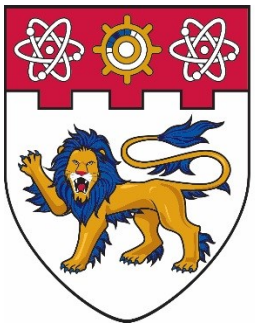

NANYANG TECHNOLOGICAL UNIVERSITY
SINGAPORE

ENTEROCOCCUS FAECALIS MEMBRANE MICRO-DOMAIN FORMATION AND ANTIMICROBIAL TARGETING

NAIR ZEUS JAREN
Interdisciplinary Graduate School
Singapore Centre for Environmental Life Sciences Engineering (SCELSE)

ENTEROCOCCUS FAECALIS MEMBRANE MICRO-DOMAIN FORMATION AND ANTIMICROBIAL TARGETING

NAIR ZEUS JAREN

Interdisciplinary Graduate School
Singapore Centre for Environmental Life Sciences Engineering (SCELSE)

A thesis submitted to the Nanyang Technological University in partial fulfillment of the requirement for the degree of
Doctor of Philosophy

2020

Statement of Originality

I hereby certify that the work embodied in this thesis is the result of original research, is free of plagiarised materials, and has not been submitted for a higher degree to any other University or Institution.

28th October 2020

. . . . . .
Date

. . . . . .
Nair Zeus Jaren

Supervisor Declaration Statement

I have reviewed the content and presentation style of this thesis and declare it is free of plagiarism and of sufficient grammatical clarity to be examined. To the best of my knowledge, the research and writing are those of the candidate except as acknowledged in the Author Attribution Statement. I confirm that the investigations were conducted in accord with the ethics policies and integrity standards of Nanyang Technological University and that the research data are presented honestly and without prejudice.

28th October 2020

. . . . . .
Date

. . . . . .
Associate Professor Kimberly Kline

Authorship Attribution Statement

This thesis **does not** contain any materials from papers published in peer-reviewed journals or from papers accepted at conferences in which I am listed as an author.

28th October 2020

. . . . . .
Date

. . . . . .
Nair Zeus Jaren

Acknowledgements

This Ph.D journey has been a challenging yet rewarding one, it would not have been possible without the support and encouragement from my supervisors, collaborators, colleagues, friends and family.

First and foremost, I would like to extend my immeasurable gratitude and appreciation to my supervisor **Kimberly Kline** for taking me into her lab and for the guidance since my very first day as an undergraduate student till today. Thank you for your unwavering support, and patience over the past 5 years, and giving me the freedom to develop my research at my own pace and to pursue research questions that interests me. I am lucky to have you as my supervisor and would not have achieved what I have today without your guidance.

I would like to also extend my deepest gratitude to **Rafi Rashid**, for his support throughout this journey, and for handing down not just technical expertise and supervision but advice along the way as well. I would not have made it this far in the initially unfamiliar lipidomics field without your input and support. I am also thankful for my co-supervisor **Chng Shu Sin** and mentor **Scott Rice** for their invaluable advice, and critical input and suggestions given all throughout this project.

Special thanks to **Markus Wenk** and members of the **Singapore Lipidomics Incubator (SLING)** for supporting the lipidomic work. I am immensely grateful to **Amaury** and **Juat Chin** for their invaluable role in imparting technical knowledge to someone who had little knowledge of the field and assisting in the use of the mass spectrometers. I would also like to thank again Chng Shu Sin and members of the **Chng Lab,** especially **Tan Wee Boon** for the help and guidance with radiolabelling work. I am also thankful for **Julien Lescar's Lab** for

the help with size exclusion chromatography and **Michael Overduin's Lab** for providing styrene maleic acid for our experiments.

I am also especially thankful to all members of the Kline lab and SCELSE, both past and present that not only helped in driving this project forward but for the friendships forged and unforgettable memories in working here. Thank you, **Kelvin, Pei Yi, Adeline, Ling Ning, Sumitra, Irina, Sharon, JJ, Dominic, Iris, Qingyan, Junhong, Mugil, Foo Kiong and Zhichao** for providing assistance to this project in one way or another. Special thanks to **Jermain, Dion,** and **Daryl** for their hard work and their contribution to this work. Thank you for being such fantastic students. I would also like to thank members of the localisation/molecular group for their valuable feedback along the way, and the whole of the laboratory management team and SCELSE-Graduate Studies Office for their support throughout. I would also like to also thank the other members of the Kline Lab / SCELSE / NTU (not mutually exclusive to those mentioned above) for their friendship, help and moral support throughout this journey: **Brenda, Nasren, Hafiz, Casandra, Renee, Rosalind, Alicia, Bryan, Patrick, Dickson, Wooi Keong, Shi Ming, Erica** and **Benny**. Thank you, the rest of the Kline lab who I have not mentioned in detail, but all of you played an equally important role in my journey and thank you for making it a tad bit easier.

Last but not the least, I would like to thank my family for their unwavering love and support these past 4 years and accompanying me through the ups and downs of this Ph.D. journey. I would not have made it this far without you all, and for this I dedicate this thesis to all of you.

Table of Contents

Sections **Page**

Acknowledgements ..... **i**

List of Tables ..... **vii**

List of Figures ..... **ix**

List of Abbreviations ..... **xii**

Presentations ..... **xv**

Summary ..... **xvi**

1. CHAPTER I **1**

1.1. Introduction 1

1.1.1. Background 1

1.1.2. Objectives 3

1.2. Literature Review 4

1.2.1. *Enterococci* and infections 4

1.2.2. Antimicrobial Targeting and Resistance 5

1.2.3. Antimicrobial resistance mechanisms 12

1.2.4. Enterococcal lipidome, lipid metabolism and regulation 17

1.2.5. Membrane organisation 23

1.3. Thesis Outline 25

1.4. References 27

2. CHAPTER II: Lysine modification of phosphatidylglycerol has broad and unexpected lipidomic, transcriptomic, and functional consequences for *Enterococcus faecalis* **40**

2.1. Introduction 40

2.2. Materials and methods 44

2.2.1. Bacterial strains and culture conditions 44

2.2.2. Analysis of membrane lipid content 48

2.2.3. RNA isolation and RT-qPCR 50

2.2.4. Growth curves 52

2.2.5. Fatty acid methyl esters (FAME) analysis 53

2.2.6. Radiolabelling and thin layer chromatography (TLC) 53

2.2.7. SDS-PAGE and western blot 54

2.2.8. Bulk secretion assay 54

2.2.9. Alkaline phosphatase (AP) secretion assay 55
2.2.10. Analysing membrane fluidity (microscopy) 55
2.2.11. Analysing membrane fluidity (microplate spectroscopy) 56
2.2.12. Daptomycin minimum inhibitory concentration (MIC) 57
2.2.13. Static biofilm assay with crystal violet staining 57
2.2.14. Live/Dead staining 57
2.2.15. Murine model of gut colonization 58
2.2.16. *In vitro* planktonic competitive growth assay 59
2.2.17. Molecular cloning 59
2.3. Results 62
2.3.1. *mprF* deletion alters Lys-PG and PG levels 62
2.3.2. Loss of *mprF* leads to changes in other lipid classes 65
2.3.3. *mprF* deletion decreases expression of genes involved in fatty acid biosynthesis 70
2.3.4. Palmitic acid, Stearic acid and Arachidic acid restores *mprF* growth in chemically defined media (CDM) 72
2.3.5. Fatty acid profiles are altered in the *mprF* mutants in both BHI and CDM 79
2.3.6. Envelope and barrier-stress sensing two-component systems (TCS) are not involved in survival of *mprF* mutants 82
2.3.7. Loss of *mprF* leads to pleiotropic phenotypes 87
2.3.8. *mprF* does not affect *in vivo* competitive gut colonisation 92
2.4. Discussion 94
2.5. Conclusion 100
2.6. References 103
3. CHAPTER III: Adaptation of *Enterococcus faecalis* to daptomycin reveals a role for *ftsH* in resistance acquisition and essentiality for growth 110
3.1. Introduction 110
3.2. Materials and methods 115
3.2.1. Bacterial strains and culture conditions 115
3.2.2. *In vitro* evolution of *E. faecalis* to daptomycin resistance 119
3.2.3. Minimal inhibitory concentration test (microplate dilution) 119
3.2.4. Growth curves 119
3.2.5. Live-dead staining 120
3.2.6. RNA isolation and sequencing 120
3.2.7. FtsH substrate identification 122
3.2.8. Mutation rate assay (Luria-Delbrück fluctuation assay) 123

3.2.9. Western immunoblot 123
3.2.10. Immunofluorescence assay 124
3.2.11. Molecular cloning 125
3.3. Results 130
3.3.1. *ftsH* is essential in the wild type *E. faecalis* but not *mprF* mutants 130
3.3.2. *ftsH* dysfunction leads to increased rate of DAP^R acquisition ... 135
3.3.3. Transcriptomic analyses reveal altered metabolism in wild type under FtsH inactivated conditions 138
3.3.4. Identification of FtsH substrates 142
3.3.5. *trePP*, *lysS* and amidase contribute to growth defects in FtsH dysfunction 146
3.3.6. *lutA* and *yckE* contribute to accelerated DAP^R acquisition upon FtsH dysfunction while *hrcA* slows acquisition 152
3.3.7. FtsH cell membrane localisation is pole and septum excluded 155
3.4. Discussion 157
3.5. Conclusion 162
3.6. References 164
4. CHAPTER IV: *Enterococcus faecalis* membrane microdomain characterisation 171
4.1. Introduction 171
4.2. Materials and methods 175
4.2.1. Bacterial strains and culture conditions 175
4.2.2. Immunofluorescence assay 178
4.2.3. Growth curves 178
4.2.4. Membrane fluidity assay by Laurdan staining 179
4.2.5. Minimal inhibitory concentration assay (microplate dilution) 180
4.2.6. Bulk secretion assay 180
4.2.7. Western blot 181
4.2.8. Membrane isolation 182
4.2.9. Detergent-sensitive and resistant membrane fractionation 182
4.2.10. Styrene-maleic acid (SMA) based isolation of membrane microdomains 183
4.2.11. Molecular cloning 184
4.3. Results 188
4.3.1. Flotillin homologs exist in *E. faecalis* 188
4.3.2. Flotillin homologs colocalise at the septum similar to SrtA 190
4.3.3. *floA* is essential for growth in nutrient limited conditions 192

4.3.4. *floT* has a minor effect on membrane fluidity under nutrient limited conditions 195
4.3.5. Flotillins are not involved in beta-lactam resistance and secretion 197
4.3.6. Detergent-based extraction and analysis of flotillin and SrtA microdomains 199
4.3.7. Non-detergent based extraction and analysis of SrtA microdomains 204
4.4. Discussion 207
4.5. Conclusion 212
4.6. References 213
5. CHAPTER V: Conclusions and future perspectives 218
5.1. Conclusions 218
5.2. Future perspectives 223
5.2.1. Investigating the mechanism behind the observed phenotypes in Δ*mprF* 223
5.2.2. Implications of chaperone activity on DAP^R acquisition and DAP mechanisms of action 224
5.2.3. More extensive characterisation of virulence factor and flotillin associated microdomains and their dynamics 226
5.2.4. Bacterial lipidome alterations in infection 228
5.3. References 229
6. APPENDIX 233
6.1. Supplementary information for Chapter 2 233
6.1.1. Supplementary section – TLC spot identification 268
6.1.2. Supplementary method – mass spectrometry of TLC spots 269
6.2. Supplementary information for Chapter 3 271
6.3. Supplementary information for Chapter 4 281

List of Tables

Table	Page
Table 1.1. List of enterococcal antimicrobial resistances	6
Table 1.2. List of enterococcal antimicrobial resistance mechanisms	13
Table 2.1. Bacteria Strains and Culture Conditions	44
Table 2.2. Lipid standards used	48
Table 2.3. Primers used for RT-qPCR	51
Table 2.4 Components in chemically defined media (CDM)	52
Table 2.5. Antibodies and developing solution used in western immunoblots	54
Table 2.6. gBlocks Sequences for Guide RNA inserts	60
Table 2.7. PCR Primers	61
Table 3.1. Bacteria Strains and Culture Conditions	115
Table 3.2. Antibodies and developing solution used in western immunoblots	124
Table 3.3. gBlocks Sequences for Guide RNA inserts	126
Table 3.4. PCR Primers	127
Table 4.1. Flotillin deletion associated phenotypes in *B. subtilis* and *S. aureus*	173
Table 4.2. Bacteria Strains and Culture Conditions	175
Table 4.3 Components in chemically defined media (CDM)	179
Table 4.4. List of antibiotics used	180
Table 4.5. Antibodies and developing solution used in western immunoblots	181
Table 4.6. PCR Primers	186
Table S2.1. DGDAG Species detected in *E. faecalis*	233
Table S2.2 - MRM transition list for DGDAG and MGDAG	236
Table S2.3 - Untargeted MS analysis of TLC spots	237
Table S2.4 - RNAseq Results (Δ*mprF1*Δ*mprF2* vs WT)	249
Table S2.5 - Fatty acids present within BHI	256
Table S2.6 - Fatty acids detected in WT and Δ*mprF1*Δ*mprF2* grown in BHI or CDM	257

Table S3.1. List of genes with mutations and sequence of occurrence 271

Table S3.2 - RNAseq Results (WT p6his-*ftsH*(H456Y) vs WT p6his-ftsH) 272

Table S3.3 - Proteomics Results (WT p6his-*ftsH*(H456Y) vs WT p6his-*ftsH*) 276

Table S4.1. Results of proteomic analysis of p*floT*-6his DRM vs DSM 281

List of Figures

Figures	Page
Figure 1.1. Daptomycin	8
Figure 1.2. Arrangement of CAMPs bound within the membrane as described by the barrel-stave, toroidal-pore, and carpet models of CAMP-mediated membrane disruption.	10
Figure 1.3. Structures of most abundant lipid species in *E. faecalis*.	18
Figure 1.4. Fatty acid and phospholipid metabolism.	19
Figure 2.1. Deletion of either *mprF* paralog results in equal enhancement of CAMP focal binding but differential CAMP susceptibility	42
Figure 2.2. *mprF* contributes to Lys-PG and PG levels	64
Figure. 2.3. mprF deletion results in lipidomic changes in other lipid classes.	69
Figure 2.4. Loss of *mprF* leads to downregulation of fatty acid biosynthesis genes.	71
Figure 2.5. *mprF* mutants display a growth defect when grown in chemically defined media (CDM) which can be rescued by a combination of palmitic and stearic acid.	78
Figure 2.6. *mprF* mutants display an altered fatty acid profile when grown in CDM as compared to the wild type	81
Figure 2.7. LiaFSR, CroRS two-component systems (TCS) are not implicated in Δ*mprF1*Δ*mprF2* survival. However, the loss of WalKR signaling is better tolerated in Δ*mprF1*Δ*mprF2*	86
Figure. 2.8. mprF mutants exhibit pleiotropic phenotypes	90
Figure. *2.9. mprF* does not contribute to fitness in a competitive gut colonisation *model.*	93
Figure. *2.10.* Working model for the effect of the loss of mprF integrating transcriptomic, lipidomic and phenotypic observations.	102
Figure 3.1. *In vitro* evolution of *mprF* mutants to DAPR reveal novel mutations	113

Figure 3.2. Heterologous expression of *ftsH(G37X)* reveals that *ftsH* is essential in the wild type 133
Figure 3.3. Inactivation of *ftsH* leads to accelerated DAPR acquisition rate 137
Figure 3.4. Transcriptomic analysis of WT p6his-ftsH*(H456Y)* vs WT p6his-ftsH reveal metabolic changes 141
Figure 3.5. Proteomic analysis of wild type p6his-ftsH*(H456Y)* vs p6his-ftsH for FtsH substrate identification 145
Figure 3.6. Growth curves of mutant strains of depleted and accumulated protein hits 151
Figure 3.7. *In vitro* evolution to DAPR of transposon mutants 154
Figure 3.8. Localisation of FtsH is pole and septum excluded 156
Figure 3.9. Model of proposed events following FtsH dysfunction 163
Figure 4.1. Protein sequence and structural alignment of predicted FloA and FloT structures 189
Figure 4.2. Immunofluorescence microscopy of *E. faecalis* pEmpty, pAK1-srtA-2HA, pCYW2-floA-2HA, pCYW2-floT-2HA and Δ*floA*Δ*floT* pAK1-srtA-2HA 191
Figure 4.3. Growth curves of *E. faecalis* wild type, Δ*floA*, Δ*floT*, Δ*floA*Δ*floT* 194
Figure 4.4. Membrane fluidity of the flotillin mutants measured by laurdan spectroscopy 196
Figure 4.5. Antibiotic minimal inhibitory concentration (MICs) and bulk secretion of the flotillin mutants 198
Figure 4.6. Analysis of detergent resistant membrane (DRM) and detergent soluble membrane (DSM) fractions from *E. faecalis* 203
Figure 4.7. Styrene-maleic acid (SMA) based isolation of SrtA-6his SMA-lipid particles (SMALPs) 206
Figure 5.1. Model for MprF influence on *E. faecalis* cell physiology and FtsH influence on growth and DAPR acquisition 222

Figure S2.1. Anti-HA western immunoblot of *E. faecalis* strains containing pmprF1-HA and *pmprF2-HA* 258

Figure. S2.2. Loss of mprF contributes to changes in individual species of Lysyl-PG, PG and DGDAG 259

Figure. S2.3. *mprF* mutants display no difference in viability and membrane permeability to propidium iodide (PI) 260

Figure. S2.4. Identification of lipid spots in 1D- and 2D-TLCs of lipid extracts from WT and the mprF mutants 262

Figure. S2.5. mprF mutants do not display detectable differences in lipoteichoic acid (LTA) levels 263

Figure. S2.6. Membrane fluidity measurements by Laurdan 263

Figure. S2.7. *In* vitro competitive planktonic growth assay 264

Figure S2.8. *mprF* mutants grown in chemically defined media (CDM) with individual fatty acid supplementation 267

Figure S3.1. Anti-HA western immunoblot of *E. faecalis* strains expressing 6his and/or HA tagged *ftsH*, *ftsH(H456Y)*, OG1RF_10100 (*arcB*), OG1RF_11679, OG1RF_10473 278

Figure S3.2. Inducible expression of inactive *ftsH* variant, *ftsH(H456Y)* leads to growth defect in the wild type 279

Figure S3.3. PCR amplification of the *ftsH* locus of Δ*mprF1*Δ*mprF2* passage control isolates from day 3, 6, 9 of evolution 279

Figure S3.4. *ftsH* dysfunction has a minor effect on cell viability and increases cell chaining in the wild type 280

Figure S4.1. Western blot of affinity tagged flotillins and SrtA showing expression 284

Figure S4.2. Plasmid map of pMSP3545zn 285

Figure S4.3. Sliver stained SDS-PAGE gels showing partition of proteins into detergent resistant membrane (DRM) and detergent soluble membrane (DSM) fractions 286

Figure S4.4. SrtA-6his SMALP isolation 287

List of Abbreviations

1D	One dimension
2D	Two dimensions
ACC	acetyl-CoA carboxylase
Acetyl-CoA	Acetyl coenzyme A
ACP	Acyl-carrier protein
Ala-PG	Alanyl phosphatidylglycerol
AMP	Antimicrobial peptides
Arg-PG	Arginyl phosphatidylglycerol
AS	Aggregation substance
ATP	Adenosine triphosphate
BHI	Brain heart infusion
CAMP	Cationic antimicrobial peptide
CAUTI	Catheter associated urinary tract infections
CDC	Centers for Disease Control and Prevention
CDM	Chemically defined medium
CDP-diacylglycerol	Cytidine diphosphate-diacylglycerol
CETSA	Cellular thermal shift assay
CL	Cardiolipin
CMP	Cytidine monophosphate
CRISPRi	CRISPR interference
DAG	Diacylglycerol
DAP	Daptomycin
DAP^{R}	Daptomycin resistance
DAP^{S}	Daptomycin susceptible
DGDAG	Diglucosyl diacylglycerol
DPI	Days post infection
DRM	Detergent resistant membrane
DSM	Detergent soluble membrane
DTT	Dithiothreitol
ESI	Electrospray ionization
FAME	Fatty acid methyl esters
FASI	Type I fatty acid synthase
FASII	Type II fatty acid synthase
FMM	Functional membrane microdomain
G-1-P	Glycerol-1-phosphate

G-3-P	Glycerol-3-phosphate
GC	Gas chromatography
GP	Generalised polarisation
GPDGDAG	Glycerophosphoryl diglucosyl diacylglycerol
HA	Hemagglutinin
HAI	Hospital acquired infection
hBD2	Human beta defensin 2
hBD3	Human beta defensin 3
HGPC	Highest growth permissive concentration
HNP-1	Human neutrophil peptide 1
IMAC	Immobilized metal affinity chromatography
KEGG	Kyoto Encyclopedia of Genes and Genomes
LC-MS/MS	Liquid chromatography tandem mass-spectrometry
L_d	Liquid disordered
L_o	Liquid ordered
LTA	Lipoteichoic acid
Lys-PG	Lysyl-phosphatidylglycerol
MDR	Multi-drug resistant
MFI	Mean fluorescence intensity
MGDAG	Monoglucosyl diacylglycerol
MHB	Mueller Hinton broth
MIC	Minimum inhibitory concentration
MprF	Multiple peptide resistance factor
MRM	Multiple reaction monitoring
MRSA	Methicillin-resistant *S. aureus*
PB	Phosphate buffer
PBS	Phosphate buffered saline
PE	Phosphatidylethanolamine
PG	Phosphatidylglycerol
PGP	Phosphatidyl-glycerolphosphate
PHB	Prohibitin homologue
PI	Propridium iodide
pNPP	Para-nitrophenyl phosphate
PSICIC	Projected system of internal coordinates from interpolated contours
RNAseq	RNA sequencing

ROI	Region of interest
ROTS	Reproducibility-optimized test statistic
RT-qPCR	Real time quantitative PCR
SEC	Size exclusion chromatography
SMA	Styrene-maleic acid
SMALP	Styrene-maleic acid lipid particle
SNP	Single nucleotide polymorphism
SPFH domain	Stomatin, prohibitin, flotillin, and HflK/C domain
TAG	Triacylglycerol
TCA	Tricholoroacetic acid
TCS	Two component system
TEM	Transmission electron microscopy
TLC	Thin layer chromatography
Tn	Transposon
TSB	Tryptone soy broth
TSBG	Tryptone soy broth with 1.39 M glucose
UTI	Urinary tract infection
VRE	Vancomycin resistant enterococci
WHO	World Health Organisation
WT	Wild type

Presentations

Nair ZJ, Gao IH and Kline KA (2018). Role of *ftsH* in Acquisition of Daptomycin Resistance in *E. faecalis*. 5th International Conference on Enterococci, Chamonix, France. 15-20 April 2018 (poster presentation).

Nair ZJ, Rashid R, Chia DMH, Chong KKL, Wong JJ, Goh SHM, Liew TH, Yong AMH, Cazenave-Gassiot A, Chen SL, Wenk MR, Kline KA (2019). Phosphatidylglycerol modifications in the opportunistic pathogen *Enterococcus faecalis* contribute to global lipid homeostasis and secretion. CSHL Conference on Microbial Pathogenesis & Host Response, New York, USA. 10-14 September 2019 (poster presentation).

Summary

Enterococcus faecalis is an opportunistic pathogen commonly isolated with nosocomial infections where its ability to acquire resistance to last-line antimicrobials poses a public health threat. Previous literature suggests the existence of septal membrane microdomains and the tendency of cationic antimicrobials to target them. Given the importance of microdomains and antimicrobial targeting as a potential drug target for this often-resistant organism, this thesis takes a multi-faceted approach to investigate the dynamics behind microdomain targeting, microdomain assembly, and membrane and genetic factors involved in targeting and resistance. We first investigated a phosphatidyl glycerol (PG) modifying enzyme, the multiple peptide resistance factor (MprF), since it is implicated in focal targeting and resistance of cationic antimicrobial peptides (CAMPs). Apart from its catalytic activity in lysinylating PG to lysyl-PG, MprF was discovered to affect the global lipidome, *de novo* fatty acid biosynthesis regulation and dependence on exogenous fatty acids under nutrient limitation. Loss of *mprF* also leads to functional outcomes in terms of secretion defects, increased membrane rigidity and susceptibility to cationic antimicrobial peptides. Interestingly, Δ*mprF* also provides a permissive environment for loss of function of an otherwise essential metalloprotease, FtsH, which results in enhanced rate of acquisition of daptomycin resistance through increased basal mutation rates. Given their possible roles in coordinating antimicrobial targeting of the membrane, microdomains were also characterised, with results suggesting that flotillins, and sortase A associated microdomains are likely part of separate domains. Flotillin homologs in *E. faecalis* demonstrate atypical functions in growth and membrane fluidity that are only apparent under nutrient limitation, and they are not enriched within detergent resistant membrane fractions. We also provided proof of concept in the use of styrene-

maleic acid to generate lipid particles as an alternative method to sample microdomains. Together this work provides a better understanding of *E. faecalis* membrane physiology and homeostasis, and how metabolic networks, membrane lipid composition, microdomains and functional outcomes are all closely intertwined.

1. CHAPTER I

1.1. Introduction

1.1.1. Background

Enterococcus faecalis is a Gram-positive, non-motile, facultative anaerobe that can tolerate a wide range of environmental conditions such as high pH, salinity and wide temperature ranges (Fisher and Phillips, 2009). *Enterococci* are also commensals of the normal gastrointestinal microbiota of humans and animals where they are commonly isolated. Within the human gut, *E. faecium* and *E. faecalis* are the most frequently isolated species (Hayashi et al., 2005; Klein, 2003). *Enterococci* are also ubiquitous in nature, present in the gastrointestinal tract of other animals and the environment (Ator and Starzyk, 1976; Lingwood and Simons, 2010; Martin and Mundt, 1972; Mundt, 1961, 1963a, b)

Despite being a member of the human gut microbiota, *E. faecalis* is also an opportunistic pathogen involved in several nosocomial infections. *Enterococci* are the second most common cause of hospital-acquired infections (HAIs) comprising 14% of all cases in the US between 2011-14 (Weiner et al., 2016). They are implicated in a variety of HAIs such as bacteraemia, meningitis, endocarditis, urinary tract infections (UTI) as well as catheter-associated, soft-tissue and surgical wound infections which can be fatal if left untreated (Hidron et al., 2008; Murdoch et al., 2009; Patterson et al., 1995; Weiner et al., 2016).

Furthermore, *Enterococci* tend to be resistant to antimicrobials via both intrinsic (resistance present within all members of the genus) or acquired (resistance acquisition through horizontal gene transfer or mutations) resistance, which makes infections difficult to treat. *Enterococci* are intrinsically resistant to cephalosporins, aminoglycosides, lincosamides, streptogramins, trimethoprim-sulfamethoxazole and low levels of beta-lactams (Hollenbeck and Rice, 2012; Miller et al., 2014). In addition, *Enterococci* also intrinsically possess

mechanisms to circumvent the action of host-derived cationic antimicrobial peptides (CAMPs) (Bao et al., 2012). Due in part to their malleable genome and horizontal gene transfer through plasmids and transposons, *Enterococci* are also able to acquire resistance to antibiotics such as glycopeptides, linezolid, daptomycin and tigecycline, amongst others (Hollenbeck and Rice, 2012; Miller et al., 2014). Among the most clinically concerning antibiotic resistances of *Enterococci* are those acquired for vancomycin (a glycopeptide) and daptomycin, which are last-line antibiotics used in treating multi-drug resistant (MDR) infections. Vancomycin resistant enterococci (VRE) have not only been correlated with increased mortality in clinical settings, but emergence of resistance to daptomycin, which is commonly used to treat VRE, has also been reported (Arias and Murray, 2012; Kelesidis et al., 2011; Munoz-Price et al., 2005). The rise of drug resistant infections also results in rising costs for healthcare and increases the patient's length of stay in the hospital (Gandra et al., 2014; Puchter et al., 2018). The rise of such infections together with increasingly ineffective antibiotic treatment not only increases mortality rates but imparts significant economic burden. This underscores the need to better understand acquisition of resistance and resistance mechanisms in *Enterococci* to better inform drug development and mitigation of multi-drug resistant infections.

Antimicrobials, particularly those that are cationic in nature, focally target the septal domains of *E. faecalis* and this targeting is suggested to be important for exerting their killing effect. Host-derived cationic antimicrobial peptides (CAMPs) such as human beta-defensin 2 (hBD2) focally target the division septum of *E. faecalis* when treated at sub-inhibitory concentrations (Kandaswamy et al., 2013). Furthermore, in susceptible strains of *E. faecalis*, cationic daptomycin similarly focally targets the division septum, which becomes dispersed in random

foci across the membrane in resistant strains (Tran et al., 2013), suggesting that focal targeting is important for daptomycin action. Several virulence factors and lipids are colocalised within the division septum of *E. faecalis*. Anionic lipids together with SrtA, SrtC (sortase enzymes responsible for anchoring surface virulence factors onto the cell wall), and SecA (ATPase that is part of the Sec secretion translocon) are colocalised at septal domains (Kandaswamy et al., 2013; Kline et al., 2009). Taken together, these studies suggest that membrane microdomains coincide with sites of virulence factor assembly and secretion at the division septum and that cationic antimicrobials target and potentially disrupt these regions.

1.1.2. Objectives

Given the significance of the focal targeting of cationic antimicrobials in the exertion of their inhibitory activity, it is important to understand the mechanism of targeting and its implications. However, much is still unknown about the interaction of antimicrobials with the *E. faecalis* membrane, particularly in terms of the factors that govern targeting, microdomain assembly, and membrane and genetic factors involved in targeting and resistance. This thesis aims to address this gap by exploring the following aspects:

1. Investigating the physiologic response of *E. faecalis* to the genetic depletion of lysyl-phosphatidylglycerol (lysyl-PG), a phospholipid involved in CAMP resistance.
2. Membrane and genetic factors affecting cationic antimicrobial resistance to daptomycin.
3. Existence of membrane microdomains, their organisation and possible links to antimicrobial targeting.

1.2. Literature Review

1.2.1. *Enterococci* and infections

Enterococci, formerly known as group D *Streptococci*, belong to a low GC branch of Gram-positive bacteria, with a chromosomal GC content of 37.5% (Paulsen et al., 2003; Schleifer and Kilpper-Bälz, 1984). They are diplococci and facultative anaerobes that possess tolerance towards harsh environmental conditions such as wide temperature ranges (10 – 45 ^{o}C), high salt concentrations (6.5% NaCl; 40% bile salts), and wide pH ranges (pH 4.6 – 9.6) (Fisher and Phillips, 2009; Lebreton et al., 2014). *Enterococci* are also well characterised as part of the human gut microbiota with this genus being isolated with more prevalence in human faeces (10^5 – 10^7 CFU/g) than that of other mammals. In terms of species, *Enterococcus faecalis* and *Enterococcus faecium* are the most dominant comprising up to 1% of the total gut microbiota of adults (Dubin and Pamer, 2014; Franz et al., 1999; Lebreton et al., 2014). They are also present as commensals of the gastrointestinal tract in animals, insects, reptiles and birds (Martin and Mundt, 1972; Mundt, 1963a). Due in part to their robust nature, they are also widely found in the environment, in water, soil and plants (Ator and Starzyk, 1976; Mundt, 1961, 1963b)

However, *Enterococci* are also opportunistic pathogens that are implicated in hospital-acquired infections (HAIs), where over the past few decades they have been an emerging source of multi-drug resistant HAIs. In 1899, the first case of enterococcal infection was reported where *E. faecalis* was isolated from a case of lethal endocarditis (Maccallum and Hastings, 1899). Up to the 1980s, the majority of *Enterococcal* infections consisted of intraabdominal, urinary tract, pelvic, skin, and soft tissue infections, and tended to be mostly community acquired and polymicrobial in nature (Lewis and Zervos, 1990; Robert C. Moellering, 1992). However, over time enterococcal infections have become

more prominent and increasingly associated with nosocomial infections. Especially in the past decade, where they have accounted for 14% of all HAIs in the USA from 2011-14 and 10% of HAIs in Europe in 2010, highlighting the major role *Enterococcal* infections play in nosocomial infections (Weiner et al., 2016; Zarb et al., 2012). Throughout these reports, *E. faecalis* and *E. faecium* consistently account for the bulk of enterococcal HAIs, and in a large-scale global study from 1997 – 2016, both of them formed majority of all surveyed enterococcal infections (64.7% and 29% respectively) (Pfaller et al., 2019). *E. faecalis* and *E. faecium* are implicated in a wide array of HAIs such as catheter associated urinary tract infections (CAUTI), endocarditis, peritonitis, bacteraemia, colitis, diabetic foot ulcers, surgical site infections, and wound infections which can be lethal if left untreated (Edmond et al., 1999; Hidron et al., 2008; Murdoch et al., 2009; Patterson et al., 1995; Weiner et al., 2016). Of these infections, *Enterococci* account for 10.7% of bloodstream infections in North America, 24% of intra-abdominal infections in the Asia-Pacific region, and 19.8% of urinary tract infections (UTIs) in the Latin-American region from 1997-2016, further highlighting its contribution to clinical infections (Pfaller et al., 2019). Taken together, enterococcal infections present a serious healthcare problem especially with its strong association with HAIs. Hence, it is imperative that there is continuing research on enterococcal pathogenicity and physiology to improve treatment options.

1.2.2. Antimicrobial Targeting and Resistance

Adding to the challenge of treating enterococcal infections is that they tend to be more resistant to antimicrobials. *Enterococci* possess intrinsic resistance, whereby all members of the genus are resistant to cephalosporins, trimethoprim-sulfamethoxazole as well as possess low level resistance to beta-lactams, lincosamide, streptogramins and aminoglycosides **(Table 1.1)**. Due in part to its

malleable genome, *enterococci* can also acquire resistance to many other antibiotics as listed in **Table 1.1** by means of sporadic mutations, or thorough mobile genetic elements such as plasmids and transposons (Hollenbeck and Rice, 2012; Miller et al., 2014).

Table 1.1. List of enterococcal antimicrobial resistances

Intrinsic Resistance	Acquired Resistance
➢ β-Lactams (Low level) ➢ Cephalosporins ➢ Lincosamides/ streptogramins (Low level) ➢ Aminoglycosides (Low level) ➢ Trimethoprim-sulfamethoxazole	➢ β-Lactams (High level) ➢ Glycopeptides **(e.g. vancomycin)** ➢ **Daptomycin** ➢ Quinupristin/ dalfopristin ➢ Aminoglycosides (High level) ➢ Linezolid ➢ Macrolides ➢ Lincosamides/ streptogramins (High level) ➢ Tetracycline ➢ Quinolones ➢ Rifampicin

(Hollenbeck and Rice, 2012; Miller et al., 2014).

Particularly concerning is the ability of *Enterococci* to acquire resistance to drugs of last resort in treating multi-drug resistant infections, namely vancomycin and daptomycin. Especially with increased use of antibiotics in healthcare settings, there has been a stark rise in multi-drug resistant infections where vancomycin-resistance in *Enterococci* has now become more widespread. From the 1980s where vancomycin-resistant *Enterococci* (VRE) was first discovered in a few European countries, it has now spread all across Europe and to the rest of the world (O'Driscoll and Crank, 2015; Werner et al., 2008). VRE infections can lengthen hospital stay from 6 up to 22 days with a slight increase of mortality rates in some cases, ranging from 9% to 30% (Mascini and Bonten, 2005). With

the increased length of hospitalisation, the need for additional treatment and infection control also often leads to increased healthcare costs associated with such infections (Carmeli et al., 2002; Mascini and Bonten, 2005; Song et al., 2003). Recognising the serious implications of VRE infections in United States, the US Centers for Disease Control and Prevention (CDC), has even listed VRE as a serious threat in its Antibiotic Resistance Threats Report in all of its past 2 editions (CDC, 2013, 2019). It has also been listed as one of the leading resistant pathogens in hospitals by the World Health Organisation (WHO) (WHO, 2013).

In VRE infections, treatment measures typically involve the use of linezolid or daptomycin as last line drugs (Patel and Gallagher, 2015). However, alarmingly in recent years, clinical occurrence of daptomycin resistance has been reported, which is particularly concerning due to the reduced treatment options (Arias and Murray, 2012; Kelesidis et al., 2011; Munoz-Price et al., 2005). Linezolid resistance has also been reported though such cases are currently rare (Bi et al., 2018; Chen et al., 2018; Yadav et al., 2017).

Daptomycin is a lipopeptide antibiotic generally used in the treatment of Gram-positive infections including VRE (Shoemaker et al., 2006). It was first discovered in the 1980s by Eli Lilly and Company, and later licensed to Cubist Pharmaceuticals Inc in 1997 (Tally and DeBruin, 2000). It is naturally produced by *Streptomyces roseospours* and consists of a decanoyl side chain linked to a 13-member amino acid ring **(Figure 1.1A)** (Miao et al., 2005; Steenbergen et al., 2005; Tally and DeBruin, 2000). Apo-daptomycin is negatively charged and becomes cationic when complexed with its cofactor, calcium (Taylor and Palmer, 2016). The exact mechanism of action of daptomycin is still unclear, however a proposed model is that daptomycin first complexes with calcium, then inserts into the membrane and oligomerises causing membrane disruption and eventual

potassium ion-leakage and cell death **(Figure 1B)** (Steenbergen et al., 2005; Taylor and Palmer, 2016).

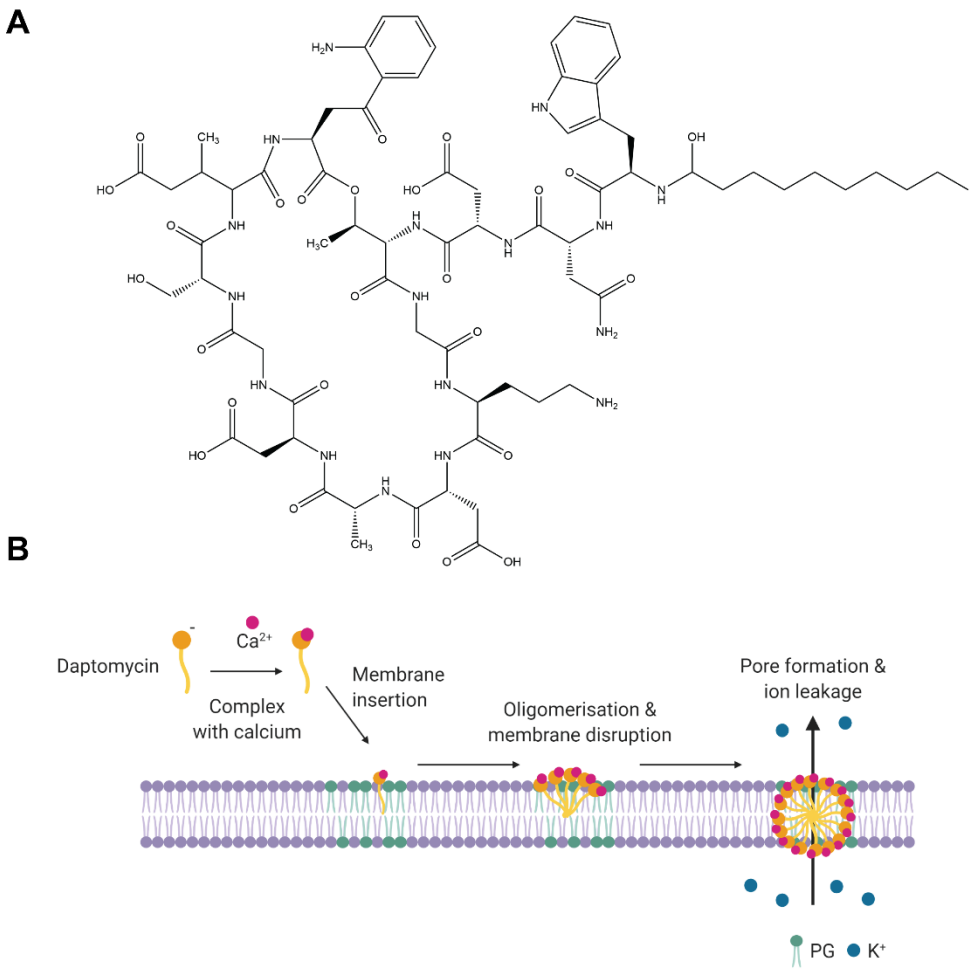

Figure 1.1. Daptomycin. (A) Daptomycin structure. (B) Proposed mechanism of action of daptomycin where PG-rich regions are targeted. Created with BioRender.com.

Interestingly, daptomycin has a preference for binding to certain regions of the cell membrane. In *Bacillus subtilis*, daptomycin has a preference for binding the nascent septum and sites of active division, with patchy foci in other parts of the cell or in the forespore membrane of sporulating cells (Hachmann et al., 2009; Pogliano et al., 2012). In *E. faecalis*, daptomycin is also enriched at the septum when treated at sub-inhibitory concentrations (Tran et al., 2013). This phenomenon however is only present in daptomycin susceptible strains of *E. faecalis* and not resistant strains, suggesting that this focal binding at the septum might be important in exerting its antimicrobial activity. Taken together these

findings suggest that daptomycin might preferentially bind membrane regions with negative curvature or have affinity to specific protein or lipid components of the membrane.

There is some evidence that daptomycin might preferably bind phosphatidylglycerol (PG) rich regions of the membrane. In *B. subtilis*, depletion of PG leads to increased daptomycin resistance and loss of enriched septal binding of daptomycin (Hachmann et al., 2009). Furthermore, daptomycin has also been shown to require PG for binding and oligomerisation in model membranes and is unable to do so in membranes lacking PG (Kreutzberger et al., 2017; Muraih et al., 2011; Muraih et al., 2012). However, detailed information on what happens after daptomycin gains entry into the cell and how resistance acquisition is mediated is scarce.

Apart from antibiotics, *Enterococci* also must contend with host derived antimicrobial peptides (AMPs) during infection. AMPs are peptides with broad spectrum activity against both Gram-positive and -negative bacteria, some enveloped viruses and fungi, that are produced by all domains of life including the human host as part of the innate immune defence system (Fox, 2013; Jenssen et al., 2006; Reddy et al., 2004). AMPs are typically amphipathic in nature which aids their insertion and partitioning into biological membranes, which is essential for their antimicrobial activity via membrane-disruption (Hancock and Rozek, 2002). AMPs are unstructured in solution and fold into their secondary structures (α-helix, β-sheet, β-hairpin loops or extended structures) once they insert and partition into membranes, and in doing so disrupt it causing cell death (Hancock and Rozek, 2002; Jenssen et al., 2006). AMPs can be divided into cationic antimicrobial peptides (CAMPs) and anionic categories based on their charged state. In this thesis we will only be focusing on CAMPs.

CAMPs are produced by human immune and epithelial cells as part of the innate immune defence and in response to infection, and are categorised into two main classes: defensins and cathelicidins (Durr et al., 2006). They disrupt membranes by targeting negatively charged phospholipid head groups by positively charged residues on CAMPs through electrostatic interaction followed by interaction of CAMP hydrophobic residues with the acyl chains of the membrane phospholipids (Pasupuleti et al., 2012; Rashid et al., 2016). In doing so, the unstructured CAMP assumes a more favourable structure for insertion and disruption of the membrane which occurs via one of the 3 proposed models: the barrel-stave, toroidal pore or carpet model (Ehrenstein and Lecar, 1977; Leontiadou et al., 2006; Pouny et al., 1992; Rashid et al., 2016) **(Figure 1.2)**.

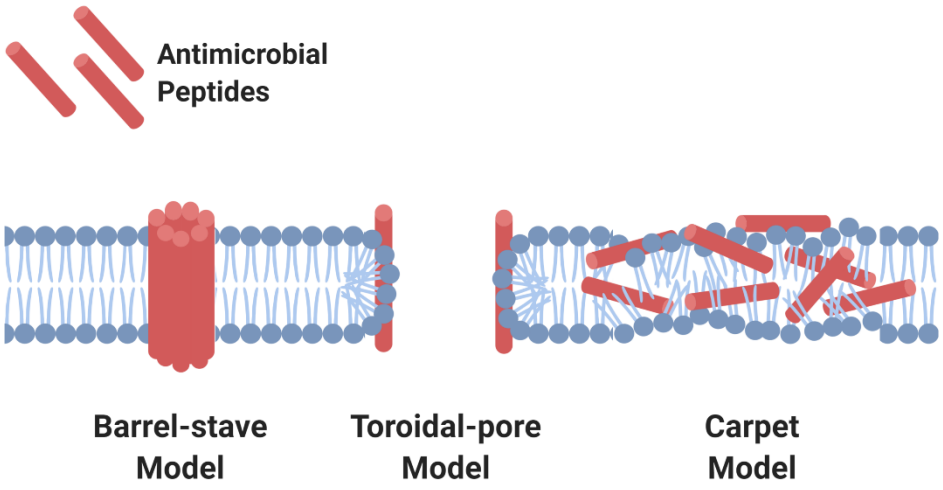

Figure 1.2. Arrangement of CAMPs bound within the membrane as described by the barrel-stave, toroidal-pore, and carpet models of CAMP-mediated membrane disruption. Diagram shows how CAMPs are arranged in the membrane post-binding. Created with BioRender.com.

In the barrel-stave model, CAMP molecules insert into the membrane and aggregate to form a barrel-like channel with hydrophobic regions facing the acyl-chains of the phospholipid bilayer, and hydrophilic regions facing an aqueous pore. This barrel/stave pore causes ion leakage and eventual cell death

(Baumann and Mueller, 1974; Ehrenstein and Lecar, 1977). In the toroidal pore model, CAMPs bind parallel to the membrane surface and when a local threshold concentration is reached, positive curvature in the membrane is induced creating an aqueous toroidal pore with phospholipid head groups and CAMPs forming the wall of the pore, which leads to eventual ion leakage (Leontiadou et al., 2006; Matsuzaki et al., 1996; Shai, 2002; Yang et al., 2001). In the carpet model, CAMPs bind the membrane surface in a parallel manner, forming a carpet of CAMPs that causes micelle formation and bilayer disruption once past threshold concentration (Pouny et al., 1992). Depending on the peptide, they disrupt membranes through one of these mechanisms. For instance, peptides such as alamethicin, pardaxin and cecropins act via the barrel-stave model; melittin and protegrins through the toroidal-pore model; LL-37 through the carpet model (Christensen et al., 1988; He et al., 1996; Kandaswamy et al., 2013; Langham et al., 2008; Porcelli et al., 2004; Porcelli et al., 2008; Rashid et al., 2016; Yang et al., 2001). Furthermore, it has been recently reviewed that CAMPs such as human beta-defensin 2 may also induce membrane disruption by delocalising membrane lipids and proteins resulting in microdomain disruption (Rashid et al., 2016).

CAMPs such as human neutrophil peptide 1 (HNP-1) and polymyxin B also tend to interact with specific regions of the cell membrane and at discrete foci (Rashid et al., 2016). In *E. faecalis*, human beta-defensin 2 (hBD2) binds the nascent septum focally and this binding disrupts the localisation of septum-localised sortase A – a cell wall sorting enzyme that attaches virulence factor substrates to the cell wall and SecA – the ATPase component of the Sec secretion machinery (Kandaswamy et al., 2013). This suggests that the initial binding of CAMPs is specifically guided to distinct foci on the membrane and this binding might disrupt the local domains and proteins situated within. This phenomenon

is not just restricted to *E. faecalis* but applies to several other bacterial species as well. In *Streptococcus pyogenes*, polymyxin B and human neutrophil peptide 1 (HNP-1), both cationic molecules, bind to the membrane at the anionic ExPortal domain disrupting it, resulting in mislocalised SecA and impaired secretion (Vega and Caparon, 2012). MP196, a 6 amino acid CAMP causes delocalisation of MurG and cytochrome c in *Bacillus subtilis* (Wenzel et al., 2014). Similarly, another CAMP, cecroprin A attacks the membrane at site of membrane curvature such as the septum of dividing cells, poles of non-septating cells (both of which are enriched in the anionic lipid, cardiolipin) in *Escherichia coli* resulting in permeabilization of the outer membrane and leakage of periplasmic contents (Mileykovskaya and Dowhan, 2009; Rangarajan et al., 2013).

Collectively, these studies indicate that the septal targeting of the positively charged calcium-daptomycin complex and CAMPs on the membrane of *E. faecalis* is a process that has functional consequences. As there is still much to be learnt about the how CAMP targeting of membranes is guided and what factors affect it, this thesis will focus on cationic antimicrobials.

1.2.3. Antimicrobial resistance mechanisms

Enterococci resist a vast array of antimicrobials through intrinsically encoded factors or acquisition of mutations or mobile genetic elements. Some of the antibiotic resistance mechanisms that *Enterococci* possess for each antibiotic class are listed in **Table 1.2.**

Table 1.2. List of enterococcal antimicrobial resistance mechanisms			
Antibiotics	**Intrinsic/ Acquired**	**Mechanism / associated genes**	**Species**
Ampilicin/ Penicillin	Intrinsic/ Acquired	Mutations or increased expression of *pbp5*, a class B PBP with low ampicillin binding affinity	*E. faecalis* *E. faecium*
	Intrinsic	β-lactamase, *blaZ*	*E. faecalis* *E. faecium*
Cephalosporin	Intrinsic	*ponA*, *pbpF*	*E. faecalis* *E. faecium*
	Intrinsic	CroRS signalling, IreKP signalling, *murAA*	*E. faecalis*
Glycopeptide (Vancomycin)	Intrinsic	VanC1/C2/C3 gene clusters D-Ala-D-Ala peptidoglycan to D-Ala-D-Ser	*E. gallinarum* *E casseliflavus*
	Acquired	VanE, VanG D-Ala-D-Ala peptidoglycan to D-Ala-D-Ser	*E. faecalis* *E. faecium*
	Acquired	VanA, VanB, VanD D-Ala-D-Ala peptidoglycan to D-Ala-D-Lac	*E. faecalis* *E. faecium*
Daptomycin	Acquired	Mutations in *liaF*, *gpdD* and *cls*	*E. faecalis*
	Acquired	Mutations in *yycFG* (*walKR*)	*E. faecium*
Aminoglycosides	Intrinsic	Naturally difficult to enter cytoplasm	*Enterococci*
	Acquired	*aadA*, streptomycin adenyltransferase	*E. faecalis*
	Acquired	APH (2')-Ic, phosphotransferase	*E. faecalis* *E. faecium* *E. gallinarum*
Oxacolidinones (Linezolid)	Acquired	Mutations in domain V of 23S rRNA Mutations in ribosomal proteins L3, L4	*E. faecalis*
	Acquired	*cfr*, methylase	*E. faecalis*
Quinupristin/ dalfopristin (Q/D)	Intrinsic	*lsa*, putative efflux pump	*E. faecalis*
	Acquired	*eatA*, *Enterococcus* ABC transporter mutations	*E. faecium*
Tetracycline	Acquired	*tetK, tetL* encoding an efflux pump	*Enterococci*
	Acquired	*tetM, tetO, tetS,* encoding alternate elongation factors	*Enterococci*
Quinolones	Acquired	Mutations in *gyrA* and *parC* targets	*E. faecalis* *E. faecium*
	Acquired	*qnr*, DNA gyrase protective protein	*E. faecalis*
Rifampicin	Acquired	Mutation in *rpoB*	*E. faecalis* *E. faecium*
Trimethoprim & sulfamethoxazole	Intrinsic	Ability to utilize exogenous folate	*Enterococci*

A non-exhaustive list of enterococcal resistance mechanisms, with particular focus on *E. faecalis* and *E. faecium* (Courvalin, 2006; Miller et al., 2014)

The resistance strategies that *enterococci* employ include decreasing antibiotic target drug affinity by mutations in the case of 23S rRNA mutations decreasing affinity to linezolid, drug inactivation via enzymes such as β-lactamases in β-lactam resistance, decreased drug uptake by intrinsic properties of the cell membrane that reduce permeability to polar aminoglycosides, increased drug efflux by Lsa efflux protein in quinupristin/dalfoprisin resistance, target protection such as Qnr binding of DNA gyrase in quinolone resistance and use of alternate pathways such as the uptake of exogenous folate in trimethoprim and sulfamethoxazole resistance (Miller et al., 2014).

Though there are many resistance mechanisms, we will be focusing on daptomycin resistance due to the interest in its intriguing septal localisation pattern and its clinical relevance as a drug of last resort in treating enterococcal MDR. *E. faecalis* is intrinsically susceptible to daptomycin and can acquire resistance based on mutations in genes related to the membrane and envelope stress-sensing.

From a genetic perspective, a study that sequenced clinical strain pairs of daptomycin resistant (DAP^R) and susceptible *E. faecalis* revealed mutations in *liaF*, *gpdD* and *cls* (Arias et al., 2011). In *B. subtilis* and *S. mutans*, *liaF* encodes the inhibitor of LiaS within the LiaFSR three-component system where LiaS is the sensor histidine kinase that senses membrane-stress and phosphorylates the response regulator LiaR (Jordan et al., 2006; Suntharalingam et al., 2009). The loss of function of LiaF in the *E. faecalis* DAP^R isolate might enhance the envelope stress response in mitigating membrane damage (Arias et al., 2011). Further investigation confirmed the involvement of the *liaFSR* three component system, where antimicrobials are sensed by a secreted *liaX* peptide that kickstarts *liaFSR* signalling. This signalling is important for mediating resistance to daptomycin and cationic antimicrobial peptides (CAMPs) (Khan et al., 2019;

Reyes et al., 2015). Furthermore, mutations in GpdD, a glycerophosphodiesterase that hydrolyses cell-membrane phosphodiesters, and Cls, a cardiolipin synthase, indicates possible changes in membrane phospholipid content that confer daptomycin resistance (Arias et al., 2011). Additionally, cardiolipin is known to prevent daptomycin penetration and permeabilization in the inner leaflet of the membranes in *in vitro* liposomes, further highlighting the possible protective role of cardiolipin in DAP^R (Zhang et al., 2014). In a separate study utilising turbidostat-based *in vitro* evolution of a daptomycin susceptible *E. faecalis* clinical isolate to DAP^R, similar mutations were found. In addition, mutations were also identified in *yvlB* – a putative *liaFSR* target of unknown function – as well as *gshF, yybT, selA* which are genes with putative function in oxidative stress response and stress signalling, and *mdpA* – a drug resistance pump – following initial mutations in LiaFSR (Miller et al., 2013). These findings further implicate envelope stress sensing, oxidative stress response, and stress signalling in DAP^R.

From a phenotypic perspective, DAP^R *E. faecalis* strains show diversion of BODIPY-daptomycin away from the septum as compared to septal enriched binding in susceptible strains, indicating daptomycin diversion as a possible strategy of resistance (Tran et al., 2013). Taking a closer look at membrane composition changes, DAP^R is associated with decrease in phospatidylglycerol (PG), and increase in glycerophosphoryl diglucosyldiacylglycerol (GPDGDAG) as well as increased membrane rigidity (Mishra et al., 2012; Rashid et al., 2017). Apart from endogenous strategies, *E. faecalis* can also incorporate exogenous fatty acid from serum and bile into its membrane altering its composition to protect itself from daptomycin (Harp et al., 2016).

Alterations in cell membrane stress response and altered membrane composition are the currently known DAP^R mechanisms. However, there is still

much to be done to uncover the full suite of DAP^R resistance mechanisms and for complete understanding of daptomycin's mechanism of action.

In addition to antibiotic resistance, *E. faecalis* also possesses mechanisms to resist the action of host-derived CAMPs. It does this primarily by altering cell surface charge to reduce affinity to CAMPs. One way is through the multiple peptide resistance factor (MprF) which aminoacylates negatively-charged PG, usually with positively charged lysine, and in doing so reduces the membrane's electrostatic affinity to CAMPs (Bao et al., 2012; Rashid et al., 2016). MprF activity has been linked with pediocin, HNP-1, nisin, alamethicin and human beta-defensin 3 (hBD-3) resistance (Bao et al., 2012; Kumariya et al., 2015). Its activity is also implicated in reducing focal binding of hBD2 to the septum of *E. faecalis* (Kandaswamy et al., 2013). Another way that surface charge can be altered is by D-alanine modifications of negatively charged lipoteichoic acid (LTA) via DltA which confers resistance in *E. faecalis* to polymyxin B, colistin and nisin by diminishing its negative charge (Fabretti et al., 2006).

Many of these CAMP and daptomycin resistances in *E. faecalis* seem to be influenced and coordinated by LiaFSR signalling and regulation. LiaR of this three-component system has been suggested to be a master regulator of cell envelope stress response to antimicrobials including CAMPs (LL-37, hBD-3, nisin, mersacidin, friulimicin) and daptomycin based on both *in vitro* and *in vivo* studies (Arias et al., 2011; Reyes et al., 2015; Rincon et al., 2019). LiaR is also implicated in the localisation of cardiolipin domains, where domain redistribution has been a suggested strategy in CAMP and daptomycin resistance (Reyes et al., 2015; Tran et al., 2013).

There remain many gaps in our knowledge about DAP^R and CAMP resistance that have yet to be addressed, such as the exact role of membrane lipids and

their regulation, of changes in domain and membrane organisation, as well as the genetic factors that determine resistance acquisition.

1.2.4. Enterococcal lipidome, lipid metabolism and regulation

Since much of the daptomycin and CAMP resistance mechanisms involve alterations in the membrane composition, it is important that we consider the enterococcal lipidome, lipid metabolism, and how its homeostasis is regulated.

Bacterial cell membranes are composed of lipids and proteins, and are particularly abundant in phospholipids of which the three major classes present are phosphatidylglycerol (PG), cardiolipin (CL) and phosphatidylethanolamine (PE) (Foss et al., 2011; López-Lara and Geiger, 2017). However, in Gram-positive bacteria, the main phospholipid classes are PG and CL while PE is generally not present (Epand and Epand, 2009).

In the case of *E. faecalis*, membrane lipids are mainly composed of phospholipid classes PG and CL as well as amino-modified forms of PG such as lysyl-PG (Lys-PG). Other lipid components of the membrane include glycerolipids, tri- and diacylglycerol (TAG, DAG), together with glycosylated glycerolipids such as mono- and diglucosyl-diacylglycerol (MGDAG, DGDAG), glycerophosphoryl-diglucosyl-diacylglycerol (GPDGDAG), and lipoteichoic acid (LTA), which is a polyglycerolphosphate chain linked to a GPDGDAG anchor that can be modified by alanine (Bao et al., 2012; Fabretti et al., 2006; Rashid et al., 2017). The structures of the most abundant lipid species of each of these lipid classes in *E. faecalis* are shown in **Figure 1.3.** These diverse lipid classes arise from integrated biochemical pathways of fatty acid and phospholipid biosynthesis **(Figure 1.4)**. Most of the studies of bacterial lipid biosynthesis have been done in *E. coli*, however, here we will only be discussing lipid classes, metabolism, and regulation relevant to Gram-positive bacteria and *E. faecalis*.

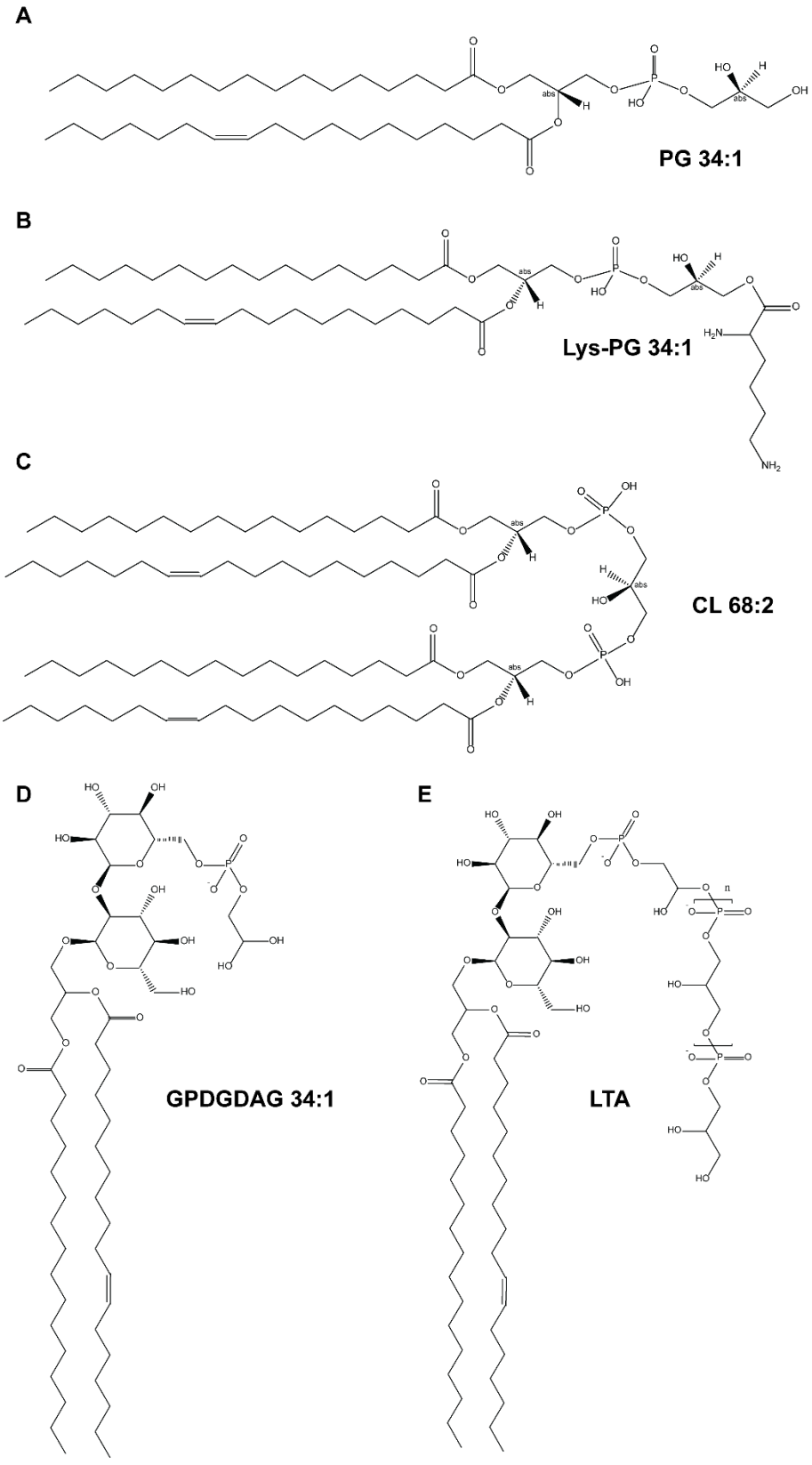

Figure 1.3. Structures of most abundant lipid species in *E. faecalis*. (A) PG 34:1, (B) lysyl-PG 34:1, (C) CL 68:2, (D) GPDGDAG 34:1, and (E) LTA with repeating glycerophosphate units. DGDAG and MGDAG structures are similar to GPDGDAG but without the glycerophosphate group and with 1 less glucosyl group for the latter.

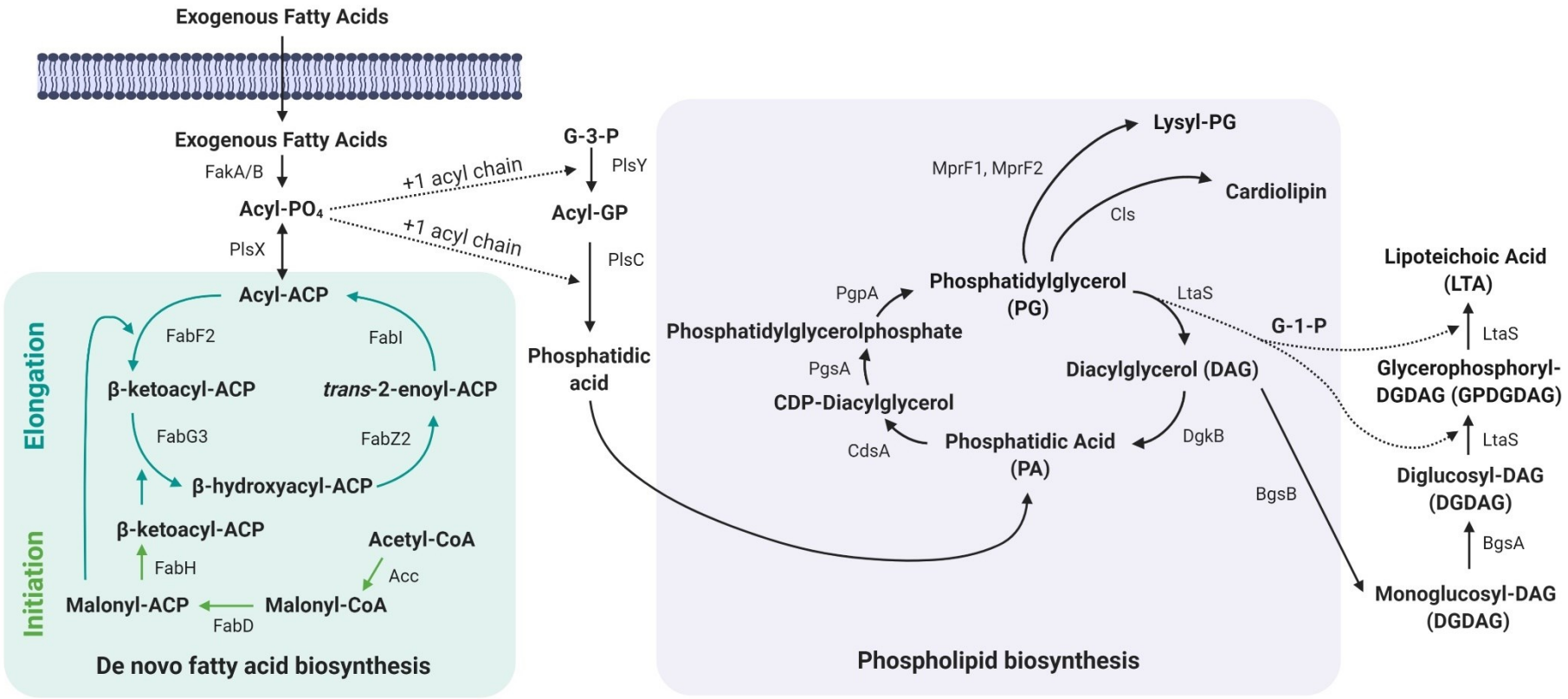

Figure 1.4. Fatty acid and phospholipid metabolism. Integrated biochemical pathway map of de novo fatty acid biosynthesis and exogenous fatty acid incorporation, phospholipid and glucosyl-modified glycerolipid biosynthesis. FabH and FabF2 catalyse the same reactions, but the FabH product determines the fatty acid structure and the product of FabF2 is only used for elongation. Enzymes specific to *E. faecalis* OG1RF are listed in the pathway based off annotation from the Kyoto Encyclopedia of Genes and Genomes (KEGG) database. Created with BioRender.com.

Fatty acid biosynthesis in bacteria is typically carried out by type II fatty acid synthase (FASII) instead of type I fatty acid synthases (FASI) used in mammals (White et al., 2005). Fatty acid biosynthesis first starts with the initiation module where acetyl-coenzyme A (acetyl-CoA) conversion to malonyl-CoA is performed by the multimeric enzyme acetyl-CoA carboxylase (ACC) enzyme encoded by *accABCD* (Cronan and Waldrop, 2002). Malonate group of malonyl-CoA is next transferred to acyl-carrier protein (ACP), by the FabD enzyme encoded by *acpB*, so that it can be recognised by the FASII enzymes (Parsons and Rock, 2013; Zhang and Rock, 2008; Zhu et al., 2019). Malonyl-ACP can either enter the elongation cycle directly to be used as a substrate for extending existing acyl-chains, or it gets condensed by FabH with a short-chain acyl-CoA to create β-ketoacyl-ACP which gets fed into the elongation cycle ultimately resulting in a new fatty acid molecule (Parsons and Rock, 2013).

The elongation cycle consists of 4 enzymes, FabG3, FabZ2, FabI and FabF2, that receive and elongate the product of FabH by 2 carbons for each cycle, which continues until a long-chain ACP of the desired length is achieved (**Figure 1.4**). In the elongation cycle, FabF2 and FabH catalyse the same reaction to yield β-ketoacyl-ACP. The difference here is that the condensation product from FabH determines the structure of fatty acids and its fate lies in forming the final fatty acid molecule, while the FabF2 product is solely used as an intermediary step in elongating existing acyl chains that are already in the elongation cycle (Parsons and Rock, 2013). In the first cycle, β-ketoacyl-ACP (product of FabH) enters the elongation cycle and gets reduced to form β-hydroxyacyl-ACP by FabG3, and dehydrated to *trans*-2-enoyl-ACP by FabZ2, followed by reduction by FabI to acyl-ACP. Acyl-ACP can be further lengthened by undergoing condensation with malonyl-ACP by FabF2 to give a β-ketoacyl-ACP with two additional carbons that initiates the cycle once more (Parsons and Rock, 2013).

In the biosynthesis of unsaturated fatty acids, there are two well described mechanisms by which the introduction of the double bond occurs. In the first mechanism commonly used by *E. coli*, the bifunctional FabA enzyme – which also converts β-hydroxyacyl-ACP to *trans*-2-enoyl-ACP – isomerises *trans*-2-decenoyl-ACP to *cis*-3-decenoyl-ACP creating a branchpoint in fatty acid biosynthesis where unsaturated fatty acid synthesis is initiated (Heath and Rock, 1996). In another mechanism commonly used by *S. pneumoniae*, a specialised enzyme, FabM catalyses the conversion of β-hydroxyacyl-ACP to trans-2-enoyl-ACP instead (Marrakchi et al., 2002). In the case of *E. faecalis*, the former occurs through a FabA homolog, FabN (Lu et al., 2005). *E. faecalis* also possesses the ability to generate *trans*-unsaturated fatty acids through the isomerisation of *cis*-unsaturated fatty acids, though the enzyme involved is currently unknown (Kondakova et al., 2019).

In Gram positive bacteria, long chain acyl-ACP of sufficient length is then converted to acyl-PO_4 by PlsX, which is then used by PlsY, a glycerol-phosphate acyltransferase that adds the acyl chain from acyl-PO_4 to *sn*-1 position on glycerol-3-phosphate (G-3-P) (Lu et al., 2006). PlsC, then transfers another acyl chain from acyl-PO_4 to the *sn*-2 position of the newly formed 1-acyl-glycerol-3-phosphate to create phosphatidic acid (López-Lara and Soto, 2019; Parsons and Rock, 2013). Exogenous fatty acids can also be incorporated, by spontaneously crossing the membrane bilayer and getting phosphorylated by fatty acid kinases FakA/B to acyl-PO_4 (López-Lara and Soto, 2019).

Phosphatidic acid acts as the precursor to phospholipid biosynthesis (Parsons and Rock, 2013) (**Figure 1.4**). It is first converted to cytidine diphosphate-diacylglycerol (CDP-diacylglcyerol) by CdsA, then to phosphatidyl-glycerolphosphate (PGP) by PgsA through the loss of cytidine monophosphate (CMP) and addition of glycerophosphate. PGP is then converted to

phosphatidylglycerol (PG) by PgpA. Cardiolipin can be synthesized from 2 PG molecules via Cls1 and/or Cls2 in *E. faecalis* or aminoacylated with lysine from lysyl-tRNA to form Lys-PG via *mprF1* and/or *mprF2* (Bao et al., 2012; Parsons and Rock, 2013). In Gram-positive bacteria, PG can get converted into DAG, when its glycerol-1-phosphate (G-1-P) group gets transferred onto the GPDGDAG membrane anchor by LtaS, yielding DAG as its by-product (Gründling and Schneewind, 2007). DAG can get glycosylated by UDP-glucose into monoglucosyl-diacylglycerol (MGDAG) by BgsB, and further glycosylated into diglucosyl-diacylglycerol (DGDAG) by BgsA (Theilacker et al., 2011). DGDAG can be converted to glycerophosphoryl-diglucosyl-diacylglycerol (GPDGDAG) by addition of G-1-P from PG by LtaS, and continual addition of G-1-P by LtaS extends the glycerophosphate chain to form mature LTA (Parsons and Rock, 2013). DAG may also be recycled back into phosphatidic acid by addition of phosphate from adenosine triphosphate (ATP) by DAG kinase, DgkB.

Given the importance of lipids in forming the cell membrane and how energetically expensive it is for biosynthesis, it is important that lipid homeostasis is maintained, and that the membrane can be altered in response to the ever-changing external environment and nutrient availability. One of the main points of regulatory control is in FASII and its reactions. *E. faecalis* does this through the global transcriptional repressor FabT which senses long-chain acyl-ACPs and enhances binding to its operator sequences located within the promoter regions of the *fabT-fabH-acpA* and *fabK-fabD-fabG-fabF-accB-fabZ-accC-accD-accA* operons (López-Lara and Soto, 2019; Schujman and de Mendoza, 2008; Zhu et al., 2019). In doing so, FabT provides feedback inhibition on fatty acid biosynthesis through the long chain acyl-ACP end products of the pathway. Additionally, the FabT repressor also allows sensing of exogenous fatty acid as well. This is done through an atypical ACP encoded in *E. faecalis*, *acpB* which

is expressed in a separate operon with *plsX* (Zhu et al., 2019). AcpB preferably accepts acyl-chains from acyl-phosphates derived from exogenous fatty acids and its acyl-AcpB form can bind to FabT (Zhu et al., 2019). This allows for sensing of exogenous fatty acids and regulation of *de novo* fatty acid biosynthesis, preventing redundant biosynthesis in the event of an excess exogenous source.

1.2.5. Membrane organisation

Unlike what was initially described of the cell membrane structure, it is not uniform as previously thought, but instead is laterally segregated in domains. One of the first models of the cell membrane structure, is the fluid mosaic model proposed by Singer and Nicolson in 1972 that describes the membrane as a homogenous mosaic of membrane lipids, proteins and other constituents that are able to diffuse freely within the membrane (Singer and Nicolson, 1972). However, advances in the field over the decades revealed that this is not the case and that certain membrane proteins and lipids segregate and organise into specific domains, termed as lipid rafts (Lingwood and Simons, 2010). These lipid rafts in eukaryotes tend to be less fluid than the rest of the membrane consisting of higher levels of certain lipids such as sterols and sphingolipids, and are responsible for organising proteins important for raft specific functions through the scaffolding activity of flotillins (Banning et al., 2011; Lajoie and Nabi, 2010; Lingwood and Simons, 2010; Zhao et al., 2011).

More recently, it has been described that lipid raft-like membrane organisation is not just restricted to eukaryotic cells but is present in bacteria as well where they are known as functional membrane microdomains (FMMs). FMMs were first described in *Bacillus subtilis* where flotillin homologs FloA and FloT are colocalised together with sensor kinase KinC in membrane microdomains enriched in polyisoprenoids (López and Kolter, 2010). *B. subtilis* flotillins are also

required for spatial organisation of FMMs, loss of which leads to functional consequences such as impaired Sec-mediated secretion, reduced FtsH activity, reduced biofilm formation due to disrupted KinC signalling, and altered membrane fluidity, suggesting that flotillins are essential in mediating microdomain formation and its associated functions (Bach and Bramkamp, 2013; Donovan and Bramkamp, 2009; Schneider et al., 2015; Yepes et al., 2012). FMMs and flotillin-homologs also exist within many other bacteria such as *S. aureus*, *Mycobacterium tuberculosis*, *Campylobacter jejuni* and *Borrelia burgdorferi* and even in archaea such as *Pyrococcus horikoshii* (Lopez and Koch, 2017). These findings highlight the ubiquity of FMMs and lipid rafts in all domains of life and their biological importance in compartmentalising cellular functions laterally within the cell membrane. Furthermore, the evidence of FMMs and lipid rafts discredits the fluid mosaic paradigm in favour of a membrane organisation that is laterally partitioned and heterogenous, and that exists in a highly coordinated fashion.

1.3. Thesis Outline

As discussed in the earlier sections, cationic antimicrobials such as CAMPs and daptomycin focally bind and target the septum of *E. faecalis*, and the septum likely consists of a distinct membrane microdomain given the localisation of sites of virulence factor assembly, secretion machinery and the enrichment of anionic lipids. However, at present there is limited information about the interplay of antimicrobials with the membrane of *E. faecalis* in terms of microdomain assembly and limited information on membrane and genetic factors involved in cationic antimicrobial resistance. This thesis aims to address this knowledge gap by (1) investigating the role of two paralogs of the multiple peptide resistance factor (*mprF*) involved in CAMP resistance and their extended functional roles in membrane homeostasis, (2) elucidating genetic factors in daptomycin resistance acquisition that might be otherwise masked by *mprF* and (3) characterising the septal and flotillin microdomains of *E. faecalis*. Chapters in this thesis are organised accordingly to address these aims:

Chapter 2: The aim of this chapter is to investigate the role of a CAMP resistance associated enzyme, *mprF* and its two paralogs (*mprF1*, *mprF2*), and how they are involved in CAMP resistance and membrane lipid homeostasis. From preliminary findings, it was observed that despite possessing similar enhancement in septal binding of CAMPs, Δ*mprF2* displayed greater CAMP-mediated killing than Δ*mprF1.* We hypothesize that the two paralogs of *mprF* (*mprF1*, *mprF2*) are involved in CAMP resistance to varying degrees based on their differential influence on the membrane lipidome. This hypothesis is addressed using mass spectrometry and thin layer chromatography-based analyses of the lipidome as well as phenotypic assays investigating membrane fluidity, CAMP killing, growth, secretion, and fatty acid uptake to give mechanistic insight into how lipid homeostasis is affected.

Chapter 3: This chapter aims to elucidate previously unknown genetic factors that might be masked by MprF activity that are involved in daptomycin resistance acquisition. We hypothesize that in vitro evolution to DAP^R in mutant backgrounds of *mprF* will uncover novel mutations that would otherwise be masked by its activity and associated contribution to cationic antimicrobial resistance, and this information will serve to further inform on the mechanism of action of daptomycin and the physiology of Δ*mprF* mutants. This is addressed through *in vitro* evolution of different *mprF* mutant backgrounds to DAP^R coupled with whole genome sequencing. A more detailed investigation on a selected hit, *ftsH*, in terms of genetic reconstitution, proteomic and transcriptomic based analyses and changes in mutation rates is also described here.

Chapter 4: Given that membrane microdomains likely exist in the septum and the septum is targeted by CAMPs, and that microdomains are typically organised by flotillins, we hypothesize that septal microdomains possess unique characteristics that guide CAMP targeting and that they are likely organised by flotillins. This chapter aims to address this by isolating and characterising septal and flotillin microdomains using detergent-resistant membrane (DRM) isolation and sampling the local environment using styrene-maleic acid (SMA) derived membrane nanodiscs. Characterisation of flotillin in terms of their localisation as well as assaying their reported mutant phenotypes in other organisms are also described here.

1.4. References

Arias, C.A., Murray, B.E., 2012. The rise of the Enterococcus: beyond vancomycin resistance. Nature reviews. Microbiology 10, 266-278.

Arias, C.A., Panesso, D., McGrath, D.M., Qin, X., Mojica, M.F., Miller, C., Diaz, L., Tran, T.T., Rincon, S., Barbu, E.M., Reyes, J., Roh, J.H., Lobos, E., Sodergren, E., Pasqualini, R., Arap, W., Quinn, J.P., Shamoo, Y., Murray, B.E., Weinstock, G.M., 2011. Genetic basis for in vivo daptomycin resistance in enterococci. The New England journal of medicine 365, 892-900.

Ator, L.L., Starzyk, M.J., 1976. Distribution of group D streptococci in rivers and streams. Microbios 16, 91-104.

Bach, J.N., Bramkamp, M., 2013. Flotillins functionally organize the bacterial membrane. Molecular microbiology 88, 1205-1217.

Banning, A., Tomasovic, A., Tikkanen, R., 2011. Functional aspects of membrane association of reggie/flotillin proteins. Current protein & peptide science 12, 725-735.

Bao, Y., Sakinc, T., Laverde, D., Wobser, D., Benachour, A., Theilacker, C., Hartke, A., Huebner, J., 2012. Role of mprF1 and mprF2 in the pathogenicity of Enterococcus faecalis. PloS one 7, e38458.

Baumann, G., Mueller, P., 1974. A molecular model of membrane excitability. Journal of supramolecular structure 2, 538-557.

Bi, R., Qin, T., Fan, W., Ma, P., Gu, B., 2018. The emerging problem of linezolid-resistant enterococci. Journal of Global Antimicrobial Resistance 13, 11-19.

Carmeli, Y., Eliopoulos, G., Mozaffari, E., Samore, M., 2002. Health and economic outcomes of vancomycin-resistant enterococci. Archives of internal medicine 162, 2223-2228.

CDC, Centers for Disease Control and Prevention, 2013. Antibiotic Resistance Threats in the United States, 2013. U.S. Department of Health and Human Services, CDC, Atlanta, GA.

CDC, Centers for Disease Control and Prevention, 2019. Antibiotic Resistance Threats in the United States, 2019. U.S. Department of Health and Human Services, CDC, Atlanta, GA.

Chen, M., Pan, H., Lou, Y., Wu, Z., Zhang, J., Huang, Y., Yu, W., Qiu, Y., 2018. Epidemiological characteristics and genetic structure of linezolid-resistant Enterococcus faecalis. Infect Drug Resist 11, 2397-2409.

Christensen, B., Fink, J., Merrifield, R.B., Mauzerall, D., 1988. Channel-forming properties of cecropins and related model compounds incorporated into planar lipid membranes. Proceedings of the National Academy of Sciences of the United States of America 85, 5072-5076.

Courvalin, P., 2006. Vancomycin Resistance in Gram-Positive Cocci. Clinical Infectious Diseases 42, S25-S34.

Cronan, J.E., Jr., Waldrop, G.L., 2002. Multi-subunit acetyl-CoA carboxylases. Progress in lipid research 41, 407-435.

Donovan, C., Bramkamp, M., 2009. Characterization and subcellular localization of a bacterial flotillin homologue. Microbiology 155, 1786-1799.

Dubin, K., Pamer, E.G., 2014. Enterococci and Their Interactions with the Intestinal Microbiome. Microbiol Spectr 5, 10.1128/microbiolspec.BAD-0014-2016.

Durr, U.H., Sudheendra, U.S., Ramamoorthy, A., 2006. LL-37, the only human member of the cathelicidin family of antimicrobial peptides. Biochimica et biophysica acta 1758, 1408-1425.

Edmond, M.B., Wallace, S.E., McClish, D.K., Pfaller, M.A., Jones, R.N., Wenzel, R.P., 1999. Nosocomial Bloodstream Infections in United States Hospitals: A Three-Year Analysis. Clinical Infectious Diseases 29, 239-244.

Ehrenstein, G., Lecar, H., 1977. Electrically gated ionic channels in lipid bilayers. Quarterly reviews of biophysics 10, 1-34.

Epand, R.M., Epand, R.F., 2009. Domains in bacterial membranes and the action of antimicrobial agents. Molecular bioSystems 5, 580-587.

Fabretti, F., Theilacker, C., Baldassarri, L., Kaczynski, Z., Kropec, A., Holst, O., Huebner, J., 2006. Alanine esters of enterococcal lipoteichoic acid play a role in biofilm formation and resistance to antimicrobial peptides. Infect Immun 74, 4164-4171.

Fisher, K., Phillips, C., 2009. The ecology, epidemiology and virulence of Enterococcus. Microbiology 155, 1749-1757.

Foss, M.H., Eun, Y.J., Weibel, D.B., 2011. Chemical-biological studies of subcellular organization in bacteria. Biochemistry 50, 7719-7734.

Fox, J.L., 2013. Antimicrobial peptides stage a comeback. Nature Biotechnology 31, 379-382.

Franz, C.M., Holzapfel, W.H., Stiles, M.E., 1999. Enterococci at the crossroads of food safety? Int J Food Microbiol 47, 1-24.

Gandra, S., Barter, D.M., Laxminarayan, R., 2014. Economic burden of antibiotic resistance: how much do we really know? Clinical Microbiology and Infection 20, 973-979.

Gründling, A., Schneewind, O., 2007. Synthesis of glycerol phosphate lipoteichoic acid in Staphylococcus aureus. Proceedings of the National Academy of Sciences of the United States of America 104, 8478-8483.

Hachmann, A.-B., Angert, E.R., Helmann, J.D., 2009. Genetic analysis of factors affecting susceptibility of Bacillus subtilis to daptomycin. Antimicrobial agents and chemotherapy 53, 1598-1609.

Hancock, R.E.W., Rozek, A., 2002. Role of membranes in the activities of antimicrobial cationic peptides. FEMS Microbiology Letters 206, 143-149.

Hayashi, H., Takahashi, R., Nishi, T., Sakamoto, M., Benno, Y., 2005. Molecular analysis of jejunal, ileal, caecal and recto-sigmoidal human colonic microbiota using 16S rRNA gene libraries and terminal restriction fragment length polymorphism. Journal of medical microbiology 54, 1093-1101.

He, K., Ludtke, S.J., Worcester, D.L., Huang, H.W., 1996. Neutron scattering in the plane of membranes: structure of alamethicin pores. Biophysical journal 70, 2659-2666.

Heath, R.J., Rock, C.O., 1996. Roles of the FabA and FabZ beta-hydroxyacyl-acyl carrier protein dehydratases in Escherichia coli fatty acid biosynthesis. The Journal of biological chemistry 271, 27795-27801.

Hidron, A.I., Edwards, J.R., Patel, J., Horan, T.C., Sievert, D.M., Pollock, D.A., Fridkin, S.K., 2008. NHSN annual update: antimicrobial-resistant pathogens associated with healthcare-associated infections: annual summary of data reported to the National Healthcare Safety Network at the Centers for Disease Control and Prevention, 2006-2007. Infection control and hospital epidemiology 29, 996-1011.

Hollenbeck, B.L., Rice, L.B., 2012. Intrinsic and acquired resistance mechanisms in enterococcus. Virulence 3, 421-569.

Jenssen, H., Hamill, P., Hancock, R.E.W., 2006. Peptide Antimicrobial Agents. Clinical microbiology reviews 19, 491-511.

Jordan, S., Junker, A., Helmann, J.D., Mascher, T., 2006. Regulation of LiaRS-dependent gene expression in bacillus subtilis: identification of inhibitor proteins, regulator binding sites, and target genes of a conserved cell envelope stress-sensing two-component system. J Bacteriol 188, 5153-5166.

Kandaswamy, K., Liew, T.H., Wang, C.Y., Huston-Warren, E., Meyer-Hoffert, U., Hultenby, K., Schröder, J.M., Caparon, M.G., Normark, S., Henriques-Normark, B., Hultgren, S.J., Kline, K.A., 2013. Focal targeting by human β-defensin 2 disrupts localized virulence factor assembly sites in Enterococcus faecalis. Proceedings of the National Academy of Sciences 110, 20230-20235.

Kelesidis, T., Humphries, R., Uslan, D.Z., Pegues, D.A., 2011. Daptomycin nonsusceptible enterococci: an emerging challenge for clinicians. Clinical infectious diseases : an official publication of the Infectious Diseases Society of America 52, 228-234.

Khan, A., Davlieva, M., Panesso, D., Rincon, S., Miller, W.R., Diaz, L., Reyes, J., Cruz, M.R., Pemberton, O., Nguyen, A.H., Siegel, S.D., Planet, P.J., Narechania, A., Latorre, M., Rios, R., Singh, K.V., Ton-That, H., Garsin, D.A., Tran, T.T., Shamoo, Y., Arias, C.A., 2019. Antimicrobial sensing coupled with cell membrane remodeling mediates antibiotic resistance and virulence in

Enterococcus faecalis. Proceedings of the National Academy of Sciences 116, 26925.

Klein, G., 2003. Taxonomy, ecology and antibiotic resistance of enterococci from food and the gastro-intestinal tract. International Journal of Food Microbiology 88, 123-131.

Kline, K.A., Kau, A.L., Chen, S.L., Lim, A., Pinkner, J.S., Rosch, J., Nallapareddy, S.R., Murray, B.E., Henriques-Normark, B., Beatty, W., Caparon, M.G., Hultgren, S.J., 2009. Mechanism for Sortase Localization and the Role of Sortase Localization in Efficient Pilus Assembly in Enterococcus faecalis. Journal of Bacteriology 191, 3237-3247.

Kondakova, T., Kumar, S., Cronan, J.E., 2019. A novel synthesis of trans-unsaturated fatty acids by the Gram-positive commensal bacterium Enterococcus faecalis FA2-2. Chemistry and Physics of Lipids 222, 23-35.

Kreutzberger, M.A., Pokorny, A., Almeida, P.F., 2017. Daptomycin-Phosphatidylglycerol Domains in Lipid Membranes. Langmuir 33, 13669-13679.

Kumariya, R., Sood, S.K., Rajput, Y.S., Saini, N., Garsa, A.K., 2015. Increased membrane surface positive charge and altered membrane fluidity leads to cationic antimicrobial peptide resistance in Enterococcus faecalis. Biochimica et biophysica acta 1848, 1367-1375.

Lajoie, P., Nabi, I.R., 2010. Lipid rafts, caveolae, and their endocytosis. International review of cell and molecular biology 282, 135-163.

Langham, A.A., Ahmad, A.S., Kaznessis, Y.N., 2008. On the nature of antimicrobial activity: a model for protegrin-1 pores. Journal of the American Chemical Society 130, 4338-4346.

Lebreton, F., Willems, R.J.L., Gilmore, M.S., 2014. Enterococcus Diversity, Origins in Nature, and Gut Colonization. In: Gilmore, M.S., Clewell, D.B., Ike, Y., Shankar, N. (Eds.), Enterococci: From Commensals to Leading Causes of Drug Resistant Infection. Massachusetts Eye and Ear Infirmary, Boston.

Leontiadou, H., Mark, A.E., Marrink, S.J., 2006. Antimicrobial peptides in action. Journal of the American Chemical Society 128, 12156-12161.

Lewis, C.M., Zervos, M.J., 1990. Clinical manifestations of enterococcal infection. European Journal of Clinical Microbiology and Infectious Diseases 9, 111-117.

Lingwood, D., Simons, K., 2010. Lipid rafts as a membrane-organizing principle. Science (New York, N.Y.) 327, 46-50.

López-Lara, I.M., Geiger, O., 2017. Bacterial lipid diversity. Biochimica et Biophysica Acta (BBA) - Molecular and Cell Biology of Lipids 1862, 1287-1299.

López-Lara, I.M., Soto, M.J., 2019. Fatty Acid Synthesis and Regulation. In: Geiger, O. (Ed.), Biogenesis of Fatty Acids, Lipids and Membranes. Springer International Publishing, Cham, pp. 391-407.

Lopez, D., Koch, G., 2017. Exploring functional membrane microdomains in bacteria: an overview. Curr Opin Microbiol 36, 76-84.

López, D., Kolter, R., 2010. Functional microdomains in bacterial membranes. Genes Dev 24, 1893-1902.

Lu, Y.J., White, S.W., Rock, C.O., 2005. Domain swapping between Enterococcus faecalis FabN and FabZ proteins localizes the structural determinants for isomerase activity. The Journal of biological chemistry 280, 30342-30348.

Lu, Y.J., Zhang, Y.M., Grimes, K.D., Qi, J., Lee, R.E., Rock, C.O., 2006. Acyl-phosphates initiate membrane phospholipid synthesis in Gram-positive pathogens. Molecular cell 23, 765-772.

Maccallum, W.G., Hastings, T.W., 1899. A case of acute endocarditis caused by *Micrococcus zymogenes*. J Exp Med 4, 521-534.

Marrakchi, H., Choi, K.H., Rock, C.O., 2002. A new mechanism for anaerobic unsaturated fatty acid formation in Streptococcus pneumoniae. The Journal of biological chemistry 277, 44809-44816.

Martin, J.D., Mundt, J.O., 1972. Enterococci in insects. Applied microbiology 24, 575-580.

Mascini, E.M., Bonten, M.J.M., 2005. Vancomycin-resistant enterococci: consequences for therapy and infection control. Clinical Microbiology and Infection 11, 43-56.

Matsuzaki, K., Murase, O., Fujii, N., Miyajima, K., 1996. An antimicrobial peptide, magainin 2, induced rapid flip-flop of phospholipids coupled with pore formation and peptide translocation. Biochemistry 35, 11361-11368.

Miao, V., Coëffet-LeGal, M.-F., Brian, P., Brost, R., Penn, J., Whiting, A., Martin, S., Ford, R., Parr, I., Bouchard, M., Silva, C.J., Wrigley, S.K., Baltz, R.H., 2005. Daptomycin biosynthesis in Streptomyces roseosporus: cloning and analysis of the gene cluster and revision of peptide stereochemistry. Microbiology (Reading, England) 151, 1507-1523.

Mileykovskaya, E., Dowhan, W., 2009. Cardiolipin membrane domains in prokaryotes and eukaryotes. Biochimica et biophysica acta 1788, 2084-2091.

Miller, C., Kong, J., Tran, T.T., Arias, C.A., Saxer, G., Shamoo, Y., 2013. Adaptation of Enterococcus faecalis to daptomycin reveals an ordered progression to resistance. Antimicrobial agents and chemotherapy 57, 5373-5383.

Miller, W.R., Munita, J.M., Arias, C.A., 2014. Mechanisms of antibiotic resistance in enterococci. Expert Review of Anti-infective Therapy 12, 1221-1236.

Mishra, N.N., Bayer, A.S., Tran, T.T., Shamoo, Y., Mileykovskaya, E., Dowhan, W., Guan, Z., Arias, C.A., 2012. Daptomycin Resistance in Enterococci Is Associated with Distinct Alterations of Cell Membrane Phospholipid Content. PloS one 7, e43958.

Mundt, J.O., 1961. Occurrence of Enterococci: Bud, Blossom, and Soil Studies. Applied microbiology 9, 541-544.

Mundt, J.O., 1963a. Occurrence of enterococci in animals in a wild environment. Applied microbiology 11, 136-140.

Mundt, J.O., 1963b. Occurrence of Enterococci on Plants in a Wild Environment. Applied microbiology 11, 141-144.

Munoz-Price, L.S., Lolans, K., Quinn, J.P., 2005. Emergence of Resistance to Daptomycin during Treatment of Vancomycin-Resistant Enterococcus faecalis Infection. Clinical Infectious Diseases 41, 565-566.

Muraih, J.K., Pearson, A., Silverman, J., Palmer, M., 2011. Oligomerization of daptomycin on membranes. Biochimica et Biophysica Acta (BBA) - Biomembranes 1808, 1154-1160.

Muraih, J.K., Harris, J., Taylor, S.D., Palmer, M., 2012. Characterization of daptomycin oligomerization with perylene excimer fluorescence: stoichiometric binding of phosphatidylglycerol triggers oligomer formation. Biochimica et biophysica acta 1818, 673-678.

Murdoch, D.R., Corey, G.R., Hoen, B., Miro, J.M., Fowler, V.G., Jr., Bayer, A.S., Karchmer, A.W., Olaison, L., Pappas, P.A., Moreillon, P., Chambers, S.T., Chu, V.H., Falco, V., Holland, D.J., Jones, P., Klein, J.L., Raymond, N.J., Read, K.M., Tripodi, M.F., Utili, R., Wang, A., Woods, C.W., Cabell, C.H., 2009. Clinical presentation, etiology, and outcome of infective endocarditis in the 21st century: the International Collaboration on Endocarditis-Prospective Cohort Study. Archives of internal medicine 169, 463-473.

O'Driscoll, T., Crank, C.W., 2015. Vancomycin-resistant enterococcal infections: epidemiology, clinical manifestations, and optimal management. Infect Drug Resist 8, 217-230.

Parsons, J.B., Rock, C.O., 2013. Bacterial lipids: metabolism and membrane homeostasis. Progress in lipid research 52, 249-276.

Pasupuleti, M., Schmidtchen, A., Malmsten, M., 2012. Antimicrobial peptides: key components of the innate immune system. Critical reviews in biotechnology 32, 143-171.

Patel, R., Gallagher, J.C., 2015. Vancomycin-resistant enterococcal bacteremia pharmacotherapy. Ann Pharmacother 49, 69-85.

Patterson, J.E., Sweeney, A.H., Simms, M., Carley, N., Mangi, R., Sabetta, J., Lyons, R.W., 1995. An analysis of 110 serious enterococcal infections. Epidemiology, antibiotic susceptibility, and outcome. Medicine 74, 191-200.

Paulsen, I.T., Banerjei, L., Myers, G.S., Nelson, K.E., Seshadri, R., Read, T.D., Fouts, D.E., Eisen, J.A., Gill, S.R., Heidelberg, J.F., Tettelin, H., Dodson, R.J., Umayam, L., Brinkac, L., Beanan, M., Daugherty, S., DeBoy, R.T., Durkin, S., Kolonay, J., Madupu, R., Nelson, W., Vamathevan, J., Tran, B., Upton, J., Hansen, T., Shetty, J., Khouri, H., Utterback, T., Radune, D., Ketchum, K.A., Dougherty, B.A., Fraser, C.M., 2003. Role of mobile DNA in the evolution of vancomycin-resistant Enterococcus faecalis. Science (New York, N.Y.) 299, 2071-2074.

Pfaller, M.A., Cormican, M., Flamm, R.K., Mendes, R.E., Jones, R.N., 2019. Temporal and Geographic Variation in Antimicrobial Susceptibility and Resistance Patterns of Enterococci: Results From the SENTRY Antimicrobial Surveillance Program, 1997-2016. Open Forum Infect Dis 6, S54-S62.

Pogliano, J., Pogliano, N., Silverman, J.A., 2012. Daptomycin-mediated reorganization of membrane architecture causes mislocalization of essential cell division proteins. Journal of bacteriology 194, 4494-4504.

Porcelli, F., Buck, B., Lee, D.K., Hallock, K.J., Ramamoorthy, A., Veglia, G., 2004. Structure and orientation of pardaxin determined by NMR experiments in model membranes. The Journal of biological chemistry 279, 45815-45823.

Porcelli, F., Verardi, R., Shi, L., Henzler-Wildman, K.A., Ramamoorthy, A., Veglia, G., 2008. NMR structure of the cathelicidin-derived human antimicrobial peptide LL-37 in dodecylphosphocholine micelles. Biochemistry 47, 5565-5572.

Pouny, Y., Rapaport, D., Mor, A., Nicolas, P., Shai, Y., 1992. Interaction of antimicrobial dermaseptin and its fluorescently labeled analogues with phospholipid membranes. Biochemistry 31, 12416-12423.

Puchter, L., Chaberny, I.F., Schwab, F., Vonberg, R.-P., Bange, F.-C., Ebadi, E., 2018. Economic burden of nosocomial infections caused by vancomycin-resistant enterococci. Antimicrobial Resistance and Infection Control 7, 1.

Rangarajan, N., Bakshi, S., Weisshaar, J.C., 2013. Localized permeabilization of E. coli membranes by the antimicrobial peptide Cecropin A. Biochemistry 52, 6584-6594.

Rashid, R., Veleba, M., Kline, K.A., 2016. Focal Targeting of the Bacterial Envelope by Antimicrobial Peptides. Frontiers in Cell and Developmental Biology 4.

Rashid, R., Cazenave-Gassiot, A., Gao, I.H., Nair, Z.J., Kumar, J.K., Gao, L., Kline, K.A., Wenk, M.R., 2017. Comprehensive analysis of phospholipids and glycolipids in the opportunistic pathogen Enterococcus faecalis. PloS one 12, e0175886.

Reddy, K.V., Yedery, R.D., Aranha, C., 2004. Antimicrobial peptides: premises and promises. International journal of antimicrobial agents 24, 536-547.

Reyes, J., Panesso, D., Tran, T.T., Mishra, N.N., Cruz, M.R., Munita, J.M., Singh, K.V., Yeaman, M.R., Murray, B.E., Shamoo, Y., Garsin, D., Bayer, A.S., Arias, C.A., 2015. A liaR deletion restores susceptibility to daptomycin and antimicrobial peptides in multidrug-resistant Enterococcus faecalis. The Journal of infectious diseases 211, 1317-1325.

Rincon, S., Panesso, D., Miller, W.R., Singh, K.V., Cruz, M.R., Khan, A., Dinh, A.Q., Diaz, L., Rios, R., Shamoo, Y., Reyes, J., Tran, T.T., Garsin, D.A., Arias, C.A., 2019. Disrupting Membrane Adaptation Restores In Vivo Efficacy of Antibiotics Against Multidrug-Resistant Enterococci and Potentiates Killing by Human Neutrophils. The Journal of infectious diseases 220, 494-504.

Robert C. Moellering, Jr., 1992. Emergence of Enterococcus as a Significant Pathogen. Clinical Infectious Diseases 14, 1173-1176.

Schleifer, K.H., Kilpper-Bälz, R., 1984. Transfer of Streptococcus faecalis and Streptococcus faecium to the Genus Enterococcus nom. rev. as Enterococcus faecalis comb. nov. and Enterococcus faecium comb. nov. International Journal of Systematic and Evolutionary Microbiology 34, 31-34.

Schneider, J., Mielich-Süss, B., Böhme, R., Lopez, D., 2015. In vivo characterization of the scaffold activity of flotillin on the membrane kinase KinC of Bacillus subtilis. Microbiology (Reading, England) 161, 1871-1887.

Schujman, G.E., de Mendoza, D., 2008. Regulation of type II fatty acid synthase in Gram-positive bacteria. Current Opinion in Microbiology 11, 148-152.

Shai, Y., 2002. Mode of action of membrane active antimicrobial peptides. Biopolymers 66, 236-248.

Shoemaker, D.M., Simou, J., Roland, W.E., 2006. A review of daptomycin for injection (Cubicin) in the treatment of complicated skin and skin structure infections. Ther Clin Risk Manag 2, 169-174.

Singer, S.J., Nicolson, G.L., 1972. The fluid mosaic model of the structure of cell membranes. Science (New York, N.Y.) 175, 720-731.

Song, X., Srinivasan, A., Plaut, D., Perl, T.M., 2003. Effect of nosocomial vancomycin-resistant enterococcal bacteremia on mortality, length of stay, and costs. Infection control and hospital epidemiology 24, 251-256.

Steenbergen, J.N., Alder, J., Thorne, G.M., Tally, F.P., 2005. Daptomycin: a lipopeptide antibiotic for the treatment of serious Gram-positive infections. The Journal of antimicrobial chemotherapy 55, 283-288.

Suntharalingam, P., Senadheera, M.D., Mair, R.W., Lévesque, C.M., Cvitkovitch, D.G., 2009. The LiaFSR System Regulates the Cell Envelope Stress Response in *Streptococcus mutans*. Journal of Bacteriology 191, 2973-2984.

Tally, F.P., DeBruin, M.F., 2000. Development of daptomycin for gram-positive infections. The Journal of antimicrobial chemotherapy 46, 523-526.

Taylor, S.D., Palmer, M., 2016. The action mechanism of daptomycin. Bioorganic & Medicinal Chemistry 24, 6253-6268.

Theilacker, C., Sava, I., Sanchez-Carballo, P., Bao, Y., Kropec, A., Grohmann, E., Holst, O., Huebner, J., 2011. Deletion of the glycosyltransferase bgsB of Enterococcus faecalis leads to a complete loss of glycolipids from the cell membrane and to impaired biofilm formation. BMC Microbiol 11, 67-67.

Tran, T.T., Panesso, D., Mishra, N.N., Mileykovskaya, E., Guan, Z., Munita, J.M., Reyes, J., Diaz, L., Weinstock, G.M., Murray, B.E., Shamoo, Y., Dowhan, W., Bayer, A.S., Arias, C.A., 2013. Daptomycin-resistant Enterococcus faecalis diverts the antibiotic molecule from the division septum and remodels cell membrane phospholipids. mBio 4.

Vega, L.A., Caparon, M.G., 2012. Cationic antimicrobial peptides disrupt the Streptococcus pyogenes ExPortal. Molecular microbiology 85, 1119-1132.

Weiner, L.M., Webb, A.K., Limbago, B., Dudeck, M.A., Patel, J., Kallen, A.J., Edwards, J.R., Sievert, D.M., 2016. Antimicrobial-Resistant Pathogens Associated With Healthcare-Associated Infections: Summary of Data Reported to the National Healthcare Safety Network at the Centers for Disease Control and Prevention, 2011-2014. Infection control and hospital epidemiology 37, 1288-1301.

Wenzel, M., Chiriac, A.I., Otto, A., Zweytick, D., May, C., Schumacher, C., Gust, R., Albada, H.B., Penkova, M., Kramer, U., Erdmann, R., Metzler-Nolte, N., Straus, S.K., Bremer, E., Becher, D., Brotz-Oesterhelt, H., Sahl, H.G., Bandow, J.E., 2014. Small cationic antimicrobial peptides delocalize peripheral membrane proteins. Proceedings of the National Academy of Sciences of the United States of America 111, E1409-1418.

Werner, G., Coque, T.M., Hammerum, A.M., Hope, R., Hryniewicz, W., Johnson, A., Klare, I., Kristinsson, K.G., Leclercq, R., Lester, C.H., Lillie, M., Novais, C., Olsson-Liljequist, B., Peixe, L.V., Sadowy, E., Simonsen, G.S., Top, J., Vuopio-Varkila, J., Willems, R.J., Witte, W., Woodford, N., 2008. Emergence and spread of vancomycin resistance among enterococci in Europe. Euro surveillance : bulletin Europeen sur les maladies transmissibles = European communicable disease bulletin 13.

White, S.W., Zheng, J., Zhang, Y.-M., Rock, C.O., 2005. The structural biology of type II fatty acid biosynthesis. Annual Review of Biochemistry 74, 791-831.

WHO, World Health Organisation, 2013. Public Health Importance of Antimicrobial Resistance, WHO. World Health Organization.

Yadav, G., Thakuria, B., Madan, M., Agwan, V., Pandey, A., 2017. Linezolid and Vancomycin Resistant Enterococci: A Therapeutic Problem. J Clin Diagn Res 11, GC07-GC11.

Yang, L., Harroun, T.A., Weiss, T.M., Ding, L., Huang, H.W., 2001. Barrel-stave model or toroidal model? A case study on melittin pores. Biophysical journal 81, 1475-1485.

Yepes, A., Schneider, J., Mielich, B., Koch, G., García-Betancur, J.C., Ramamurthi, K.S., Vlamakis, H., López, D., 2012. The biofilm formation defect of a Bacillus subtilis flotillin-defective mutant involves the protease FtsH. Molecular microbiology 86, 457-471.

Zarb, P., Coignard, B., Griskeviciene, J., Muller, A., Vankerckhoven, V., Weist, K., Goossens, M.M., Vaerenberg, S., Hopkins, S., Catry, B., Monnet, D.L., Goossens, H., Suetens, C., National Contact Points for the ECDC pilot point prevalence survey, C., Hospital Contact Points for the ECDC pilot point prevalence survey, C., 2012. The European Centre for Disease Prevention and Control (ECDC) pilot point prevalence survey of healthcare-associated infections and antimicrobial use. Eurosurveillance 17, 20316.

Zhang, T., Muraih, J.K., Tishbi, N., Herskowitz, J., Victor, R.L., Silverman, J., Uwumarenogie, S., Taylor, S.D., Palmer, M., Mintzer, E., 2014. Cardiolipin prevents membrane translocation and permeabilization by daptomycin. The Journal of biological chemistry 289, 11584-11591.

Zhang, Y.M., Rock, C.O., 2008. Membrane lipid homeostasis in bacteria. Nat Rev Microbiol 6, 222-233.

Zhao, F., Zhang, J., Liu, Y.-S., Li, L., He, Y.-L., 2011. Research advances on flotillins. Virology Journal 8, 479.

Zhu, L., Zou, Q., Cao, X., Cronan, J.E., 2019. *Enterococcus faecalis* Encodes an Atypical Auxiliary Acyl Carrier Protein Required for Efficient Regulation of Fatty Acid Synthesis by Exogenous Fatty Acids. mBio 10, e00577-00519.

2. CHAPTER II:

Lysine modification of phosphatidylglycerol has broad and unexpected lipidomic, transcriptomic, and functional consequences for *Enterococcus faecalis*

2.1. Introduction

Enterococci colonise various niches and sites in the human host such as the gut, surgical wounds, heart valves and the urinary tract (Hidron et al., 2008; Murdoch et al., 2009; Patterson et al., 1995; Weiner et al., 2016). One of the first barriers to successful colonisation that *Enteroccoci* must contend with and overcome is the host's innate immune defences present at these sites. One important component of the innate immunity are antimicrobial peptides (AMPs), which serve as a first line of defence against invading pathogens and are produced not just by mammals but in non-mammalian vertebrates, plants and even insects (Brown and Hancock, 2006; Pasupuleti et al., 2012). AMPs in the human host are typically secreted by circulating phagocytes and mucosal epithelial cells and have broad specificity against Gram-positive and -negative bacteria. The vast majority of AMPs possess a cationic charge with a large hydrophobic region that is key to targeting negatively charged bacterial membranes (Diamond et al., 2009; Lei et al., 2019). Most of these cationic antimicrobial peptides (CAMPs) in humans fall into 2 classes, defensins such as human β-defensins (hBDs) and human neutrophil peptides (HNP); and cathelicidins such as LL-37 (Diamond et al., 2009; Durr et al., 2006; Ganz, 2003).

To overcome the inhibitory activity of CAMPs, many bacterial species possess evolutionarily conserved defence mechanisms. One such mechanism in Gram-positive bacteria is through the modification of negatively charged membrane phospholipids to diminish their charge and electrostatic affinity to CAMPs.

Several Gram-positive organisms such as *Bacillus anthracis*, *Staphylococcus aureus*, *Listeria monocytogenes* as well as *E. faecalis* can do this through the membrane bound enzyme multiple peptide resistance factor (MprF) (Bao et al., 2012; Peschel et al., 2001; Samant et al., 2009; Thedieck et al., 2006). MprF consists of a *C*-terminal aminoacyltransferase present in the inner leaflet of the membrane bilayer domain responsible for aminoacylating phosphatidylglycerol (PG) typically with lysine from lysyl-tRNA to form lysyl-PG (Lys-PG). Lys-PG then gets flipped to the outer leaflet by the *N*-terminal transmembrane flippase domain of MprF and in doing so, reduces the overall negative charge of the membrane (Ernst et al., 2009). While many organisms possess only one *mprF* gene, *E. faecalis* encodes two paralogs of *mprF* in its genome (*mprF1* and *mprF2*) (Bao et al., 2012; Ernst et al., 2009). In an encapsulated *E. faecalis* strain 12030, *mprF2* appears to be more involved in aminoacylation and CAMP resistance and the aminoacyl-PG in this strain includes not just Lys-PG but possibly Arg-PG and Ala-PG as well (Bao et al., 2012).

MprF also has an influence on CAMP targeting. In *E. faecalis* OG1RF the septum has been previously established to be focally targeted by CAMPs (Kandaswamy et al., 2013). When either paralog of *mprF* was deleted, focal binding of CAMPs to the septum was intensified to similar extents (Kumaravel Kandaswamy, unpublished) **(Figure 2.1A, B)**. Interestingly, despite the equal contributions to CAMP focal targeting, *mprF2* appears to play a greater role in CAMP resistance as compared to *mprF1* when tested with human beta defensin 2 (Dominic Chia, unpublished) **(Figure 2.1C)**.

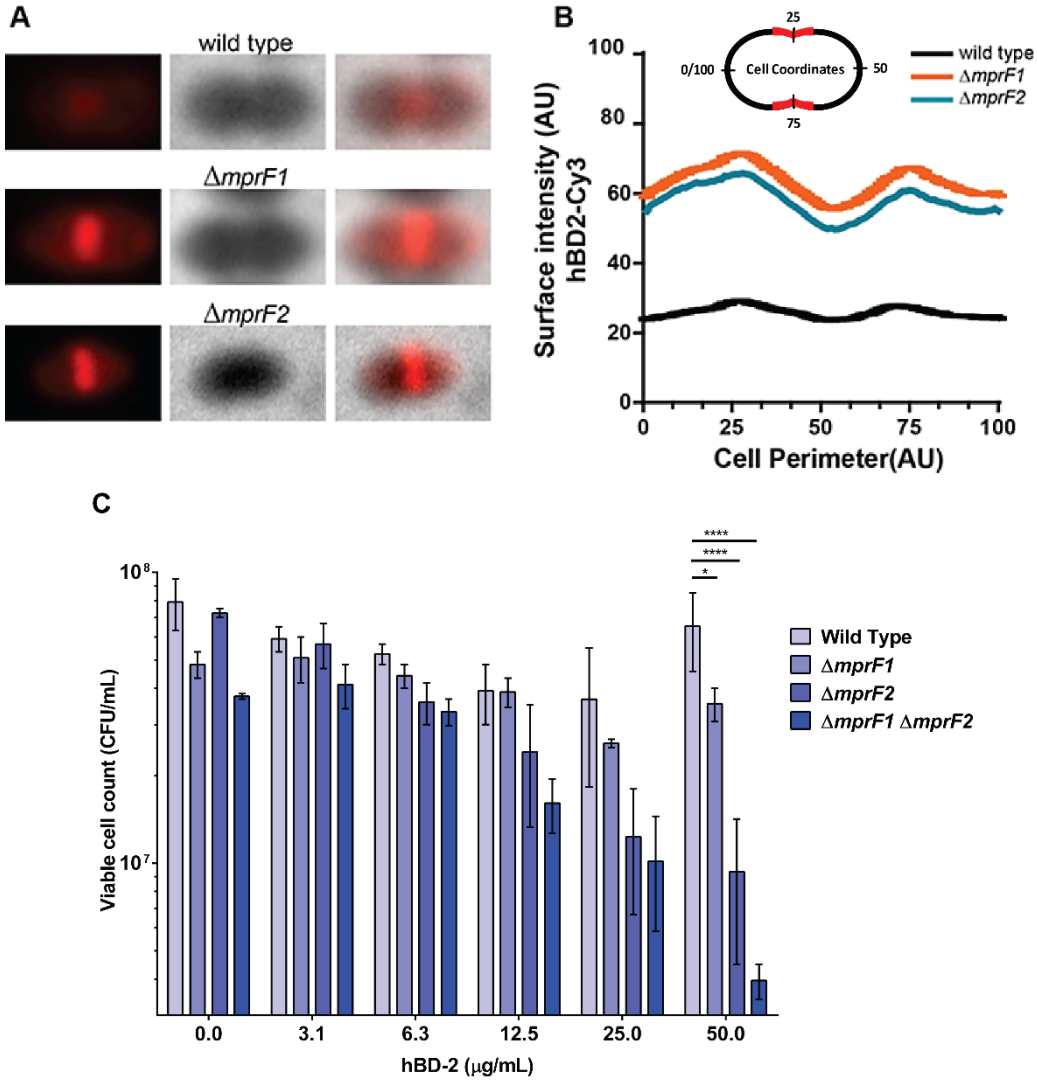

Figure 2.1. Deletion of either *mprF* paralog results in equal enhancement of CAMP focal binding but differential CAMP susceptibility (Kumaravel Kandaswamy and Dominic Chia, unpublished) (A) Equally enhanced focal binding of Cy3-hBD2 to the septum of Δ*mprF1* and Δ*mprF2*. Red fluorescence corresponds to Cy3-hBD2. **(B)** PSICIC analysis of cell perimeter fluorescence whereby fluorescence intensity across the perimeter of the cell is represented as a graph. Positions 0/100 and 50 refer to the cell poles while positions 25 and 75 refer to the septum of mid-log phase cells. Fluorescence of at least 100 mid-log phase cells were quantified. **(C)** CFU enumerated after 2-hour exposure to increasing concentrations of hBD2. Error bars represent the standard error of mean from 2 biological replicates with 6 technical replicates each. Each biological replicate consists of averaged values from their constituent technical replicates. Statistical comparisons made for mutants against wild type of each concentration. * p=0.05 to 0.01; ****, p⩽0.0001; Fisher's LSD test for ANOVA.

At present it is unclear why there is a disparity between CAMP targeting and susceptibility in the two *mprF* paralogs. We hypothesize that there might be differences at the membrane composition that results in this phenomenon and there are likely other differences in membrane and cell physiology that has not been previously explored.

In this chapter, we sought to characterize the function of these two paralogs in terms of their effect on PG-aminoacylation as well as their influence on the cell envelope lipidome via liquid chromatography tandem mass-spectrometry (LC-MS/MS) and thin layer chromatographic analyses of *mprF* mutants. To give mechanistic insight into the changes observed upon *mprF* deletion and to determine their functional outcome, transcriptomic analysis together with phenotypic assays investigating membrane fluidity, secretion, biofilm formation and survival in fatty acid limited conditions were carried out.

This chapter provides insight into the extended role of *mprF* beyond just its enzymatic function, where the loss of a single phospholipid modification can have a far-reaching effect in affecting the lipidome composition and generating seemingly unrelated phenotypes. Understanding the full extent that *mprF* paralogs and lysine modifications of PG has on the cell, will better position future research on *mprF* or other branches of phospholipid metabolism as targets for inhibition.

2.2. Materials and methods

2.2.1. Bacterial strains and culture conditions

The wild-type (WT) parental strain used was *E. faecalis* OG1RF (Dunny et al., 1978) and Δ*mprF1* and Δ*mprF2* mutants used were described previously (Chong et al., 2017; Kandaswamy et al., 2013). Unless stated, all bacterial strains were grown overnight to late stationary phase for 16-18 hours in their respective media at 37 °C in static conditions and stored in 25% glycerol solution at -80 °C when long-term storage was required. If mid-log phase cultures were required, late stationary phase cultures were sub-cultured 1:10 dilution into fresh media and grown at 37 °C, 250 rpm shaking conditions until an OD_{600} of 0.5 ± 0.05 was reached. When normalisation of cultures was required, they were centrifuged at 6,000 rcf for 5 min at 4 °C and cell pellets were washed twice with 1mL of phosphate buffered saline (PBS). Cell suspensions were then normalised to an OD_{600} of 0.7 or required optical density by diluting with PBS. All strains, their respective genotypes, sources, and growth media are listed in **Table 2.1** below.

Table 2.1. Bacteria Strains and Culture Conditions

Bacterial Strains	Relevant Information / Genotype	References / Source	Media Used
	E. coli		
Stellar™ Competent Cells (*E. coli* HST08)	*F–, endA1, supE44, thi-1, recA1, relA1, gyrA96, phoA, Φ80d lacZΔM15, Δ(lacZYA - argF) U169, Δ(mrr - hsdRMS - mcrBC), ΔmcrA, λ–*	Clontech, Takara Bio Inc., Japan	-
DH5α pCYW2	DH5α harbouring pCYW2*; Kan^r *pCYW2: pGCP123 parent plasmid (Nielsen et al., 2012) with PsrtA promoter. Expression vector.	Lab stock	LB, Miller broth (BD, USA) with 50 µg/mL kanamycin (Thermo Scientific, USA)

DH5α pMSP3535	DH5α harbouring pMSP3535*; Erm^r *pMSP3535: Shuttle vector for nisin-controlled inducible expression.	pMSP3535 was a gift from Gary Dunny, University of Minnesota (Addgene plasmid # 46886) (Bryan et al., 2000)	LB, Miller broth (BD, USA) with 300 µg/mL erythromycin (Sigma Alrdrich, USA)
Stellar™ Competent Cells pMSP3545-d*cas9*	DH5α harbouring pMSP3545-d*cas9**; Erm^r *pMSP3535-dcas9: Shuttle vector for nisin-inducible expression of dcas9	Constructed by Irina Afonina (Afonina et al., 2020)	LB, Miller broth (BD, USA) with 300 µg/mL erythromycin (Sigma Alrdrich, USA)
DH5α pABG5.2mini	DH5α harbouring pABG5.2mini* *pABG5.2mini: Shuttle expression vector	(Nielsen et al., 2012)	LB, Miller broth (BD, USA) with 50 µg/mL kanamycin (Thermo Scientific, USA)
DH5α pGCP123-*mprF1-HA* DH5α pGCP123-*mprF2-HA*	DH5α harbouring pGCP123-*mprF1*-HA* * pGCP123-*mprF1*-HA: Shuttle expression vector for *mprF1* complementation DH5α harbouring pGCP123-*mprF2*-HA* * pGCP123-*mprF2*-HA*:* Shuttle expression vector for mprF2 complementation	Constructed by Liew Horng Tze (Rashid et al., unpublished)	LB, Miller broth (BD, USA) with 50 µg/mL kanamycin (Thermo Scientific, USA)
	E. faecalis		
OG1X	Strep^r, wild type	Lab stock	BHI (Neogen, USA)
OG1RF	Fus^r, Rif^r, wild-type strain	American Type Culture Collection (ATCC© 47077™)	
OG1RF Δ*mprF1*	Fus^r, Rif^r, Δ*mprF1*	(Kandaswamy et al., 2013)	
OG1RF Δ*mprF2*	Fus^r, Rif^r, Δ*mprF2*	(Kandaswamy et al., 2013)	

OG1RF Δ*mprF1*Δ*mprF2*	Fus^r, Rif^r, Δ*mprF1*Δ*mprF2*	Constructed by Liew Horng Tze (Rashid et al., unpublished)	
OG1RF Δ*mprF1* *pGCP123-mprF1-HA*	Fus^r, Rif^r, Δ*mprF1* *pGCP123-mprF1-HA*	This study	BHI (Neogen, USA) with 500 µg/mL kanamycin (Thermo Scientific, USA)
OG1RF Δ*mprF2* *pGCP123-mprF2-HA*	Fus^r, Rif^r, Δ*mprF2* *pGCP123-mprF2-HA*	This study	
OG1RF Δ*mprF1*Δ*mprF2* *pGCP123-mprF1-HA*	Fus^r, Rif^r, Δ*mprF1*Δ*mprF2* *pGCP123-mprF1-HA*	This study	
OG1RF Δ*mprF1*Δ*mprF2* *pGCP123-mprF2-HA*	Fus^r, Rif^r, Δ*mprF1*Δ*mprF2* *pGCP123-mprF2-HA*	This study	
OG1RF Δ*mprF2* *pGCP123-mprF2*	Fus^r, Rif^r, Δ*mprF2* *pGCP123-mprF2*	This study	
OG1RF Δ*mprF1*Δ*mprF2* *pGCP123-mprF2*	Fus^r, Rif^r, Δ*mprF1*Δ*mprF2* *pGCP123-mprF2*	This study	
OG1RF Δ*mprF1*Δ*mprF2* *pGCP123-mprF2 (D731A,R734S)*	Fus^r, Rif^r, Δ*mprF2* *pGCP123-mprF2 (D731A,R734S)*	This study	
OG1RF Δ*mprF1*Δ*mprF2* *pGCP123-mprF2 (D731A,R734S)*	Fus^r, Rif^r, Δ*mprF1*Δ*mprF2* *pGCP123-mprF2 (D731A,R734S)*	This study	
OG1RF *pABG5*	Fus^r, Rif^r, *pABG5*	Constructed by Dominic Ming Hao Chia (Rashid et al., unpublished)	BHI (Neogen, USA) with 500 µg/mL kanamycin (Thermo Scientific, USA)
OG1RF Δ*mprF1* *pABG5*	Fus^r, Rif^r, Δ*mprF1*, *pABG5*		
OG1RF Δ*mprF2* *pABG5*	Fus^r, Rif^r, Δ*mprF2*, *pABG5*		
OG1RF Δ*mprF1*Δ*mprF2* *pABG5*	Fus^r, Rif^r, Δ*mprF1*Δ*mprF2* *pABG5*		
OG1RF pMSP3545-*dcas9* pABG5.2mini	Fus^r, Rif^r, pMSP3545-*dcas9* pABG5.2mini*1*	This study	BHI (Neogen, USA) with 500 µg/mL kanamycin, 100 µg/mL erythromycin
OG1RF Δ*mprF1*Δ*mprF2* pMSP3545-*dcas9* pABG5.2mini	Fus^r, Rif^r, Δ*mprF1*Δ*mprF2* pMSP3545-*dcas9* pABG5.2mini	This study	
OG1RF pMSP3545-*dcas9* pABG5.2mini-*croR_g1*	Fus^r, Rif^r, pMSP3545-*dcas9* pABG5.2mini-*croR_g1*	This study	
OG1RF Δ*mprF1*Δ*mprF2* pMSP3545-*dcas9* pABG5.2mini-*croR_g1*	Fus^r, Rif^r, Δ*mprF1*Δ*mprF2* pMSP3545-*dcas9* pABG5.2mini-*croR_g1*	This study	

OG1RF pMSP3545-*dcas9* pABG5.2mini-*liaF_g1*	Fus^r, Rif^r, pMSP3545-*dcas9* pABG5.2mini-*liaF_g1*	This study
OG1RF Δ*mprF1*Δ*mprF2* pMSP3545-*dcas9* pABG5.2mini-*liaF_g1*	Fus^r, Rif^r, Δ*mprF1*Δ*mprF2* pMSP3545-*dcas9* pABG5.2mini-*liaF_g1*	This study
OG1RF pMSP3545-*dcas9* pABG5.2mini-*walK_g1*	Fus^r, Rif^r, pMSP3545-*dcas9* pABG5.2mini-*walK_g1*	This study
OG1RF Δ*mprF1*Δ*mprF2* pMSP3545-*dcas9* pABG5.2mini-*walK_g1*	Fus^r, Rif^r, Δ*mprF1*Δ*mprF2* pMSP3545-*dcas9* pABG5.2mini-*walK_g1*	This study

2.2.2. Analysis of membrane lipid content

Lipids were extracted from lyophilised cell pellets from late stationary phase cultures using a modified Bligh & Dyer method in which the extraction solvent contained chloroform/methanol in a ratio of 1:2 (v/v) as previously described (Bligh and Dyer, 1959; Rashid et al., 2017). For method validation and quantification, known amounts of internal standards for phosphatidylglycerol (PG) and lysyl-PG (Lys-PG) were added to the samples. Nine hundred microliters of chilled extraction solvent containing internal standards (Avanti polar lipids, Alabaster, AL, USA) was added to the cell pellets except monoglucosyl-diacylglycerol (MGDAG) 34:1 which was used as a surrogate external standard for diglucosyl-diacylglycerol (DGDAG) instead **(Table 2.2)**:

Table 2.2. Lipid standards used

Standard	Usage	Catalogue #	Stock conc. [mg/ml]	Final conc. [µg/ml]	Precursor ion (m1) m/z	Fragment ion (m3) m/z
PG 14:0	Internal	840445P	1	5	665.5 $[M-H]^-$	153
Lys-PG 16:0	Internal	840520P	0.1	4	849.6 $[M-H]^-$	145
MGDAG 34:1	External	840522P	1	variable	774.6 $[M+NH_4]^+$	313

Lipid extraction was then carried out as previously described (Rashid et al., 2017). The dried lipid extract was resuspended in a mixture of chloroform and methanol (1:1 v/v), to a final lipid concentration of 10 mg/ml. This solution was stored at -80°C until the mass spectrometry analysis was performed. PG and Lys-PG in *E. faecalis* were quantified by LC-MS/MS using multiple reaction monitoring (MRM) using a previously described methodology (Rashid et al., 2017). An Agilent 6490 QqQ mass spectrometer connected to a 1290 series chromatographic system was used with a Kinetex® 2.6 µm HILIC column (100 Å, 150 x 2.1 mm) (Phenomenex, USA). Electrospray ionization (ESI) was used to ionize lipids. Each lipid molecular species was analysed using a targeted

multiple reaction monitoring (MRM) approach containing transitions for known precursor/product mass-to-charge ratio (m1/m3). Signal intensities were normalized to the spiked internal standards (PG 14:0 and Lys-PG 16:0) to obtain relative measurements, as described previously (Rashid et al., 2017).

To determine the species of DGDAG present in *E. faecalis*, untargeted analysis of lipid extracts of WT, Δ*mprF1*, Δ*mprF2* and Δ*mprF1* Δ*mprF2* was carried out. Lipid extracts were analysed using an Agilent 6550 QToF mass spectrometer connected to a 1290 series chromatographic system with a Kinetex® 2.6 µm HILIC column (100 Å, 150 x 2.1 mm) (Phenomenex, USA). The QToF instrument was set to positive ion mode, at an electrospray voltage of -3500 V (Vcap), a temperature of 200 °C, a drying gas rate of 14 L/min. Spectra were acquired in auto-MS2 mode with MS1 acquisition rate at 4 spectra/s and the MS2 acquisition rate at 20 spectra/s with fixed collision energy at 40 eV. The list of detected species of DGDAG in the samples can be found in the Appendix **(Table S2.1)**.

Due to the absence of suitable internal standards, semi-quantitative analysis of DGDAG was carried out instead. Lipid extraction was performed as described above without addition of internal standards. Analysis of DGDAG lipid species was performed by LC-MS/MS via MRMs using monoglucosyl-diacylglycerol (MGDAG) 34:1 as a surrogate standard **(Table 2.2)** for external calibration curves. Measurements of MGDAG 34:1 dilution from 0.2 ng/mL to 1000 ng/mL were used to construct external calibration curves to estimate the levels of DGDAG. Estimated DGDAG levels were then normalized against dry cell pellet of the respective samples. The MRM transitions for DGDAG molecular species and MGDAG 34:1 are listed in the Appendix **(Supplementary Table S2.2)**. The mobile phase gradients used for all experiments are as previously described (Rashid et al., 2017).

For semiquantitative analysis of glycerophosphoryl-diglucosyl-diacylglycerol (GPDGDAG), lipid extracts were analysed using an Agilent 6550 QToF mass spectrometer connected to a 1290 series chromatographic system with a Kinetex® 2.6 u HILIC column (100 Å, 150 x 2.1 mm) in negative mode. The most abundant GPDGDAG was quantified with the following transition (MS1 m/z: 1071.6, MS2 m/z: 153.0). Integrated peak areas were normalised against cell weight.

2.2.3. RNA isolation and RT-qPCR

Real time quantitative PCR (RT-qPCR) was performed on RNA isolated from WT and Δ*mprF1*Δ*mprF2* strains for *pgsA* and fatty acid biosynthesis genes. Overnight cultures were subcultured 1:10 in BHI and grown to mid-log phase (OD_{600} 0.5 ± 0.05). One millilitre of RNAprotect Bacteria Reagent (Qiagen, Germany) was added to 500 µL of mid-log phase culture and incubated for 5 minutes at room temperature. Cells were then pelleted and rinsed with PBS to thoroughly remove the RNAprotect reagent. Cell pellets were then resuspended in 20 mg/mL lysozyme (Sigma-aldrich, USA) in lysis buffer (10 mM Tris-HCl pH 7.0, 1 mM EDTA, 50 mM NaCl and 0.74 M sucrose) and incubated for 1 hour. Cells were then pelleted and washed once with PBS. One millilitre of ice-cold TRIzol™ Reagent (Ambion, USA) was added and the cell pellet resuspended by pipetting action. After which, 200 µL of ice-cold chloroform (Fisher, USA) was added to the tube and the suspension mixed by shaking gently before incubating on ice for 2 minutes. The mixture was then centrifuged for 15 minutes at 12, 000 x g at 4 ^{o}C to induce phase separation. Next, 500 µL of the upper aqueous phase was carefully removed and added to the spin-column from the RNeasy Mini Kit (Qiagen, USA). Purification was then carried as specified by the manufacturer's instructions and eluted in 40 µL of Nuclease-free water (Ambion, USA). Quantification of RNA and DNA was performed using Qubit™ RNA Assay Kits

and Qubit™ dsDNA HS Assay Kits (Invitrogen, USA), respectively. Integrity of RNA was analyzed by gel electrophoresis using Agilent RNA ScreenTape (Agilent Technologies, USA). cDNA synthesis was performed on the total isolated RNA using SuperScript™ III First-Strand Synthesis SuperMix (Invitrogen™, USA) according to the manufacturer's instructions. RT-qPCR was next performed using the KAPA SYBR® FAST qPCR Kit Master Mix (2X) Universal (Kapa biosystem, USA) with the respective primers listed in **Table 2.3** below on a StepOnePlus™ Real-Time PCR System (Applied Biosystems, USA). The product from cDNA synthesis run without template added was used as a negative control.

Table 2.3. Primers used for RT-qPCR

Primer	Target	Gene Type	Sequence (5' → 3')	Tm (°C)
gyrA_F	*gyrA*	Housekeeping	TGTTCGTCGGGATGTGAGTG	55
gyrA_R	*gyrA*	Housekeeping	GGTACGCCTTTTTCGATGGC	55
pgsA_F	*pgsA*	Target	CGACACAACGTTAGCCGTTA	55
pgsA_R	*pgsA*	Target	AAGGCGGTCATCACTAGCAT	55
accA_F	*accA*	Target	GCGATACCCTTCAGGATTAG	55
accA_R	*accA*	Target	CTTTGCCGATGATTTAGCTG	55
accB_F	*accB*	Target	GCTTCAACGATACACACAACG	55
accB_R	*accB*	Target	ACCGACAACCAATGAAAAGA	55
accC_F	*accC*	Target	CGATATGACGTGCTGGATAA	55
accC_R	*accC*	Target	TACCCAGTGATGTTAAAGGCA	55
accD_F	*accD*	Target	GTTGGATCAGTCAATACCGTAAG	55
accD_R	*accD*	Target	TGATTTTCACTGCATCTGGTG	55
fabD_F	*fabD*	Target	TCACGATTTGTTGTGGTGTAT	55
fabD_R	*fabD*	Target	GTCAGTACATGACAGAAGCAGC	55
fabF2_F	*fabF2*	Target	CTGGTGTTGGTGATGTCATA	55
fabF2_R	*fabF2*	Target	TGGATTTGTGATGGGAGAAGG	55
fabG3_F	*fabG3*	Target	TATCATTCGTAATCCCAGCG	55
fabG3_R	*fabG3*	Target	ATTGAAGCCTTTGGGGTAAAAT	55
fabK_F	*fabK*	Target	TCAATGATTTCTTGGGCTGT	55
fabK_R	*fabK*	Target	TCCAAAAAGAAGTGCCTGAT	55
fabZ2_F	*fabZ2*	Target	CCCTTTGAATTCAGGCATTG	55
fabZ2_F	*fabZ2*	Target	GCGTTGTAGCGAAAAAGAATG	55

2.2.4. Growth curves

Overnight cultures were normalised to OD_{600} of 0.7 and diluted 200-fold (for BHI) or 100-fold (for chemically defined media (CDM)) before inoculation in 200 µL of media in 96-well plates in a ratio of 1:25. The 96-well plates were incubated at 37 °C in a Tecan Infinite© M200 Pro spectrophotometer (Tecan, Switzerland) and absorbance was read at 600 nm every 10 minutes for 18 hours (for BHI) or 72 hours (for CDM). The components of the CDM used are shown in **Table 2.4** below.

Table 2.4 Components in chemically defined media (CDM)

Component	g/L	Component	g/L
KH_2PO_4	3.6000	D-glucose	15.0000
NaCl	3.0000	L-histidine	0.1700
$(NH_4)_2SO_4$	1.0000	L-isoleucine	0.2400
MOPS	13.0500	L-leucine	1.0000
K-acetate	0.9000	L-methionine	0.0600
$(NH_4)_6Mo_7O_{24} \cdot 4H_2O$	0.0002	L-valine	0.7000
$ZnSO_4 \cdot 7H_2O$	0.0050	L-arginine	0.7200
$CoCl_2 \cdot 6H_2O$	0.0002	L-glutamic acid	0.7200
$CuSO_4 \cdot 5H_2O$	0.0002	Glycine	0.3600
H_3BO_3	0.0008	L-serine	0.6000
K_2SO_4	0.0230	L-threonine	0.6000
KI	0.0001	$MgSO_4 \cdot 7H_2O$	1.0000
L-tryptophan	0.2400	$CaCl_2 \cdot 2H_2O$	0.0400
L-cysteine HCl	0.2400	Inositol	0.0020
Ca-pantothenate	0.0012	Biotin	0.0060
Pyridoxal HCl	0.0048	Niacin	0.0009
Riboflavin	0.0009	p-aminobenzoic acid	0.0001
Folic acid	0.0006	Tricine	1.3050
Thiamine-HCl	0.0006	Glutathione	0.0150
		Iron (II) sulfate heptahydrate	0.0040

If fatty acid supplementation was required, fatty acids were prepared as 10 mg/mL stocks in ethanol for linoleic acid, oleic acid, *cis*-vaccenic acid, palmitoleic acid, stearic acid, palmitic acid, and lauric acid, and as 1 mg/mL in ethanol for arachidic acid.

2.2.5. Fatty acid methyl esters (FAME) analysis

Late stationary phase cultures of wild-type and Δ*mprF1*Δ*mprF2* grown in either BHI (overnight) or CDM (72 hours) were lyophilised and sent together with powdered BHI for GC-FAME analysis at the Identification Service of Deutsche Sammlung von Mikroorganismen und Zellkulturen GmbH (DSMZ), Braunschweig, Germany.

2.2.6. Radiolabelling and thin layer chromatography (TLC)

[^{14}C]-acetate or [^{32}P]-disodium phosphate (Perkin Elmer, USA) was added into 5 mL of media at 0.2 µCi/mL or 1 µCi/mL respectively before culturing strains overnight at 37 ºC for 16-18 hours at static conditions. Lipids were then extracted as previously described and resuspended in 50 µL of chloroform-methanol solution (1:1 v/v) (Rashid et al., 2017). 10 µL of lipid extracts were mixed with 2 mL of Ultima Gold™ scintillation fluid (Perkin Elmer, USA), and radioactive counts were measured using a MicroBeta2® scintillation counter (Perkin Elmer, USA). The lipid extracts were spotted on to silica-gel coated TLC plates (Merck, USA) and normalised according to the scintillation counts. TLC plates were developed in pre-equilibrated TLC chambers with chloroform:methanol:water (65:25:4) solvent system for 1 dimension (1D) TLCs. For 2 dimensional (2D) TLCs, TLC plates were developed using chloroform:methanol:water (65:25:4) solvent system for the first dimension and chloroform:hexane:methanol:acetic acid (50:30:10:5). TLC plates were then visualised by exposure to a storage phosphor screen (GE healthcare, USA) overnight, and read using a Storm Phosphorimager (GE healthcare, USA). For iodine and ninhydrin-stained TLC plates, no radiolabelling was carried out and TLC spots were normalised based on dry cell weight instead. Iodine crystals (Sigma-Aldrich, USA) were used to develop TLC plates in a chamber, while for ninhydrin staining, ninhydrin was

applied to the plates, allowed to air dry before heating with a hairdryer till spots appeared.

2.2.7. SDS-PAGE and western blot

SDS-PAGE and western blot were performed as described in a previous study (Nielsen et al., 2012). 4-12% or 12% NuPAGE® Bis-Tris mini gel in a XCell SureLock® Mini-Cell filled with either 1x MES or 1x MOPs SDS running buffer (Invitrogen, USA) was used and run at 140 V for 90 min. Proteins were transferred to nitrocellulose membranes using the iBlot™ Dry Blotting System (Invitrogen, USA) according to the manufacturer's protocol. The antibodies and developing solutions used are shown in **Table 2.5**.

Table 2.5. Antibodies and developing solution used in western immunoblots

Target of interest	Primary Antibody Dilution; Host	Secondary Antibody Dilution; Host	Developing Solution; Dilution Ratios (Luminol:Peroxide:Water)
LTA	Mouse anti-LTA 1:1000 (Hycult Biotech, Netherlands)	Goat anti-mouse HRP 1:5000 (Thermoscientific, USA)	SuperSignal™ West Femto Maximum Sensitivity Substrate 1:1:8
2HA	Mouse anti-HA 1:1000 (Thermoscientific, USA)	Goat anti-mouse HRP 1:5000 (Thermoscientific, USA)	SuperSignal™ West Femto Maximum Sensitivity Substrate 1:1:8
SecA	Rabbit anti-SecA 1:3000 (Kline et al., 2009)	Goat anti-rabbit HRP 1:6000 (Thermoscientific, USA)	SuperSignal™ West Femto Maximum Sensitivity Substrate 1:1:8

2.2.8. Bulk secretion assay

Late stationary phase cultures were prepared by growing cultures in BHI broth overnight for 16-18 hours at 37 °C, static conditions. OD_{600} readings of the cultures were measured. Cell-free supernatants were obtained by centrifugation at 6,000 rcf for 5 minutes at 4 °C and filtering the supernatants into fresh Eppendorf tubes using 0.2 µm syringe filters. 1.6 mL of filtered supernatant was mixed with 400 µL of 100% w/v tricholoroacetic acid (TCA) solution (1:4 ratio of

TCA to sample) and incubated at 4 ºC for 10 minutes. Tubes were centrifuged at 20,000 rcf for 15 minutes at 4 ºC. The precipitated protein pellet was washed once with 2 mL of 100% ice-cold acetone and placed on a 98 ºC heat block to evaporate residual acetone. The pellets were resuspended in 500 µL of PBS. Twenty-five microliters of these protein solutions were used for estimation of protein content using the Pierce BCA Protein Assay Kit (Thermoscientific, USA) in a microtiter plate format according to the manufacturer's protocol. Protein concentrations of the samples were then normalized to OD_{600} of 1.0 based on the respective OD_{600} readings of the individual cultures.

2.2.9. Alkaline phosphatase (AP) secretion assay

Mid-log phase cultures of strains harbouring the pABG5 plasmid containing a chimeric alkaline phosphatase (PhoZF) were normalised to OD_{600} of 0.5. Cell-free supernatants were obtained by centrifuging samples at 6,000 rcf for 5 minutes at 4 ºC and filtering the supernatant through 0.2 µm syringe filters. 25 µL of supernatant was added to 200 µL of 1M Tris-HCl, pH 8.0, in a 96-well microtitre plates. 25 µL of 4 mg/mL para-nitrophenyl phosphate (pNPP) (Sigma-Aldrich, USA) was then added to each well to start the reaction. pNPP will get converted to a coloured substrate in the presence of PhoZF, that can be detected by measuring absorbance at 405nm. The plate was then placed into a Tecan Infinite© M200 Pro spectrophotometer and incubated at 37 ºC with the absorbance read at 405 nm every 10 minutes for 18 hours.

2.2.10. Analysing membrane fluidity (microscopy)

1mM Laurdan stock solutions were prepared by dissolving Laurdan powder (Sigma-Aldrich, USA) in methanol and stored at -20 ºC. Late stationary and mid-log phase cultures were normalised to OD_{600} of 0.7 in PBS and incubated with 100 µM of Laurdan for 10 minutes at 37 ºC. Cells were washed twice with PBS and 10 µL of the cell suspension was spotted onto PBS-agarose pads (1% w/v)

mounted on glass slides. Coverslips were placed over the agarose pads and sealed using paraffin wax.

Slides were imaged using a Zeiss LSM 880 Laser Scanning Microscope with Airyscan, using a Plan-Apochromat 63x/1.4 Oil DIC objective with an incubation chamber set to 37 ºC. The slides were equilibrated for 10 minutes within the chamber before imaging and excited using a 405nm laser with emission collected between 419-455nm (blue) and 480-520nm (green) simultaneously. Digital images were acquired using the Zen (Zeiss) software and analysed using ImageJ. Using ImageJ, regions of interests (ROIs) of individual cells or cell clusters were selected and mean fluorescence intensities (MFIs) of each ROI for each channel were measured and tabulated in Microsoft excel. Using the following formula, the average GP values for each ROI were calculated and then plotted using graphpad prism software:

$$GP = \frac{I_{Blue} - I_{Green}}{I_{Blue} + I_{Green}} = \frac{I_{419-455\,nm} - I_{480-520\,nm}}{I_{419-455\,nm} + I_{480-520\,nm}}$$

2.2.11. Analysing membrane fluidity (microplate spectroscopy)

Late stationary phase cultures were normalised to OD_{600} of 1.0 in 1 mL of PBS and incubated with 10 µM of Laurdan for 10 minutes at 37 ºC. Cells were then washed twice with PBS and resuspended in 1mL of PBS. 200 µL of the cell suspension, and supernatant of the preceding wash (to serve as an unbound dye control) were loaded into wells of a 96-well microtiter plate which was further incubated at 37 ºC for 30 minutes. Fluorescence measurements were taken with a Tecan Infinite© M200 Pro spectrophotometer with excitation at wavelength of 350 nm and emission at wavelengths of 435 and 500 nm, every 10 minutes for 1 hour at 37 ºC to monitor for GP value stability. Readings at 30 minutes where GP values start to become stable were used for analysis. GP values were calculated using the following formula:

$$GP = \frac{I_{Blue} - I_{Green}}{I_{Blue} + I_{Green}} = \frac{I_{435\,nm} - I_{500\,nm}}{I_{435\,nm} + I_{500\,nm}}$$

2.2.12. Daptomycin minimum inhibitory concentration (MIC)

Mid-log phase cultures of the strains were tested for their daptomycin minimum inhibitory concentration (MIC) using the microplate broth dilution methods as previously described (Rashid et al., 2017).

2.2.13. Static biofilm assay with crystal violet staining

Late stationary phase cultures were normalised to OD_{600} of 0.7 and inoculated in a ratio of 1:25 into 200 µL of Tryptone Soy Broth (TSB) (Oxoid, Singapore) supplemented with 1.39 M D-glucose (VWR, USA) (TSBG) in a 96-well plate (Thermo Scientific, USA), and incubated at 37 °C in static conditions. Crystal violet staining of total adherent biomass was performed next. Supernatants were discarded, adherent cells were washed twice with PBS, stained with 0.1% v/v crystal violet solution for 30 minutes at 4 °C, washed twice with 1X PBS again followed by dye solubilization in 4:1 ethanol-acetone solution (Merck, USA) for 30 minutes at room temperature. Absorbance was read at 595 nm with a Tecan Infinite© M200 Pro spectrophotometer (Tecan Group Ltd, Switzerland) as a measure of biomass levels.

2.2.14. Live/Dead staining

Late stationary and mid-log phase cultures were normalised to OD_{600} 0.5 in 1 mL of PBS and washed twice with PBS. Two microliters of SYTO9 and propridium iodide (PI) mix (LIVE/DEAD™ BacLight™ Bacterial Viability Kit, for microscopy, Invitrogen, USA) was added to the cell suspensions and incubated at 15 minutes at room temperature in the dark. Stained cells were washed once with PBS and resuspended in 200 µL 0.01M phosphate buffer (PB). Five microliters of stained cells were wet mounted on 1.0-1.2mm microscope slides (Biomedia, Singapore) with 0.13-0.16 mm coverslips. Slides were imaged with

a Zeiss Axio observer Z1 inverted microscope (Carl-Zeiss, Germany) with a 100X oil immersion objective (NA 1.4, optovar 1.6X), AF488/FITC filter cube (460-490 nm band pass excitation filter, 515-550 nm band pass barrier filter) and AF568/Cy3 filter cube (530-550 nm band pass excitation filter, 590 nm long pass barrier filter). Phase contrast, green (460-490 nm) and red (530-550 nm) fluorescence images were captured.

2.2.15. Murine model of gut colonization

Male wild-type mice (C57BL/6, 7-8 weeks old, 21 to 25 g; InVivos Pte Ltd, Singapore) were supplied with *E. faecalis* in the drinking water for a period of 7 days as reported previously (Kommineni et al., 2015). Bacteria were inoculated into 200 mL of drinking water as follows: 10^8 CFU/mL *E. faecalis* OG1X with either 10^8 CFU/mL *E. faecalis* OG1RF wild-type or 10^8 CFU/mL *E. faecalis* Δ*mprF1*Δ*mprF2*. Freshly bacteria-inoculated water was replaced every two days. At the same time, body weight was monitored, and faecal pellets collected for enumeration of viable bacteria. Bacteria-inoculated water was replaced with sterile water at day 7 and the mice were euthanized 3 days post infection (dpi) by carbon dioxide induced hypoxia and cervical dislocation. Mouse ceca were removed aseptically, and the contents were separated from the cecal tissue. Cecal tissues were washed once in sterile PBS prior to homogenization in 1 mL sterile PBS. Viable bacteria from cecal tissue homogenates, cecal contents, and faecal pellets were enumerated by plating on MacConkey agar and BHI agar supplemented with 10 μg/mL colistin, 10 μg/mL nalidixic acid and 25 μg/mL rifampicin to select for *E. faecalis* OG1RF or BHI agar supplemented with 500 μg/mL streptomycin to select for *E. faecalis* OG1X. Data were combined from two independent experiments (5 mice per infection group). Experiment was performed with assistance from Wong Jun Jie and Sharon Goh.

2.2.16. *In vitro* planktonic competitive growth assay

Late stationary phase cultures of *E. faecalis* OG1RF, *E. faecalis* OG1RF Δ*mprF1*Δ*mprF2* and OG1X were normalised to 10^8 CFU/mL. Cultures were mixed to 1:1 ratio of either *E. faecalis* OG1RF with OG1X or *E. faecalis* OG1RF Δ*mprF1*Δ*mprF2* with OG1X. Cultures were then diluted 100X with fresh BHI in a flask and incubated in a shaker at 37 °C for up to 24 hours. CFU were enumerated at 0, 1, 2, 3, 4, 5, 6, 7, 8, 9 and 24 hours on the following selection plates: BHI with 25 µg/mL Rifampicin (to select for OG1RF) or 500 µg/mL Streptomycin (to select for OG1X).

2.2.17. Molecular cloning

pGCP123-*mprF1*-HA and pGCP123-*mprF2*-HA plasmids were extracted from *E. coli* DH5α strains harbouring these plasmids using the Monarch® Plasmid Miniprep Kit (New England BioLabs, USA) according to the manufacturer's instructions. They were then transformed into electrocompetent *E. faecalis* Δ*mprF1*, Δ*mprF2* and Δ*mprF1*Δ*mprF2*. Expression was verified by SDS-PAGE and western immunoblot as described above. It was discovered that only the pGCP123-*mprF2*-HA plasmids displayed expression **(Supplementary Figure S2.1)**. To create the pGCP123-*mprF2* and pGCP123-*mprF2*(D731A,R734S) plasmids, site directed mutagenesis was performed on the pGCP123-*mprF2*-HA plasmid by inverse PCR to introduce the D731A,R734S mutation using Q5® High-Fidelity DNA Polymerase (New England BioLabs, USA). The linearised PCR product was circularised using the In-Fusion HD Cloning system (Takara, Japan) and transformed into Stellar™ Competent Cells (Takara, Japan) according to the manufacturer's instructions. Plasmids were then extracted from the stellar competent cells using the Monarch® Plasmid Miniprep Kit. Inverse PCR was again performed to remove the hemagglutinin (HA) affinity tag and the

rest of the steps repeated to introduce the plasmid into *E. coli*. Plasmids were then transformed into electrocompetent *E. faecalis* Δ*mprF2* and Δ*mprF1*Δ*mprF2*.

To create strains for CRISPRi knockdowns, the pABG5.2mini plasmid was first linearized by PCR and ligated with inserts containing the guide RNA by using the In-Fusion HD Cloning system. These inserts were in the form of gBlocks ordered from Integrated DNA Technologies Pte. Ltd, Singapore. gBlock (insert) sequences can be found in the **Table 2.6** below. pMSP3545-dcas9 was first transformed into *E. faecalis* wild type and Δ*mprF1*Δ*mprF2*, followed by the respective pABG5.2mini based guide RNA plasmids.

Table 2.6. gBlocks Sequences for Guide RNA inserts

gBlock	Sequence
*croR*_g1	TATCGACGGAAGATCCTGCAGAGATCTATCTAAAACAGTCTTAATT CTATCTTGAGAAAGTATTGGTAATAATATTATTGTCGATAACGCGA GCATAATAAACGGCTCTGATTAAATTCTGAAGTTTGTTAGATACAAT GATTTCACTTCCATTCCATCCATGATGTTTTAGAGCTAGAAATAGC AAGTTAAAATAAGGCTAGTCCGTTATCAACTTGAAAAAGTGGCACC GAGTCGGTGCTTTTTTTGGATCCACTAGTGGTACCGAATTCAACCC GAACAATTGGCATGCGGCCGCCACCGCGGT
*liaF*_g1	TATCGACGGAAGATCCTGCAGAGATCTATCTAAAACAGTCTTAATT CTATCTTGAGAAAGTATTGGTAATAATATTATTGTCGATAACGCGA GCATAATAAACGGCTCTGATTAAATTCTGAAGTTTGTTAGATACAAT GATTTCTGACAATAAAAACAACGCCGGTTTTAGAGCTAGAAATAGC AAGTTAAAATAAGGCTAGTCCGTTATCAACTTGAAAAAGTGGCACC GAGTCGGTGCTTTTTTTGGATCCACTAGTGGTACCGAATTCAACCC GAACAATTGGCATGCGGCCGCCACCGCGGT
*walR*_g1	TATCGACGGAAGATCCTGCAGAGATCTATCTAAAACAGTCTTAATT CTATCTTGAGAAAGTATTGGTAATAATATTATTGTCGATAACGCGA GCATAATAAACGGCTCTGATTAAATTCTGAAGTTTGTTAGATACAAT GATTTCTGGTTTCGTTACATAGTCATGTTTTAGAGCTAGAAATAGC AAGTTAAAATAAGGCTAGTCCGTTATCAACTTGAAAAAGTGGCACC GAGTCGGTGCTTTTTTTGGATCCACTAGTGGTACCGAATTCAACCC GAACAATTGGCATGCGGCCGCCACCGCGGT

Transformants were selected using by BHI or LB agar containing the appropriate antibiotics as listed in **Table 2.1**. Screening of transformants was performed using colony PCR using Taq DNA Polymerase, recombinant (5 U/μL) (Thermo Scientific, USA) according to the manufacturer's instructions. Gel electrophoresis to assess for product sizes was performed using 1% w/v agarose gel in TAE buffer ran at 100 V for 30 minutes followed by ethidium

bromide staining for 10-15 minutes. After each transformation step, if plasmids passed the colony PCR check, they were extracted and sent for Sanger sequencing for their inserts to ensure the correct sequence was present (1st BASE DNA Sequencing Services, Singapore). PCR purification was performed using Wizard® SV Gel and PCR Clean-Up System (Promega, USA) according to the manufacturer's instructions. Primers used for the described PCR steps are shown in **Table 2.7** below.

Table 2.7. PCR Primers

Primer	Target(s)	Sequence	Purpose
F1	- pGCP123-*mprF1*-HA - pGCP123-*mprF2*-HA - pGCP123-*mprF2* (*D731A, R734S*)-HA - pGCP123-*mprF2* - pGCP123-*mprF2* (*D731A, R734S*)	GTAAAACGACGGCCAGT	Screening for transformants containing pGCP123-mprF2 Same primers used for Sanger sequencing
R3		ACGCTAAAACGTCTCAGAAAC	
pmprF2-MT-F	- pGCP123-*mprF2*	ATGAAGTTGGTACCATCGCATTGATGAGCCACCATAAAGAAAAAGCCCC	Inverse PCR to create D731A, R734S mutation on *mprF2*
pmprF2-MT-R		TGGTACCAACTTCATTTGTGTAACTAGGAATGA	
pmprF2-delHA_F	- pGCP123-*mprF2* (*D731A, R734S*)-HA - pGCP123-*mprF2*	TTAATAAAAAATCGATTATTAGTCAATATTTTTTTGATCGACAATGAGTAAAGCAATCATCACGTA	Inverse PCR to create remove HA affinity tag
pmprF2-delHA_F		TCGATTTTTTATTAAAACGTCTCAAAATCGTTTCTG	
5.2mini_Linearise_F	pABG5.2mini	GGCCGCCACCGCGGTGGAGCTC	To linearize plasmid
5.2mini_Linearise_R		GATCTTCCGTCGATACTATGTTATACG	

2.3. Results

2.3.1. *mprF* deletion alters Lys-PG and PG levels

Previous findings in the lab describe similar levels of enhanced focal binding of CAMPs in both Δ*mprF1* and Δ*mprF2*, yet the deletion of each *mprF* paralog yielded different degrees of CAMP susceptibility in CAMP killing assays where *mprF2* appears to be more involved in conferring CAMP resistance than *mprF1* (Kumaravel Kandaswamy & Dominic Chia, unpublished). To explain the differences in CAMP susceptibility between the mutants, we hypothesized that the *mprF* paralogs might be producing different amounts of CAMP-protective lysyl-PG (Lys-PG). To address this, we quantified the Lys-PG of extracted lipids from wild type and the *mprF* mutants via liquid chromatography tandem mass spectrometry (LC-MS/MS), with multiple reaction monitoring (MRMs) for Lys-PG. We observed that Δ*mprF1* had about 30% lower Lys-PG than the wildtype, while Δ*mprF2* and Δ*mprF1*Δ*mprF2* had Lys-PG below detection limits **(Figure 2.2A)**. Furthermore, the Lys-PG levels were restored in Δ*mprF2* and Δ*mprF1*Δ*mprF2* with plasmid-based complementation by *mprF2*-HA **(Figure 2.2A).** In terms of individual species, Lys-PG 32:1, 33:2, 34:1, and 36:2 were significantly lower in Δ*mprF1* than wild type **(Supplementary Figure S2.2A)**. Complementation with *mprF1*-HA was not possible due to the lack expression based on western blot analysis **(Supplementary Figure S2.1)**.

To determine if loss of *mprF* had any effect on its substrate, phosphatidylglycerol (PG), PG levels were also quantified by LC-MS/MS with MRMs for PG. We observed that loss of *mprF* led to decreased PG levels in all the mutants **(Figure 2.2B)**. This was particularly surprising as PG is the major phospholipid in the membrane of gram-positive bacteria, is thought to be essential, and such a major change from the loss of a single phospholipid modification has not been reported to our knowledge (Bao et al., 2012; Epand and Epand, 2009). As compared to

wild type, we saw a slight decrease in PG levels in Δ*mprF1* of about ~20% when compared to the wild type and a stronger decrease in Δ*mprF2* of ~60% **(Figure 2.2B)**. Interestingly, we observed that Δ*mprF1*Δ*mprF2* displayed a weaker degree of PG reduction of ~30% reduction as compared to ~60% reduction observed in Δ*mprF2* **(Figure 2.2B)**. However, complement of Δ*mprF2* and Δ*mprF1*Δ*mprF2* with plasmid-based expression of *mprF2*-HA failed to restore PG levels back to wild type levels **(Figure 2.2B)**. This failure of full complementation might be due to plasmid-based expression levels being different from native expression, or the hemagglutinin (HA) tag might be interfering with native interactions required for the restoration of PG levels. In terms of individual species, some of the PG species had different trends across the mutants. PG 34:1 and 36:2 had sequentially lower values in Δ*mprF1,* Δ*mprF2* and Δ*mprF1*Δ*mprF2* as compared to the wild type. PG 32:0 and 32:2 had similar levels across strains. PG 34:0 and 36:1 were greatly lowered in Δ*mprF1*Δ*mprF2* as compared to the wild type, while Δ*mprF1* and Δ*mprF2* were at similar intermediate values between the wild type and the double mutant (**Supplementary Figure S2.2B).**

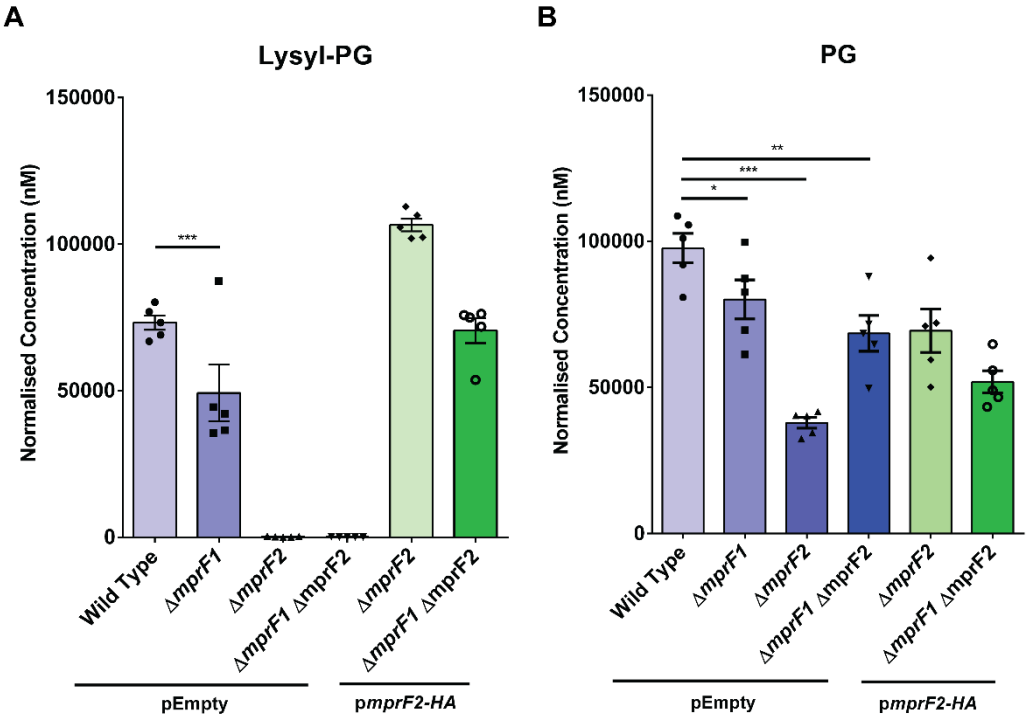

Figure 2.2. *mprF* contributes to Lys-PG and PG levels. The normalised amounts of **(A)** total lysyl-phosphatidylglycerol (Lys-PG) and **(B)** total PG in *E. faecalis* wild-type and *mprF* mutants are shown. Each bar represents the mean ± standard error of measurement calculated from 5 biological replicates. *, p=0.05 to 0.01; **, p=0.001 to 0.01; ***, p=0.0001 to 0.001; ****, p⩽0.0001; Fisher's LSD test for ANOVA. Samples were normalised against internal standards and dry sample weight. Representative data from 3 independent experiments.

2.3.2. Loss of *mprF* leads to changes in other lipid classes

With the observed decreased Lys-PG and PG levels in the *mprF* mutants, and since PG is essential in many bacteria, we hypothesized that there might be other compensatory changes in the lipidome that might be compensating for these decreased abundances (Dowhan, 1997; Furse, 2016; Heacock and Dowhan, 1987). We first conducted 1-dimensional thin layer chromatography (TLC) of lipids extracted from wild type, Δ*mprF1*, Δ*mprF2*, Δ*mprF1*Δ*mprF2* as well as p*mprF2*-HA complemented Δ*mprF2* and Δ*mprF1*Δ*mprF2* using ^{14}C radiolabelling and iodine staining **(Figure 2.3A)**.

6 major spots were observed in the 1D-TLC which were identified to be diglucosyl-diacylglycerol (DGDAG), Lys-PG, glycerophosporyl diglucosyl-diacylglycerol (GPDGDAG), D-ala-GPDGDAG, PG and cardiolipin (CL) co-migrating in the same spot, as well as a spot of unknown identity containing phosphorus **(Figure 2.3A)**. Identities of these spots were determined through a combination of TLCs with lipid standards as well as mass spectrometry of the spots. Detailed information on how spot identities were assigned can be found in the Appendix **(Supplementary section 2.1 – TLC spot identification, Figure S2.4, Table S2.3)**.

Spot intensities of Lys-PG were decreased in Δ*mprF2*, Δ*mprF1*Δ*mprF2* but not in wild type and Δ*mprF1* in both the ^{14}C radiolabelled and iodine-stained TLC plates. This decrease was restored upon complementation with p*mprF2*-HA **(Figure 2.3A, B)**. These findings are consistent with the reduced Lys-PG levels in the MRM analysis **(Figure 2.2A)**. There is also a nearly 2x increase in intensities of a phosphorus containing spot of unknown identity, together with the slight increase in a D-ala-GPDGDAG spot intensity in Δ*mprF2*, Δ*mprF1*Δ*mprF2* but not Δ*mprF1* when compared to the wild type in the ^{14}C radiolabelled samples. These increases can be complemented by p*mprF2*-HA

(Figure 2.3A, B). The spot intensities of GPDGDAG and the PG and CL spot intensities do not appear to be vastly different across the different mutants **(Figure 2.3A, B)**. Though there seems to be some differences in the DGDAG spot, the trend is not very clear **(Figure 2.3A, B)**. Positions of PG, CL and Lys-PG can be confirmed based on the standards in the iodine-stained TLC plate **(Figure 2.3A)**. Interestingly, we also observed an absence of a spot above DGDAG present in the ^{14}C radiolabelled TLC that is not iodine-stained in Δ*mprF2* and Δ*mprF1*Δ*mprF2* that is otherwise present in the rest of the samples **(Figure 2.3A).** It is unknown as to what this spot corresponds to, which warrants future investigation.

To verify if GPDGDAG levels were significantly altered in the mutants, semi-quantitative mass spectrometry analysis was performed on the species GPDGDAG 34:1 that was previously determined to be the most abundant amongst the class (Rashid et al., 2017) **(Figure 2.3C)**. MRMs were not possible due the lack of a commercially available standard. But semi-quantitative analysis showed that GPDGDAG 34:1 levels were increased as compared to the wild type across the *mprF* mutants in increasing order from Δ*mprF1*, Δ*mprF2*, Δ*mprF1*Δ*mprF2* with Δ*mprF1*Δ*mprF2* showing a 5-fold increase. This increase was not detected in the TLC possibly due to the low proportion of GPDGDAG in the samples and the inherent lower sensitivity of TLC-based assays.

Due to the uncertainty over the DGDAG spot intensities, we performed semi-quantitative MRMs for DGDAG in the *mprF* mutants using monoglucosyl-diacylglycerol (MGDAG) as a surrogate standard due to the lack of a commercially available one **(Figure 2.3D)**. Interestingly, Δ*mprF1* and Δ*mprF2* had increased levels over the wild type, while Δ*mprF1*Δ*mprF2* was not significantly altered **(Figure 2.3D)**. This trend was also observed across most of the DGDAG species **(Supplementary Figure S2.2C)**.

To determine if there were any differences in PG and CL spot intensities, we performed 2 dimensional TLCs to further separate the co-migrating PG and CL spots in the first dimension **(Figure 2.3E).** Identities of the assigned spots were determined as explained in the Appendix **(Supplementary section 2.1 – TLC spot identification, Figure S2.4)**. We observed that the PG spot intensity had a barely noticeable decrease in the Δ*mprF1*Δ*mprF2* while CL appears to be slightly increased **(Figure 2.3E, F)**. This difference between PG spot intensities from TLC analysis and data from mass spectrometry-based analysis **(Figure 2.2D)** could also be due to the inherent lower sensitivity of TLC-based assays and justifies for the need of mass spectrometric based analysis where possible as a complementary method especially when differences are not as apparent.

Taken together, these data suggest that in the *mprF* mutants, and particularly in Δ*mprF1*Δ*mprF2*, the decrease in Lys-PG and PG appears to be compensated for by the increases in a phosphorus containing lipid of unknown identity, D-ala-GPDGDAG, GPDGDAG, as well as a slight increase in CL.

Since GPDGDAG was increased in the *mprF* mutants, it was possible that its downstream product, lipoteichoic acid – which is poly-glycerophosphate polymerised onto a GPDGDAG membrane anchor – might be affected as well. To investigate this, immunoblots of whole cell lysates and supernatant of wild type and the *mprF* mutants were carried out **(Supplementary Figure S2.5)**. We observed no difference in LTA levels in the whole cell lysates, and LTA shedding was not detected in the supernatants of any strain, suggesting that LTA levels remain unchanged in these mutant backgrounds **(Supplementary Figure S2.5)**.

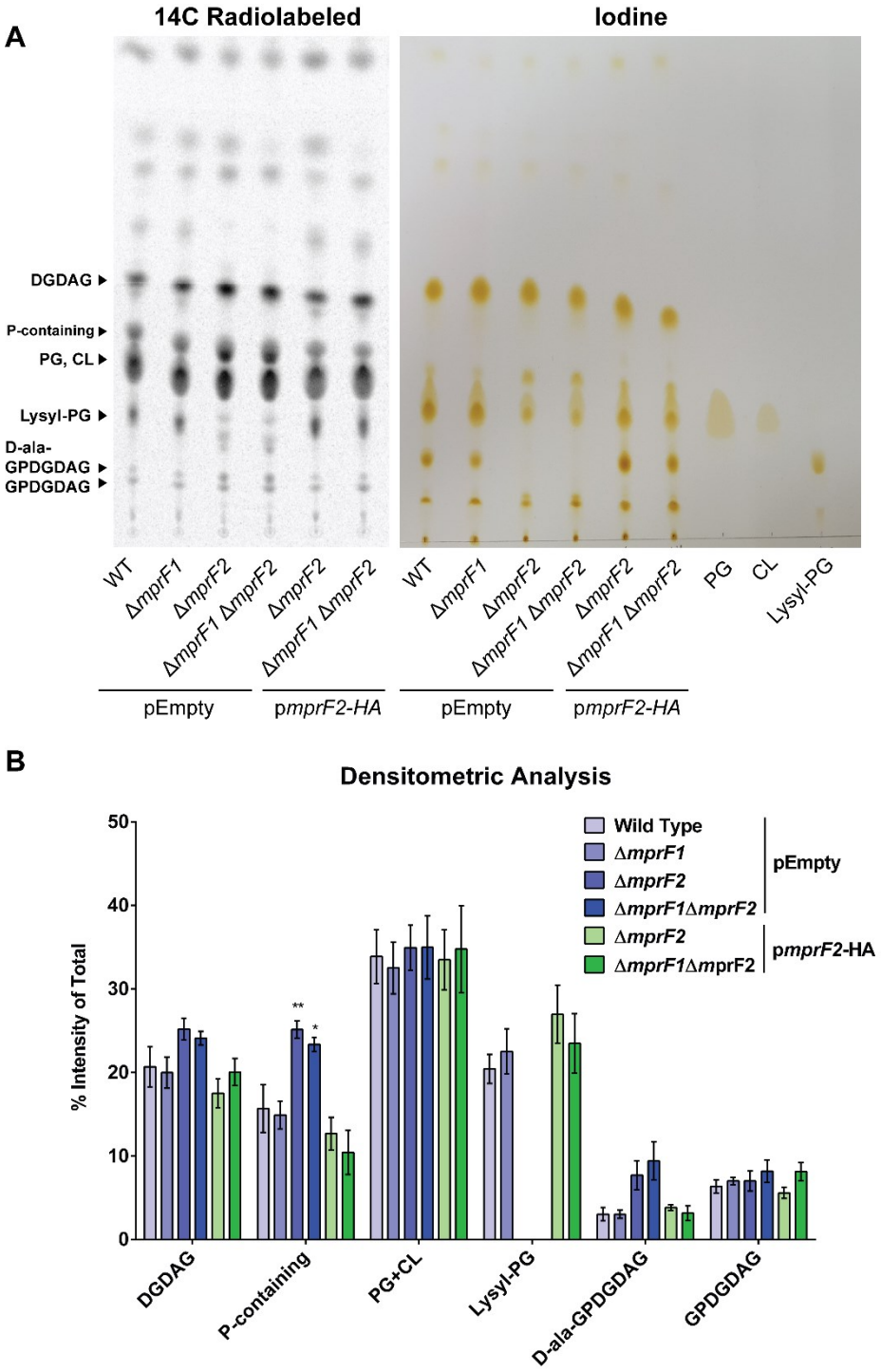
A
14C Radiolabeled
Iodine
DGDAG
P-containing
PG, CL
Lysyl-PG
D-ala-GPDGDAG
GPDGDAG
WT
ΔmprF1
ΔmprF2
ΔmprF1 ΔmprF2
ΔmprF2
ΔmprF1 ΔmprF2
WT
ΔmprF1
ΔmprF2
ΔmprF1 ΔmprF2
ΔmprF2
ΔmprF1 ΔmprF2
PG
CL
Lysyl-PG
pEmpty
pmprF2-HA
pEmpty
pmprF2-HA
B
Densitometric Analysis
% Intensity of Total
50
40
30
20
10
0
Wild Type
ΔmprF1
ΔmprF2
ΔmprF1ΔmprF2
ΔmprF2
ΔmprF1ΔmprF2
pEmpty
pmprF2-HA
**
*
DGDAG
P-containing
PG+CL
Lysyl-PG
D-ala-GPDGDAG
GPDGDAG

C

Relative levels of GPDGDAG 34:1	
Strain	% of Wild type
Wild type	100
ΔmprF1	226
ΔmprF2	443
ΔmprF1 ΔmprF2	500

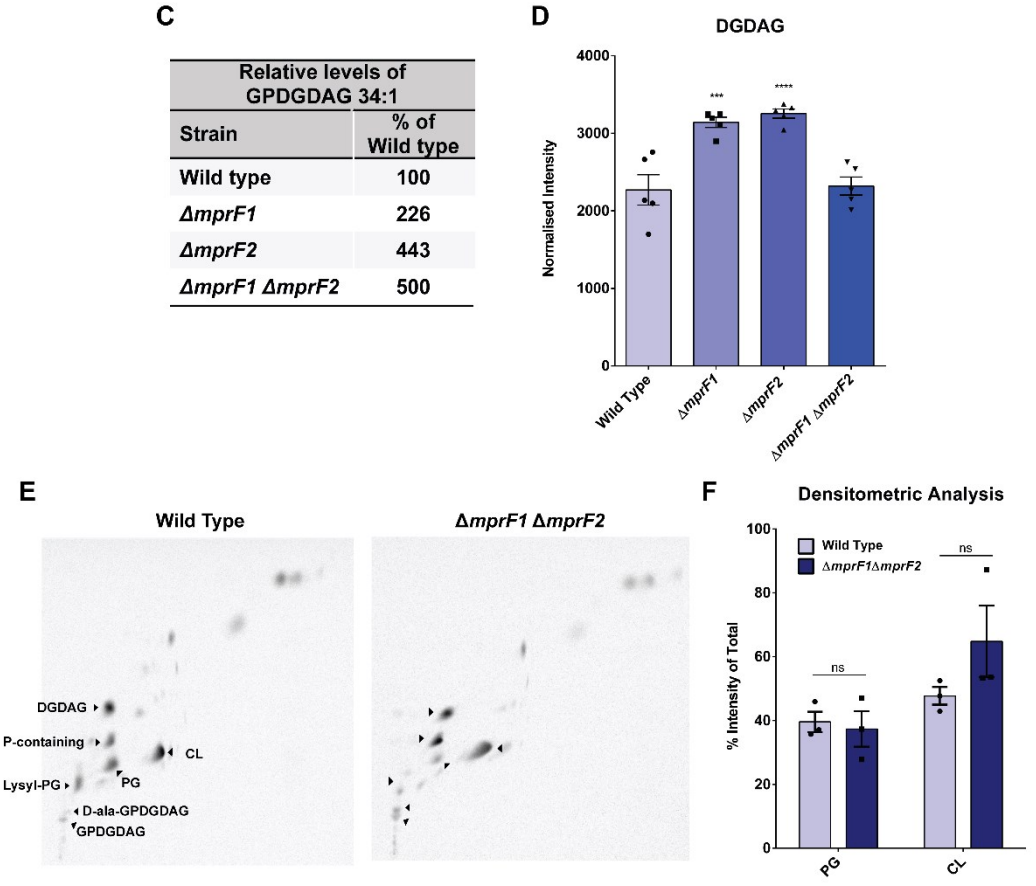

Figure. 2.3. *mprF* deletion results in lipidomic changes in other lipid classes. (A) Representative ^{14}C radiolabelled and iodine stained 1D-TLC of lipid extracts from the *mprF* mutants using chloroform: methanol: water (65:25:4). Identification of the lipid spots can be found in the supplement (Supplementary section S2.1). **(B)** Densitometric analysis of ^{14}C radiolabelled 1D TLC spots. Each bar represents the mean ± standard error of measurement calculated from 4 biological replicates. **(C)** Semiquantitative analysis of dominant GPDGDAG species, GPDGDAG 34:1. **(D)** Semiquantitative quantification of DGDAG levels across the *mprF* mutants. Each bar represents the mean ± standard error of measurement calculated from 5 biological replicates. Samples concentrations were obtained using a MGDAG 34:1 standard curve and normalised against dry sample weight. **(E)** Representative 2D-TLC of lipid extracts from wild type and *ΔmprF1ΔmprF2* for further spot separation to visualise changes in PG and CL. **(F)** Densitometric analysis of ^{14}C radiolabelled 2D TLC spots. Each bar represents the mean ± standard error of measurement calculated from 3 biological replicates. Statistical comparisons made for mutants against wild type. *, p=0.05 to 0.01; **, p=0.001 to 0.01; ***, p 0.0001 to 0.001; ****, p less than 0.0001; Fisher's LSD test for ANOVA.

2.3.3. *mprF* deletion decreases expression of genes involved in fatty acid biosynthesis

Having observed unexpected global membrane lipid changes in the *mprF* mutants, we hypothesized that there might be transcriptomic changes in genes related to phospholipid and general lipid metabolism. Based on a previously conducted RNAseq experiment in the lab comparing wild type and the three *mprF* mutant strains, while there were no transcriptional change in genes involved in phospholipid biosynthesis or *pgsA* (involved in PG synthesis), there was a global downregulation of genes in the *de novo* fatty acid biosynthesis pathway (Kelvin Chong, Adeline Yong, Swaine Chen, unpublished) **(Supplementary Table S2.4)**. To verify the findings of the RNAseq results, real time quantitative PCR (RT-qPCR) was performed for *pgsA* and the implicated genes of *de novo* fatty acid biosynthesis (*accA, accB, accC, accD, fabD, fabF2, fabG3, fabK,* and *fabZ2*) in the wild type and Δ*mprF1*Δ*mprF2* **(Figure 2.4)**. Δ*mprF1*Δ*mprF2* displayed significant downregulation of the *de novo* fatty acid biosynthesis genes of about half the levels of the wild type ($p \leq 0.0001$), which is consistent with the RNAseq data **(Figure 2.4)**. However, there was also a slight increase in *pgsA* expression in Δ*mprF1*Δ*mprF2* ($P = 0.001$ to 0.01) observed **(Figure 2.4)**. This could explain the PG levels being higher in Δ*mprF1*Δ*mprF2* and compared to Δ*mprF2*.

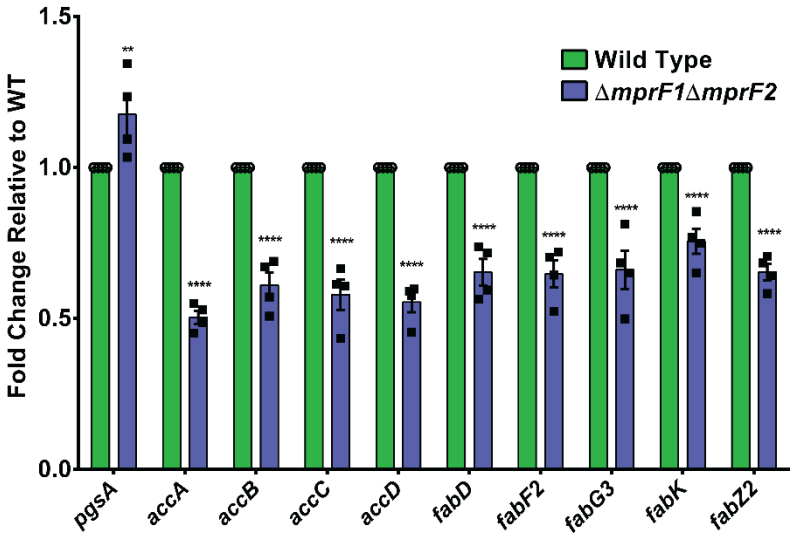

Figure 2.4. Loss of *mprF* leads to downregulation of fatty acid biosynthesis genes. RT-qPCR of mid-log phase cultures of wild type and Δ*mprF1*Δ*mprF2* showing a slight increase in *pgsA* and decrease in fatty acid biosynthesis gene expression levels. Each bar represents the mean ± standard error of measurement calculated from 4 biological replicates with 3 technical replicates. Each biological replicate consists of averaged values from its constituent technical replicates. Statistical comparisons made for Δ*mprF1*Δ*mprF2* against wild type. **, p=0.001 to 0.01; ****, p⩽0.0001; Fisher's LSD test for ANOVA.

2.3.4. Palmitic acid, Stearic acid and Arachidic acid restores *mprF* growth in chemically defined media (CDM)

Since genes encoding *de novo* fatty acid biosynthesis enzymes were downregulated in Δ*mprF1*Δ*mprF2*, we speculated that *E. faecalis* must have a strategy for Δ*mprF1*Δ*mprF2* to overcome this downregulation to allow for unaffected growth. It has been previously reported that *E. faecalis* can incorporate exogenous fatty acids into its membrane (Saito et al., 2017). Since BHI (the growth media used in the preceding experiments) is likely to be abundant in fatty acids, we hypothesized that *E. faecalis* might be utilising free fatty acids present in BHI to overcome the downregulation in *de novo* fatty acid biosynthetic genes. To test this, we grew the *mprF* mutants in a more nutrient-limited chemically defined media (CDM) that does not contain any fatty acids **(Figure 2.5A)**. As predicted, we observed growth defects for the *mprF* mutants in CDM, which had lower absorbance at the stationary phase than the wild type, where the Δ*mprF1*Δ*mprF2* had an extended lag phase of about 51 hours from the 34-36 hours lag phase observed in the single mutants and the wild type **(Figure 2.5A, F)**.

To determine which missing fatty acids in CDM that might be supporting growth in BHI, fatty acids in BHI were analysed by GC-FAME. Palmitic acid ($C_{16:0}$) and stearic acid ($C_{18:0}$) were the only fatty acids detected in BHI **(Supplementary Table S2.5)**. To confirm the potential role of these two fatty acids in supporting growth of Δ*mprF1*Δ*mprF2*, they were supplemented into CDM individually at 500, 250 and 125 ng/mL **(Figure 2.5B, C)**. Supplementing with either palmitic or stearic acid resulted in significant enhancement in specific growth rates (doubling time) and stationary phase absorbances in Δ*mprF1*Δ*mprF2* close to wild type levels at lower concentrations of 125 ng/mL of either fatty acid **(Figure 2.5B, C, F)**. This effect however is dose dependent, where higher concentrations

of either fatty acid is either inhibitory or less effective at enhancing growth, which become growth promoting at lower concentrations **(Figure 2.5B, C, F)**.

Next, palmitic, and stearic acid were added into CDM in similar ratios (3:1) as they were present in BHI **(Supplementary Table S2.5)**. Supplementation at higher concentrations of 1, 5 and 10 µg/mL of total fatty acid in the palmitic:stearic acid (3:1) mix, resulted in no growth of both wild type and Δ*mprF1*Δ*mprF2* (data not shown). At lower concentrations of 250 and 500 ng/mL, this fatty acid mix was still growth inhibitory to both the wild type and Δ*mprF1*Δ*mprF2* by increasing the lag phase duration and/or reducing stationary phase absorbance values. However, at 125 ng/mL, palmitic:stearic acid (3:1) had growth promoting effects on Δ*mprF1*Δ*mprF2* by increasing stationary phase absorbance close to wild type levels, reduced lag phase duration and increasing specific growth rates **(Figure 2.5D, F)**. At increasingly lower concentrations of 62.5 and 31.25 ng/mL, there was less pronounced growth enhancement in Δ*mprF1*Δ*mprF2* in terms of stationary phase absorbance values, growth rates and specific growth rates. At 15.63 ng/mL, supplementation failed to rescue the growth of Δ*mprF1*Δ*mprF2* and instead was inhibitory to growth in terms of stationary phase absorbance values **(Figure 2.5E)**. In the wild type, all supplementations appear to decrease the lag phase time while decreasing stationary phase absorbance values **(Figure 2.5A-F)**. Taken together there seems to be a dose dependent enhancement in growth when supplementing with either or both fatty acids, where 125 ng/mL of fatty acid is optimal and higher or lower concentrations results in reduced enhancement or inhibition **(Figure 2.5A-F).**

It had been previously reported that *E. faecalis* responds differently to supplementation of individual fatty acid species and supplementation of unsaturated fatty acids may override inhibition of *de novo* fatty acid biosynthesis

by cerulenin (Saito et al., 2017). We therefore hypothesized that other fatty acids might support the growth of Δ*mprF1*Δ*mprF2*, since its *de novo* fatty acid biosynthesis genes are also downregulated. To investigate this, wild type and Δ*mprF1*Δ*mprF2* were grown in CDM supplemented with a single species of unsaturated fatty acids: palmitoleic acid ($C_{16:1\ cis-9}$), oleic acid ($C_{18:1\ cis-9}$), *cis*-vaccenic acid ($C_{18:1\ cis-11}$) or linoleic acid ($C_{18:2\ cis-9,12}$); or saturated fatty acids: lauric acid ($C_{12:0}$), myristic acid ($C_{14:0}$), palmitic acid ($C_{16:0}$), stearic acid ($C_{18:0}$) or arachidic acid ($C_{20:0}$) at similar concentrations of 5 µg/mL **(Supplementary Figure S2.8)**.

For unsaturated fatty acids, supplementation of either palmitoleic acid ($C_{16:1\ cis-9}$), oleic acid ($C_{18:1\ cis-9}$), *cis*-vaccenic acid ($C_{18:1\ cis-11}$) or linoleic acid ($C_{18:2\ cis-9,12}$) led to delayed and reduced growth in both wild-type and Δ*mprF1*Δ*mprF2* **(Supplementary Figure S2.8A, B)**.

For the saturated fatty acids, wild type growth was negatively affected when supplemented with myristic acid ($C_{14:0}$) and palmitic acid ($C_{16:0}$), while lauric acid ($C_{12:0}$), stearic acid ($C_{18:0}$) and arachidic acid ($C_{20:0}$) had relatively minor effects on growth **(Supplementary Figure S2.8C, D)**. In Δ*mprF1*Δ*mprF2*, lauric acid ($C_{12:0}$), myristic acid ($C_{14:0}$), palmitic acid ($C_{16:0}$) and stearic acid ($C_{18:0}$) had negative effects on growth while arachidic acid ($C_{20:0}$) promoted growth slightly **(Supplementary Figure S2.8C, D)**. At lower concentrations of arachidic acid, growth enhancement became even more pronounced with stationary phase absorbance approaching wild type levels at 1 µg/mL supplementation, even though growth was still delayed **(Supplementary Figure S2.8E)**.

For both unsaturated and saturated fatty acid supplementations in CDM, growth inhibition was more intense than previously reported in BHI (Saito et al., 2017). This could be due to the different composition of CDM and its complete absence of exogenous fatty acids.

Taken together, these findings suggest that the *mprF* mutants may utilise the exogenous fatty acids palmitic and stearic acid for survival when *de novo* fatty acid biosynthesis is downregulation. Arachidic acid may also promote the growth of *mprF* mutants. However, it is important to note that neither of these supplementations brought growth back to levels seen in BHI, suggesting that there might be other missing components in CDM that are needed to support growth.

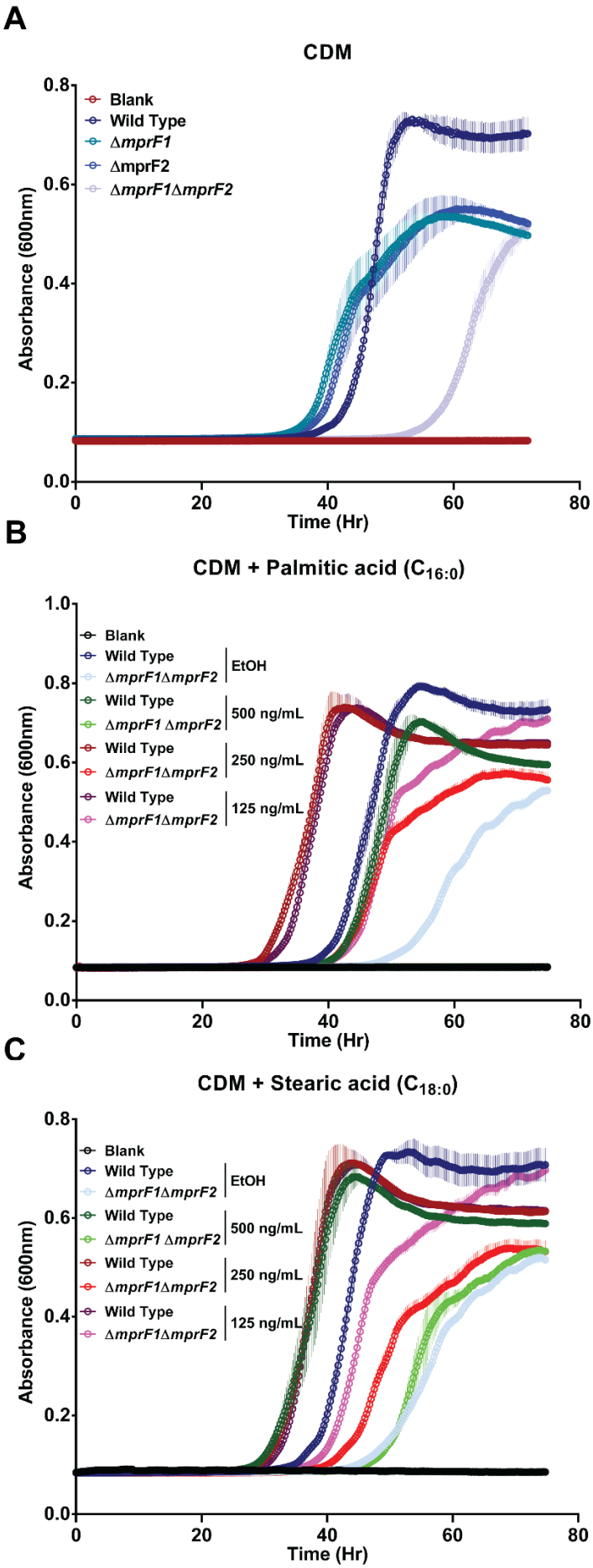
A
CDM
Blank
Wild Type
ΔmprF1
ΔmprF2
ΔmprF1ΔmprF2
Absorbance (600nm)
Time (Hr)
B
CDM + Palmitic acid (C16:0)
EtOH
500 ng/mL
250 ng/mL
125 ng/mL
C
CDM + Stearic acid (C18:0)

D

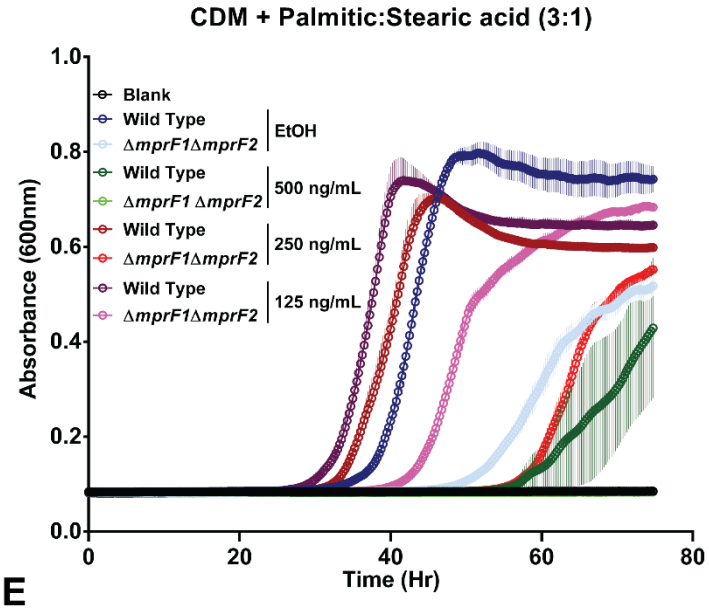
CDM + Palmitic:Stearic acid (3:1)
Absorbance (600nm)
Time (Hr)
Blank
Wild Type
ΔmprF1ΔmprF2
EtOH
Wild Type
ΔmprF1 ΔmprF2
500 ng/mL
Wild Type
ΔmprF1ΔmprF2
250 ng/mL
Wild Type
ΔmprF1ΔmprF2
125 ng/mL

E

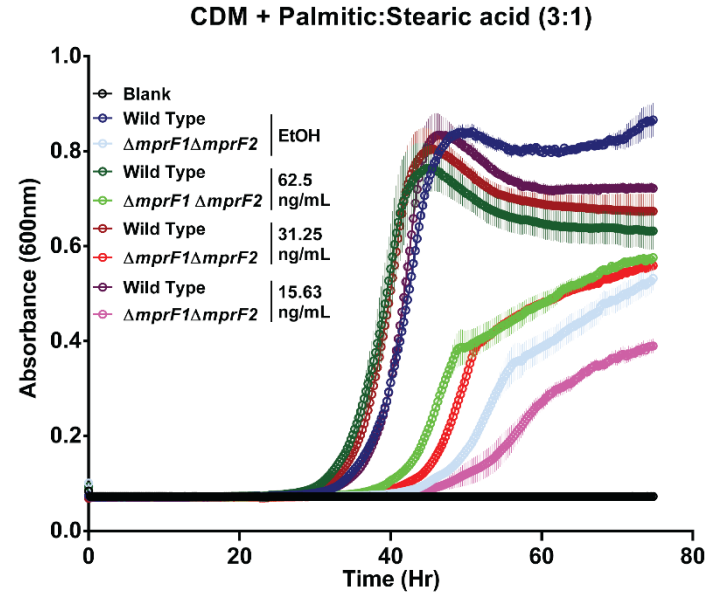
CDM + Palmitic:Stearic acid (3:1)
Absorbance (600nm)
Time (Hr)
Blank
Wild Type
ΔmprF1ΔmprF2
EtOH
Wild Type
ΔmprF1 ΔmprF2
62.5 ng/mL
Wild Type
ΔmprF1ΔmprF2
31.25 ng/mL
Wild Type
ΔmprF1ΔmprF2
15.63 ng/mL

F

Figure	Strain	Supplement	Concentration (ng/mL)	Mean specific growth rate (h^{-1})		Mean endpoint absorbance (600nm)		Mean lag phase duration (h)
2.5A	WT	-	-	0.215 ± 0.022	-	0.702 ± 0.048	-	36
	Δ*mprF1*	-	-	0.151 ± 0.026	ns	0.497 ± 0.017	***	35
	Δ*mprF2*	-	-	0.178 ± 0.036	ns	0.521 ± 0.009	***	34
	Δ*mprF1* Δ*mprF2*	-	-	0.142 ± 0.015	ns	0.518 ± 0.029	***	51
2.5B	WT	EtOH	-	0.182 ± 0.007	-	0.733 ± 0.039	-	37
		Palmitic acid	500.00	0.182 ± 0.019	ns	0.594 ± 0.008	***	39
		Palmitic acid	250.00	0.174 ± 0.017	ns	0.644 ± 0.012	**	27
		Palmitic acid	125.00	0.193 ± 0.009	ns	0.649 ± 0.006	*	29
	Δ*mprF1* Δ*mprF2*	EtOH	-	0.090 ± 0.019	-	0.529 ± 0.020	-	46
		Palmitic acid	500.00	No growth	-	No growth	-	No growth
		Palmitic acid	250.00	0.167 ± 0.017	**	0.556 ± 0.028	ns	39
		Palmitic acid	125.00	0.188 ± 0.004	**	0.710 ± 0.015	***	39
2.5C	WT	EtOH	-	0.177 ± 0.011	-	0.708 ± 0.049	-	34
		Stearic acid	500.00	0.149 ± 0.017	ns	0.589 ± 0.006	**	26
		Stearic acid	250.00	0.177 ± 0.019	ns	0.613 ± 0.015	*	26
		Stearic acid	125.00	0.198 ± 0.005	ns	0.614 ± 0.003	*	26
	Δ*mprF1* Δ*mprF2*	EtOH	-	0.108 ± 0.011	-	0.516 ± 0.015	-	43
		Stearic acid	500.00	0.164 ± 0.029	*	0.533 ± 0.011	ns	44
		Stearic acid	250.00	0.133 ± 0.015	ns	0.532 ± 0.032	ns	38
		Stearic acid	125.00	0.189 ± 0.006	**	0.697 ± 0.015	****	36
2.5D	WT	EtOH	-	0.210 ± 0.001	-	0.743 ± 0.040	-	34
		Palmitic + Stearic acid	500.00	0.074 ± 0.048	**	0.429 ± 0.209	*	54
		Palmitic + Stearic acid	250.00	0.169 ± 0.010	ns	0.599 ± 0.008	ns	32
		Palmitic + Stearic acid	125.00	0.199 ± 0.007	ns	0.646 ± 0.015	ns	29
	Δ*mprF1* Δ*mprF2*	EtOH	-	0.106 ± 0.008	-	0.518 ± 0.031	-	49
		Palmitic + Stearic acid	500.00	No growth	-	No growth	-	No growth
		Palmitic + Stearic acid	250.00	0.162 ± 0.034	ns	0.552 ± 0.017	ns	54
		Palmitic + Stearic acid	125.00	0.179 ± 0.012	*	0.683 ± 0.004	***	39
2.5E	WT	EtOH	-	0.194 ± 0.014	-	0.866 ± 0.050	-	32
		Palmitic + Stearic acid	62.50	0.189 ± 0.014	ns	0.632 ± 0.055	**	30
		Palmitic + Stearic acid	31.25	0.222 ± 0.004	ns	0.674 ± 0.051	**	31
		Palmitic + Stearic acid	15.63	0.241 ± 0.010	**	0.722 ± 0.016	*	32
	Δ*mprF1* Δ*mprF2*	EtOH	-	0.139 ± 0.033	-	0.532 ± 0.035	-	42
		Palmitic + Stearic acid	62.50	0.165 ± 0.014	ns	0.576 ± 0.012	ns	38
		Palmitic + Stearic acid	31.25	0.179 ± 0.003	ns	0.559 ± 0.019	ns	40
		Palmitic + Stearic acid	15.63	0.100 ± 0.035	ns	0.390 ± 0.021	***	44

Figure 2.5. *mprF* mutants display a growth defect when grown in chemically defined media (CDM) which can be rescued by a combination of palmitic and stearic acid. (A) Growth curves of wild type and *mrpF* mutants grown in chemically defined media. Growth curves of wild type and Δ*mprF1*Δ*mprF2* grown under fatty acid supplementation of **(B)** palmitic acid ($C_{16:0}$), **(C)** stearic acid ($C_{18:0}$), and **(D, E)** a combination of palmitic and stearic acid in a 3:1 ratio at varying concentrations. Equal volumes of ethanol (EtOH) were used as the solvent control for comparison. Each data point represents the mean ± standard error of measurement calculated from 3 biological replicates with 3 technical replicates each. Each biological replicate consists of averaged values from its constituent technical replicates. **(F)** Calculated specific growth rate (doubling time), lag phase duration and end point absorbances for each of the graphs are shown. *, p=0.05 to 0.01; **, p=0.001 to 0.01; ***, p=0.0001 to 0.001; ****, p≤0.0001; Dunnett's test for ANOVA. Comparisons made between each fatty acid concentration against the EtOH solvent control of the respective strain.

2.3.5. Fatty acid profiles are altered in the *mprF* mutants in both BHI and CDM

Since genes in the *de novo* fatty acid biosynthesis pathway are downregulated and growth impaired when Δ*mprF1*Δ*mprF2* was grown in CDM, it seemed likely that the fatty acid profiles of *mprF* mutants would be different from wild type in BHI versus CDM. To investigate this, GC-FAME was conducted on lyophilised cell pellets of the wild type and Δ*mprF1*Δ*mprF2* grown to stationary phase in either BHI or CDM **(Figure 2.6)**. Similar to previous reports, *E. faecalis* fatty acid composition is dominated by palmitic acid ($C_{16:0}$) and *cis*-vaccenic acid ($C_{18:1\ \omega7\ cis}$) (Chilambi et al., 2018; Saito et al., 2014) **(Figure 2.6, Supplementary Table S2.6)**.

As compared to the wild type, Δ*mprF1*Δ*mprF2* had a largely similar fatty acid profile in BHI with a slight increase of ~2% in palmitic acid ($C_{16:0}$) and a slight decrease of ~2% in stearic acid ($C_{18:0}$). However, in CDM, Δ*mprF1*Δ*mprF2* had a large increase of ~11% in palmitic acid ($C_{16:0}$) coupled with decreases of ~11% in *cis*-vaccenic acid ($C_{18:1\ \omega7\ cis}$) and ~2.5% in $C_{19\ cyclo\ \omega7}$ as compared to the wild type **(Figure 2.6)**. Furthermore, in CDM, $C_{14:1\ \omega5\ cis}$, $C_{17:1\ \omega7\ trans}$, $C_{19:1\ \omega9\ trans}$ were detected in Δ*mprF1*Δ*mprF2* at low abundances of about 0.11-0.16% of total fatty acids that were absent in the wild type **(Supplementary Table S2.6)**.

As compared to BHI, wild type grown in CDM possessed a slight decrease of 2% and 3% in palmitic acid ($C_{16:0}$) and stearic acid ($C_{18:0}$), respectively, coupled with a ~6% increase in *cis*-vaccenic acid ($C_{18:1\ \omega7\ cis}$) **(Figure 2.6)**. In CDM, $C_{16:1\ \omega6\ cis}$ and $C_{18:1\ \omega9\ cis}$ were absent in the wild type but present in BHI, while $C_{19:1\ \omega7\ cis}$ and $C_{19:1\ \omega7\ trans}$ were detected in CDM and were absent in BHI **(Supplementary Table S2.6)**. These fatty acids were present at low abundances of less than 1% of total fatty acids.

When Δ*mprF1*Δ*mprF2* was grown in CDM, it possessed a ~7% increase in palmitic acid ($C_{16:0}$) and ~5% decrease in *cis*-vaccenic acid ($C_{18:1\ \omega7\ cis}$) and ~3.5% decrease in $C_{19\ cyclo\ \omega7}$ as compared to growth in BHI **(Figure 2.6)**. Similarly, in CDM, $C_{16:1\ \omega6\ cis}$ and $C_{18:1\ \omega9\ cis}$ were absent in wild type but present in BHI, while $C_{14:1\ \omega5\ cis}$, $C_{17:1\ \omega7\ trans}$, $C_{19:1\ \omega9\ trans}$, $C_{19:1\ \omega7\ cis}$ and $C_{19:1\ \omega7\ trans}$ were detected in CDM but absent in BHI **(Supplementary Table S2.6)**. Likewise, these fatty acids were present at low abundances of less than 1% of total fatty acids.

Taken together, these findings suggest that the way Δ*mprF1*Δ*mprF2* alters its fatty acid composition when switching from BHI to CDM is very different from the way wild type does so. The wild type makes less $C_{16:0}$ and more $C_{18:1\ \omega7c}$ in CDM while Δ*mprF1*Δ*mprF2* displays the opposite with more $C_{16:0}$ and less $C_{18:1\ \omega7c}$. This difference could be the reason, or the consequence, of the growth defect observed for Δ*mprF1*Δ*mprF2* in CDM.

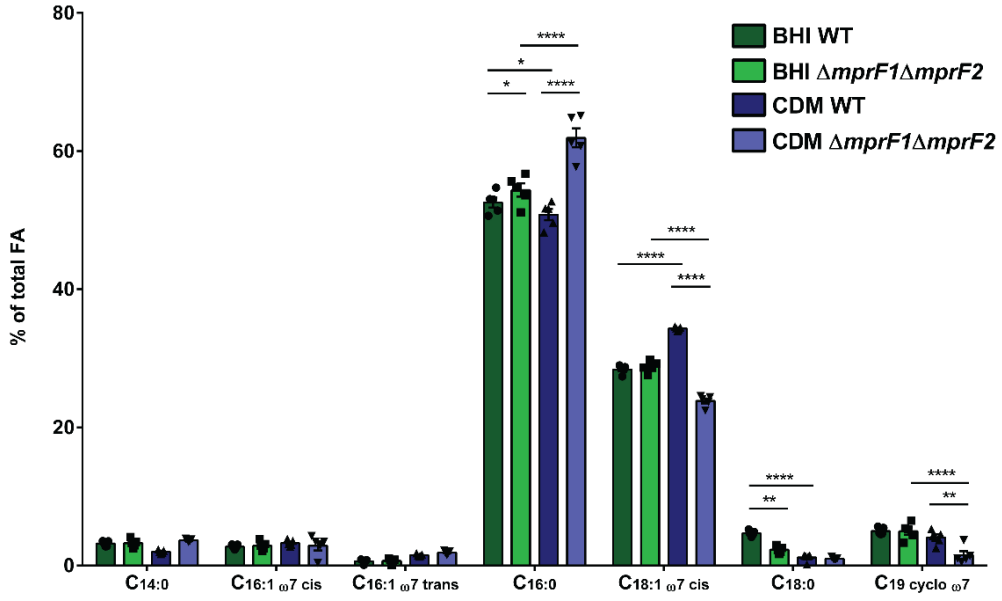

Figure 2.6. *mprF* mutants display an altered fatty acid profile when grown in CDM as compared to the wild type. GC-FAME analysis of fatty acids in WT and Δ*mprF1*Δ*mprF2* grown to stationary phase in either BHI or CDM. The most abundant fatty acid species that account for at least 1% or more of the total fatty acids (FA) present within the sample are displayed here. The full list of detected fatty acid methyl esters are shown in Supplementary Table S2.6. Each bar represents the mean ± standard error of measurement calculated from 5 biological replicates. *, p=0.05 to 0.01; **, p=0.001 to 0.01; ****, p≤0.0001; Tukey test for ANOVA.

2.3.6. Envelope and barrier-stress sensing two-component systems (TCS) are not involved in survival of *mprF* mutants

Changes in the lipidome and transcriptomic downregulation of *de novo* fatty acid biosynthesis genes in the *mprF* mutants may impart some amount of membrane stress to these strains. Previous transcriptional analysis revealed the upregulation of genes in the arginine deiminase pathway (*arcAB* and *arcC*) as well as stress response related genes *gls24,* general stress proteins, *gspA1* and *gspA2* in Δ*mprF1*Δ*mprF2* as compared to wild type (Kelvin Chong, Adeline Yong, Swaine Chen, unpublished). *gls24* is involved in adaptation to stress conditions such as high bile-salt, cadmium ions and glucose starvation (Choudhury et al., 2011; Teng et al., 2005). Furthermore, the upregulation of the arginine deiminase pathway is frequently associated with stress responses to acid and oxidative stress in other Gram positive organisms (Cotter and Hill, 2003; Lindgren et al., 2014; Rochat et al., 2012). Taken together, these observations suggest that the *mprF* mutants are likely in a stressed state.

However, previously conducted growth kinetics assays performed in BHI revealed no growth defect in the mutants, and Δ*mrpF2* and Δ*mprF1*Δ*mprF2* grew faster and to a higher stationary phase absorbance than wild type (Dominic Chia). Furthermore, there was no observed difference in viability or increased membrane permeability to propidium iodide (PI) based on live-dead staining **(Supplementary Figure S2.3)**. These findings suggest that, in addition to the role of exogenous fatty acids described earlier, there could be some compensatory mechanisms at play that might be supporting *E. faecalis mprF* mutant growth, resulting in the lack of an observed fitness defect.

Hence, we hypothesized that there might be membrane stress present that are sensed by two component systems (TCSs) resulting in adaptations that allow for survival of the *mprF* mutants. We shortlisted the WalKR essential two-

component system as a potential candidate since it has been reported that in *Streptococcus pneumoniae* that YycF (WalR) modulates expression of fatty acid biosynthesis genes (Mohedano et al., 2005). Though not directly involved in lipid homeostasis, we also shortlisted TCS candidates, LiaFSR and CroRS which have known functions in sensing cell barrier and envelope stress that could be involved in generating compensatory responses for investigation (Djorić and Kristich, 2015; Eldholm et al., 2010; Kellogg and Kristich, 2016; Suntharalingam et al., 2009).

To investigate the role of these two-component systems, we utilised a dual plasmid nisin-inducible CRISPR interference (CRISPRi) system for *E. faecalis* (Afonina et al., 2020) to knock down *walKR*, *liaFSR* and *croRS* expression by targeting the first gene of each of their respective operons (*walR ,liaF* and *croR*). In this system, dCas9 and respective guide RNAs targeting the selected TCS genes for knockdown are placed in 2 separate plasmids under control of a nisin inducible promoter. When induced for expression by nisin, expression of these 2 components results in knockdown of the target gene.

Wild-type and Δ*mprF1*Δ*mprF2* containing these plasmids were induced for knockdown and growth kinetics measured to determine if any of the TCSs are responsible for supporting survival of *E. faecalis* in the absence of *mprF* **(Figure 2.7)**. We predicted that knockdown of any TCS required for normal growth in Δ*mprF1*Δ*mprF2* would attenuate this strain's growth as compared to wild type. At low nisin induction of knockdown, targeting *liaF* or *croR* had mild effects on growth, whereby there is minimal changes in specific growth rates with a reduction in stationary phase absorbance values by 0.02 to 0.03 **(Figure 2.7A, D)**. However, at higher nisin induction of knockdown, targeting *liaF* or *croR* led to slowing of growth rates for both wild-type and Δ*mprF1*Δ*mprF2* **(Figure 2.7B, D)**. One reason for this could be that nisin being a membrane targeting antibiotic

could be causing increased membrane stress at higher concentrations that might be otherwise compensated by LiaFSR or CroRS signalling but is now unable to do so with these TCSs knocked down. Since the nisin promoter of this CRISPRi system has leaky expression, no induction was required for the knockdown of *walKR*, which is essential, conferring a growth defect in the wild type compared to the pEmpty vector control by reducing growth rates **(Figure 2.7C, D)**. Surprisingly, and opposite to our prediction, Δ*mprF1*Δ*mprF2* tolerates *walR* knockdown better than the wild type.

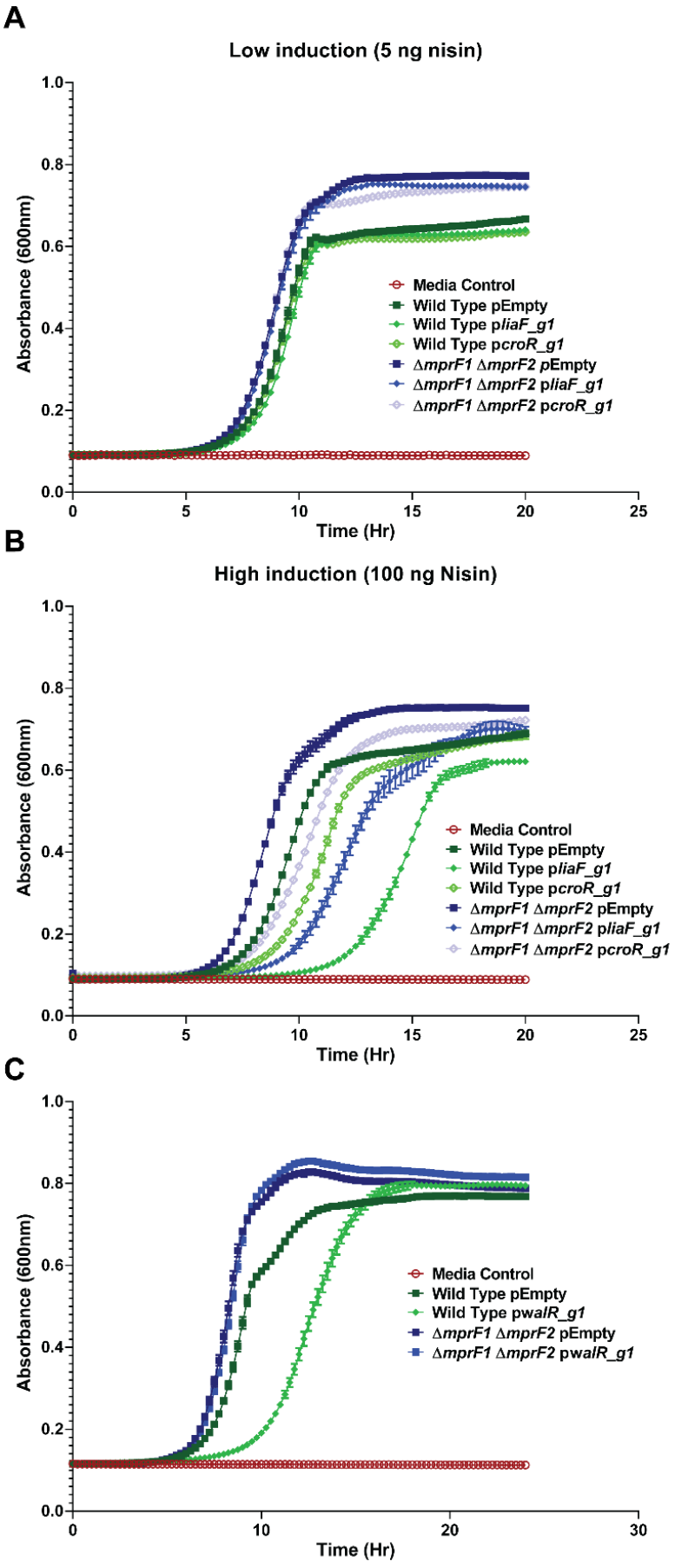
A
Low induction (5 ng nisin)
Absorbance (600nm)
Time (Hr)
Media Control
Wild Type pEmpty
Wild Type pliaF_g1
Wild Type pcroR_g1
ΔmprF1 ΔmprF2 pEmpty
ΔmprF1 ΔmprF2 pliaF_g1
ΔmprF1 ΔmprF2 pcroR_g1
B
High induction (100 ng Nisin)
Absorbance (600nm)
Time (Hr)
Media Control
Wild Type pEmpty
Wild Type pliaF_g1
Wild Type pcroR_g1
ΔmprF1 ΔmprF2 pEmpty
ΔmprF1 ΔmprF2 pliaF_g1
ΔmprF1 ΔmprF2 pcroR_g1
C
Absorbance (600nm)
Time (Hr)
Media Control
Wild Type pEmpty
Wild Type pwalR_g1
ΔmprF1 ΔmprF2 pEmpty
ΔmprF1 ΔmprF2 pwalR_g1

D

Figure	Strain	Plasmid	Nisin induction (ng/mL)	Mean specific growth rate (h^{-1})		Mean endpoint absorbance (600nm)		Mean lag phase duration (h)
2.5A	WT	pEmpty	5	0.468 ± 0.017	-	0.667 ± 0.009	-	5.25
		p*liaF*_g1	5	0.524 ± 0.012	*	0.641 ± 0.003	*	5.25
		p*croR*_g1	5	0.473 ± 0.018	ns	0.636 ± 0.010	*	5.25
	Δ*mprF1* Δ*mprF2*	pEmpty	5	0.467 ± 0.008	-	0.772 ± 0.003	-	5.25
		pliaF_g1	5	0.491 ± 0.020	ns	0.746 ± 0.003	****	5.25
		pcroR_g1	5	0.479 ± 0.007	ns	0.746 ± 0.002	****	5.25
2.5B	WT	pEmpty	100	0.427 ± 0.010	-	0.689 ± 0.004	-	5.50
		p*liaF*_g1	100	0.344 ± 0.041	*	0.621 ± 0.007	***	9.50
		p*croR*_g1	100	0.395 ± 0.007	ns	0.686 ± 0.014	ns	6.25
	Δ*mprF1* Δ*mprF2*	pEmpty	100	0.511 ± 0.020	-	0.751 ± 0.002	-	5.50
		pliaF_g1	100	0.337 ± 0.027	***	0.697 ± 0.014	**	6.75
		pcroR_g1	100	0.342 ± 0.006	***	0.722 ± 0.004	*	6.25
2.5C	WT	pEmpty	0	0.515 ± 0.013	-	0.768 ± 0.006	-	5.25
		p*walR*_g1	0	0.309 ± 0.002	****	0.795 ± 0.005	**	7.00
	Δ*mprF1* Δ*mprF2*	pEmpty	0	0.572 ± 0.013	-	0.788 ± 0.010	-	5.25
		pwalR_g1	0	0.580 ± 0.002	ns	0.815 ± 0.009	ns	5.25

Figure 2.7. LiaFSR, CroRS two-component systems (TCS) are not implicated in Δ*mprF1*Δ*mprF2* survival. However, the loss of WalKR signaling is better tolerated in Δ*mprF1*Δ*mprF2*. Growth curves of CRISPRi nisin-inducible knockdowns of selected TCS by targeting the first gene in the TCS operon under **(A)** low induction (5 ng nisin) and **(B)** high induction (100 ng nisin). **(C)** *walR* knockdown under leaky induction without inducer (0 ng nisin). Each data point represents the mean ± standard error of measurement calculated from 3 biological replicates with 3 technical replicates each. Each biological replicate consists of averaged values from its constituent technical replicates. **(D)** Calculated specific growth rate (doubling time), lag phase duration and end point absorbances for each of the graphs are shown. *, p=0.05 to 0.01; ***, p=0.0001 to 0.001; ****, p≤0.0001; Dunnett's test for ANOVA for figure 2.5A and B; T-test for figure 2.5C. Comparisons made between each plasmid against the pEmpty vector control of within each strain.

2.3.7. Loss of *mprF* leads to pleiotropic phenotypes

Membrane Fluidity

Based on the global changes in the lipidome we observed upon deletion of *mprF*, we expected that there might be concomitant changes in the cell physiology. The fluidity of the cell membrane is influenced by the amount of unsaturated lipids present, where a higher degree of unsaturation results in more fluid membranes (Alberts, 2002). Since the lysyl-PG species present in *E. faecalis* are predominantly unsaturated fatty acids and we observe decreases in them **(Figure S2.2A)**, coupled with alterations in lipid homeostasis, we hypothesized that membrane fluidity might be affected as well. Membrane fluidity was assayed using a fluorescent dye sensitive to fluidity changes, Laurdan. The dye inserts into membrane bilayers and depending on how liquid ordered (L_o) or disordered (L_d) the local lipid environment is, its emission spectra will blue-shift in L_o regions (rigid regions) or red-shift in L_d regions (fluid regions) respectively (Bach and Bramkamp, 2013; Harris et al., 2002). This spectral shift can be detected by measuring the green and blue wavelengths and expressing the readings as a ratio, generalised polarisation (GP), where higher GP values imply more rigid membranes and lower GP values imply more fluid membranes.

By staining late stationary phase cultures of the wild-type and *mprF* mutants with Laurdan and imaging cells by microscopy, we observed that Δ*mprF2* and Δ*mprF1*Δ*mprF2* had a slight increase in GP values indicating slightly more rigid membranes in these mutants as compared to the wild type (P = 0.0001 to 0.001), while Δ*mprF1* had no significant difference in GP values **(Figure 2.8A)**. Hence, this suggests that the lipidomic changes correlated with more rigid membranes in the *mprF* mutants.

To ensure that Laurdan and this assay can accurately measure differences in membrane fluidity, control experiments were conducted. Wild type cells were

incubated at a range of temperatures to ensure that the altered fluidity of the membrane across temperatures could be measured **(Supplementary Figure S2.6A)**. In another control experiment, membrane fluidizer, benzyl alcohol was also used to fluidize wild type membranes, which was successfully detected by a spectrophotometer in a microtiter plate format. A microplate format was used instead due to the technical difficulties in applying benzyl alcohol to microscope samples **(Supplementary Figure S2.6B)**. The higher GP value of Δ*mprF1*Δ*mprF2* as compared to the wild type was also accurately detected by this method **(Supplementary Figure S2.6B)**. Taken together, these experiments show that the Laurdan assay is sensitive and accurate enough in detecting for membrane fluidity changes, confirming that membranes of Δ*mprF1*Δ*mprF2* are indeed measured to be more rigid than the wild type.

Intriguingly, the ratios of saturated/unsaturated fatty acids were largely similar between the wild type and Δ*mprF1*Δ*mprF2*, suggesting that the fluidity differences is not due to the differences in saturation at a global level and might be influenced by other factors such as the differential packing of proteins within the lipid bilayer or presence of isoprenoid lipids within the membrane **(Supplementary Table S2.6)**.

Secretion

Efficient Sec-mediated secretion requires the presence of anionic lipids present in the vicinity of the Sec-secretion machinery (Crane and Randall, 2017; de Vrije et al., 1988; Koch et al., 2019; Kusters et al., 1991; Rosch et al., 2007). Given that the septum in *E. faecalis* are enriched in anionic lipids and components of the Sec-secretion machinery, it has been proposed that anionic lipid microdomains are present at this location (Kandaswamy et al., 2013; Kline et al., 2009). Since we observed increased membrane rigidity and altered lipid profiles in the *mprF* mutants, particularly the decrease in anionic PG, we predicted that

these anionic lipid microdomains may be disrupted and the functions of the resident Sec-machinery might also be affected. Consistent with this prediction, disruptions of microdomains has also been associated with impaired secretion in *B. subtilis* (Bach and Bramkamp, 2013).

To assess whether secretion is indeed affected in the *mprF* mutants, we quantified the overall proteins in the supernatants of overnight stationary phase of wild type and *mprF* mutants as a measure of bulk secretion. We observed significantly decreased bulk secretion ($P \leqslant 0.0001$) in the *mprF* mutants with the greatest decrease observed for Δ*mprF1*Δ*mprF2* (~50% decrease) followed by Δ*mprF2* (~40% decrease) and Δ*mprF1* (~25% decrease) **(Figure 2.8B)**.

To validate the disruption of Sec-mediated secretion, a chimeric alkaline phosphatase PhoZF (*E. faecalis* native PhoZ fused to the secretion domain of protein F from *S. pyogenes*) was expressed in wild type and the *mprF* mutants. As compared to the wild type, the *mprF* mutants displayed significant impairment in secretion ($P \leqslant 0.0001$) and Δ*mprF1*Δ*mprF2* showed the greatest reduction of almost half that of wild type **(Figure 2.8C)**.

Biofilm formation

It was previously reported in another strain, *E. faecalis* 12030, that the loss of *mprF* enhances biofilm formation (Bao et al., 2012). To determine if the same might occur in strain OG1RF, we assayed biofilm formation of the wild type and *mprF* mutants by growing them in microtiter plates with crystal violet staining for detection of adherent biomass. We observed slight increases in biofilm formation for the Δ*mprF1* and Δ*mprF2* mutants with a significant 2-fold increase for Δ*mprF1*Δ*mprF2* ($P \leq 0.001$) across all daily timepoints for the 5-day period tested, as compared to wild type **(Figure 2.8D)**. The previous study attributed this increase to higher extracellular DNA (eDNA) release in the *mprF* mutants (Bao

et al., 2012). This could also be occurring with our mutants and should be investigated in future experiments by measuring the extracellular DNA in biofilms using cell membrane impermeable DNA stains.

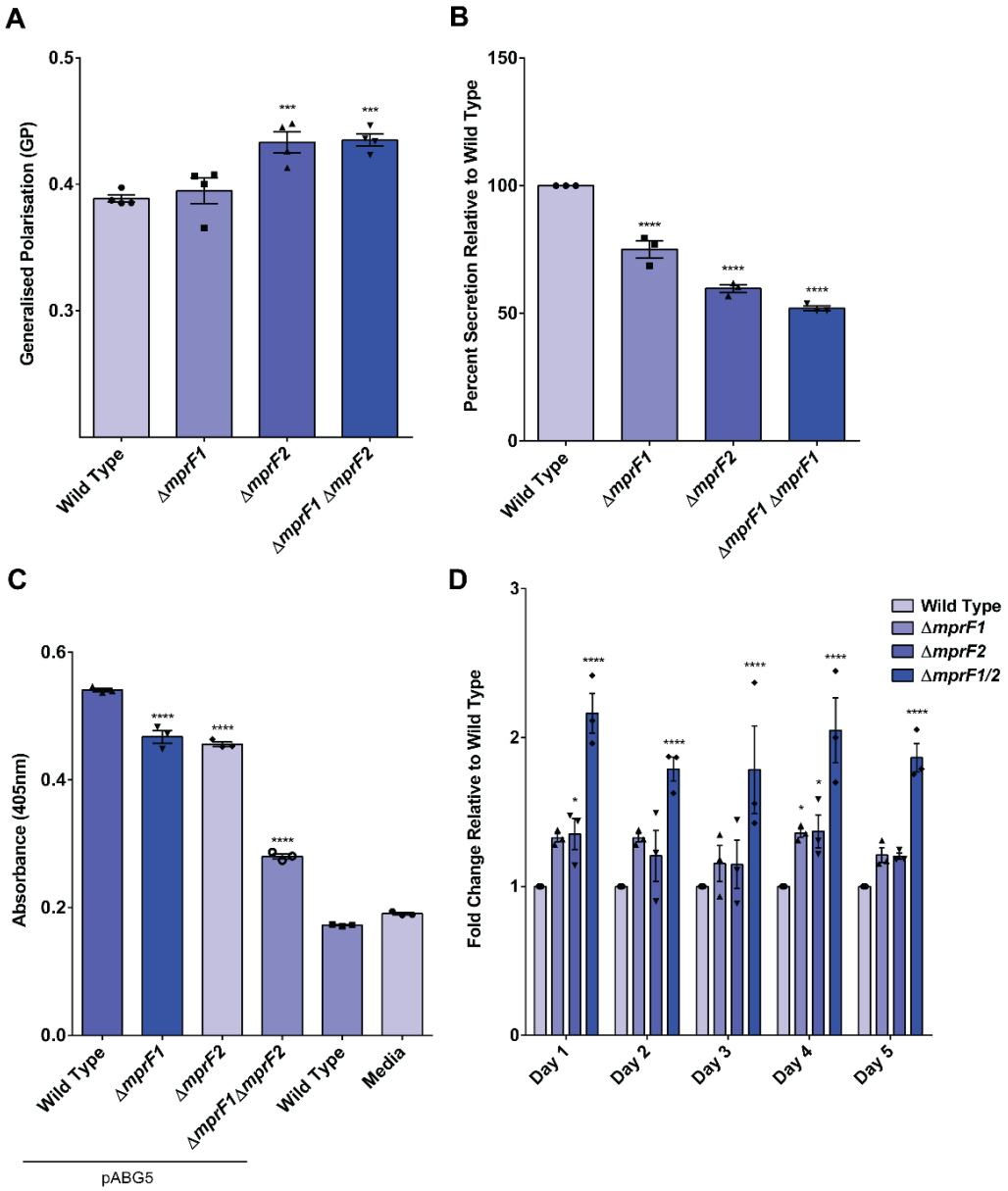

Figure. 2.8. *mprF* mutants exhibit pleiotropic phenotypes. (A) Overnight late stationary phase cultures were labelled with Laurdan and analyzed microscopically to assess for membrane fluidity changes. Higher GP values indicate more rigid membranes. Error bars represent the standard error of the mean of GP values from 4 separate experiments. Each experiment consists of 1 biological replicate with average GP values tabulated from >100 ROIs of cells/cell clusters. **(B)** Relative amounts of proteins secreted into the growth media by wild-type and mutant strains grown to late stationary phase are shown. Each bar represents the mean ± standard error of the mean calculated from 3

biological replicates with 3 technical replicates each. Each biological replicate consists of averaged values from its constituent technical replicates. **(C)** Relative amounts of alkaline phosphatase secreted into the growth media by wild-type and mutant strains growth to mid-logarithmic phase are shown. Each bar represents the mean ± standard error of the mean calculated from 3 biological replicates with 3 technical replicates each. Each biological replicate consists of averaged values from its constituent technical replicates. **(D)** Static biofilm assay with crystal violet staining across 5-days. Fold-change of absorbance 595nm readings of the crystal violet stain were reported. Each bar represents the mean ± standard error of the mean calculated from 3 biological replicates with 3 technical replicates each. Each biological replicate consists of averaged values from its constituent technical replicates. Statistical comparisons made for mutants against wild type. *, p=0.05 to 0.01; **, p=0.001 to 0.01; ***, p=0.0001 to 0.001; ****, p⩽ 0.0001; Fisher's LSD test for ANOVA.

2.3.8. *mprF* does not affect *in vivo* competitive gut colonisation

In a competitive wound infection model, wild type outcompetes another *E. faecalis* strain OG1X to a greater extent than does the Δ*mprF1*Δ*mprF2* mutant, suggesting that *mprF* contributes to fitness in this infection model (Chong et al., 2017). To determine if *mprF* affects fitness in another niche where CAMPs might be abundant, we tested wild type and Δ*mprF1*Δ*mprF2* in a competitive gut colonisation model **(Figure 2.9)**. We observed no significant difference in competitive indices for the cecum, cecum contents or the combination of both between wild type and Δ*mprF1*Δ*mprF2*, suggesting that *mprF* does not affect fitness in *in vivo* gut tissue colonisation **(Figure 2.9A)**. However, interestingly, the amount of viable Δ*mprF1*Δ*mprF2* recovered from the faeces was significantly higher than the wild type **(Figure 2.9B)**. Faecal competitive indices also reveal that Δ*mprF1*Δ*mprF2* outcompetes OG1X better than wild type OG1RF in the faeces **(Figure 2.9C)**.

To also determine how these strains fair in *in vitro* planktonic growth conditions, a competitive planktonic growth assay with OG1RF wild type and Δ*mprF1*Δ*mprF2* together with OG1X over the course of 24 hours. Δ*mprF1*Δ*mprF2* had significantly higher CFU/mL than OG1X at later timepoints of 4, 5, 6, 8 and 24 hours (P = 0.05 to 0.01), while CFU/mL values of OG1RF WT was similar to OG1X at all timepoints **(Supplementary Figure S2.7)**.

Taken together, these findings suggest that under co-culture with OG1X in planktonic *in vitro* conditions and in the faeces of mice, loss of *mprF* improves the fitness of OG1RF. However, *mprF* does not contribute to the fitness of OG1RF in the colonisation of the murine cecum.

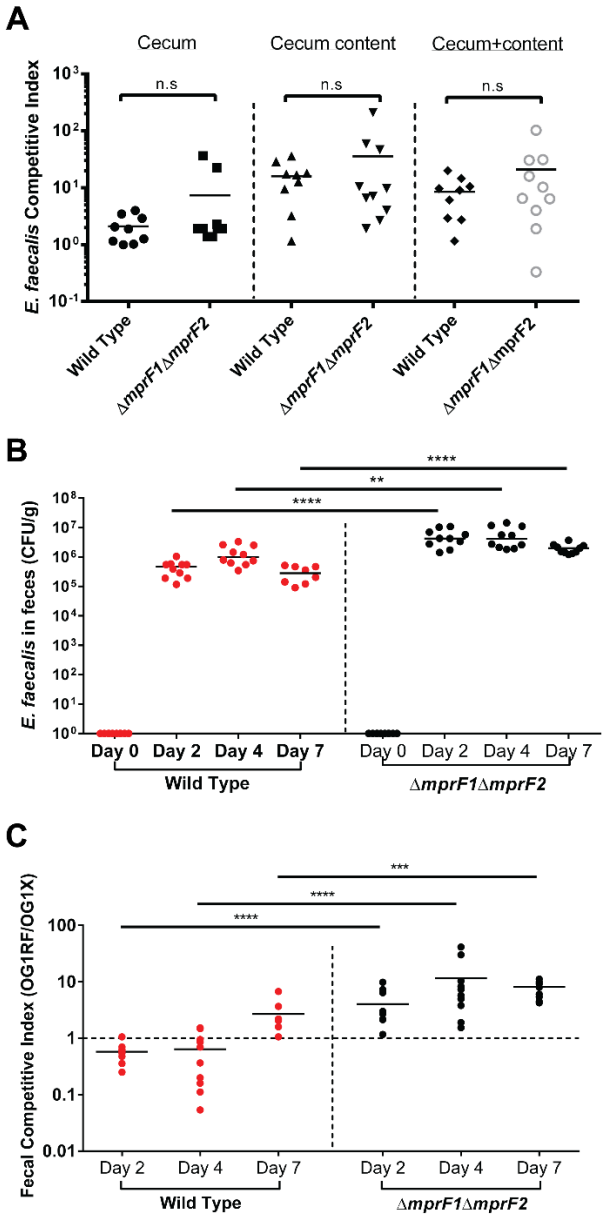

Figure. 2.9. *mprF* does not contribute to fitness in a competitive gut colonisation model. Mice were supplied with *E. faecalis* in the drinking water for a period of 7 days. 200 ml of drinking water was inoculated with 10^8 CFU/mL *E. faecalis* OG1X with either 10^8 CFU/mL *E. faecalis* OG1RF wild type or 10^8 CFU/ml *E. faecalis* Δ*mprF1*Δ*mprF2*. Viable bacteria from cecal tissue homogenates and cecal contents and faecal pellets were enumerated on selective media for each strain. **(A)** Competitive indices of *E. faecalis* OG1RF WT and Δ*mprF1*Δ*mprF2* against OG1X in the cecum and cecal contents. **(B)** OG1RF WT and Δ*mprF1*Δ*mprF2* CFU/g enumerated from faeces of mice in a single species colonisation experiment over 7 days. **(C)** Competitive indices of *E. faecalis* OG1RF WT and Δ*mprF1*Δ*mprF2* against OG1X in the faeces of mice in a mixed species competitive colonisation experiment. Each symbol represents one mouse, and the solid horizontal lines indicate the median, N=3, n=5. Mann-Whitney U test. ***, p=0.0001 to 0.001; ****, p⩽0.0001. Performed with assistance from Wong Jun Jie and Sharon Goh.

2.4. Discussion

Key to establishing colonisation and infection in the host is the ability to avoid clearance by the immune system. Part of the first barriers to colonisation and infection that *E. faecalis* encounters are cationic antimicrobial peptides (CAMPs) of the innate immune system produced by epithelial cells of mucosal surfaces or immune cells such as neutrophils. One of the adaptions that *E. faecalis* possesses to circumvent CAMP action is through the alteration of surface charge, for example modifying phospholipids to reduce electrostatic affinity to CAMPs through the action of the multiple peptide resistance factor (MprF) enzyme that lysinylates PG to lysyl-PG. *E. faecalis* possesses two paralogs of *mprF*, *mprF1* and *mprF2. mprF2* has been described to be solely involved in aminoacylation of PG to Lys-PG and possibly Arg-PG and Ala-PG in the encapsulated *E. faecalis* strain 12030 (Bao et al., 2012).

In our model strain of interest, OG1RF, we describe unexpected lipidomic and transcriptomic changes in the Δ*mprF* mutants that results in functional physiological changes to the cell **(Figure 2.10)**. In OG1RF, both *mprF1* and *mprF2* contribute to PG aminoacylation albeit to different degrees as evidenced by the partial loss of Lys-PG in Δ*mprF1* and its complete absence in Δ*mprF2* from MRM analysis by LC-MS/MS **(Figure 2.2A).** Accompanying the loss of Lys-PG are a series of previously unreported lipidomic changes with a decrease in the major phospholipid PG, with compensatory increases in GPDGDAG, D-ala-GPDGDAG, a phosphate containing lipid of unknown identity and a slight increase in CL uncovered by a combination of TLC and MRM analysis **(Figure 2.2B, 2.3, S2.4 and supplementary section 2.1)**. None of these changes can be explained transcriptomically as no changes in phospholipid biosynthesis genes were observed from transcriptomic analysis (Kelvin Chong, Adeline Yong, Swaine Chen, unpublished).

From a fatty acid perspective, *de novo* fatty acid biosynthesis genes were globally downregulated in Δ*mprF1*Δ*mprF2* as compared to the wild type from RT-qPCR analysis, in spite of having a largely similar fatty acid profile as wild type when grown in BHI **(Figure 2.4, 2.6).** Despite downregulation of the essential *de novo* fatty acid biosynthesis pathway and large lipidomic changes, the Δ*mprF* mutants were just as viable as the wild type and even displayed accelerated growth rates when grown in BHI (containing palmitic and stearic acid), but in contrast experienced growth inhibition when grown in CDM (without exogenous fatty acids) **(Figure 2.5A, Supplementary Table S2.3, S2.5, and Dominic Chia, unpublished)**. The ability of Δ*mprF1*Δ*mprF2* to survive in BHI is also unlikely due to the envelope and barrier-sensing two-component systems (*walKR*, *CroRS* or *LiaFSR*) since their knockdowns do not affect Δ*mprF1*Δ*mprF2* more than the wild type **(Figure 2.7)**. Instead, it is likely that Δ*mprF1*Δ*mprF2* has the ability to utilise the exogenous fatty acids in BHI to overcome the downregulation of *de novo* fatty acid biosynthesis genes, given that the supplementation of palmitic and stearic acid present in BHI or another long chain fatty acid, arachidic acid were able to partially rescue its growth in CDM **(Figure 2.5, Supplementary Figure 2.8)**.

These lipidomic and transcriptomic changes in Δ*mprF1*Δ*mprF2* also results in functional consequences to the cell. Membrane fluidity of Δ*mprF1*Δ*mprF2* at stationary phase was more rigid as compared to the wild type when assessed by Laurdan staining while Sec-mediated secretion was impaired in terms of both bulk secretion and secretion of a heterologously-expressed alkaline phosphatase **(Figure 2.8A, B)** - both of which are likely due to direct effects of lipidomic changes. In a mouse model of gastrointestinal colonization, Δ*mprF1*Δ*mprF2* was as fit as wild type in competitive colonisation of the cecum with *E. faecalis* OG1X **(Figure 2.9A)**. However, Δ*mprF1*Δ*mprF2* possessed

higher CFU titres in the faeces than the wild type, with higher competitive indices at all timepoints tested **(Figure 2.9B, C)**. This observation can be attributed to the enhanced biofilm formation and enhanced growth of Δ*mprF1*Δ*mprF2* in co-culture with OG1X **(Figure 2.8D)**. There was increased biofilm formation of Δ*mprF1*Δ*mprF2* as compared to the wild type when it was a static biofilm assay across a 5-day period. In addition, Δ*mprF1*Δ*mprF2* also displayed increased CFU titres when compared to the wild type when grown as a co-culture with OG1X over a 24-hour period **(Supplementary Figure S2.7)**.

Some of our findings are consistent with previous findings. We observed no growth defect in the Δ*mprF* mutants which was similarly reported in the Δ*mprF* mutants of *E. faecalis* 12030 (Bao et al., 2012) **(Supplementary Figure S2.3 and Dominic Chia, unpublished)**. Enhanced biofilm formation that we observed for Δ*mprF2* of *E. faecalis* OG1RF was similarly reported in *E. faecalis* 12030 Δ*mprF2* (Bao et al., 2012). We also observed an even greater enhancement in biofilm formation in *E. faecalis* OG1RF Δ*mprF1*Δ*mprF2* **(Figure 2.8C)**.

In previous studies involving *E. faecalis mprF*, the complete loss of Lys-PG was similarly only observed in Δ*mprF2* but not Δ*mprF1* in *E. faecalis* 12030 (Bao et al., 2012). However, Δ*mprF1* was described to have similar Lys-PG levels as compared to the wild type and no additional lipidomic changes were reported except for possible changes in Arg-PG and Ala-PG (Bao et al., 2012). This difference of that with our findings could be due to the inherent lower sensitivity in TLCs as compared to mass spectrometric methods as we similarly observe minimal changes in Lys-PG in Δ*mprF1*, when a ~20% decrease was detected in Lys-PG MRMs from LC-MS/MS **(Figure 2.3A, B, 2.2)**. This highlights the need for complementary analysis by mass spectrometry where possible to validate findings from TLC-based analyses especially when differences are not as

apparent. Additionally, we also detected a surprising decrease in the major phospholipid PG coupled with increased GPDGDAG, D-ala-GPDGDAG and a phosphate-containing lipid of unknown identity coupled with slightly increased CL that were not previously reported to knowledge, both in other *E. faecalis* strains and other organisms **(Figure 2.2, 2.3)** (Bao et al., 2012; Ernst and Peschel, 2011). The reason could be that these changes were simply undetected, and this is the first study taking a comprehensive look into the lipidome of the Δ*mprF* mutants.

From fatty acid supplementation experiments, growth inhibition by both unsaturated (palmitoleic, oleic, *cis*-vaccenic and linoleic acid) and saturated fatty acid (myristic and palmitic acid) supplementation for the wild type in CDM was more severe than previously reported for supplementation in BHI (Saito et al., 2017) **(Supplementary Figure S2.8)**. This could be due to the vastly different media composition of CDM compared to BHI. Furthermore, we report that our BHI contains palmitic and stearic acid while a previous study from the same group reported no fatty acids present within BHI (Saito et al., 2014). This could be due to different sources of BHI used or that their detection methods were not able to pick up palmitic or stearic acid from the media.

Previous studies have shown that *mprF* contributes to fitness in a murine wound competitive infection model, while it did not contribute to fitness in a murine bacteraemia model in single infections (Bao et al., 2012; Chong et al., 2017). We also show that *mprF* does not contribute to fitness in a murine gut colonisation model of the cecum, but instead it increased the CFU titres in the shed faeces **(Figure 2.9)**. Hence, this suggests that *mprF*'s role in fitness is niche specific and likely depends on the site of infection or colonisation.

Taken together, our findings show that the loss of a phospholipid modifying enzyme *mprF* has unexpected and wide-reaching effects on lipidome

composition and has phenotypic consequences affecting secretion, membrane fluidity and biofilm formation. These findings highlight the need to consider the wider lipidomic implications when studying lipid modifying or biosynthesis enzymes. One must not assume that losing an enzyme or gene only directly affects the reaction it catalyses, and a more holistic approach should be taken in investigating lipidomic phenotypes to avoid missing seemingly unrelated changes. Our work in identifying most of the lipid spots in the 1D and 2D TLC assays provides a now more complete TLC-based tool for quick and easy assessment of lipidomic changes in *E. faecalis* that can be followed up by mass spectrometric-based analysis for validation. CDM based supplementation also presents itself as a useful tool for looking at the effects of specific fatty acids without the background of exogenous lipids present in commonly used complex media such as BHI.

This study also brings forth intriguing observations that should be investigated further. Wild type *E. faecalis* responds to the absence of exogenous fatty acids in CDM by decreasing the proportion of palmitic acid ($C_{18:0}$) while increasing *cis*-vaccenic acid ($C_{18:1\ \omega7c}$), while the opposite happens in Δ*mprF1*Δ*mprF2* **(Figure 2.6)**. Whether this change in fatty acid profile in the wild type is a compensatory response to the lack of exogenous fatty acids and the reason behind the lack of this response in Δ*mprF1*Δ*mprF2* is at present unclear. Better understanding of this will shed light on the fatty acid responses and requirements needed for optimal growth. Future work, looking at palmitic and stearic acid supplementation experiments into CDM to give it a more BHI-like exogenous fatty acid environment, followed by fatty acid analysis by GC-FAME post supplementation should be done to address this. In addition, the exact mechanism of how the loss of *mprF* leads to the large lipidomic changes is still elusive. Future work should cover other avenues that could be mediating these changes, for instance

characterising the interacting partners of *mprF* and proteins within its vicinity might give better understanding on potentially novel regulatory mechanisms. Like previous reports, *E. faecalis* appears to only respond to select species of fatty acids and it is still currently unclear why this is so (Saito et al., 2014). Investigations in *S. aureus* reveal that the fatty acid kinases (FakA/B) responsible for phosphorylating exogenous fatty acids for incorporation have preference for binding specific fatty acids (Cuypers et al., 2019). It is possible that *E. faecalis* fatty acid kinases might possess a similar form of selectivity that might explain our observations and should be investigated from a structural perspective. This information will help better predict *E. faecalis'* behaviour under fatty acid supplementation.

However, this study has a few limitations. At present, whether the lipidomic changes observed are unique to *E. faecalis* or apply to all *mprF* enzymes from other species and strains is not known and should be investigated in detail in future studies. The fact that *Listeria* display altered listeriolysin O secretion in *mprF* mutants suggests that it is quite possible that a similar phenomenon may occur in other species (Zemansky et al., 2009). Furthermore, the transcriptomic responses of *E. faecalis* in the presence of CDM may not be the same as in BHI due to the differences in media composition, which should be addressed in future transcriptomic analyses. In addition, we observed that the supplementation of palmitic and stearic acid supports the growth of Δ*mprF1*Δ*mprF2* in CDM **(Figure 2.5)**. However, despite stationary phase absorbance reaching that of the wild type, the growth rate is still slowed suggesting that exogenous fatty acids might not be the sole missing component resulting in growth inhibition in Δ*mprF1*Δ*mprF2*. The differences between BHI and CDM should be further investigated by metabolomic analyses fill in this gap. Nonetheless, this method

still serves as a useful tool to uncover factors contributing to growth through supplementation experiments.

From a technical perspective, there are some aspects of the experiments performed that should be improved in future. At present only semi-quantitative analysis of a single GPDGDAG was conducted, which trends may or may not be representative of the whole class **(Figure 2.3C)**. To improve this, other species should also be measured, and MRMs conducted when GPDGDAG standards are next available. Furthermore, measurement of whole cell GP values done in this thesis, does not give spatial information of local GP distributions within the membrane which might be altered in the *mprF* mutants. Due to incompatibility of the thicker slide set-ups used with higher magnification objectives, lower magnification of 640X was used for GP measurements using laurdan resulting in insufficient resolution for spatial information to be obtained. In future, super resolution microscopy such as structured illumination microscopy (SIM) should be used instead together with thinner slides compatible with 1000X magnification to allow for the membrane distribution of GP values to be obtained.

2.5. Conclusion

In summary, we have shown in this chapter that the loss of a phospholipid modifying enzyme *mprF*, has far reaching and unexpected effects on cell physiology **(Figure 2.10)**. The lipidome in the *mprF* mutants is drastically altered with decreases in Lys-PG and PG, coupled with increases in D-ala-GPDGDAG, GPDGDAG and a phosphorous lipid of unknown identity. Furthermore, fatty acid biosynthesis genes are downregulated in the *mprF* mutants which results in growth defects in chemically defined media that can be overcome by using exogenously fatty acids. The combination of lipidomic and transcriptomic changes in the cell leads to functional outcomes in terms of enhanced CAMP binding and susceptibility, increased membrane rigidity and compromised Sec-

mediated secretion. This is the first report of a single phospholipid modification enzyme being able to generate such a large degree of pleiotropic effects on cell physiology in its absence. This report underscores the need for more thorough characterisation when studying genes and products of lipidomic pathways, and the need to consider their context in the wider metabolic network. Taken together, this study paints a much more complete picture of *mprF*'s role in cell physiology beyond just its catalytic function and provides vital information for future studies utilising it as an anti-resistance target for therapeutic development.

In the next chapter, *mprF's* role in acquiring resistance to a last line antibiotic, daptomycin, are examined in detail where genetic factors masked by MprF activity are elucidated. Further investigations focused on one factor, *ftsH* and its contribution to daptomycin resistance acquisition are also described in the next chapter.

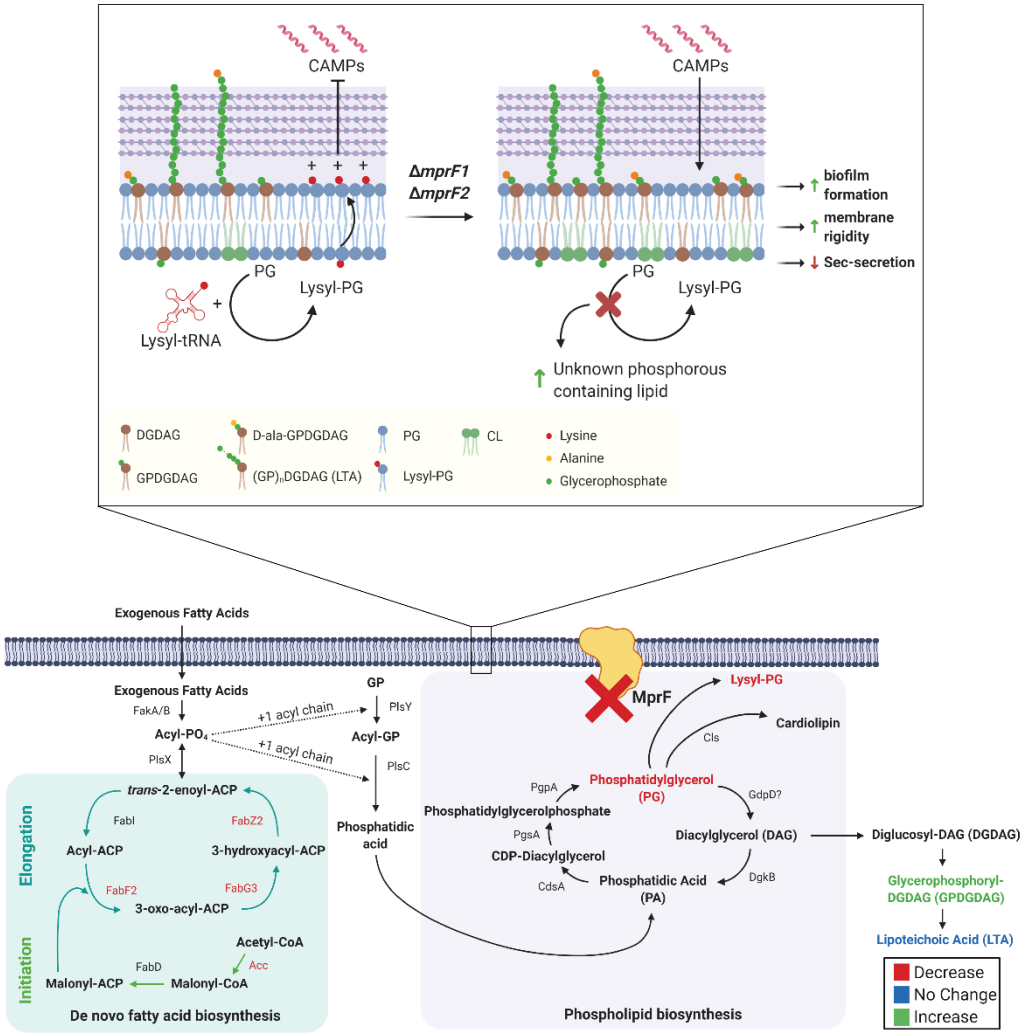

Figure. 2.10. Working model for the effect of the loss of *mprF* integrating transcriptomic, lipidomic and phenotypic observations. The loss of *mprF* leads to downregulation of fatty acid biosynthesis genes and decreases in lysyl-PG (Lys-PG), PG coupled with increases in GPDGDAG, cardiolipin as well as a phosphorus containing lipid and D-ala-GPDGDAG. These large lipidomic changes lead to functional impairment in Sec-mediated secretion, increased rigidity as well as enhanced CAMP binding. Created with BioRender.com.

2.6. References

Afonina, I., Ong, J., Chua, J., Lu, T., Kline, K.A., 2020. Multiplex CRISPRi-Cas9 silencing of planktonic and stage-specific biofilm genes in *Enterococcus faecalis*. bioRxiv, 2020.2004.2030.071571.

Alberts, B.J., A.; Lewis, J.; Raff, M.; Roberts, K. ; Walter, P, 2002. Molecular biology of the cell. 4th edition., The Lipid Bilayer. Garland Science, New York.

Bach, J.N., Bramkamp, M., 2013. Flotillins functionally organize the bacterial membrane. Molecular microbiology 88, 1205-1217.

Bao, Y., Sakinc, T., Laverde, D., Wobser, D., Benachour, A., Theilacker, C., Hartke, A., Huebner, J., 2012. Role of mprF1 and mprF2 in the pathogenicity of Enterococcus faecalis. PloS one 7, e38458.

Bligh, E.G., Dyer, W.J., 1959. A rapid method of total lipid extraction and purification. Can J Biochem Physiol 37, 911-917.

Brown, K.L., Hancock, R.E., 2006. Cationic host defense (antimicrobial) peptides. Current opinion in immunology 18, 24-30.

Bryan, E.M., Bae, T., Kleerebezem, M., Dunny, G.M., 2000. Improved vectors for nisin-controlled expression in gram-positive bacteria. Plasmid 44, 183-190.

Chilambi, G.S., Gao, I.H., Yoon, B.K., Park, S., Kawakami, L.M., Ravikumar, V., Chan-Park, M.B., Cho, N.-J., Bazan, G.C., Kline, K.A., Rice, S.A., Hinks, J., 2018. Membrane adaptation limitations in Enterococcus faecalis underlie sensitivity and the inability to develop significant resistance to conjugated oligoelectrolytes. RSC Advances 8, 10284-10293.

Chong, K.K.L., Tay, W.H., Janela, B., Yong, A.M.H., Liew, T.H., Madden, L., Keogh, D., Barkham, T.M.S., Ginhoux, F., Becker, D.L., Kline, K.A., 2017. Enterococcus faecalis Modulates Immune Activation and Slows Healing During Wound Infection. The Journal of infectious diseases 216, 1644-1654.

Choudhury, T., Singh, K.V., Sillanpää, J., Nallapareddy, S.R., Murray, B.E., 2011. Importance of Two Enterococcus faecium Loci Encoding Gls-like Proteins for In Vitro Bile Salts Stress Response and Virulence. The Journal of infectious diseases 203, 1147-1154.

Cotter, P.D., Hill, C., 2003. Surviving the acid test: responses of gram-positive bacteria to low pH. Microbiology and molecular biology reviews : MMBR 67, 429-453, table of contents.

Crane, J.M., Randall, L.L., 2017. The Sec System: Protein Export in Escherichia coli. EcoSal Plus 7, 10.1128/ecosalplus.ESP-0002-2017.

Cuypers, M.G., Subramanian, C., Gullett, J.M., Frank, M.W., White, S.W., Rock, C.O., 2019. Acyl-chain selectivity and physiological roles of Staphylococcus aureus fatty acid-binding proteins. The Journal of biological chemistry 294, 38-49.

de Vrije, T., de Swart, R.L., Dowhan, W., Tommassen, J., de Kruijff, B., 1988. Phosphatidylglycerol is involved in protein translocation across Escherichia coli inner membranes. Nature 334, 173-175.

Diamond, G., Beckloff, N., Weinberg, A., Kisich, K.O., 2009. The roles of antimicrobial peptides in innate host defense. Curr Pharm Des 15, 2377-2392.

Djorić, D., Kristich, C.J., 2015. Oxidative stress enhances cephalosporin resistance of Enterococcus faecalis through activation of a two-component signaling system. Antimicrobial agents and chemotherapy 59, 159-169.

Dowhan, W., 1997. Molecular basis for membrane phospholipid diversity: Why Are There So Many Lipids? Annual Review of Biochemistry 66, 199-232.

Dunny, G.M., Brown, B.L., Clewell, D.B., 1978. Induced cell aggregation and mating in Streptococcus faecalis: evidence for a bacterial sex pheromone. Proceedings of the National Academy of Sciences of the United States of America 75, 3479-3483.

Durr, U.H., Sudheendra, U.S., Ramamoorthy, A., 2006. LL-37, the only human member of the cathelicidin family of antimicrobial peptides. Biochimica et biophysica acta 1758, 1408-1425.

Eldholm, V., Gutt, B., Johnsborg, O., Brückner, R., Maurer, P., Hakenbeck, R., Mascher, T., Håvarstein, L.S., 2010. The pneumococcal cell envelope stress-sensing system LiaFSR is activated by murein hydrolases and lipid II-interacting antibiotics. Journal of bacteriology 192, 1761-1773.

Epand, R.M., Epand, R.F., 2009. Domains in bacterial membranes and the action of antimicrobial agents. Molecular bioSystems 5, 580-587.

Ernst, C.M., Peschel, A., 2011. Broad-spectrum antimicrobial peptide resistance by MprF-mediated aminoacylation and flipping of phospholipids. Molecular microbiology 80, 290-299.

Ernst, C.M., Staubitz, P., Mishra, N.N., Yang, S.-J., Hornig, G., Kalbacher, H., Bayer, A.S., Kraus, D., Peschel, A., 2009. The Bacterial Defensin Resistance Protein MprF Consists of Separable Domains for Lipid Lysinylation and Antimicrobial Peptide Repulsion. PLOS Pathogens 5, e1000660.

Furse, S., 2016. Is phosphatidylglycerol essential for terrestrial life? J Chem Biol 10, 1-9.

Ganz, T., 2003. Defensins: antimicrobial peptides of innate immunity. Nature reviews. Immunology 3, 710-720.

Harris, F.M., Best, K.B., Bell, J.D., 2002. Use of laurdan fluorescence intensity and polarization to distinguish between changes in membrane fluidity and phospholipid order. Biochimica et biophysica acta 1565, 123-128.

Heacock, P.N., Dowhan, W., 1987. Construction of a lethal mutation in the synthesis of the major acidic phospholipids of Escherichia coli. The Journal of biological chemistry 262, 13044-13049.

Hidron, A.I., Edwards, J.R., Patel, J., Horan, T.C., Sievert, D.M., Pollock, D.A., Fridkin, S.K., 2008. NHSN annual update: antimicrobial-resistant pathogens associated with healthcare-associated infections: annual summary of data reported to the National Healthcare Safety Network at the Centers for Disease Control and Prevention, 2006-2007. Infection control and hospital epidemiology 29, 996-1011.

Kandaswamy, K., Liew, T.H., Wang, C.Y., Huston-Warren, E., Meyer-Hoffert, U., Hultenby, K., Schröder, J.M., Caparon, M.G., Normark, S., Henriques-Normark, B., Hultgren, S.J., Kline, K.A., 2013. Focal targeting by human β-defensin 2 disrupts localized virulence factor assembly sites in Enterococcus faecalis. Proceedings of the National Academy of Sciences 110, 20230-20235.

Kellogg, S.L., Kristich, C.J., 2016. Functional Dissection of the CroRS Two-Component System Required for Resistance to Cell Wall Stressors in *Enterococcus faecalis*. Journal of Bacteriology 198, 1326.

Kline, K.A., Kau, A.L., Chen, S.L., Lim, A., Pinkner, J.S., Rosch, J., Nallapareddy, S.R., Murray, B.E., Henriques-Normark, B., Beatty, W., Caparon, M.G., Hultgren, S.J., 2009. Mechanism for Sortase Localization and the Role of Sortase Localization in Efficient Pilus Assembly in Enterococcus faecalis. Journal of Bacteriology 191, 3237-3247.

Koch, S., Exterkate, M., López, C.A., Patro, M., Marrink, S.J., Driessen, A.J.M., 2019. Two distinct anionic phospholipid-dependent events involved in SecA-mediated protein translocation. Biochimica et Biophysica Acta (BBA) - Biomembranes 1861, 183035.

Kommineni, S., Bretl, D.J., Lam, V., Chakraborty, R., Hayward, M., Simpson, P., Cao, Y., Bousounis, P., Kristich, C.J., Salzman, N.H., 2015. Bacteriocin production augments niche competition by enterococci in the mammalian gastrointestinal tract. Nature 526, 719-722.

Kusters, R., Dowhan, W., de Kruijff, B., 1991. Negatively charged phospholipids restore prePhoE translocation across phosphatidylglycerol-depleted Escherichia coli inner membranes. The Journal of biological chemistry 266, 8659-8662.

Lei, J., Sun, L., Huang, S., Zhu, C., Li, P., He, J., Mackey, V., Coy, D.H., He, Q., 2019. The antimicrobial peptides and their potential clinical applications. Am J Transl Res 11, 3919-3931.

Lindgren, J.K., Thomas, V.C., Olson, M.E., Chaudhari, S.S., Nuxoll, A.S., Schaeffer, C.R., Lindgren, K.E., Jones, J., Zimmerman, M.C., Dunman, P.M., Bayles, K.W., Fey, P.D., 2014. Arginine deiminase in Staphylococcus epidermidis functions to augment biofilm maturation through pH homeostasis. J Bacteriol 196, 2277-2289.

Mohedano, M.L., Overweg, K., de la Fuente, A., Reuter, M., Altabe, S., Mulholland, F., de Mendoza, D., López, P., Wells, J.M., 2005. Evidence that the essential response regulator YycF in Streptococcus pneumoniae

modulates expression of fatty acid biosynthesis genes and alters membrane composition. Journal of bacteriology 187, 2357-2367.

Murdoch, D.R., Corey, G.R., Hoen, B., Miro, J.M., Fowler, V.G., Jr., Bayer, A.S., Karchmer, A.W., Olaison, L., Pappas, P.A., Moreillon, P., Chambers, S.T., Chu, V.H., Falco, V., Holland, D.J., Jones, P., Klein, J.L., Raymond, N.J., Read, K.M., Tripodi, M.F., Utili, R., Wang, A., Woods, C.W., Cabell, C.H., 2009. Clinical presentation, etiology, and outcome of infective endocarditis in the 21st century: the International Collaboration on Endocarditis-Prospective Cohort Study. Archives of internal medicine 169, 463-473.

Nielsen, H.V., Guiton, P.S., Kline, K.A., Port, G.C., Pinkner, J.S., Neiers, F., Normark, S., Henriques-Normark, B., Caparon, M.G., Hultgren, S.J., 2012. The Metal Ion-Dependent Adhesion Site Motif of the Enterococcus faecalis EbpA Pilin Mediates Pilus Function in Catheter-Associated Urinary Tract Infection. mBio 3.

Pasupuleti, M., Schmidtchen, A., Malmsten, M., 2012. Antimicrobial peptides: key components of the innate immune system. Critical reviews in biotechnology 32, 143-171.

Patterson, J.E., Sweeney, A.H., Simms, M., Carley, N., Mangi, R., Sabetta, J., Lyons, R.W., 1995. An analysis of 110 serious enterococcal infections. Epidemiology, antibiotic susceptibility, and outcome. Medicine 74, 191-200.

Peschel, A., Jack, R.W., Otto, M., Collins, L.V., Staubitz, P., Nicholson, G., Kalbacher, H., Nieuwenhuizen, W.F., Jung, G., Tarkowski, A., van Kessel, K.P., van Strijp, J.A., 2001. Staphylococcus aureus resistance to human defensins and evasion of neutrophil killing via the novel virulence factor MprF is based on modification of membrane lipids with l-lysine. J Exp Med 193, 1067-1076.

Rashid, R., Cazenave-Gassiot, A., Gao, I.H., Nair, Z.J., Kumar, J.K., Gao, L., Kline, K.A., Wenk, M.R., 2017. Comprehensive analysis of phospholipids and glycolipids in the opportunistic pathogen Enterococcus faecalis. PloS one 12, e0175886.

Rochat, T., Boudebbouze, S., Gratadoux, J.J., Blugeon, S., Gaudu, P., Langella, P., Maguin, E., 2012. Proteomic analysis of spontaneous mutants of

Lactococcus lactis: Involvement of GAPDH and arginine deiminase pathway in H2O2 resistance. Proteomics 12, 1792-1805.

Rosch, J.W., Hsu, F.F., Caparon, M.G., 2007. Anionic lipids enriched at the ExPortal of Streptococcus pyogenes. Journal of bacteriology 189, 801-806.

Saito, H.E., Harp, J.R., Fozo, E.M., 2014. Incorporation of exogenous fatty acids protects Enterococcus faecalis from membrane-damaging agents. Appl Environ Microbiol 80, 6527-6538.

Saito, H.E., Harp, J.R., Fozo, E.M., 2017. Enterococcus faecalis Responds to Individual Exogenous Fatty Acids Independently of Their Degree of Saturation or Chain Length. Appl Environ Microbiol 84, e01633-01617.

Samant, S., Hsu, F.-F., Neyfakh, A.A., Lee, H., 2009. The *Bacillus anthracis* Protein MprF Is Required for Synthesis of Lysylphosphatidylglycerols and for Resistance to Cationic Antimicrobial Peptides. Journal of Bacteriology 191, 1311-1319.

Suntharalingam, P., Senadheera, M.D., Mair, R.W., Lévesque, C.M., Cvitkovitch, D.G., 2009. The LiaFSR System Regulates the Cell Envelope Stress Response in <em>Streptococcus mutans</em&gt. Journal of Bacteriology 191, 2973.

Teng, F., Nannini, E.C., Murray, B.E., 2005. Importance of gls24 in Virulence and Stress Response of Enterococcus faecalis and Use of the gls24 Protein as a Possible Immunotherapy Target. The Journal of infectious diseases 191, 472-480.

Thedieck, K., Hain, T., Mohamed, W., Tindall, B.J., Nimtz, M., Chakraborty, T., Wehland, J., Jansch, L., 2006. The MprF protein is required for lysinylation of phospholipids in listerial membranes and confers resistance to cationic antimicrobial peptides (CAMPs) on Listeria monocytogenes. Molecular microbiology 62, 1325-1339.

Weiner, L.M., Webb, A.K., Limbago, B., Dudeck, M.A., Patel, J., Kallen, A.J., Edwards, J.R., Sievert, D.M., 2016. Antimicrobial-Resistant Pathogens Associated With Healthcare-Associated Infections: Summary of Data Reported to the National Healthcare Safety Network at the Centers for Disease Control

and Prevention, 2011-2014. Infection control and hospital epidemiology 37, 1288-1301.

Zemansky, J., Kline, B.C., Woodward, J.J., Leber, J.H., Marquis, H., Portnoy, D.A., 2009. Development of a mariner-based transposon and identification of Listeria monocytogenes determinants, including the peptidyl-prolyl isomerase PrsA2, that contribute to its hemolytic phenotype. Journal of bacteriology 191, 3950-3964.

3. CHAPTER III:

Adaptation of *Enterococcus faecalis* to daptomycin reveals a role for *ftsH* in resistance acquisition and essentiality for growth

3.1. Introduction

Enterococci are a major healthcare concern due to their association with hospital acquired infections (HAIs) and ability to acquire resistance to drugs of last resort such as vancomycin. Vancomycin resistant *enterococci* (VRE) are associated with increased mortality rates, lengthened hospital stays and increased economic burden associated with treatment and infection control costs (Carmeli et al., 2002; Mascini and Bonten, 2005; Song et al., 2003).

To manage VRE infections, treatment measures typically involve antibiotics such as linezolid and daptomycin (Patel and Gallagher, 2015). Daptomycin is a lipopeptide antibiotic that is positively charged when complexed with its cofactor calcium, and targets the negatively charged bacterial membrane by inserting into and oligomerising within it to cause membrane disruption, ion leakage and eventual cell death (Steenbergen et al., 2005; Taylor and Palmer, 2016). Daptomycin has broad activity against Gram-positive infections and has been largely successful in treating VRE infections (Munita et al., 2014; Shoemaker et al., 2006). However, VRE can acquire resistance to daptomycin (DAP), which is alarming as it further reduces the already limited treatment options available for VRE infections (Arias and Murray, 2012; Kelesidis et al., 2011; Munoz-Price et al., 2005).

Recognising the severe implications if daptomycin resistance (DAP^R) becomes widespread, previous studies have attempted to determine mutations and genes associated with DAP^R. Mutations found in *liaF* encoding the LiaF negative

regulator of the LiaFSR three-component system as well as in *yylB* – a putative LiaFSR target – in DAP^R strains suggest possible involvement of this membrane stress sensing system (Arias et al., 2011; Miller et al., 2013). DAP^R-associated mutations in *gdpD* (glycerophosphodiesterase) and *cls* (cardiolipin synthase), decreased levels of phosphatidylglycerol (PG) and increased glycerophosphoryl-diglucosyldiacylglycerol (GPDGDAG), together with increased membrane rigidity and diversion of daptomycin away from the septum in DAP^R strains indicate that resistance is also likely mediated through membrane remodelling (Arias et al., 2011; Mishra et al., 2012; Rashid et al., 2017; Tran et al., 2013). Furthermore, genes related to oxidative stress response (*gsh, yybT, selA*) and *mdpA* – a drug efflux pump – have also been linked to DAP^R (Miller et al., 2013). At present, daptomycin resistance appears to be mediated by LiaFSR signalling, membrane remodelling associated with lipidomic changes as well as oxidative stress responses. However, information on what governs the rate of DAP^R acquisition and daptomycin's mechanism of action after it gains entry to the cell is scarce. Having complete understanding of DAP^R mechanisms and factors affecting resistance acquisition is essential in developing anti-resistance strategies to mitigate potential widespread resistance in future.

There is also evidence that the multiple peptide resistance factor (MprF) might be implicated in daptomycin resistance. MprF is a membrane bound enzyme that aminoacylates PG in the inner leaflet of the membrane and flips it to the outer leaflet and in doing so reduces the membrane's overall negative charge and consequently the cell's affinity to cationic antimicrobials (Bao et al., 2012; Rashid et al., 2016). *E. faecalis* possess two paralogs of *mprF* – *mprF1* and *mprF2* – and we have shown in **chapter II** that *mprF2* plays a greater role than *mprF1* in aminoacylation. In *S. aureus*, DAP^R isolates have been shown to

possess *mprF* gain of function mutations and increased MprF expression (Ernst et al., 2018; Mishra et al., 2009; Sabat et al., 2018). In daptomycin susceptible *E. faecalis*, deletion of *mprF2* led to further decreases of MIC by 1.5 to 2-fold (Iris Gao, unpublished).

Given that *mprF* expression has daptomycin protective effects, we hypothesized that *mprF* activity might be masking daptomycin resistance events during *in vitro* evolution screens and in clinical isolates of *E. faecalis*. We therefore performed an *in vitro* evolution assay to DAP^R in the background of the *mprF* mutants to reveal novel mutations and genes implicated in daptomycin resistance. Information gathered here will help inform daptomycin resistance mechanisms, its mechanism of action as well as the physiology of the *mprF* mutants.

In previous work, this *in vitro* evolution assay was conducted and revealed several genes in which DAP^R–associated mutations were enriched only in certain mutant backgrounds, and these mutations were not previously reported in wild type backgrounds (Iris Gao, unpublished) **(Figure 3.1A, B)**. One of the hits, encoding a conserved metalloprotease, FtsH, was found to only possess mutations in the Δ*mprF1*Δ*mprF2* background, and these mutations always arose only early in evolution (Iris Gao, unpublished) **(Figure 3.1B)**. We hypothesized that these mutations result in FtsH loss of function, which helps accelerate the speed of DAP^R acquisition.

This chapter investigates the contribution of one of the commonly occurring FtsH mutations, G37X, in contributing to accelerated DAP^R acquisition and essentiality in the wild type through a targeted *in vitro* evolution assay and growth curves. A proteolytically inactive substrate-trapping variant of FtsH was used in proteomic and transcriptomic analyses to identify potential substrates of FtsH as well as the physiologic response to loss of FtsH function. Proteomic hits were also investigated through targeted *in vitro* evolution and growth assays.

Information gained from this detailed investigation presents a novel link between FtsH function and DAP^{R} acquisition. This study also sheds light on factors governing resistance acquisition rates, which may serve as potential targets in the future development of anti-resistance strategies.

A

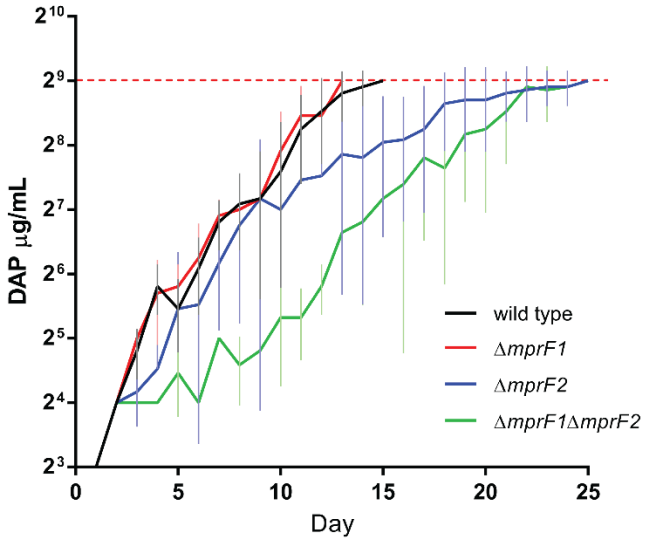

B

***In vitro* evolution list of hits**			
Gene ID	**Gene hits**	**Sequence of occurrence**	**Enriched in which strain?**
OG1RF_10209	*ftsH*	Early	Δ*mprF1*Δ*mprF2*
OG1RF_10364 OG1RF_11324	*cls1, cls2*	Intermediate	All
OG1RF_11464	*liaX*	Intermediate	Wild type Δ*mprF1* Δ*mprF2*
OG1RF_11507	Putative membrane protein	Intermediate	Δ*mprF1*Δ*mprF2*
OG1RF_10437	Putative Permease	Late	Δ*mprF1*Δ*mprF2*
OG1RF_11901	Putative HD domain protein	Late	Wild type Δ*mprF1*

Figure 3.1. *In vitro* evolution of *mprF* mutants to DAP^{R} reveal novel mutations (Iris Gao, unpublished). (A) Highest growth permissive concentration (HGPC) of daptomycin over time for each of the evolved strains. 8 lines of evolution were performed. **(B)** Whole genome sequencing across evolution reveals an ordered progression of acquired mutations, some of which are enriched in certain mutant backgrounds. Sequence of occurrence of mutations is based of DAP HGPC where the mutation first

occurred (early, ≤ 16 μg/mL; intermediate, ≤ 64 μg/mL; Late, ≤ 256 μg/mL). Detailed information on mutations observed are shown in **Supplementary Table S3.1**.

3.2. Materials and methods

3.2.1. Bacterial strains and culture conditions

The wild-type (WT) parental strain used was *E. faecalis* OG1RF (Dunny et al., 1978) and Δ*mprF1* and Δ*mprF2* mutants used were described previously (Chong et al., 2017; Kandaswamy et al., 2013). Unless stated, all bacterial strains were grown overnight to late stationary phase for 16-18 hrs in their respective media at 37 °C in static conditions and stored in 25% glycerol solution at -80 °C when long-term storage was required. If mid-log phase cultures were required, late stationary phase cultures were sub-cultured 1:10 dilution into fresh media and grown at 37 °C, 250 rpm shaking conditions till an OD_{600} of 0.5 ± 0.05 was reached. When normalisation of cultures was required, they were centrifuged at 6,000 rcf for 5 mins at 4 °C and cell pellets were washed twice with 1mL of phosphate buffered saline (PBS). Cell suspensions were then normalised to an OD_{600} of 0.7 or required optical density by diluting with PBS. Strains, their respective genotype, source, and growth media used are listed in **table 3.1** below.

Table 3.1. Bacteria Strains and Culture Conditions

Bacterial Strains	Relevant Information / Genotype	References / Source	Media Used
	E. coli		
Stellar™ Competent Cells (*E. coli* HST08)	*F–, endA1, supE44, thi-1, recA1, relA1, gyrA96, phoA, Φ80d lacZΔM15, Δ(lacZYA - argF) U169, Δ(mrr - hsdRMS - mcrBC), ΔmcrA, λ–*	Clontech, Takara Bio Inc., Japan	-
DH5α pCYW2* (*Alternative name: pGCP123-PsrtA)	DH5α harbouring pCYW2*; Kan^r *pCYW2: pGCP123 parent plasmid (Nielsen et al., 2012) with PsrtA promoter. Expression vector.	Lab stock	LB, Miller broth (BD, USA) with 50 µg/mL kanamycin (Thermo Scientific, USA)

DH5α pMSP3535	DH5α harbouring pMSP3535*; Erm^r *pMSP3535: Shuttle vector for nisin-controlled inducible expression.	pMSP3535 was a gift from Gary Dunny, University of Minnesota (Addgene plasmid # 46886) (Bryan et al., 2000)	LB, Miller broth with 300 µg/mL erythromycin (Sigma Aldrich, USA)
Stellar™ Competent Cells pMSP3545-d*cas9*	*E. coli* HST08 harbouring pMSP3545-d*cas9**; Erm^r *pMSP3535-dcas9: Shuttle vector for nisin-inducible expression of dcas9	Constructed by Irina Afonina (Afonina et al., 2020)	LB, Miller broth with 300 µg/mL erythromycin
DH5α pABG5.2mini* (*alternative name: pGCP123)	DH5α harbouring pABG5.2mini* *pABG5.2mini: Shuttle expression vector	(Nielsen et al., 2012)	LB, Miller broth with 50 µg/mL kanamycin
TOP10 pGCP213	TOP10 harbouring pGCP213*; Erm^r *pGCP213: Temp-sensitive shuttle vector used for allelic replacement in E. faecalis	(Nielsen et al., 2012)	LB, Miller broth with 500 µg/mL erythromycin
Stellar™ Competent Cells pGCP213-*ftsH(G37X)*	*E. coli* HST08 harbouring pGCP213-*ftsH(G37X)*; Erm^r	This study	LB, Miller broth with 500 µg/mL erythromycin
	E. faecalis		
OG1RF	Fus^r, Rif^r, wild-type strain	American Type Culture Collection (ATCC© 47077™)	BHI (Neogen, USA)
OG1RF Δ*mprF1*	Fus^r, Rif^r, Δ*mprF1*	(Kandaswamy et al., 2013)	
OG1RF Δ*mprF2*	Fus^r, Rif^r, Δ*mprF2*	(Kandaswamy et al., 2013)	
OG1RF Δ*mprF1*Δ*mprF2*	Fus^r, Rif^r, Δ*mprF1*Δ*mprF2*	Constructed by Liew Horng Tze (Rashid et al., unpublished)	
OG1RF pCYW2-*ftsH(G37X)*	Fus^r, Rif^r, pCYW2-*ftsH(G37X)*	This study	

OG1RF Δ*mprF1*Δ*mprF2* pCYW2-*ftsH(G37X)*	Fus^r, Rif^r, Δ*mprF1*Δ*mprF2* pCYW2-*ftsH(G37X)*	This study	BHI with 500 µg/mL kanamycin
OG1RF pGCP123	Fus^r, Rif^r, pGCP123	This study	
OG1RF Δ*mprF1*Δ*mprF2* pGCP123	Fus^r, Rif^r, Δ*mprF1*Δ*mprF2* pGCP123	This study	
OG1RF pMSP3535	Fus^r, Rif^r, pMSP3535	This study	BHI with 100 µg/mL erythromycin
OG1RF pMSP3535-6his-*ftsH*	Fus^r, Rif^r, pMSP3535-6his-*ftsH*	This study	
OG1RF pMSP3535-2HA-*ftsH*	Fus^r, Rif^r, pMSP3535-2HA-*ftsH*	This study	
OG1RF pMSP3535-6his-*ftsH(H456Y)*	Fus^r, Rif^r, pMSP3535-6his-*ftsH(H456Y)*	This study	
OG1RF pMSP3535-2HA-*ftsH(H456Y)*	Fus^r, Rif^r, pMSP3535-2HA-*ftsH(H456Y)*	This study	
OG1RF pMSP3535-*cls1*	Fus^r, Rif^r, pMSP3535-*cls1*	Constructed by Chen Qingyan (Chen Qingyan, unpublished)	
OG1RF pMSP3535-OG1RF_10100-HA	Fus^r, Rif^r, pMSP3535-OG1RF_10100-HA	This study	
OG1RF pMSP3535-OG1RF_11679-HA	Fus^r, Rif^r, pMSP3535-OG1RF_11679-HA	This study	
OG1RF pMSP3535-OG1RF_10473-HA	Fus^r, Rif^r, pMSP3535-OG1RF_10473-HA	This study	
OG1RF Tn::OG1RF_11014	Fus^r, Rif^r, Tn::OG1RF_11014 (Strain ID: 007A07, 114D11, 013G10)	From a transposon library gifted by Gary Dunny, University of Minnesota (Kristich et al., 2008)	BHI
OG1RF Tn::OG1RF_10886	Fus^r, Rif^r, Tn::OG1RF_10886 (Strain ID: 030F11, 070D04, 070C04)		
OG1RF Tn::OG1RF_11526	Fus^r, Rif^r, Tn::OG1RF_11526 (Strain ID: 100E05, 148F04)		

OG1RF Tn::OG1RF_12425	Fus^r, Rif^r, Tn::OG1RF_12425 (Strain ID: 064F10, 095E07, 018D03, 110D12)		
OG1RF Tn::OG1RF_11427	Fus^r, Rif^r, Tn::OG1RF_11427 (Strain ID: 006D07, 034D02)		
OG1RF Tn::OG1RF_11383	Fus^r, Rif^r, Tn::OG1RF_11383 (Strain ID: 040B07)		
OG1RF Tn::OG1RF_11076	Fus^r, Rif^r, Tn::OG1RF_11076 (Strain ID: 075A04, 016F09)		
OG1RF pMSP3545-*dcas9* pABG5.2mini	Fus^r, Rif^r, pMSP3535-*dcas9* pABG5.2mini	This study	
OG1RF Δ*mprF1*Δ*mprF2* pMSP3545-*dcas9* pABG5.2mini	Fus^r, Rif^r, Δ*mprF1*Δ*mprF2* pMSP3535-*dcas9* pABG5.2mini	This study	
OG1RF pMSP3545-*dcas9* pABG5.2mini-*lysS*_g1	Fus^r, Rif^r, pMSP3535-*dcas9* pABG5.2mini-*lysS*_g1	This study	BHI with 100 µg/mL erythromycin, 500 µg/mL kanamycin
OG1RF Δ*mprF1*Δ*mprF2* pMSP3545-*dcas9* pABG5.2mini-*lysS*_g1	Fus^r, Rif^r, Δ*mprF1*Δ*mprF2* pMSP3535-*dcas9* pABG5.2mini-*lysS*_g1	This study	
OG1RF pMSP3545-*dcas9* pABG5.2mini-*pyrB*_g1	Fus^r, Rif^r, pMSP3535-*dcas9* pABG5.2mini-*pyrB*_g1	This study	
OG1RF Δ*mprF1*Δ*mprF2* pMSP3545-*dcas9* pABG5.2mini-*pyrB*_g1	Fus^r, Rif^r, Δ*mprF1*Δ*mprF2* pMSP3535-*dcas9* pABG5.2mini-*pyrB*_g1	This study	
OG1RF *ftsH(G37X)*	Fus^r, Rif^r, *ftsH(G37X)*	This study	BHI
OG1RF DAP-passage control	Fus^r, Rif^r, passage control strain	This study	
OG1RF pGCP213-*ftsH(G37X)*	Fus^r, Rif^r, pGCP213-*ftsH(G37X)*	This study	BHI with 50 µg/mL erythromycin
OG1RF Δ*mprF1*Δ*mprF2* pGCP213-*ftsH(G37X)*	Fus^r, Rif^r, Δ*mprF1*Δ*mprF2* pGCP213-*ftsH(G37X)*	This study	

3.2.2. *In vitro* evolution of *E. faecalis* to daptomycin resistance

The protocol was adapted from a previously published *in vitro* evolution experiment done in *E. faecalis* V583 (Palmer et al., 2011). For each strain, multiple parallel lines of evolution experiment were performed. First, 10X dilutions of overnight bacterial cultures of each strain were made in BHI supplemented with 1.25 mM calcium chloride (Sigma, USA) (50 mg/L Ca^{2+}) containing daptomycin (DAP) (Peptide Institute Inc, Japan) concentrations of 1X MIC, 2X MIC and 4X MIC and incubated at 37 °C at static conditions for 22 to 26 hrs. Cultures of every evolution line were examined for visible bacterial growth. Bacterial cultures at the highest growth-permissive concentrations (HGPCs) are diluted 10 times into fresh DAP-containing medium at 0.5X HGPC, 1X HGPC and 2X HGPC. This was repeated till HGPC of 512 µg/mL was achieved.

3.2.3. Minimal inhibitory concentration test (microplate dilution)

Stationary phase cultures to be tested were grown till mid-log phase and normalised to OD_{600} of 0.7. MIC assays were performed in a 96-well plate as described previously (Wiegand et al., 2008), with the following modifications. Antibiotics were diluted in BHI media supplemented with 1.25 mM calcium chloride (50 mg/L Ca^{2+}), in 2-fold dilutions, from 256.0 µg/mL to 0.5 µg/mL of daptomycin (AG Scientific, USA). Cultures with daptomycin were incubated for 16-18 hrs at 37 °C in static conditions before assessing for growth in the wells to estimate the MIC.

3.2.4. Growth curves

Overnight stationary phase cultures were normalised to OD_{600} of 0.7 and diluted 200-fold before inoculating in 200 µL of media in 96-well plates in a ratio of 1:25. The 96-well plates were incubated at 37 °C in a Tecan Infinite© M200 Pro

spectrophotometer (Tecan, Switzerland) with absorbance read at 600 nm every 10 mins for 18 hrs.

3.2.5. Live-dead staining

Late stationary and mid-log phase cultures were normalised to OD_{600} 0.5 in 1mL of PBS and washed twice with PBS. 2 µL of SYTO9 and propridium iodide (PI) mix (LIVE/DEAD™ BacLight™ Bacterial Viability Kit, for microscopy, Invitrogen, USA) were added to the cell suspensions and incubated at 15 mins at room temperature in the dark. Stained cells were washed once with PBS and resuspended in 200 µL 0.01 M phosphate buffer (PB). 5 µL of stained cells were wet mounted on 1.0-1.2 mm microscope slides (Biomedia, Singapore) with 0.13-0.16 mm coverslips. Slides were imaged with a Zeiss Axio observer Z1 inverted microscope (Carl-Zeiss, Germany) with a 100X oil immersion objective (NA 1.4, optovar 1.6X), AF488/FITC filter cube (460-490 nm band pass excitation filter, 515-550nm band pass barrier filter) and AF568/Cy3 filter cube (530-550nm band pass excitation filter, 590nm long pass barrier filter). Phase contrast, green (460-490 nm) and red (530-550nm) fluorescence images were captured.

3.2.6. RNA isolation and sequencing

Sequencing of RNA was done on WT pMSP3535-6his-*ftsH*(H456Y) and WT pMSP3535-*ftsH*(H456Y) strains. Overnight cultures were subcultured 1:10 in BHI and grown to mid-log phase, cultures were then induced for expression of their respective plasmids' gene constructs with 125 ng/mL of nisin for 16-18 hrs at 37 °C in static conditions. 2 mL of RNAprotect© Bacteria Reagent (Qiagen, Germany) was added to 1 mL of induced culture and incubated for 5 mins at room temperature. Cells were then pelleted and rinsed with PBS to thoroughly remove the RNAprotect© reagent. Cell pellets were then resuspended in 20 mg/mL lysozyme (Sigma-Aldrich, USA) in lysis buffer (10 mM Tris-HCl pH 7.0, 1 mM EDTA, 50 mM NaCl and 0.74 M Sucrose) and incubated for 1 hr at 37 °C.

Cells were then pelleted and washed once with PBS. 1 mL of ice-cold TRIzol™ Reagent (Ambion, USA) was next added and the cell pellet resuspended by pipetting. 200 µL of ice-cold chloroform (Fisher, USA) was next added to the tube and the suspension mixed by shaking gently before incubating on ice for 2 mins. The mixture was then centrifuged for 15 mins at 12, 000 rcf at 4 °C to induce phase separation. Next, 500 µL of the upper aqueous phase was carefully removed and added to the spin-column from the PureLink™ RNA Mini Kit (Thermofisher, USA). Purification was then carried as specified by the manufacturer's instructions and eluted in 30 µL of Nuclease-free water (Ambion, USA). Quantification of RNA and DNA were performed using Qubit™ RNA Assay Kits and Qubit™ dsDNA HS Assay Kits (Invitrogen, USA), respectively. Integrity of RNA was analyzed by gel electrophoresis using Agilent RNA ScreenTape (Agilent Technologies, USA). Extracted RNA samples were subjected to ribosomal depletion with Ribo-Zero™ Magnetic Kits (Lucigen, USA) and purified using RNAclean® XP beads (Beckman Coulter, USA) according to their respective manufacturers' protocol. cDNA synthesis was done using NEBNext® RNA First Strand Synthesis Module and NEBNext® Ultra Directional RNA Second Strand Synthesis Module (New England Biolabs, USA), and purified using AMPure XP beads (Beckman Coulter, USA). RNA library preparation and sequencing were done by the sequencing facility of Singapore Centre of Life Science Engineering (SCELSE, Singapore) using MiSeq.

Sequencing reads were mapped to the *E. faecalis* OG1RF reference genome (NCBI accession: NC_017316.1) using BWA (version 0.5.9) on default settings (Li and Durbin, 2009; Nagalakshmi et al., 2010). Reads mapping onto predicted open reading frames (ORFs) were counted on HTseq and ribosomal reads were filtered out (Anders et al., 2015). Pairwise comparisons were performed in in R program with the Bioconductor package, edgeR (Robinson et al., 2010).

Significant differentially expressed genes were determined using a cutoff of false discovery rate (FDR) and p-value of 0.05. Kyoto Encyclopedia of Genes and Genomes (KEGG) annotation along with manual curation using BLASTP and cross-referencing of other functional data from literature were performed. Gene ontologies were obtained from KEGG (identifier: efi) and genes were classified based on membership of a pathway with their respective log fold change (log_2FC).

3.2.7. FtsH substrate identification

WT pMSP3535-6his-*ftsH*(H456Y) and WT pMSP3535-*ftsH*(H456Y) strains were grown to mid-log phase and induced for expression of their respective plasmids' gene constructs with 125 ng/mL of nisin for 16-18 hrs at 37 °C in static conditions and cell pellets were harvested. The membrane fraction was isolated from the harvested pellets as previously described, resuspended with 100 µL of 50 mM Tris-HCl, pH 8.0, and boiled with 33.3 µL of NuPAGE® LDS Sample Buffer (4X) (Thermofisher, USA) and 10µL of 1M DTT (Maddalo et al., 2011). Samples were then run on SDS-PAGE on a 4-12% NuPAGE® Bis-Tris mini gel in a XCell SureLock® Mini-Cell filled with MES SDS running buffer (Invitrogen, USA) till samples just entered the gel. Gels were then silver-stained by fixing with 50% v/v methanol and 5% v/v acetic acid solution, sensitizing with 0.02% w/v sodium thiosulfate solution, silver-stained with 0.1% w/v silver nitrate and 3% v/v formalin solution and developed using 2% w/v sodium carbonate and 1.5% v/v formalin solution. The concentrated protein band of each lane was excised and stored in Eppendorf tubes filled with water. Samples were then sent to the Taplin Mass Spectrometry Facility, Harvard Medical School, Boston, Massachusetts, USA for peptide mass spectrometry and proteomic analysis. Peptide counts were normalised using tweeDEseq (TMM normalisation) and statistics were

done using Reproducibility-Optimized Test Statistic (ROTS) (Esnaola et al., 2013; Suomi et al., 2017).

3.2.8. Mutation rate assay (Luria-Delbrück fluctuation assay)

Overnight stationary phase cultures were diluted 10, 000X in 40 mL of BHI supplemented with 1.25 mM calcium chloride (50 mg/L Ca^{2+}). 100 µL of diluted culture was then added into each well of a 96-well microtiter plate, sealed and incubated at 37 °C in static conditions for 16-18 hrs. 24 wells from the plate were pooled and sonicated gently for 1 min in a bath sonicator to break up cell clumps followed by serial dilution and plating on non-selective BHI agar plate for CFU enumeration. This determines the average cell number (N). Whole volumes (100 µL) of each of the 72 wells/cultures were then transferred into wells of a 24-well microtiter plate containing 900 µL BHI supplemented with 1.25 mM calcium chloride and daptomycin (dilution was taken into account such that final daptomycin concentration is 4X MIC). Plates were incubated for 24 hrs at 37 °C in static conditions and observed for growth visually by the presence of turbid wells. Plates were then left in the incubator for up to 7 days, and monitored daily to determine if any more wells had turn turbid. The fraction of wells/cultures with zero growth indicating zero mutant cells is defined as p_0. The expected number of mutation events per culture (m) is calculated as, $m = -\ln(p_0)$. The mutation rate (µ) is calculated as: $\mu = \frac{m}{N}$.

3.2.9. Western immunoblot

SDS-PAGE and western blot were performed as described in a previous study (Nielsen et al., 2012). 4-12% or 12% NuPAGE® Bis-Tris mini gel in a XCell SureLock® Mini-Cell filled with either 1x MES or 1x MOPs SDS running buffer (Invitrogen, USA) were used and ran at 140 V for 90 mins. Proteins were transferred to nitrocellulose membranes using the iBlot™ Dry Blotting System

(Invitrogen, USA) according to the manufacturer's protocol. The antibodies and developing solutions used are shown in below **(table 3.2)**.

Table 3.2. Antibodies and developing solution used in western immunoblots

Target of interest	Primary Antibody Dilution; Host	Secondary Antibody Dilution; Host	Developing Solution; Dilution Ratios (Luminol:Peroxide:Water)
6his	Mouse anti-6his 1:1000 (Thermoscientific, USA)	Goat anti-mouse HRP 1:5000 (Thermoscientific, USA)	SuperSignal™ West Femto Maximum Sensitivity Substrate 1:1:8
2HA	Mouse anti-HA 1:1000 (Thermoscientific, USA)	Goat anti-mouse HRP 1:5000 (Thermoscientific, USA)	SuperSignal™ West Femto Maximum Sensitivity Substrate 1:1:8

3.2.10. Immunofluorescence assay

Immunofluorescence microscopy was performed as previously described with the following modifications (Kandaswamy et al., 2013). Overnight cultures of wild type pMSP3535-2HA-*ftsH* were subcultured twice and grown to mid-log phase, where the cultures were induced throughout with 125 ng/mL of nisin. After fixation, cells were treated with 10 mg/mL lysozyme in lysis buffer for 45 mins at 37 °C followed by permeabilization with 0.1% (v/v) triton-X for 5 mins at 37 °C. The primary and secondary antibodies used were rabbit anti-HA (1:500 dilution) and anti-rabbit Alexa Fluor™ 488 (1:1000 dilution).

Slides were imaged with a Zeiss Axio observer Z1 inverted microscope (Carl-Zeiss, Germany) with a 100X oil immersion objective (NA 1.4, optovar 1.6X), AF488/FITC filter cube (460-490 nm band pass excitation filter, 515-550 nm band pass barrier filter). Phase contrast and green (460-490 nm) fluorescence images were captured. Fluorescence along the cell perimeter was quantified using Projected System of Internal Coordinates from Interpolated Contours (PSICIC) on MATLAB (Guberman et al., 2008). This software works by detecting the cell perimeter and detecting the fluorescence intensity along that perimeter.

The perimeter is divided into 100 sections (where 0/100 and 50 refer to the cell poles; points 25 and 75 refer to each side of the septum), each with a fluorescence intensity value. Perimeter fluorescence intensities from at least 100 cells are plotted against the cell perimeter coordinates to visualise fluorescence localisation along the membrane. Only mid-log phase cells (4.8 – 8.0 μm) were selected.

3.2.11. Molecular cloning

The respective plasmids were extracted from *E. coli* strains harbouring them using the Monarch® Plasmid Miniprep Kit (New England BioLabs, USA) according to the manufacturer's instructions.

To generate constructs and ligate inserts into vectors, plasmids were first linearized by PCR and inserts generated by PCR using *E. faecalis* OG1RF genomic DNA as a template. PCR was done using Q5® High-Fidelity DNA Polymerase (New England BioLabs, USA) according to the manufacturer's instructions. Linearized plasmids and their corresponding inserts were then ligated using the In-Fusion HD Cloning system (Takara, Japan) and transformed into Stellar™ Competent Cells (Takara, Japan) according to the manufacturer's instructions. Plasmids were then extracted from the stellar competent cells using the Monarch® Plasmid Miniprep Kit and then transformed into electrocompetent *E. faecalis*. PCR to create *ftsH(H456Y)* related inserts were done by overlap extension PCR.

To create strains for CRISPRi knockdowns, the pABG5.2mini plasmid was first linearized by PCR and ligated with inserts containing the guide RNA by using the In-Fusion HD Cloning system. These inserts were in the form of gBlocks ordered from Integrated DNA Technologies Pte. Ltd, Singapore. gBlock (insert) sequences can be found in the **table 3.3** below. pMSP3545-dcas9 was first

transformed into *E. faecalis* wild type and Δ*mprF1*Δ*mprF2*, followed by the respective pABG5.2mini based guide RNA plasmids.

Table 3.3. gBlocks Sequences for Guide RNA inserts	
gBlock	**Sequence**
*lysS*_g1	TATCGACGGAAGATCCTGCAGAGATCTATCTAAAACAGTCTTAATTCTATCTT GAGAAAGTATTGGTAATAATATTATTGTCGATAACGCGAGCATAATAAACGG CTCTGATTAAATTCTGAAGTTTGTTAGATACAATGATTTCCGATCGAAACGTT TACCGAAGTTTTAGAGCTAGAAATAGCAAGTTAAAATAAGGCTAGTCCGTTA TCAACTTGAAAAAGTGGCACCGAGTCGGTGCTTTTTTTGGATCCACTAGTGG TACCGAATTCAACCCGAACAATTGGCATGCGGCCGCCACCGCGGT
*pyrB*_g1	TATCGACGGAAGATCCTGCAGAGATCTATCTAAAACAGTCTTAATTCTATCTT GAGAAAGTATTGGTAATAATATTATTGTCGATAACGCGAGCATAATAAACGG CTCTGATTAAATTCTGAAGTTTGTTAGATACAATGATTTCTAACCCCATGACT TCACGGTGTTTTAGAGCTAGAAATAGCAAGTTAAAATAAGGCTAGTCCGTTA TCAACTTGAAAAAGTGGCACCGAGTCGGTGCTTTTTTTGGATCCACTAGTGG TACCGAATTCAACCCGAACAATTGGCATGCGGCCGCCACCGCGGT

Transformants were selected by BHI or LB agar containing the appropriate antibiotics as listed in **table 3.1**. All screening of transformants were done using colony PCR using Taq DNA Polymerase, recombinant (5 U/μL) (Thermo Scientific, USA) according to the manufacturer's instructions. Gel electrophoresis to assess for product sizes were done using 1% w/v agarose gel in TAE buffer ran at 100 V for 30 mins followed by ethidium bromide staining for 10-15 mins. After each transformation step, if plasmids passed the colony PCR check, they were extracted and sent for Sanger sequencing for their inserts to ensure the correct sequence is present (1st BASE DNA Sequencing Services, Singapore). PCR purification was done using Wizard® SV Gel and PCR Clean-Up System (Promega, USA) according to the manufacturer's instructions. Sequences of the primers used for PCR are shown below **(table 3.4)**. Verification of protein expression of the affinity tagged constructs (6his or 2HA) were done by western blot **(Supplementary Figure S3.1)**.

Table 3.4. PCR Primers			
Primer	**Target(s)**	**Sequence**	**Purpose / Remarks**
M13F	- pCYW2-*ftsH(G37X)* - pABG5.2mini-*lysS*_g1 - pABG5.2mini-*pyrB*_g1 - pGCP213-*ftsH(G37X)*	GTAAAACGACGGCCAG	Screening for transformants targeting the insert
M13R		CAGGAAACAGCTATGAC	Same primers used for Sanger sequencing
pMSP3535-Screen_R	- pMSP3535-6his-*ftsH* - pMSP3535-2HA-*ftsH* - pMSP3535-6his-*ftsH(H456Y)* - pMSP3535-2HA-*ftsH(H456Y)* - pMSP3535-*cls1* - pMSP3535-OG1RF_10100-HA - pMSP3535-OG1RF_11679-HA - pMSP3535-OG1RF_10473-HA	CGAAATTAATACGACTCACTATAGGG	Screening for transformants targeting the insert
pMSP3535-Screen_F		TTTTGAAAACCGCTACGGATC	Same primers used for Sanger sequencing
pMSP3545-Screen-F	pMSP3545-*dcas9*	TAATACGACTCACTATAGGG	Screening for transformants targeting the insert
pMSP3545-Screen-R		GGTTGCAAATTTTGAAAACCGC	Same primers used for Sanger sequencing
Amp_FtsH_F	*E. faecalis* colonies from strains obtained from *in vitro* evolution	AGCTGACTACGTAGGGTTTG	Screening of FtsH locus for truncation of FtsH size on the genome
Amp_FtsH_R		GTGCAGTATTCGTCAACTCG	
Nil	pGCP213	Nil	EcoRI and NotI restriction enzymes used to linearise instead
pMSP3535-BamHI-F	pMSP3535	GATCCATGCAGAGTCTCCTGTTTTACAACCGGGTGTACATAGCGAAATACTTGTAATGCGTGGT	To linearize plasmid
pMSP3535-PstI-R		GGAATTCGCATGCGAGCTCGTCGACAGCGCTTCTAGAC	

Nil	pCYW2	Nil	EcoRI and NotI restriction enzymes used to linearise instead
5.2mini_ Linearise_F	pABG5.2mini	GGCCGCCACCGCGGTG GAGCTC	To linearize plasmid
5.2mini_ Linearise_R		GATCTTCCGTCGATACT ATGTTATACG	
FtsH_STOP_ Cmpl_F	Genomic DNA of DAP^{R} strain from *in vitro* evolution: DAP#50	GCTTGATATCGAATTAAT GATGAGCATAAGGAGGA	To create insert: *ftsH(G37X)*
FtsH_STOP_ Cmpl_R		ACCGCGGTGGCGGCCT TATTTATAACGATCTTCG TAG	
6his-FtsH_F	*E. faecalis* OG1RF gDNA	GACTCTGCATGGATCAT GCATCATCACCATCACC ACATGAGCATAAGGAGG ACAGG	To create insert: 6his-*ftsH*
FtsH_R		TCGCATGCGAATTCCCT GCACCTTCTACTAATTG GTTATT	
2HA-FtsH_F	*E. faecalis* OG1RF gDNA	GACTCTGCATGGATCAT GTACCCATACGATGTTC CAGATTACGCTTACCCA TACGATGTTCCAGATTA CGCTAGCATAAGGAGGA CAGGC	To create insert: 2HA-*ftsH*
FtsH_R		TCGCATGCGAATTCCCT GCACCTTCTACTAATTG GTTATT	
(1) 6his-FtsH_F	First PCR template is *E. faecalis* OG1RF gDNA Second PCR template is a 1:1 mix of the PCR products from the first reaction: (1+2) and (3+4)	GACTCTGCATGGATCAT GCATCATCACCATCACC ACATGAGCATAAGGAGG ACAGG	To create insert: 6his-*ftsH(H456Y)* Overlap extension PCR. First PCR using primers (1)+(2), (3)+(4). Second PCR using primers (1)+(4)
(2) FtsH(H456Y)_ R		GTGTCCCGCTTCGTAGT AAGCCACC	
(3) FtsH_(H456Y) _F		GGTGGCTTACTACGAAG CGGGACAC	
(4) FtsH_R		TCGCATGCGAATTCCCT GCACCTTCTACTAATTG GTTATT	
(1) 2HA-FtsH_F	First PCR template is *E. faecalis* OG1RF gDNA Second PCR template is a 1:1 mix of the PCR products from the first reaction: (1+2) and (3+4)	GACTCTGCATGGATCAT GTACCCATACGATGTTC CAGATTACGCTTACCCA TACGATGTTCCAGATTA CGCTAGCATAAGGAGGA CAGGC	To create insert: 2HA-*ftsH(H456Y)* Overlap extension PCR. First PCR using primers (1)+(2), (3)+(4). Second PCR using primers (1)+(4)
(2) FtsH(H456Y)_ R		GTGTCCCGCTTCGTAGT AAGCCACC	
(3) FtsH_(H456Y) _F		GGTGGCTTACTACGAAG CGGGACAC	
(4) FtsH_R		TCGCATGCGAATTCCCT GCACCTTCTACTAATTG GTTATT	
arcB_F	*E. faecalis* OG1RF gDNA	GACTCTGCATGGATCTA GGAGGAATCATCATGAA TTCAGT	To create insert: OG1RF_10100-HA
arcB_HA_R		TCGCATGCGAATTCCCT ACTAAGCGTAATCTGGA ACATCGTATGGGTACAC ACGAGGAATGAATAAGT TGC	

11679_F	*E. faecalis* OG1RF gDNA	GACTCTGCATGGATCTG GAGGAATCAACGAATGA AAAAATT	To create insert: OG1RF_11679-HA
11679_HA_R		TCGCATGCGAATTCCTT ATTAAGCGTAATCTGGA ACATCGTATGGGTATTTA CTCATTAAGCCATCATG GATTTT	
10473_F	*E. faecalis* OG1RF gDNA	GACTCTGCATGGATCTG GTATAGGAGGATAAAAA TGTCTAAATTTTTA	To create insert: OG1RF_10473-HA
10473_HA_R		TCGCATGCGAATTCCTT ATTAAGCGTAATCTGGA ACATCGTATGGGTACTG CTCATCTCTATTTATTTT TTTACTGTTTG	

3.3. Results

3.3.1. *ftsH* is essential in the wild type *E. faecalis* but not *mprF* mutants

MprF has been implicated in daptomycin resistance in *S. aureus*, where *mprF* gain of function mutations and increased *mprF* expression were found in DAP^R isolates (Ernst et al., 2018; Mishra et al., 2009; Sabat et al., 2018). Similarly, in *E. faecalis*, loss of *mprF2* led to a 1.5 to 2-fold decrease in the daptomycin MIC in daptomycin susceptible (DAP^S) strains (Iris Gao, unpublished). These observations suggested that MprF contributes to DAP^R and its activity might be masking other mutations related to DAP^R previously reported in clinical isolates and *in vitro* evolution assays. Preliminary work to uncover these masked mutations involved an *in vitro* evolution assay conducted in the wild type and the *mprF* mutant backgrounds (Δ*mprF1*, Δ*mprF2* and Δ*mprF1*Δ*mprF2*) (Iris Gao, unpublished). Novel DAP^R-associated mutations were discovered. *ftsH*, encoding a putative membrane protein (OG1RF_11507) and a putative permease (OG1RF_10437) were found to occur in only in the Δ*mprF1*Δ*mprF2* background in intermediate, and late stages of evolution respectively (intermediate, ≤ 64 μg/mL; Late, ≤ 256 μg/mL highest growth permissive concentration (HGPC) of daptomycin). Mutations in a gene encoding a putative HD domain protein (OG1RF_11901) was also discovered to occur both in the wild type and Δ*mprF1* at late stages of evolution (Iris Gao, unpublished).

Due to the enrichment of *ftsH* mutants in the Δ*mprF1*Δ*mprF2* background and since *ftsH* has not been studied in *E. faecalis*, this chapter focuses on the *ftsH* hit from the in vitro evolution assay and investigate the relationship between *ftsH* and DAP^R acquisition.

FtsH is a membrane-bound cytoplasmic protease that is highly conserved in bacteria, where it is essential in some species like *E. coli* but dispensable in others such as *B. subtilis* (Bittner et al., 2017; Deuerling et al., 1997). FtsH

consists of a 2 transmembrane domains at the N-terminal region which is linked by a glycine-rich linker to a AAA+ domain that is responsible for threading substrate proteins into its homohexamer complex through the use of ATP, and a zinc-metalloprotease domain that is responsible for its endopeptidase activity (Langklotz et al., 2012) **(Figure 3.2A)**. From whole genome sequencing of the *in vitro* evolution isolates, we observed that most of the DAP^R mutations in *ftsH* resulted in mutations clustering within the ATP-binding site of the AAA+ domain or resulting in a nonsense mutation (G37X) in the N-terminal region, truncating *ftsH* to just its first transmembrane domain which are highly indicative of loss of function **(Figure 3.2A)**.

To examine the effect of these loss of function mutations in *E. faecalis*, the G37X variant was picked for further investigation since it was an obvious loss of function mutation. *ftsH(G37X)* was heterologously expressed in the wild type and Δ*mprF1*Δ*mprF2* with constitutive expression under a *srtA* promoter. When growth was assessed, expression of the *ftsH(G37X)* variant resulted in slightly slowed growth rates in wild type as compared to its empty vector control, which was not observed in Δ*mprF1*Δ*mprF2*. It was also noted that there were large variations in absorbance readings during the mid-log phase of the wild type expressing *ftsH(G37X)* **(Figure 3.2B)**. When cultures of the wild type expressing *ftsH(G37X)* were spotted onto agar, small and large colony variants were observed which were absent in the empty vector control that displayed only large colonies **(Figure 3.2C)**. When colony PCR of the plasmid inserts were conducted on these colony variants of the wild type expressing *ftsH(G37X)*, the *ftsH(G37X)* sequence was truncated or lost in the large colony variants, whereas the sequence was intact in the small colony variants **(Figure 3.2C)**. Furthermore, attempts to reconstitute the G37X mutation onto genomic *ftsH* were only successful in Δ*mprF1*Δ*mprF2* under daptomycin pressure at sub-inhibitory

concentrations (1 µg/mL) **(Figure 3.2D)**, suggesting that FtsH loss of function is beneficial in the presence of DAP and permitted only in the absence of MprF.

Taken together, this suggests that *ftsH* is essential in the wild type but dispensable in ∆*mprF1*∆*mprF2*. FtsH forms homo-hexamers facilitated by its transmembrane domains (Langklotz et al., 2012; Makino et al., 1999). Upon heterologous expression of *ftsH(G37X)*, it is likely that this defective FtsH variant possessing only one transmembrane region oligomerises with native FtsH, disrupting FtsH hexamer formation with full length subunits resulting in complex dysfunction, which then manifests as a dominant negative growth defect.

To verify if oligomerisation with defective monomers does indeed cause dysfunction of FtsH resulting in the growth defect in wild type *E. faecalis*, a proteolytically inactive *ftsH* variant was constructed and expressed. The zincin motif – a conserved HEXXH sequence (HEAGH) of the protease active centre in the protease domain – was mutated to an inactive variant (YEAGH) by introducing a previously reported inactivating-mutation (H456Y) (Arends et al., 2016; Bieniossek et al., 2006). Inducible expression of proteolytically inactive *ftsH*, 6his-*ftsH(H456Y)* in the wild type led to slowed growth while expression of wild type 6his-*ftsH* showed similar growth as the empty vector control **(Supplementary Figure S3.2)**. Hence it is likely that oligomerisation with inactive FtsH monomers leads to a wild type specific growth defect.

A

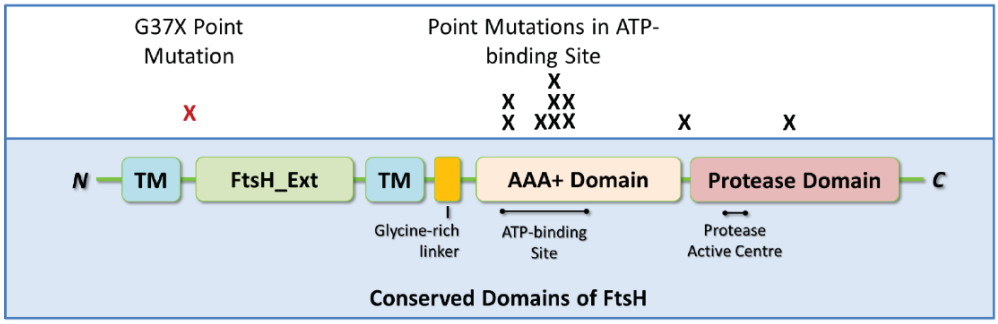

B

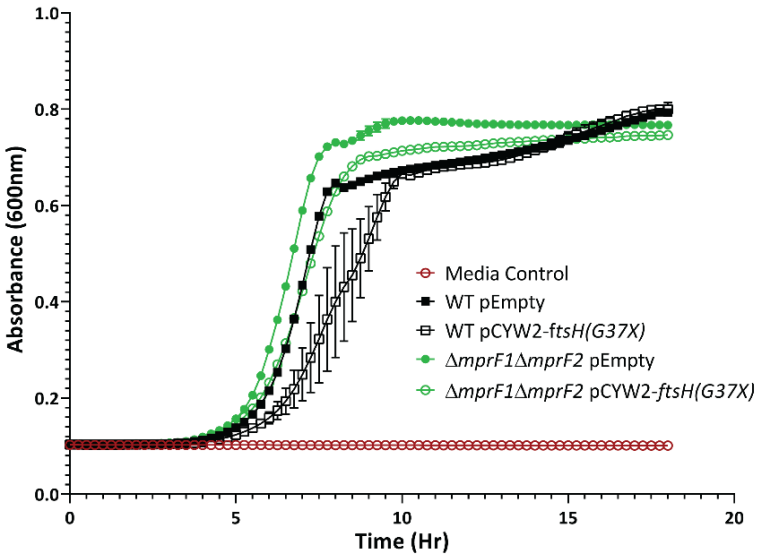

Strain	Plasmid	Mean specific growth rate (h^{-1})		Mean endpoint absorbance (600nm)		Mean lag phase duration (h)
WT	pEmpty	0.660 ± 0.007	-	0.793 ± 0.003	-	3.75
	pftsH(G37X)	0.388 ± 0.064	**	0.800 ± 0.019	ns	3.75
ΔmprF1 ΔmprF2	pEmpty	0.625 ± 0.015	-	0.767 ± 0.006	-	3.75
	pftsH(G37X)	0.582 ± 0.008	*	0.746 ± 0.007	*	3.75

C

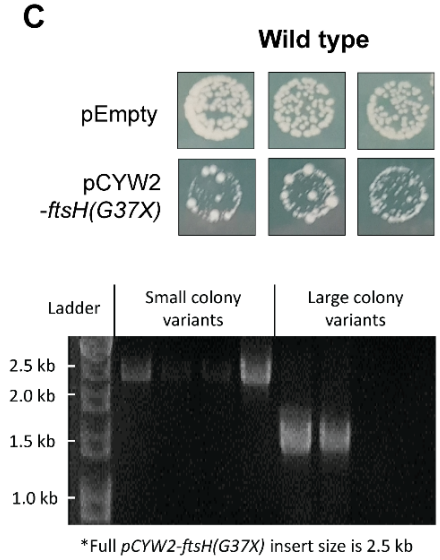

*Full *pCYW2-ftsH(G37X)* insert size is 2.5 kb

D

Introducing G37X mutation on genomic *ftsH*		
Strain	**Manipulation**	**Outcome**
Wild type	Genomic *ftsH* to G37X variant	✗
ΔmprF1ΔmprF2	Genomic *ftsH* to G37X variant	✓ Under DAP selective pressure

Figure 3.2. Heterologous expression of *ftsH(G37X)* reveals that *ftsH* is essential in the wild type. (A) Map of FtsH domains. "x" refers to the location of point mutations

observed. **(B)** Growth curves of wild type and Δ*mprF1*Δ*mprF2* with *ftsH(G37X)* expression. Each data point represents the mean ± standard error of measurement calculated from 3 biological replicates with 3 technical replicates each. Each biological replicate consists of averaged values from its constituent technical replicates. Mean specific growth rates, end point absorbance and lag phase durations are also displayed. Comparisons made between pftsH(G37X) against pEmpty of each strain. *, p=0.05 to 0.01; **, p=0.001 to 0.01; T-test. **(C)** *ftsH(G37X)* results in small and large colony variants in the wild type, where large colony variants show reduced/absent inserts. **(D)** The G37X mutation can only be introduced in Δ*mprF1*Δ*mprF2* but not the wildtype.

3.3.2. *ftsH* dysfunction leads to increased rate of DAP^R acquisition

Since the loss of function mutations occurred only in *ftsH* early in DAP^R evolution, we wanted to determine if *ftsH* inactivation has any significant impact on DAP MIC of *E. faecalis*. To address this, we assessed the MIC of the genomic *ftsH(G37X)* mutant, Δ*mprF1*Δ*mprF2 ftsH(G37X)* and a passage-controlled counterpart of its parental strain **(Figure 3.3A)**. The passage control counterpart refers to the parental strain, Δ*mprF1*Δ*mprF2*, that was passaged alongside Δ*mprF1*Δ*mprF2 ftsH(G37X)* during the process to introduce the G37X mutation on genomic *ftsH* by homologous recombination. This strain will henceforth be referred to as Δ*mprF1*Δ*mprF2* passage control. We observed that Δ*mprF1*Δ*mprF2 ftsH(G37X)* had a slightly higher MIC at 32 µg/mL DAP as compared to Δ*mprF1*Δ*mprF2* passage control which had an MIC range of 16 – 32 µg/mL, with most replicates displaying 16 µg/mL DAP MIC **(Figure 3.3A)**. These data suggested that the G37X inactivating mutation in *ftsH* only directly affects *E. faecalis'* resistance to DAP to a small extent, which is unsurprising since this mutation occurs early in evolution (≤ 16 µg/mL DAP HGPC).

Since this mutation frequently occurs in early evolution, we next hypothesized that this is not directly affecting resistance to DAP, but instead affects the rate of DAP^R acquisition. To investigate this, we performed *in vitro* evolution to DAP^R on the Δ*mprF1*Δ*mprF2* passage control and Δ*mprF1*Δ*mprF2 ftsH(G37X)* **(Figure 3.3B)**. Δ*mprF1*Δ*mprF2 ftsH(G37X)* achieved endpoint DAP^R of 512 µg/mL HGPC of DAP faster than its passage control, suggesting that the G37X mutation accelerates the rate of DAP^R acquisition **(Figure 3.3B)**. To determine if mutation in *ftsH* is required to achieve high level HGPC of DAP later in evolution, PCR amplification of the *ftsH* locus inclusive of its native promoter was conducted on Δ*mprF1*Δ*mprF2* passage control on day 3, 6 and 9 of evolution **(Supplementary Figure S3.3)**. Only a small fraction of the colonies tested had

reduced or absent PCR products from amplification indicative of mutations in the locus across all time points **(Figure S3.3)**. This suggests that mutations in *ftsH* is not a required trajectory to achieve higher levels of HGPC later in evolution, though these mutations certainly help in increasing the DAP^R acquisition rate. Since this method only detects large deletions, it is possible that small inserts/deletions or single nucleotide polymorphisms (SNPs) might be missed which can be addressed by whole genome sequencing. However, this will likely replicate the mutation trajectory of the initial *in vitro* evolution of the *mprF* mutants which also showed that *ftsH* is not a required trajectory (Iris Gao, unpublished).

We therefore hypothesized that the accelerated DAP^R acquisition rate of Δ*mprF1*Δ*mprF2 ftsH(G37X)* could be due to increased basal mutation rates as compared to its passage control. To address this, we assayed the basal mutation rates of Δ*mprF1*Δ*mprF2 ftsH(G37X)* and Δ*mprF1*Δ*mprF2* passage control using the Luria-Delbrück fluctuation assay **(Figure 3.3C)**. Δ*mprF1*Δ*mprF2 ftsH(G37X)* was observed to have 2 log-fold increase in mutation rate as compared to the passage control strain, which explains the accelerated DAP^R acquisition rate.

A

MIC of *ftsH* mutant strains by microplate dilution	
Strain	**Daptomycin MIC (µg/mL)**
Δ*mprF1*Δ*mprF2* passage control	**16** – 32
Δ*mprF1*Δ*mprF2 ftsH(G37X)*	32

B

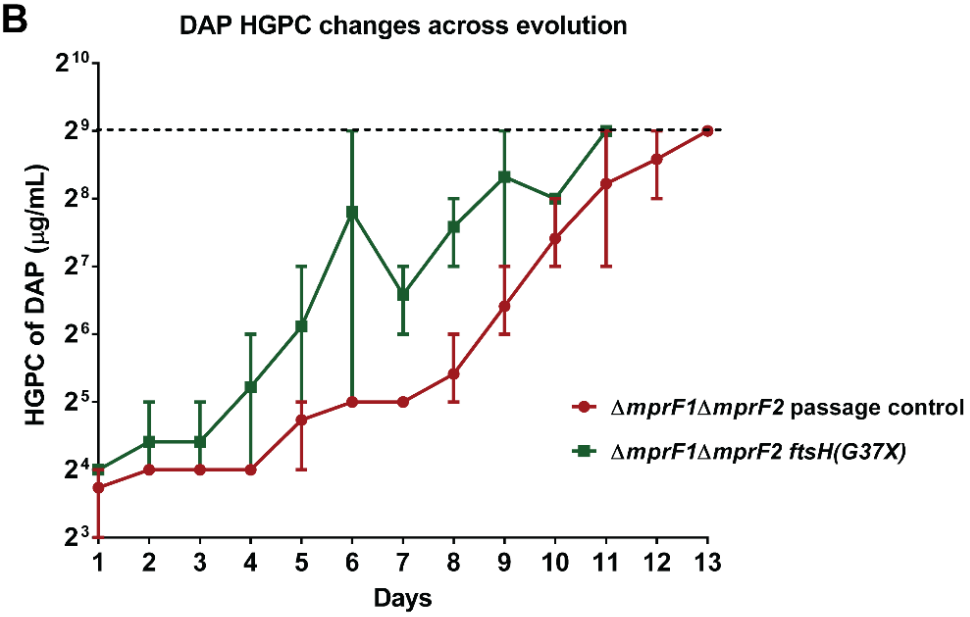

C

Mutation rate of Δ*mprF1*Δ*mprF2 ftsH(G37X)*	
Strain	**Mean mutation rate**
Δ*mprF1*Δ*mprF2* passage control	$4.08 \times 10^{-10} \pm 4.66 \times 10^{-10}$
Δ*mprF1*Δ*mprF2 ftsH(G37X)*	$2.44 \times 10^{-8} \pm 2.65 \times 10^{-8}$

Figure 3.3. Inactivation of *ftsH* leads to accelerated DAP^R acquisition rate. (A) MIC of Δ*mprF1*Δ*mprF2* passage control and Δ*mprF1*Δ*mprF2 ftsH(G37X)* measured by microplate dilution assay. The MIC that most of the tested replicates display are shown in bold. Data obtained from 3 biological replicates with 3 technical replicates each. Representative data from 2 experiments. **(B)** *In vitro* evolution of Δ*mprF1*Δ*mprF2* passage control and Δ*mprF1*Δ*mprF2* to highest growth permissive concentration (HGPC) of DAP of 512 µg/mL. HGPC of DAP progression displayed against time. 3 lines of evolution were conducted. **(C)** Mean mutation rate with standard deviation of Δ*mprF1*Δ*mprF2* passage control and Δ*mprF1*Δ*mprF2* assayed by the Luria-Delbrück fluctuation assay from 3 independent experiments.

3.3.3. Transcriptomic analyses reveal altered metabolism in wild type under FtsH inactivated conditions

To understand why FtsH dysfunction leads to the growth defect in the wild type background, RNA sequencing was performed on RNA extracted upon inducible expression of 6his-*ftsH(H456Y)* or 6his-*ftsH* encoded on plasmids in the wild type background **(Figure 3.4)**.

Gene set enrichment analysis was performed on the transcriptomic data obtained where the gene sets which are significantly differentially regulated and their pathways are highlighted **(Figure 3.4A, B)**. In this analysis, genes involved in oxidative phosphorylation, the shikimate pathway and carbon utilisation were differentially regulated **(Figure 3.4C)**. In the oxidative phosphorylation pathway, there was an upregulation of V-type ATPases involved in ATP utilisation (*atpABDGI)* as well as a F-type ATPase involved in ATP generation (*atpA2* – α-subunit) as well as downregulation a F-type ATPase involved in ATP generation (*atpC2* ε-subunit), cytochrome bd complex (*cydB)* and NADH dehydrogenase (*ndh3*) in wild type p6his-*ftsH(H456Y)* **(Figure 3.4C)**. This suggests that there might be an overall net increase in ATP utilisation and decrease in ATP generation, together with possible disruption of the electron transport chain in wild type p6his-*ftsH(H456Y)*. We also observed a down regulation of genes involved in the shikimate pathway involved in chorismate biosynthesis (*aroABCF*) in wild type p6his-*ftsH(H456Y)* **(Figure 3.4C)**. Since chorismate is a precursor to aromatic amino acid biosynthesis and is part of the folate biosynthetic pathway, it is likely that there is reduced aromatic amino acid and folate production under FtsH dysfunction in the wild type (Dosselaere and Vanderleyden, 2001). Furthermore, we also observed that an up-regulation of genes encoding enzymes between glyceraldehyde-3-phosphate and glycerate-3-phosphate steps in glycolysis (*tpiA, gap, pqk, gap2*) suggesting possible increased

glycolysis in wild type p6his-*ftsH(H456Y)* **(Figure 3.4C)**. Taken together these data led us to hypothesize that there might be metabolic changes under FtsH dysfunction in the wild type that could be leading to decreased ATP generation, aromatic amino acid and folate production as well as increased glycolysis which could in concert be the reason for the slowed growth when expressing defective FtsH monomers in the wild type. However, to confirm this future work to investigate ATP production through fluorometric assays, mass spectrometric quantification of chorismate, folate and aromatic amino acids, and extracellular acidification assays to indirectly measure the extent of glycolysis by detecting lactate production should be done to validate this hypothesis. Furthermore, qRT-PCR should also be conducted to validate these findings and CRISPRi knockdowns of these implicated genes should be done to validate their essentiality for growth.

To determine if FtsH dysfunction leads to impaired cell integrity in terms of membrane permeability, live-dead staining was carried out on stationary phase cultures of wild type and Δ*mprF1*Δ*mprF2* expressing the *ftsH(G37X)* defective monomer as well as wild type with inducible expression of inactive *ftsH*, *ftsH(H456Y)* to determine if there is any compromise in cell membrane permeability to propidium iodide (PI) **(Supplementary Figure S3.4A)**. It was observed that expressing *ftsH(G37X)* did not have a significant effect on permeability to PI as compared to empty vector controls, however expression of *ftsH(H456Y)* resulted a minor increase in PI staining of about 10% when compared to expression of *ftsH* (P = 0.05 to 0.01) **(Figure S3.4A)**. A more pronounced effect seen with *ftsH(H456Y)* could be due to higher expression levels with nisin induction as compared to the PsrtA promoter-controlled expression of *ftsH(G37X)*. However, through microscopy we also noticed that there was significant increase in cell chaining when either *ftsH(G37X)* or

ftsH(H456Y) was overexpressed in the wildtype of about 20% (P = 0.0001 to 0.001), which was not observed when *ftsH(G37X)* was expressed in ∆*mprF1*∆*mprF2* **(Supplementary Figure S3.4B)**. This increased chaining in the wild type expressing defective FtsH monomers could be indicative of defects in cell division which could be partly contributed by the metabolic changes observed.

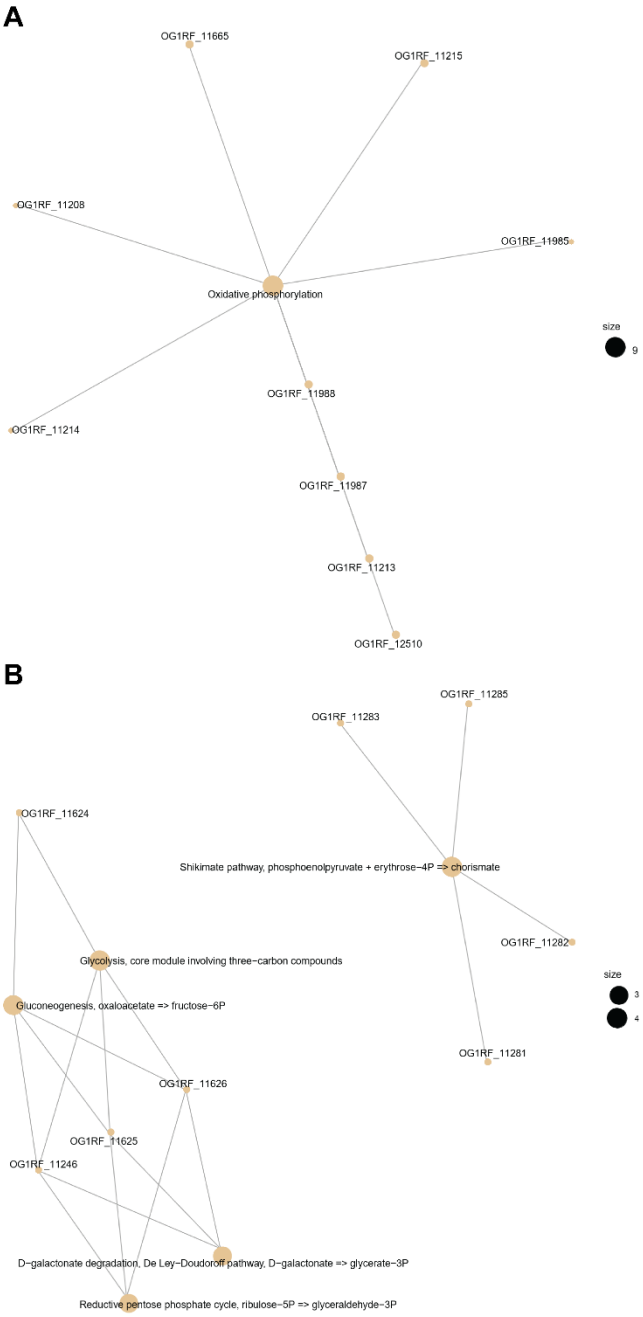

C

Oxidative Phosphorylation

Locus tag	log_2FC	Name
OG1RF_11214	1.34	*atpB*
OG1RF_11208	1.13	*atpI*
OG1RF_11665	-0.86	*cydB*
OG1RF_11215	1.07	*atpD*
OG1RF_11985	-1.57	*atpC2*
OG1RF_11988	0.79	*atpA2*
OG1RF_11987	0.72	*atpG*
OG1RF_11213	0.88	*atpA*
OG1RF_12510	-0.68	*ndh3*

Shikimate Pathway

Locus tag	log_2FC	Name
OG1RF_11285	-1.16	*aroA*
OG1RF_11283	-0.71	*aroC*
OG1RF_11282	-1.49	*aroB*
OG1RF_11281	-1.47	*aroF*

Carbon Utilisation

Locus tag	log_2FC	Name
OG1RF_11624	0.79	*tpiA*
OG1RF_11246	0.70	*gap*
OG1RF_11625	0.81	*pgk*
OG1RF_11626	1.45	*gap2*

Figure 3.4. Transcriptomic analysis of WT p6his-*ftsH(H456Y)* vs WT p6his-ftsH reveal metabolic changes. (A, B) Gene set enrichment analysis (GSEA) results. Plots showing interconnectivity between each gene in the respective differentially regulated pathways. Size of node represents number of genes in the respective category. Gene over-representation test comparing categories differentially expressed genes in each KEGG category comparing WT p6his-*ftsH(H456Y)* vs WT p6his-*ftsH*. **(B)** Tables showing the Log_2FC of the individual genes within the differentially regulated pathways in **(A)**. Data obtained from 3 biological replicates. Full table of fold-changes are shown in **Supplementary table S3.2.** Analysis carried out with assistance from Kelvin Chong.

3.3.4. Identification of FtsH substrates

It appears from our data that in FtsH dysfunctional conditions, wild type growth is impaired while the Δ*mprF1*Δ*mprF2* is not, and this dysfunction is beneficial to DAP^R acquisition in Δ*mprF1*Δ*mprF2*. Since FtsH is a protease, it is likely that the growth and DAP^R acquisition effects are mediated by accumulation of a substrate or substrates when FtsH is inactivated. Hence, to further investigate this, we first needed to identify the substrates of FtsH.

To do this, we used a protease inactive variant of FtsH, FtsH(H456Y), where its HEXXH zincin motif in the protease active centre was mutated, to identify accumulated substrates, similar to an approach employed to identify FtsH substrates in *E. coli* (Arends et al., 2016; Westphal et al., 2012). As suggested above, heterologous expression of this variant will oligomerise with native FtsH to form a dysfunctional complex. Here, the AAA+ domain is still active and able to thread in unfolded proteins into the hexamer core, but due to the disabled protease active centre, degradation will be inefficient allowing substrates to be "trapped" within the complex. Since FtsH acts on both unfolded membrane proteins and SsrA-tagged cytoplasmic proteins, we analysed the proteome of both the membrane fraction and whole cell lysate (Langklotz et al., 2012; Okuno and Ogura, 2013). This approach allowed us to better capture both types of substrates and the membrane fraction samples allowed for reduced sample complexity and better detection of the trapped substrates and membrane proteome changes.

From the proteomic analysis, we observed both accumulation and depletion of proteins in the membrane fractions and the whole cell lysates in wild type p6his-*ftsH(H456Y)* **(Figure 3.5A, B)**. However, due to lysozyme contamination of the whole cell lysate and resulting reduced sensitivity, there were fewer proteins detected in this sample **(Figure 3.5B)**. Nonetheless, we used both samples to

identify proteins that were accumulated only in the absence of of FtsH-mediated degradation. Among these short-listed proteins, those whose genes were up regulated in RNAseq experiments, indicating that their protein levels are most likely influenced by increased transcription instead of FtsH dysfunction, were excluded. The refined list of likely FtsH substrates are shown in **Figure 3.5D**. These proteins include YcKE (beta-glucosidase), LysS (lysine-tRNA ligase), PyrB (aspartate carbamoyltransferase), LutA (a homolog to *B. subtilis* lactate utilisation Fe-S protein, LutA), GelE (gelatinase E), TrePP (carbamoyl-phosphate synthase), CryZ (putative NADPH:quinone reductase) and HrcA (heat-inducible transcription repressor).

Interestingly, depletion (rather than enrichment) of several proteins in both samples was also observed **(Figure 3.5A, B)**. This could be due to a compensatory response, where other proteases could display increased activity (and hence increased degradation of their own targets) in response to the accumulation of FtsH substrates, in order to control the overall amount of unfolded proteins in the cell. A similar criterion for short-listing these hits was employed, by selecting depleted proteins common to both samples, whose genes were also are not downregulated in RNAseq to rule out transcriptomic effects. The list of these short-listed proteins is shown in **Figure 3.5C**. They include ArcB (ornithine carbamoyltransferase), Cls1 (Cardiolipin synthase 1), OG1RF_11679 (a metal ABC transporter) and OG1RF_10473 (an amidase). To validate if these proteins are indeed accumulated or depleted as observed here, westernblot should be done for these implicated proteins. For implicated proteins where antibodies are not available, affinity tagging of those proteins can be done to allow for immunoblotting.

A

Wild type p6his-*ftsH(H456Y)* vs p6his-*ftsH*
(Membrane Fraction)

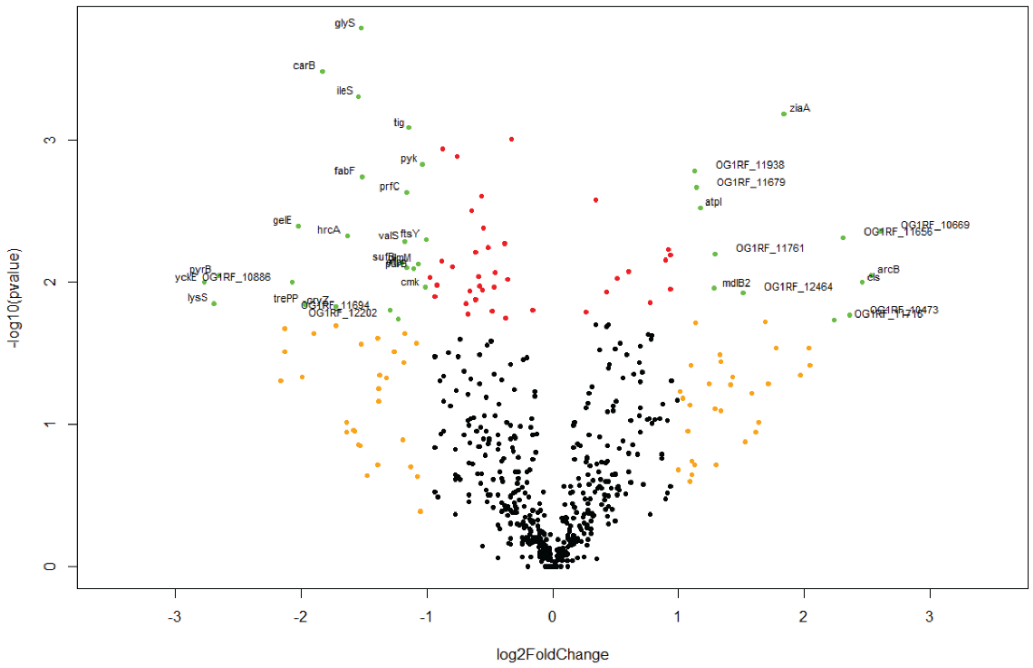

B

Wild type p6his-*ftsH(H456Y)* vs p6his-*ftsH*
(Whole cell lysate)

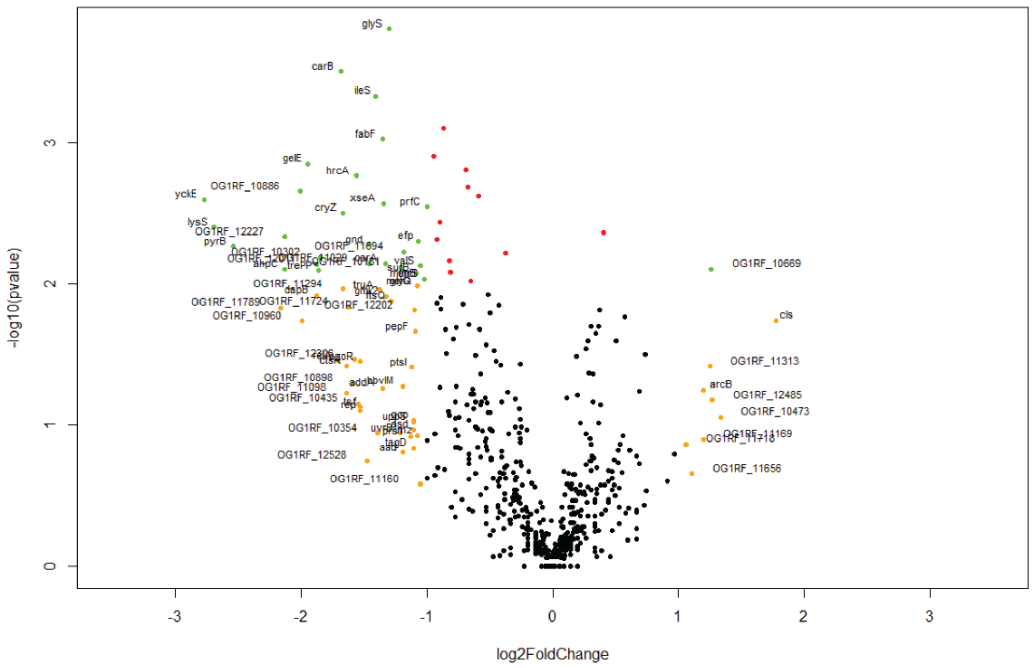

C

Depleted Proteins				
Gene	**Gene Number**	**Identity**	**Proteomics log_2FC**	**RNAseq log_2FC**
yckE	OG1RF_11014	beta-glucosidase	-2.77	-
lysS	OG1RF_10212	lysine--tRNA ligase	-2.69	-
pyrB	OG1RF_11430	aspartate carbamoyltransferase	-2.54	-
lutA	OG1RF_10886	Putative lactate utilisation Fe-S protein Homologous to *B. subtilis lutA*	-2.01	1.22
gelE	OG1RF_11526	gelatinase E	-1.95	-
trePP	OG1RF_12425	glycosyl hydrolase	-1.86	-
carB	OG1RF_11427	carbamoyl-phosphate synthase large subunit	-1.69	0.67
cryZ	OG1RF_11383	putative NADPH:quinone reductase	-1.67	-
hrcA	OG1RF_11076	heat-inducible transcription repressor HrcA	-1.56	-

D

Accumulated Proteins				
Gene	**Gene Number**	**Identity**	**Proteomics log_2FC**	**RNAseq log_2FC**
arcB	OG1RF_10100	ornithine carbamoyltransferase	2.53	-0.89
OG1RF_11679	OG1RF_11679	metal ABC transporter substrate-binding protein	1.14	-1.59
cls1	OG1RF_10364	cardiolipin synthase 1	2.46	-
OG1RF_10473	OG1RF_10473	amidase	2.36	-

Figure 3.5. Proteomic analysis of wild type p6his-*ftsH(H456Y)* vs p6his-*ftsH* for FtsH substrate identification. Membrane fraction and whole cell lysates of wild type cells with induced expression of inactive *ftsH* – *ftsH(H456Y)* – and wild type *ftsH*. Volcano plot of differential abundances of proteins detected in p6his-*ftsH(H456Y)* vs p6his-*ftsH* samples in **(A)** membrane fractions and **(B)** whole cell lysate. Red, FDR<0.05; orange, $log_2FC>1$; green, FDR<0.05 and $log_2FC>1$. Lists of short-listed proteins that are **(C)** depleted or **(D)** accumulated in wild type p6his-*ftsH(H456Y)* samples. Proteomic log_2FC values listed in **(C, D)** are from the membrane fraction. These short-listed proteins are protein hits which are common in both whole cell lysates and the membrane fraction and are not upregulated by RNAseq for the accumulated protein hits and not down regulated in the depleted protein hits. This is since we are interested in proteins which are accumulated/depleted due to the FtsH protease dysfunction that are not due to a transcriptional response. Data obtained from 3 biological replicates. Membrane fraction hits are filtered by P-value<0.05, FDR<0.05, $log_2FC>1$. Whole cell lysates are filtered by P-value<0.1, $log_2FC>1$ instead due to high lysozyme contamination reducing sensitivity of detection. Full table of fold-changes are shown in **Supplementary table S3.3.**

3.3.5. *trePP*, *lysS* and amidase contribute to growth defects in FtsH dysfunction

To determine if any of the depleted proteins identified in the proteomic analysis **(Figure 3.5 C, D)** were associated with the growth defects observed in the wild type background upon FtsH dysfunction, the available transposon (Tn) mutants of the depleted protein hits (*yckE, lutA*, *gelE, trePP, carB, cryZ* and *hrcA*) and CRISPR interference (CRISPRi) knockdowns for those which we had no Tn mutant (*lysS* and *pyrB*) were assayed for growth **(Figure 3.6A, B, C)**. Tn mutants of glycosyl hydrolase, *trePP* (3 out of the 4 available *trePP* Tn mutants), displayed a growth defect in terms of reduced stationary phase absorbance of between 0.100 to 0.200 as compared to wild type, as well as Tn::*gelE* which had a minor decrease in stationary phase absorbance of 0.040 whereas the others grew normally **(Figure 3.6A, B, C, G).** Tn mutants of *hrcA* also possessed a slight reduction in growth rates and slight increase in lag phase duration, while the other Tn mutants grew just as well as the wild type **(Figure 3.6A, B, C, G)**. Furthermore, in the CRISPRi knockdowns of *pyrB* and *lysS*, utilising a previously optimised dual plasmid inducible knockdown system for *E. faecalis* (Afonina et al., 2020), knockdowns of lysyl-tRNA ligase (*lysS*) in the wild type displayed slowed growth in terms of increased lag phase duration while knockdowns of aspartate carbamoyltransferase (*pyrB*) had minimal effect. Hence, it is likely that the depletion of *trePP* and *lysS* could be partly responsible for the growth defect observed under FtsH dysfunction in the wild type.

To determine if there were any differential effects when these knockdowns were conducted in the absence of *mprF*, the same CRISPRi knockdowns were done in the Δ*mprF1*Δ*mprF2* background. When we tested knockdowns of *pyrB* in Δ*mprF1*Δ*mprF2* there was similarly no effect on growth **(Figure 3.6D, G)**. Since depletion of LysS interfered with wild type growth under FtsH dysfunction, we

wondered what effect might be for Δ*mprF1*Δ*mprF2*. Given that *mprF* utilises lysyl-tRNA for lysyl-PG production, we hypothesize that in the Δ*mprF1*Δ*mprF2* there is lesser utilisation of lysyl-tRNA, and it might tolerate the knockdown of *lysS* better. However, unexpectedly we observed that *lysS* knockdown was less tolerated in Δ*mprF1*Δ*mprF2*, where there was significantly decreased growth rates and increased stationary phase absorbance and lag phase durations (**Figure 3.6D, G)**. It is possible that the compensatory changes observed in the lipidome and transcriptome of Δ*mprF1*Δ*mprF2* made it less tolerant of the loss of *lysS* expression. The exact mechanism however requires further investigation.

Returning to the original question of which FtsH targets must be degraded in sustain normal growth, we examined the role of the accumulated protein hits (*arcB, cls1*, OG1RF_11679, OG1RF_10473) in inhibiting growth. To force their accumulation in a wild type background, each gene was cloned into a nisin inducible expression vector pMSP3535 for inducible overexpression and assayed for growth **(Figure 3.6E, G)**. None of these overexpressed genes strongly affected growth except OG1RF_10473 (amidase) which resulted in slowed growth in both wild type and Δ*mprF1*Δ*mprF2* backgrounds in terms of growth rate and stationary phase absorbance. Since some amidases are involved in cell wall hydrolysis and septation during cell division, if OG1RF_10473 is indeed a cell wall amidase, it is possible that dysregulation by overexpression could affect cell division and in turn growth (Do et al., 2020; Priyadarshini et al., 2007). This situation could also explain the increased cell chaining that observed in the FtsH dysfunctional mutants during microscopy **(Supplementary Figure S3.4B)**.

Taken together, the reduced levels of TrePP and LysS, and increased levels of amidase (OG1RF_10473) appear to affect growth. We hypothesize that it is the combination of these differential regulation of genes which are contributing

factors to the growth defect observed in wild type under FtsH dysfunction. This will need to be tested via combinatorial CRISPRi knockdowns combined with genetic overexpression of amidase.

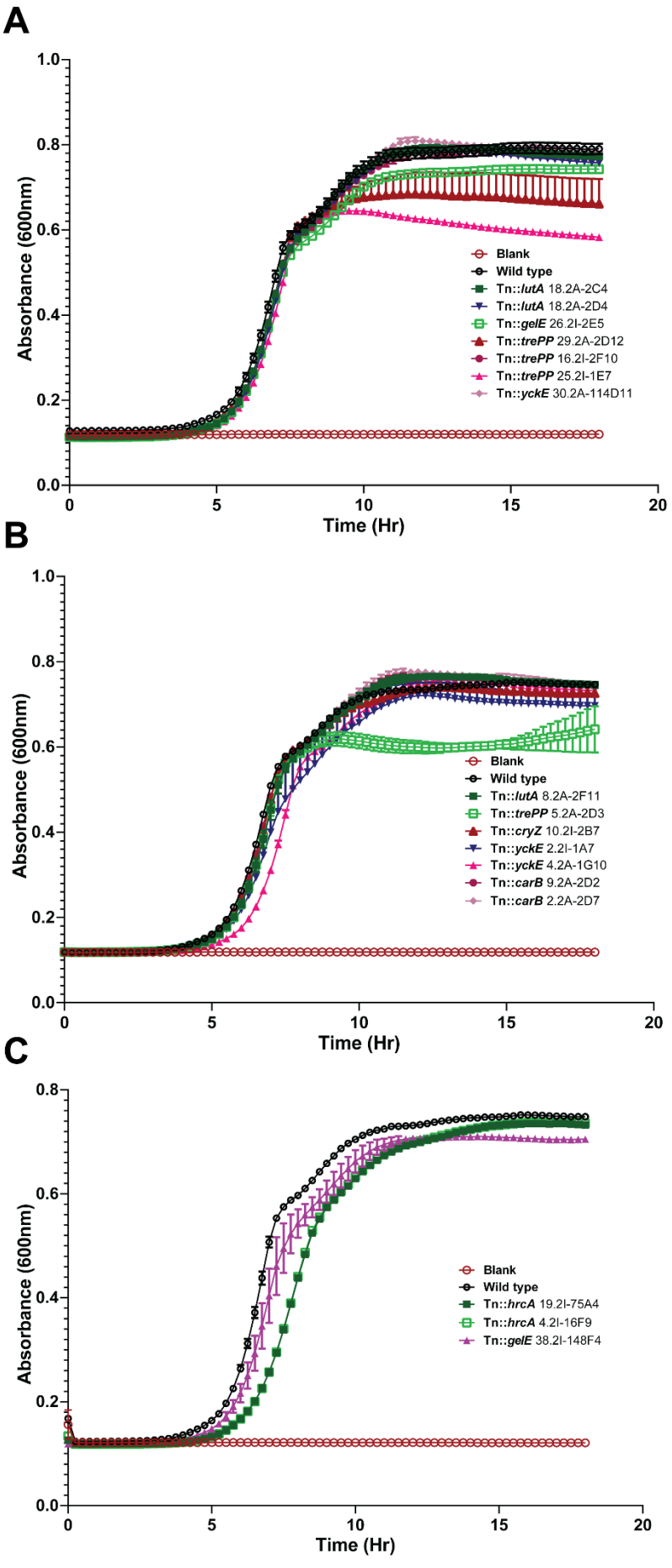
A
Absorbance (600nm)
Time (Hr)
Blank
Wild type
Tn::lutA 18.2A-2C4
Tn::lutA 18.2A-2D4
Tn::gelE 26.2I-2E5
Tn::trePP 29.2A-2D12
Tn::trePP 16.2I-2F10
Tn::trePP 25.2I-1E7
Tn::yckE 30.2A-114D11
B
Absorbance (600nm)
Time (Hr)
Blank
Wild type
Tn::lutA 8.2A-2F11
Tn::trePP 5.2A-2D3
Tn::cryZ 10.2I-2B7
Tn::yckE 2.2I-1A7
Tn::yckE 4.2A-1G10
Tn::carB 9.2A-2D2
Tn::carB 2.2A-2D7
C
Absorbance (600nm)
Time (Hr)
Blank
Wild type
Tn::hrcA 19.2I-75A4
Tn::hrcA 4.2I-16F9
Tn::gelE 38.2I-148F4

D

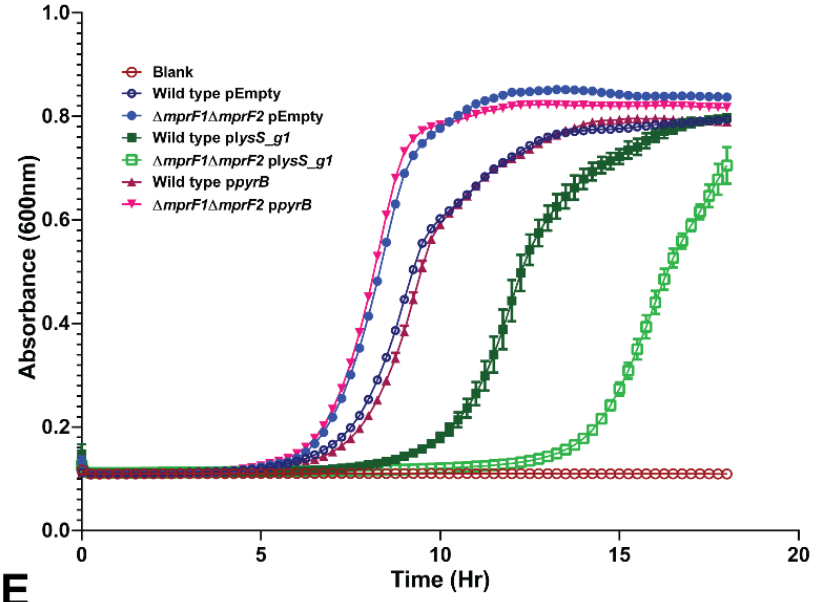
Blank
Wild type pEmpty
ΔmprF1ΔmprF2 pEmpty
Wild type plysS_g1
ΔmprF1ΔmprF2 plysS_g1
Wild type ppyrB
ΔmprF1ΔmprF2 ppyrB
Absorbance (600nm)
Time (Hr)

E

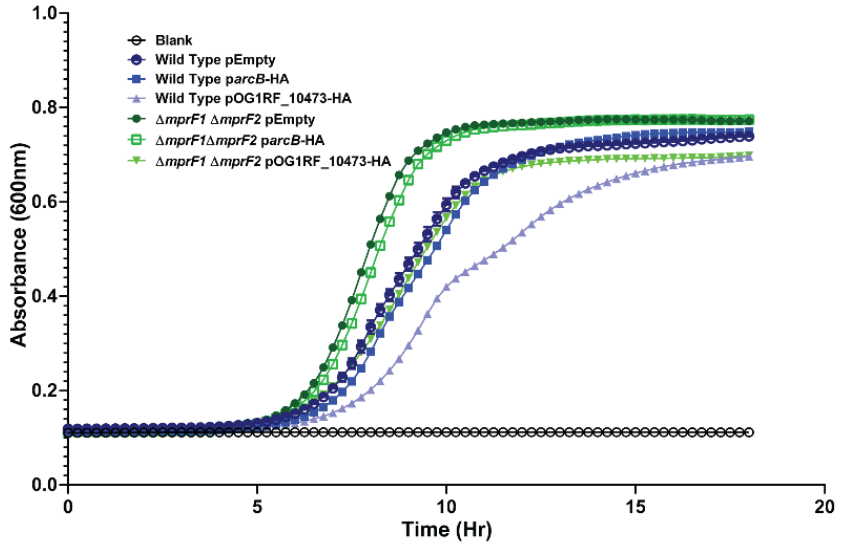
Blank
Wild Type pEmpty
Wild Type parcB-HA
Wild Type pOG1RF_10473-HA
ΔmprF1 ΔmprF2 pEmpty
ΔmprF1ΔmprF2 parcB-HA
ΔmprF1 ΔmprF2 pOG1RF_10473-HA
Absorbance (600nm)
Time (Hr)

F

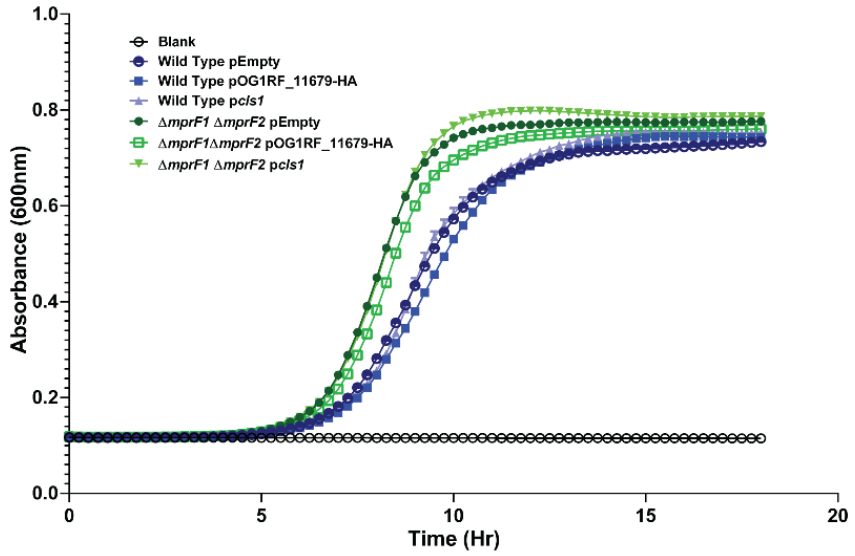
Blank
Wild Type pEmpty
Wild Type pOG1RF_11679-HA
Wild Type pcls1
ΔmprF1 ΔmprF2 pEmpty
ΔmprF1ΔmprF2 pOG1RF_11679-HA
ΔmprF1 ΔmprF2 pcls1
Absorbance (600nm)
Time (Hr)

G

Figure	Strain	Mean specific growth rate (h^{-1})		Mean endpoint absorbance (600nm)		Mean lag phase duration (h)
2.5A	WT	0.619 ± 0.018	-	0.790 ± 0.017	-	3.00
	Tn::lutA 18.2A-2C4	0.649 ± 0.005	*	0.772 ± 0.008	ns	3.00
	Tn::lutA 18.2A-2D4	0.648 ± 0.006	*	0.757 ± 0.007	ns	3.00
	Tn::gelE 26.2I-2E5	0.637 ± 0.003	ns	0.742 ± 0.004	ns	3.00
	Tn::trePP 29.2A-2D12	0.635 ± 0.008	ns	0.662 ± 0.081	**	3.00
	Tn::trePP 16.2I-2F10	0.652 ± 0.003	**	0.767 ± 0.007	ns	3.00
	Tn::trePP 25.2I-1E7	0.643 ± 0.002	*	0.583 ± 0.004	****	3.00
	Tn::yckE 30.2A-114D11	0.646 ± 0.010	*	0.774 ± 0.014	ns	3.00
2.5B	WT	0.657 ± 0.004	-	0.746 ± 0.002	-	3.00
	Tn::lutA 8.2A-2F11	0.645 ± 0.024	ns	0.746 ± 0.005	ns	3.00
	Tn::trePP 5.2A-2D3	0.657 ± 0.002	ns	0.641 ± 0.077	*	3.00
	Tn::cryZ 10.2I-2B7	0.648 ± 0.006	ns	0.726 ± 0.005	ns	3.00
	Tn::yckE 2.2I-1A7	0.563 ± 0.121	ns	0.696 ± 0.035	ns	3.00
	Tn::yckE 4.2A-1G10	0.653 ± 0.007	ns	0.732 ± 0.002	ns	3.75
	Tn::carB 9.2A-2D2	0.659 ± 0.004	ns	0.742 ± 0.008	ns	3.00
	Tn::carB 2.2A-2D7	0.643 ± 0.003	ns	0.740 ± 0.012	ns	3.00
2.5C	WT	0.655 ± 0.010	-	0.748 ± 0.004	-	2.50
	Tn::hrcA 19.2I-75A4	0.529 ± 0.002	***	0.732 ± 0.008	ns	3.25
	Tn::hrcA 4.2I-16F9	0.541 ± 0.004	***	0.736 ± 0.010	ns	4.00
	Tn::gelE 38.2I-148F4	0.604 ± 0.033	*	0.705 ± 0.003	***	4.00
2.5D	WT pEmpty	0.523 ± 0.005	-	0.794 ± 0.008	-	5.00
	WT plysS_g1	0.482 ± 0.029	ns	0.797 ± 0.009	ns	7.75
	WT ppyrB	0.553 ± 0.002	ns	0.790 ± 0.008	ns	5.00
	ΔmprF1 ΔmprF2 pEmpty	0.602 ± 0.008	-	0.837 ± 0.008	-	4.25
	ΔmprF1 ΔmprF2 plysS_g1	0.446 ± 0.013	****	0.705 ± 0.050	**	12.25
	ΔmprF1 ΔmprF2 ppyrB	0.605 ± 0.001	ns	0.817 ± 0.005	ns	4.25
2.5E	WT pEmpty	0.300 ± 0.014	-	0.739 ± 0.009	-	4.25
	WT parcB-HA	0.337 ± 0.002	*	0.749 ± 0.009	ns	4.25
	WT pOG1RF_10473-HA	0.391 ± 0.002	****	0.696 ± 0.006	**	4.25
	ΔmprF1 ΔmprF2 pEmpty	0.466 ± 0.011	-	0.772 ± 0.001	-	4.25
	ΔmprF1 ΔmprF2 parcB-HA	0.491 ± 0.003	*	0.774 ± 0.005	ns	4.25
	ΔmprF1 ΔmprF2 pOG1RF_10473-HA	0.299 ± 0.006	****	0.698 ± 0.002	****	4.25
2.5F	WT pEmpty	0.418 ± 0.005	-	0.734 ± 0.004	-	4.50
	WT pOG1RF_11679-HA	0.422 ± 0.004	ns	0.743 ± 0.009	ns	4.50
	WT pcls1	0.520 ± 0.006	****	0.754 ± 0.007	*	4.50
	ΔmprF1 ΔmprF2 pEmpty	0.475 ± 0.004	-	0.777 ± 0.002	-	4.50
	ΔmprF1 ΔmprF2 pOG1RF_11679-HA	0.502 ± 0.006	**	0.760 ± 0.002	***	4.50
	ΔmprF1 ΔmprF2 pcls1	0.496 ± 0.003	**	0.787 ± 0.002	**	4.50

Figure 3.6. Growth curves of mutant strains of depleted and accumulated protein hits. (A, B, C) Transposon (Tn) mutants of depleted protein hits tested assayed individually for growth. **(D)** For depleted hits where no Tn mutants are available, CRISPRi knockdowns of the respective genes were done instead, and growth assayed. **(E, F)** For accumulated protein hits, overexpressing strains of the respective genes were used, and growth assayed. Genes to be overexpressed are placed under a nisin inducible plasmid pMSP3535 and induced with 200 ng nisin for overexpression. Each data point for all graphs consists of 3 biological replicates, with each replicate consisting of averaged values from 3 biological replicates. Representative data of 2 experiments. **(G)** Mean specific growth rates, end point absorbance and lag phase durations. *, p=0.05 to 0.01; **, p=0.001 to 0.01; ***, p=0.0001 to 0.001; ****, p⩽0.0001; Dunnett's test for ANOVA. Comparisons made between transposon mutants and the wild type; plasmid containing strains against the empty vector control within the same strain background.

3.3.6. *lutA* and *yckE* contribute to accelerated DAP^R acquisition upon FtsH dysfunction while *hrcA* slows acquisition

To determine if any of the depleted protein hits contribute to accelerated DAP^R acquisition, one Tn mutant of each hit was evolved to DAP^R **(Figure 3.7)**. First, the DAP MIC and HGPC of the Tn mutants were assessed by microplate dilution, which remained similar to that of wild type **(Figure 3.7A)**. This was not surprising since, under FtsH dysfunction, DAP MIC did not differ greatly between ∆*mprF1*∆*mprF2 ftsH(G37X)* and the passage control **(Figure 3.3A)**.

The Tn mutants together with the wild type were then evolved to DAP^R using the MIC/HGPCs determined as starting points **(Figure 3.7B)**. Only Tn mutants of *lutA* (homolog of lactate utilisation Fe-S binding protein, *lutA* in *B. subtilis*) and *yckE* (beta glucosidase) displayed faster evolution to DAP^R (512 µg/mL) of about 1 day on average **(Figure 3.7B).** This difference may seem relatively minor. However, this is unsurprising since the evolution to DAP^R of 512 µg/mL in ∆*mprF1*∆*mprF2 ftsH(G37X)* was accelerated by 2 days as compared to its passage control counterpart. Given that contribution to DAP^R acquisition rate is likely multi-factorial, it is not unexpected that single mutants display an intermediate acceleration in acquisition. *lutA* (OG1RF_10886) is a homolog of *B. subtilis lutA* that is part of the *lutABC* operon which is essential for lactate utilisation (Chai et al., 2009). The involvement of *lutA* and *yckE* (beta-glucosidase) suggest that the possible impairments in lactate and complex sugar breakdown might be contributing to accelerated DAP^R acquisition. Whether this is due to direct effects on mutation rate or due to alleviation of metabolic constraints in acquiring DAP^R related mutations, needs to be investigated further.

Interestingly, the transposon mutant of *hrcA* displayed a large impediment in DAP^R acquisition rate, taking more than 20 days to achieve DAP^R of 512 µg/mL, while the wild type only took 12-14 days **(Figure 3.7B)**. *hrcA* encodes a negative

regulator of the *grpE-dnaK-dnaJ* and *groEL-groES* operons in *B. subtilis* (Roncarati and Scarlato, 2017; Schulz and Schumann, 1996). From transcriptomic data of FtsH dysfunction in the wild type, we indeed observe upregulation of *grpE*, *dnaK* and *groEL* (Log_2FC 1.13, 1.53, 1.58 respectively) **(Supplementary Table S3.2)**. This suggests that the loss of *hrcA* could relieve transcriptional repression of these operons allowing for their increased expression and chaperone activity that results in reduced rate of DAP^R acquisition. Whether this is due to direct effects on mutation rate needs to be further investigated.

Though it might also appear that *trePP* mutation might also be slowing DAP^R acquisition, this is unlikely to be the case as only 1 outlier took 18 days to reach DAP^R of 512 µg/mL while the rest took around 12 days on average which is similar to the wild type **(Figure 3.7B)**. To verify these findings, more parallel lines of evolution should be conducted in future.

A

MIC and HGPC of Tn mutant strains by microplate dilution		
Strain	**Daptomycin MIC (µg/mL)**	**Daptomycin HGPC (µg/mL)**
WT	**2**-4	**1**-2
Tn::*trePP* 5.2A-2D3	**2**-4	**1**-2
Tn::*gelE* 26.2I-2E5	**2**-4	**1**-2
Tn::*yckE* 30.2A-114D11	**2**-4	**1**-2
Tn::*cryZ* 10.2I-2B7	2-**4**	1-**2**
Tn::*hrcA* 19.2I-75A4	2	1
Tn::*lutA* 1.8A-2C4	**2**-4	**1**-2
Tn::*carB* 9.2A-2D2	4	2

B

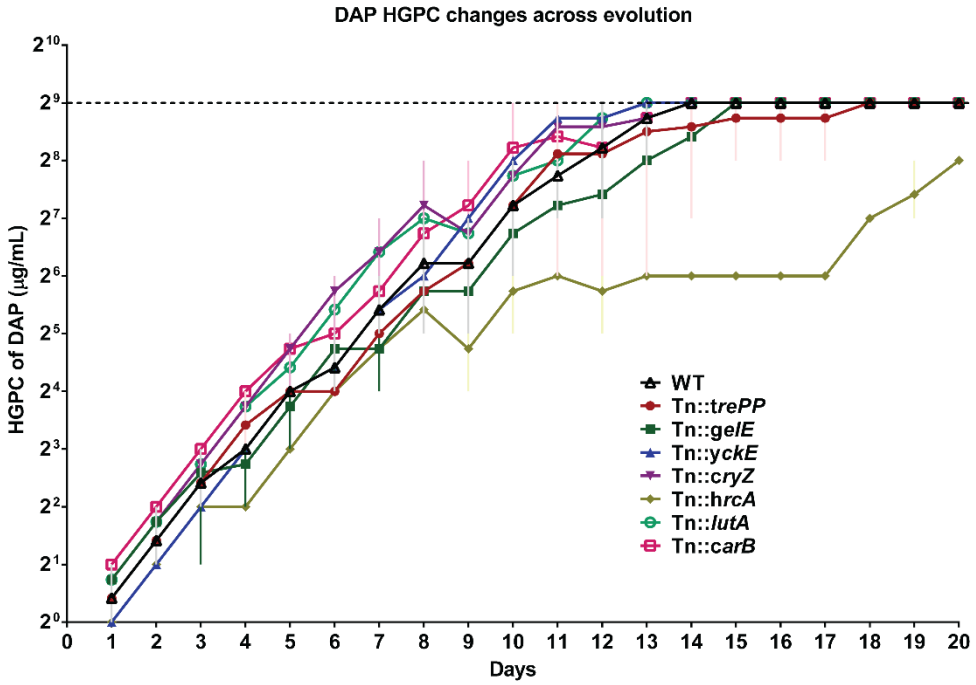

Figure 3.7. *In vitro* evolution to DAP^R of transposon mutants. (A) DAP MIC and HGPC of selected transposon (Tn) mutants corresponding to the depleted protein hits from FtsH dysfunction assayed by microplate dilution. The MIC that most of the tested replicates display are shown in bold. Data represents 3 biological replicates. **(B)** Average HGPC progression of the wild type and Tn mutants across evolution to DAP^R (512 µg/mL). 3 parallel lines of evolution were carried out per strain.

3.3.7. FtsH cell membrane localisation is pole and septum excluded

It has been reported in *S. aureus*, *E. coli, B. subtilis* and *B. burgdorferi* that FtsH is closely associated with functional membrane microdomains in these organisms (Lopez and Koch, 2017). Furthermore, given that anionic microdomains are likely to exist in the septum of *E. faecalis* which are enriched in SecA of the sec-secretion machinery, sortase A and are targets of CAMPs, it is possible that FtsH could be coordinated within these domains as well (Kandaswamy et al., 2013). To determine where FtsH might be spatially organised on the cell membrane, we conducted immunofluorescence microscopy on wild type cells with induced expression of 2HA-*ftsH.* We observed that cells at mid log phase display fluorescence along the cell perimeter which is excluded at the cell poles and septum **(Figure 3.8 A, B)**. Hence, they are likely coordinated at regions separate from septal domains. This is in contrast with what was observed in *B. subtilis* where FtsH localises to the septum during cell division and at the onset of sporulation with functions linked to regulatory initiation of sporulation (Thi Nguyen and Schumann, 2012; Wehrl et al., 2000).

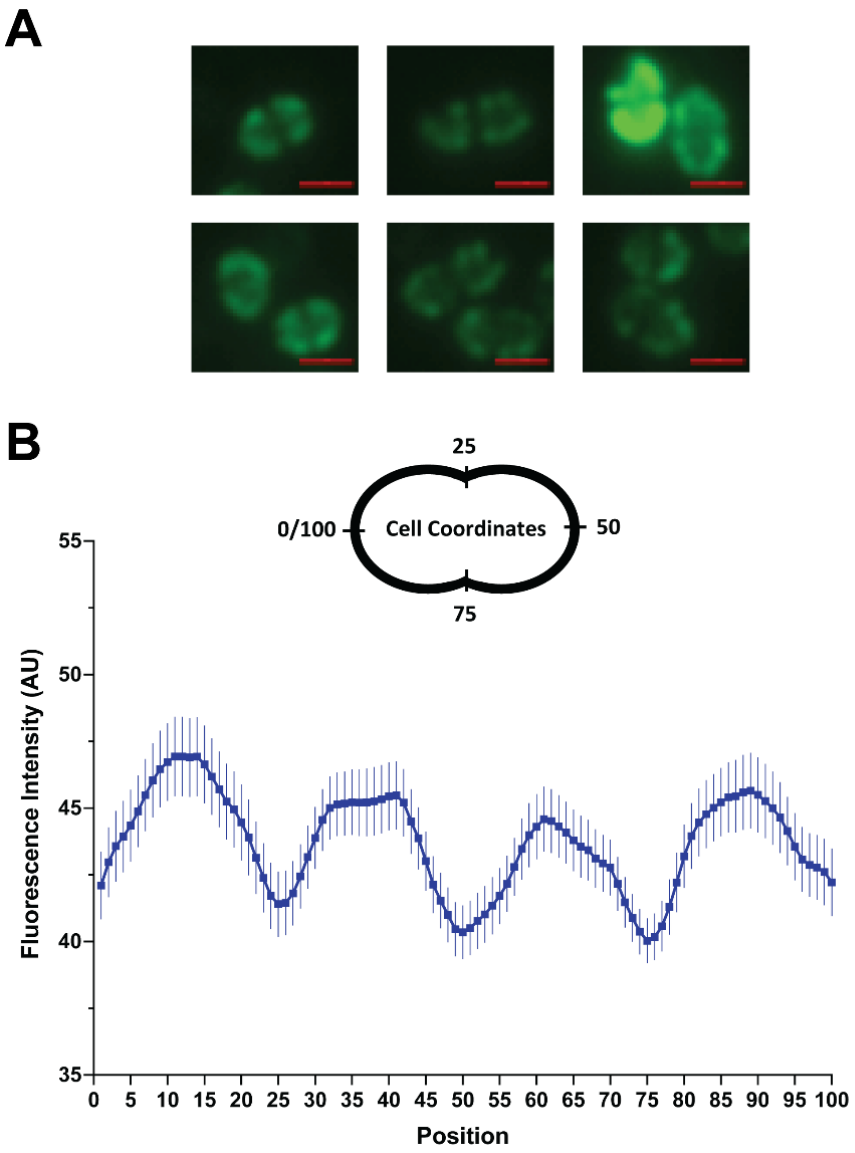

Figure 3.8. Localisation of FtsH is pole and septum excluded. **(A)** Representative images of WT pMSP3535-2HA-*ftsH* at mid-log phase with nisin induction of 125 ng/mL. Green fluorescence corresponds to 2HA-FtsH. Cells were stained with mouse anti-HA primary antibodies and anti-mouse Alexa Fluor 488 secondary antibodies. Scale bar = 1 µm. **(B)** Quantification of fluorescence across the cell perimeter. The positions numbers 0/100 and 50 correspond to the cell poles, while 25 and 75 correspond to the nascent septum. Error bars refer to the standard deviation of fluorescence quantified from 218 cells. Representative data from 3 independent experiments.

3.4. Discussion

Daptomycin (DAP) is one of the last line drugs used in the treatment of vancomycin resistant enterococcal (VRE) infections apart from linezolid (Patel and Gallagher, 2015). While it has largely been successful in treating VRE infections, there has been reports of daptomycin resistance (DAP^R) occurring in *Enterococci* which is particularly alarming as it can further reduce the already limited treatment options (Arias and Murray, 2012; Kelesidis et al., 2011; Munoz-Price et al., 2005). As part of investigations into *Enterococcal* DAP^R mechanisms, resistance strategies such membrane composition remodelling (via *gpdD*, *cls,* and diversion of DAP away from the septum), enhanced envelope stress response (via LiaFSR signalling), oxidative stress response (via *gsh*, *yybT*, *selA*) and drug efflux (via *mdpA*) have been described in *E. faecalis* (Arias et al., 2011; Khan et al., 2019; Miller et al., 2013; Reyes et al., 2015; Tran et al., 2013).

Besides these, the multiple peptide resistance factor (*mprF*) has also been shown to be protective against DAP. In *S. aureus* where only 1 *mprF* gene is present, *mprF* gain of function mutations with increased expression were detected in DAP^R clinical isolates (Ernst et al., 2018; Mishra et al., 2009; Sabat et al., 2018). While in *E. faecalis*, deletion of *mprF2* in a daptomycin susceptible strain, OG1RF, led to further decrease in MIC of 1.5 to 2 folds (Iris Gao, unpublished). To uncover mutations that would otherwise be masked by *mprF* activity, *in vitro* evolution was carried out on the Δ*mprF* mutants (Iris Gao, unpublished) **(Figure 3.1)**. In this chapter, follow up investigations were focused on one hit, *ftsH*, due to enrichment of *ftsH* mutant in Δ*mprF1*Δ*mprF2* early in evolution, and because *ftsH* was previously unstudied in *E. faecalis*.

We discovered that *ftsH* is essential in wild type *E. faecalis* but dispensable in the Δ*mprF1*Δ*mprF2* background, through a series of genetic approaches where heterologous expression of inactive variants of *ftsH* in the wild type affected

growth **(Figure 3.2, S3.2)**. Loss of function mutations in *ftsH* also accelerate DAP^R acquisition in Δ*mprF1*Δ*mprF2* in a targeted *in vitro* evolution to DAP^R, which is likely due to increased basal mutation rates that results from the inactivation of *ftsH* **(Figure 3.3B, C)**.

FtsH dysfunction in a wild type background also led to transcriptomic changes in genes in oxidative phosphorylation, the shikimate pathway and glycolysis, and depletion of TrePP and LysS at a proteomic level. A combination of these effects could be the reason for the growth defect and its essentiality in the wild type. RNAseq analysis of wild type strains encoding dysfunctional FtsH revealed an overall net increase in ATPases involved in ATP (*atpABDGI*) utilisation and decrease in ATP generation (*atpC2* ε-subunit) and electron transport chain components (cytochrome b – *cydB*, NADH dehydrogenase – *ndh3*) **(Figure 3.4)**. In addition, under FtsH dysfunction there was down regulation of genes in the chorismate biosynthesis pathway (*aroABCF*) and upregulation of enzymes between glyceraldehyde-3-phosphate and glycerate-3-phosphate (*tpiA*, *gap*, *pqk* and *gap2*) indicating increased glycolysis **(Figure 3.4)**. Proteomic analysis of the dysfunctional FtsH background in the wild type also revealed several depleted proteins, notably TrePP (glycosyl hydrolase) and LysS (lysine tRNA-ligase) which were confirmed to affect growth of wild type when reconstituted via transposon disruption and CRISPRi knockdown, respectively **(Figure 3.5, 3.6)**. Hence, it is possible that these changes might impart metabolic stress onto the wild type cell resulting in the observed growth defects. We also hypothesize that this metabolic stress might also be occurring in Δ*mprF1*Δ*mprF2*, where it is better tolerated in that background such that growth is unaffected. It is possible that it is this metabolic stress induces stress responses that enhances mutation rates, a phenomenon that is widely known to occur in bacteria (Bjedov et al., 2003; Ferenci, 2019; Foster, 2007; Galhardo et al., 2007). However, whether

such metabolic stress exists in Δ*mprF1*Δ*mprF2,* and if this mediates increased mutation rates needs to be investigated.

The putative substrates for *E. faecalis* FtsH are YcKE (beta-glucosidase), LysS (lysine-tRNA ligase), PyrB (aspartate carbamoyltransferase), LutA (a homolog to *B. subtilis* lactate utilisation Fe-S protein, LutA), GelE (gelatinase E), TrePP (carbamoyl-phosphate synthase), CryZ (putative NADPH:quinone reductase) and HrcA (heat-inducible transcription repressor), which were found to accumulate under FtsH dysfunction and are not due to transcriptomic upregulation **(Figure 3.5D)**. Several proteins were also depleted by proteomics that were not due to transcriptomic downregulation **(Figure 3.5C)**. Of these, loss of function of *lutA* (lactate utilisation Fe-S protein homolog) and *yckE* (beta-glucosidase) accelerates DAP^R acquisition rates while *hrcA* (heat-inducible transcription repressor) drastically slows acquisition rates in targeted *in vitro* evolution of their respective Tn mutants **(Figure 3.7)**. With *lutA* and *yckE* roles in lactate utilisation and breakdown of complex sugars respectively, it is possible that their inactivation could be relieving metabolic constraints in acquiring DAP^R. While *hrcA's* role in repressing the *grpE-dnaKJ* and *groELS* operons suggest that enhancement in chaperone expression from loss of transcriptomic repression could be reducing mutation rates. However, how these chaperones directly mediate the change in mutation rates needs to be further investigated.

Our findings that inactivating mutations of *ftsH*, namely *ftsH(G37X)* and *ftsH(H456Y)*, exerted a dominant negative growth inhibition in a wild type background suggest that, consistent with FtsH in other organisms such as *E. coli*, FtsH in *E. faecalis* likely forms homo-oligomers since this inhibition likely stems from disruption of the FtsH hexamer complex and its function (Akiyama and Ito, 2000; Bieniossek et al., 2006) **(Figure 3.2)**. Similar to *E. coli*, FtsH in *E. faecalis* is also essential under wild type conditions (Okuno and Ogura, 2013).

However, unlike FtsH in other organisms, *E. faecalis* FtsH likely has very different functions. The putative FtsH substrates identified in *E. faecalis* in this work have not been described in other organisms (Arends et al., 2016; Narberhaus et al., 2009; Westphal et al., 2012). Moreover, FtsH on is excluded from the poles and septum of mid-log phase cells **(Figure 3.8)**, whereas in *B. subtilis* FtsH is specifically localised to the septum (Wehrl et al., 2000).

Furthermore, this study is the first, to our knowledge, which links FtsH function to DAP^R acquisition. This is likely a result of FtsH essentiality in wild type backgrounds, which is the typical background that studies tend to use, so inactivating mutations could not be detected.

Our findings provide the first description of FtsH phenotypes in *E. faecalis* involving growth through its influence on metabolic genes, as well as mutation rate. This, together with the unique putative substrates, gives valuable insight in the functions of FtsH and provides a framework for future studies investigating FtsH function and related phenotypes in *E. faecalis* and possible related strains. This also provides evidence that, despite being a conserved gene, FtsH functions are diverse and organism dependent due to its differing substrates and its function cannot be simply extrapolated from another species. Having discovered a role for FtsH loss of function in accelerating DAP^R acquisition in *E. faecalis*, it is possible that it could have similar functions in restricting DAP^R resistance acquisition in other *Enteroccoci* or other organisms which is worth investigating using similar methods as we describe here. Furthermore, our finding that *hrcA* and the likely consequent upregulation of *grpE-dnaK-dnaJ* and *groEL-groES* operons highlights the potential role of chaperones in restricting DAP^R acquisition rates and presents the *hrcA* regulon as potential targets for investigation in anti-resistance therapies.

However, there are still several outstanding questions from our study. Whether the proteomic hits that affect DAP^R acquisition rates (*lutA*, *yckE* and *hrcA*) do so by directly affecting basal mutation rates or by relieving metabolic constraints imposed by subsequent DAP^R-linked mutations needs to be investigated in detail. Future work measuring mutation rates of these Tn mutants and investigating their transcriptomic effects on metabolism can be considered. These proteomic hits were tested in the wild type background, and it is possible that they may not possess the same phenotype in the Δ*mprF1*Δ*mprF2*, which should be verified in future work. However, results from investigation in the wild type background is still useful in providing information on general DAP^R acquisition-linked factors. Furthermore, the putative substrates identified may or may not be the actual targets of FtsH and should be verified in future by *in vivo* stability assays in both FtsH functional and dysfunctional conditions, or by *in vitro* biochemical assays measuring degradation of these putative substrates. The other gene hits enriched in the Δ*mprF1*Δ*mprF2* from the initial *in vitro* evolution to DAP^R should also be followed up in future work.

From a technical perspective, there are also some limitations to the experiments performed in this chapter. For instance, MIC measurements were done in BHI instead of the commonly used Mueller Hinton Broth (MHB), which can make comparisons to antibiotic breakpoints in literature difficult. In future, MIC measurements should also be done in MHB. Furthermore, for the *in vitro* evolution assays, only 3 biological replicates were performed which is rather few for the comparisons made. Future work should look at increasing experiment repeats with increased amounts of biological replicates to verify the trends observed.

3.5. Conclusion

In summary, we have shown in this chapter that *ftsH* is essential in wild type *E. faecalis* but dispensable in the Δ*mprF1*Δ*mprF2* background, while its loss of function is able to accelerate acquisition of DAP^R **(Figure 3.9)**. The combined metabolic effects involving oxidative phosphorylation, shikimate pathway and carbon utilisation as well as a down regulation of glycosyl hydrolase (*trePP)* and lysine-tRNA ligase (*lysS)* in wild type, in the absence of functional *ftsH* likely is the reason for the wild type specific growth defects observed. Loss of FtsH activity results in accelerated DAP^R acquisition rates due to the increased basal mutation rates. This accelerated DAP^R acquisition is influenced by positive contribution of a lactose utilisation protein (*lutA)* and beta-glucosidase (*yckE*), and negative contribution of a heat inducible transcription repressor (*hrcA*). Putative substrates of FtsH has also been discovered, which are YcKE (beta-glucosidase), LysS (lysine-tRNA ligase), PyrB (aspartate carbamoyltransferase), LutA (a homolog to B. subtilis lactate utilisation Fe-S protein, LutA), GelE (gelatinase E), TrePP (carbamoyl-phosphate synthase), CryZ (putative NADPH:quinone reductase) and HrcA (heat-inducible transcription repressor). These findings provide the first major insight into FtsH function and putative substrates in *E. faecalis*, information which will benefit future studies investigating FtsH function. FtsH involvement in accelerating DAP^R acquisition, together with the influence of *lutA, yckE* and *hrcA*, highlights their potential as targets for anti-resistance strategies in future therapeutic development.

In the next chapter, membrane microdomains and their organising factors, flotillins, are characterised in detail. In previous studies, membrane microdomains are commonly organised by flotillins, where flotillin-associated domains tend to be enriched with FtsH in other organisms such as *B. subtilis*, *S. aureus* and *B. burgdorferi* (Lopez and Koch, 2017). With FtsH's close

association with membrane microdomains in other organisms and that the septum of *E. faecalis* are likely sites of an anionic membrane microdomain, this chapter will provide insight into how they are organised with respect to flotillins.

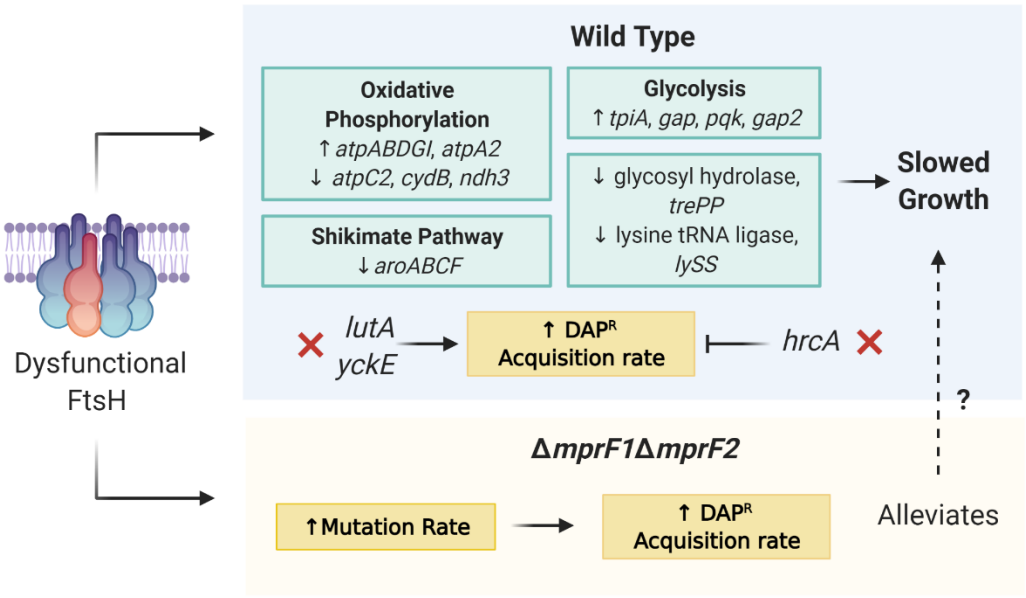

Figure 3.9. Model of proposed events following FtsH dysfunction. FtsH dysfunction results in metabolic changes in oxidative phosphorylation, shikimate pathway, glycolysis together with decreases in a glycosyl hydrolase and lysine tRNA ligase, which in combination results in slowed growth in the wild type. In Δ*mprF1*Δ*mprF2* environment, the slowed growth is alleviated by an unknown mechanism. FtsH dysfunction also leads to increased mutation rates ultimately resulting in increased DAP^R acquisition rates. Acquisition rate is positively influenced by loss of function of *lutA* and *yckE*, while is negatively influenced by loss of function of *hrcA*. Created with BioRender.com.

3.6. References

Afonina, I., Ong, J., Chua, J., Lu, T., Kline, K.A., 2020. Multiplex CRISPRi-Cas9 silencing of planktonic and stage-specific biofilm genes in *Enterococcus faecalis*. bioRxiv, 2020.2004.2030.071571.

Akiyama, Y., Ito, K., 2000. Roles of multimerization and membrane association in the proteolytic functions of FtsH (HflB). EMBO J 19, 3888-3895.

Anders, S., Pyl, P.T., Huber, W., 2015. HTSeq--a Python framework to work with high-throughput sequencing data. Bioinformatics (Oxford, England) 31, 166-169.

Arends, J., Thomanek, N., Kuhlmann, K., Marcus, K., Narberhaus, F., 2016. In vivo trapping of FtsH substrates by label-free quantitative proteomics. Proteomics 16, 3161-3172.

Arias, C.A., Murray, B.E., 2012. The rise of the Enterococcus: beyond vancomycin resistance. Nature reviews. Microbiology 10, 266-278.

Arias, C.A., Panesso, D., McGrath, D.M., Qin, X., Mojica, M.F., Miller, C., Diaz, L., Tran, T.T., Rincon, S., Barbu, E.M., Reyes, J., Roh, J.H., Lobos, E., Sodergren, E., Pasqualini, R., Arap, W., Quinn, J.P., Shamoo, Y., Murray, B.E., Weinstock, G.M., 2011. Genetic basis for in vivo daptomycin resistance in enterococci. The New England journal of medicine 365, 892-900.

Bao, Y., Sakinc, T., Laverde, D., Wobser, D., Benachour, A., Theilacker, C., Hartke, A., Huebner, J., 2012. Role of mprF1 and mprF2 in the pathogenicity of Enterococcus faecalis. PloS one 7, e38458.

Bieniossek, C., Schalch, T., Bumann, M., Meister, M., Meier, R., Baumann, U., 2006. The molecular architecture of the metalloprotease FtsH. Proceedings of the National Academy of Sciences of the United States of America 103, 3066-3071.

Bittner, L.M., Arends, J., Narberhaus, F., 2017. When, how and why? Regulated proteolysis by the essential FtsH protease in Escherichia coli. Biological chemistry 398, 625-635.

Bjedov, I., Tenaillon, O., Gérard, B., Souza, V., Denamur, E., Radman, M., Taddei, F., Matic, I., 2003. Stress-Induced Mutagenesis in Bacteria. Science (New York, N.Y.) 300, 1404-1409.

Bryan, E.M., Bae, T., Kleerebezem, M., Dunny, G.M., 2000. Improved vectors for nisin-controlled expression in gram-positive bacteria. Plasmid 44, 183-190.

Carmeli, Y., Eliopoulos, G., Mozaffari, E., Samore, M., 2002. Health and economic outcomes of vancomycin-resistant enterococci. Archives of internal medicine 162, 2223-2228.

Chai, Y., Kolter, R., Losick, R., 2009. A Widely Conserved Gene Cluster Required for Lactate Utilization in *Bacillus subtilis* and Its Involvement in Biofilm Formation. Journal of Bacteriology 191, 2423.

Chong, K.K.L., Tay, W.H., Janela, B., Yong, A.M.H., Liew, T.H., Madden, L., Keogh, D., Barkham, T.M.S., Ginhoux, F., Becker, D.L., Kline, K.A., 2017. Enterococcus faecalis Modulates Immune Activation and Slows Healing During Wound Infection. The Journal of infectious diseases 216, 1644-1654.

Deuerling, E., Mogk, A., Richter, C., Purucker, M., Schumann, W., 1997. The ftsH gene of Bacillus subtilis is involved in major cellular processes such as sporulation, stress adaptation and secretion. Molecular microbiology 23, 921-933.

Do, T., Schaefer, K., Santiago, A.G., Coe, K.A., Fernandes, P.B., Kahne, D., Pinho, M.G., Walker, S., 2020. *Staphylococcus aureus* cell growth and division are regulated by an amidase that trims peptides from uncrosslinked peptidoglycan. Nature Microbiology 5, 291-303.

Dosselaere, F., Vanderleyden, J., 2001. A metabolic node in action: chorismate-utilizing enzymes in microorganisms. Critical reviews in microbiology 27, 75-131.

Dunny, G.M., Brown, B.L., Clewell, D.B., 1978. Induced cell aggregation and mating in Streptococcus faecalis: evidence for a bacterial sex pheromone. Proceedings of the National Academy of Sciences of the United States of America 75, 3479-3483.

Ernst, C.M., Slavetinsky, C.J., Kuhn, S., Hauser, J.N., Nega, M., Mishra, N.N., Gekeler, C., Bayer, A.S., Peschel, A., 2018. Gain-of-Function Mutations in the Phospholipid Flippase MprF Confer Specific Daptomycin Resistance. mBio 9, e01659-01618.

Esnaola, M., Puig, P., Gonzalez, D., Castelo, R., Gonzalez, J.R., 2013. A flexible count data model to fit the wide diversity of expression profiles arising from extensively replicated RNA-seq experiments. BMC bioinformatics 14, 254.

Ferenci, T., 2019. Irregularities in genetic variation and mutation rates with environmental stresses. Environmental Microbiology 21, 3979-3988.

Foster, P.L., 2007. Stress-induced mutagenesis in bacteria. Crit Rev Biochem Mol Biol 42, 373-397.

Galhardo, R.S., Hastings, P.J., Rosenberg, S.M., 2007. Mutation as a stress response and the regulation of evolvability. Crit Rev Biochem Mol Biol 42, 399-435.

Guberman, J.M., Fay, A., Dworkin, J., Wingreen, N.S., Gitai, Z., 2008. PSICIC: Noise and Asymmetry in Bacterial Division Revealed by Computational Image Analysis at Sub-Pixel Resolution. PLOS Computational Biology 4, e1000233.

Kandaswamy, K., Liew, T.H., Wang, C.Y., Huston-Warren, E., Meyer-Hoffert, U., Hultenby, K., Schröder, J.M., Caparon, M.G., Normark, S., Henriques-Normark, B., Hultgren, S.J., Kline, K.A., 2013. Focal targeting by human β-defensin 2 disrupts localized virulence factor assembly sites in Enterococcus faecalis. Proceedings of the National Academy of Sciences 110, 20230-20235.

Kelesidis, T., Humphries, R., Uslan, D.Z., Pegues, D.A., 2011. Daptomycin nonsusceptible enterococci: an emerging challenge for clinicians. Clinical infectious diseases : an official publication of the Infectious Diseases Society of America 52, 228-234.

Khan, A., Davlieva, M., Panesso, D., Rincon, S., Miller, W.R., Diaz, L., Reyes, J., Cruz, M.R., Pemberton, O., Nguyen, A.H., Siegel, S.D., Planet, P.J., Narechania, A., Latorre, M., Rios, R., Singh, K.V., Ton-That, H., Garsin, D.A., Tran, T.T., Shamoo, Y., Arias, C.A., 2019. Antimicrobial sensing coupled with cell membrane remodeling mediates antibiotic resistance and virulence in

Enterococcus faecalis. Proceedings of the National Academy of Sciences 116, 26925.

Kristich, C.J., Nguyen, V.T., Le, T., Barnes, A.M., Grindle, S., Dunny, G.M., 2008. Development and use of an efficient system for random mariner transposon mutagenesis to identify novel genetic determinants of biofilm formation in the core Enterococcus faecalis genome. Appl Environ Microbiol 74, 3377-3386.

Langklotz, S., Baumann, U., Narberhaus, F., 2012. Structure and function of the bacterial AAA protease FtsH. Biochimica et biophysica acta 1823, 40-48.

Li, H., Durbin, R., 2009. Fast and accurate short read alignment with Burrows-Wheeler transform. Bioinformatics (Oxford, England) 25, 1754-1760.

Lopez, D., Koch, G., 2017. Exploring functional membrane microdomains in bacteria: an overview. Current opinion in microbiology 36, 76-84.

Maddalo, G., Chovanec, P., Stenberg-Bruzell, F., Nielsen, H.V., Jensen-Seaman, M.I., Ilag, L.L., Kline, K.A., Daley, D.O., 2011. A reference map of the membrane proteome of Enterococcus faecalis. Proteomics 11, 3935-3941.

Makino, S.-i., Makinoa, T., Abe, K., Hashimoto, J., Tatsuta, T., Kitagawa, M., Mori, H., Ogura, T., Fujii, T., Fushinobu, S., Wakagi, T., Matsuzawa, H., 1999. Second transmembrane segment of FtsH plays a role in its proteolytic activity and homo-oligomerization. FEBS Letters 460, 554-558.

Mascini, E.M., Bonten, M.J.M., 2005. Vancomycin-resistant enterococci: consequences for therapy and infection control. Clinical Microbiology and Infection 11, 43-56.

Miller, C., Kong, J., Tran, T.T., Arias, C.A., Saxer, G., Shamoo, Y., 2013. Adaptation of Enterococcus faecalis to daptomycin reveals an ordered progression to resistance. Antimicrobial agents and chemotherapy 57, 5373-5383.

Mishra, N.N., Yang, S.-J., Sawa, A., Rubio, A., Nast, C.C., Yeaman, M.R., Bayer, A.S., 2009. Analysis of cell membrane characteristics of in vitro-selected daptomycin-resistant strains of methicillin-resistant Staphylococcus aureus. Antimicrobial agents and chemotherapy 53, 2312-2318.

Mishra, N.N., Bayer, A.S., Tran, T.T., Shamoo, Y., Mileykovskaya, E., Dowhan, W., Guan, Z., Arias, C.A., 2012. Daptomycin Resistance in Enterococci Is Associated with Distinct Alterations of Cell Membrane Phospholipid Content. PloS one 7, e43958.

Munita, J.M., Murray, B.E., Arias, C.A., 2014. Daptomycin for the treatment of bacteraemia due to vancomycin-resistant enterococci. International journal of antimicrobial agents 44, 387-395.

Munoz-Price, L.S., Lolans, K., Quinn, J.P., 2005. Emergence of Resistance to Daptomycin during Treatment of Vancomycin-Resistant Enterococcus faecalis Infection. Clinical Infectious Diseases 41, 565-566.

Nagalakshmi, U., Waern, K., Snyder, M., 2010. RNA-Seq: a method for comprehensive transcriptome analysis. Current protocols in molecular biology Chapter 4, Unit 4.11.11-13.

Narberhaus, F., Obrist, M., Führer, F., Langklotz, S., 2009. Degradation of cytoplasmic substrates by FtsH, a membrane-anchored protease with many talents. Research in Microbiology 160, 652-659.

Nielsen, H.V., Guiton, P.S., Kline, K.A., Port, G.C., Pinkner, J.S., Neiers, F., Normark, S., Henriques-Normark, B., Caparon, M.G., Hultgren, S.J., 2012. The Metal Ion-Dependent Adhesion Site Motif of the Enterococcus faecalis EbpA Pilin Mediates Pilus Function in Catheter-Associated Urinary Tract Infection. mBio 3.

Okuno, T., Ogura, T., 2013. FtsH protease-mediated regulation of various cellular functions. Sub-cellular biochemistry 66, 53-69.

Palmer, K.L., Daniel, A., Hardy, C., Silverman, J., Gilmore, M.S., 2011. Genetic basis for daptomycin resistance in enterococci. Antimicrobial agents and chemotherapy 55, 3345-3356.

Patel, R., Gallagher, J.C., 2015. Vancomycin-resistant enterococcal bacteremia pharmacotherapy. Ann Pharmacother 49, 69-85.

Priyadarshini, R., de Pedro, M.A., Young, K.D., 2007. Role of Peptidoglycan Amidases in the Development and Morphology of the Division Septum in *Escherichia coli*. Journal of Bacteriology 189, 5334-5347.

Rashid, R., Veleba, M., Kline, K.A., 2016. Focal Targeting of the Bacterial Envelope by Antimicrobial Peptides. Frontiers in Cell and Developmental Biology 4.

Rashid, R., Cazenave-Gassiot, A., Gao, I.H., Nair, Z.J., Kumar, J.K., Gao, L., Kline, K.A., Wenk, M.R., 2017. Comprehensive analysis of phospholipids and glycolipids in the opportunistic pathogen Enterococcus faecalis. PloS one 12, e0175886.

Reyes, J., Panesso, D., Tran, T.T., Mishra, N.N., Cruz, M.R., Munita, J.M., Singh, K.V., Yeaman, M.R., Murray, B.E., Shamoo, Y., Garsin, D., Bayer, A.S., Arias, C.A., 2015. A liaR deletion restores susceptibility to daptomycin and antimicrobial peptides in multidrug-resistant Enterococcus faecalis. The Journal of infectious diseases 211, 1317-1325.

Robinson, M.D., McCarthy, D.J., Smyth, G.K., 2010. edgeR: a Bioconductor package for differential expression analysis of digital gene expression data. Bioinformatics (Oxford, England) 26, 139-140.

Roncarati, D., Scarlato, V., 2017. Regulation of heat-shock genes in bacteria: from signal sensing to gene expression output. FEMS Microbiology Reviews 41, 549-574.

Sabat, A.J., Tinelli, M., Grundmann, H., Akkerboom, V., Monaco, M., Del Grosso, M., Errico, G., Pantosti, A., Friedrich, A.W., 2018. Daptomycin Resistant Staphylococcus aureus Clinical Strain With Novel Non-synonymous Mutations in the mprF and vraS Genes: A New Insight Into Daptomycin Resistance. Front Microbiol 9, 2705-2705.

Schulz, A., Schumann, W., 1996. hrcA, the first gene of the Bacillus subtilis dnaK operon encodes a negative regulator of class I heat shock genes. J Bacteriol 178, 1088-1093.

Shoemaker, D.M., Simou, J., Roland, W.E., 2006. A review of daptomycin for injection (Cubicin) in the treatment of complicated skin and skin structure infections. Ther Clin Risk Manag 2, 169-174.

Song, X., Srinivasan, A., Plaut, D., Perl, T.M., 2003. Effect of nosocomial vancomycin-resistant enterococcal bacteremia on mortality, length of stay, and costs. Infection control and hospital epidemiology 24, 251-256.

Steenbergen, J.N., Alder, J., Thorne, G.M., Tally, F.P., 2005. Daptomycin: a lipopeptide antibiotic for the treatment of serious Gram-positive infections. The Journal of antimicrobial chemotherapy 55, 283-288.

Suomi, T., Seyednasrollah, F., Jaakkola, M.K., Faux, T., Elo, L.L., 2017. ROTS: An R package for reproducibility-optimized statistical testing. PLOS Computational Biology 13, e1005562.

Taylor, S.D., Palmer, M., 2016. The action mechanism of daptomycin. Bioorganic & Medicinal Chemistry 24, 6253-6268.

Thi Nguyen, H.B., Schumann, W., 2012. The sporulation control gene spo0M of Bacillus subtilis is a target of the FtsH metalloprotease. Res Microbiol 163, 114-118.

Tran, T.T., Panesso, D., Mishra, N.N., Mileykovskaya, E., Guan, Z., Munita, J.M., Reyes, J., Diaz, L., Weinstock, G.M., Murray, B.E., Shamoo, Y., Dowhan, W., Bayer, A.S., Arias, C.A., 2013. Daptomycin-resistant Enterococcus faecalis diverts the antibiotic molecule from the division septum and remodels cell membrane phospholipids. mBio 4.

Wehrl, W., Niederweis, M., Schumann, W., 2000. The FtsH Protein Accumulates at the Septum of *Bacillus subtilis* during Cell Division and Sporulation. Journal of Bacteriology 182, 3870.

Westphal, K., Langklotz, S., Thomanek, N., Narberhaus, F., 2012. A trapping approach reveals novel substrates and physiological functions of the essential protease FtsH in Escherichia coli. The Journal of biological chemistry 287, 42962-42971.

Wiegand, I., Hilpert, K., Hancock, R.E., 2008. Agar and broth dilution methods to determine the minimal inhibitory concentration (MIC) of antimicrobial substances. Nature protocols 3, 163-175.

4. CHAPTER IV:

Enterococcus faecalis membrane microdomain characterisation

4.1. Introduction

Key to successful bacterial colonisation and infection, is the ability to express and assemble virulence factors. One important class of enzymes involved in this process are sortases. They recognise secreted proteins bound for the cell wall containing a C-terminal LPXTG signal motif, and following signal sequence cleavage, mediate LPXTG cleavage and transpeptidation to attach them to lipid II precursors of the growing cell wall (Schneewind and Missiakas, 2012). Sortase A (SrtA) in *E. faecalis*, responsible for the sorting of aggregation substance (AS) and other sortase substrates, focally localises to the division septum of mid-log phase cells (Kline et al., 2009; Kristich et al., 2005). The ATPase component (SecA) of the Sec-secretion machinery also localises to the septum, suggesting that sec-mediated secretion is coordinated with sorting at this location (Kline et al., 2009). Furthermore, the division septum is also enriched in anionic lipids and is focally targeted by cationic antimicrobials such as daptomycin or cationic antimicrobial peptides (CAMPs) such as human beta defensin 2 (hBD2) (Kandaswamy et al., 2013; Tran et al., 2013). Taking these findings in consideration, it is likely that that membrane microdomains exist at the septum.

In the initial model of cell membrane organisation, the fluid mosaic model proposed by Singer and Nicolson described the membrane to be a homogenous mosaic of proteins and other constituents, which are embedded and freely diffusible within a membrane lipid bilayer (Singer and Nicolson, 1972). However, this model was later shown to be inaccurate, and that in eukaryotic membranes, proteins and lipids laterally segregate and organise into domains termed as lipid

rafts (Lingwood and Simons, 2010). These lipid rafts tend to consist of higher levels of certain lipids such as sterols and sphingolipids resulting in increased membrane rigidity, and their assembly is coordinated by flotillins (Banning et al., 2011; Lajoie and Nabi, 2010; Zhao et al., 2011).

Flotillins serve as a scaffolding protein to recruit raft-associated proteins important for lipid raft specific functions such as cytoskeleton arrangement, vesicular trafficking and insulin signalling (Langhorst et al., 2005; Zhao et al., 2011). Lipid raft-like organisation have also been described in bacteria where they are termed functional membrane microdomains (FMMs). First described in *Bacillus subtilis*, FMMs are enriched in polyisoprenoids; have functions linked to Sec-mediated secretion, FtsH protease activity and KinC signalling; and are coordinated by flotillin homologs, FloA and FloT (Bach and Bramkamp, 2013; Donovan and Bramkamp, 2009; Lopez and Kolter, 2010; Schneider et al., 2015; Yepes et al., 2012). Membrane microdomains have also been described in other bacteria such as *Staphylococcus aureus*, *Streptococcus pyogenes*, *Mycobacterium tuberculosis* and *Campylobacter jejuni* (Lopez and Koch, 2017; Rosch and Caparon, 2005).

At the outset of this thesis, membrane microdomains in *E. faecalis* were unstudied. We hypothesized that FMMs might exist at the *E. faecalis* septum since both cell wall sorting of virulence factors and secretion are coordinated at the septum, and since cationic antimicrobials preferentially target this region as well.

Homologs of *floA* and *floT* are present in *E. faecalis*. We hypothesized that these homologs may coordinate septal FMM assembly and might have functions similar to those previously described ones in *B. subtilis* and *S. aureus* as shown in **table 4.1**.

Table 4.1. Flotillin deletion associated phenotypes in *B. subtilis* and *S. aureus*		
Phenotype	***B. subtilis***	***S. aureus***
Membrane fluidity	Increased membrane rigidity (Bach and Bramkamp, 2013)	-
Antibiotic susceptibility	-	Increased susceptibility to beta-lactams (García-Fernández et al., 2017)
Protein secretion	Reduced bulk secretion (Bach and Bramkamp, 2013)	-
Localisation	FloA and FloT are present in distinct foci all along the membrane. They are not colocalised. (Donovan and Bramkamp, 2009; Schneider et al., 2015; Yepes et al., 2012)	FloA present at distinct foci (Mielich-Süss et al., 2017)

To further examine the role of *E. faecalis* flotillins, phenotypic investigations were conducted on deletion mutants of *floA* and *floT* based on phenotypes observed in other species. The flotillin mutants were assayed for their effects on growth, membrane fluidity and secretion in both nutrient-rich BHI (brain-heart infusion) and nutrient-limited CDM (chemically defined media). Beta-lactam resistance was also assayed in the mutants grown in BHI. Localisation of the flotillins on the membrane was also determined through immunofluorescence microscopy.

In order to better understand the functional roles of microdomains and flotillins in *E. faecalis*, characterisation of the membrane microdomain components in *E. faecalis* was accomplished by partitioning the cell membrane into detergent resistant membrane (DRM) fractions – where flotillins and microdomains are found in other species – and detergent soluble membrane (DSM) fractions for peptide mass spectrometric analysis. In addition, we proposed the use of nondetergent-based nanodisc preparations using styrene-maleic acid (SMA) co-

polymers to capture proteins and lipids within their immediate vicinity in the membrane. SMA extraction of nanodiscs was performed using SrtA as a septal microdomain marker to isolate septum-associated lipid nanodiscs.

This chapter provides the first detailed characterisation of flotillin function and microdomain constituents in *E. faecalis* and sets the stage for further characterisation of flotillin-associated domain functions and the use of flotillins as possible anti-virulence drug targets.

4.2. Materials and methods

4.2.1. Bacterial strains and culture conditions

The wild-type (WT) parental strain used was *E. faecalis* OG1RF (Dunny et al., 1978). Unless stated, all bacterial strains were grown overnight to late stationary phase for 16-18 hrs in their respective media at 37 ºC in static conditions and stored in 25% glycerol solution at -80 ºC when long-term storage was required. If mid-log phase cultures were required, late stationary phase cultures were sub-cultured 1:10 dilution into fresh media and grown at 37 ºC, 250 rpm shaking conditions to an OD_{600} of 0.5 ± 0.05 was reached. When normalisation of cultures was required, they were centrifuged at 6000 rcf for 5 mins at 4 ºC and cell pellets were washed twice with 1 mL of phosphate buffered saline (PBS). Cell suspensions were then normalised to an OD_{600} of 0.7 or required optical density by diluting with PBS. Strains, their respective genotype, source, and growth media used are listed in **table 4.2** below.

Table 4.2. Bacteria Strains and Culture Conditions

Bacterial Strains	Relevant Information / Genotype	References / Source	Media Used
	E. coli		
Stellar™ Competent Cells (*E. coli* HST08)	*F–, endA1, supE44, thi-1, recA1, relA1, gyrA96, phoA, Φ80d lacZΔM15, Δ(lacZYA - argF) U169, Δ(mrr - hsdRMS - mcrBC), ΔmcrA, λ–*	Clontech, Takara Bio Inc., Japan	LB, Miller broth (BD, USA)
DH5α pCYW2* (*Alternative name: pGCP123-PsrtA)	DH5α harbouring pCYW2*; Kan^r *pCYW2: pGCP123 parent plasmid (Nielsen et al., 2012) with PsrtA promoter. Expression vector.	Lab stock	LB, Miller broth with 50 µg/mL kanamycin (Thermo Scientific, USA)
DH5α pMSP3545	DH5α harbouring pMSP3545*; Erm^r *pMSP3545: Shuttle vector for nisin-	pMSP3545 was a gift from Gary Dunny, University of Minnesota	LB, Miller broth with 300 µg/mL erythromycin

	controlled inducible expression.	(Addgene plasmid # 46886) (Bryan et al., 2000)	(Sigma Aldrich, USA)
Stellar™ Competent Cells pMSP3545zn	*E. coli* HST08 harbouring pMSP3545zn *Modified shuttle expression vector of pMSP3545. Nisin two-component system removed. Nisin inducible promoter replaced with PsrtA	This study	LB, Miller broth with 300 µg/mL erythromycin
Stellar™ Competent Cells pCYW2-*floA*-2HA	*E. coli* HST08 harbouring pCYW2-*floA*-2HA	This study. Constructed by Jermain Goh.	LB, Miller broth with 50 µg/mL kanamycin
Stellar™ Competent Cells pCYW2-*floA*-6his	*E. coli* HST08 harbouring pCYW2-*floA*-6his	This study. Constructed by Jermain Goh.	
Stellar™ Competent Cells pCYW2-*floT*-2HA	*E. coli* HST08 harbouring pCYW2-*floT*-2HA	This study. Constructed by Jermain Goh.	
Stellar™ Competent Cells pCYW2-*floT*-6his	*E. coli* HST08 harbouring pCYW2-*floT*-6his	This study. Constructed by Daryl Yeong.	
TOP10 pGCP213	TOP10 harbouring pGCP213*; Erm^r *pGCP213: Temp-sensitive shuttle vector used for allelic replacement in E. faecalis	(Nielsen et al., 2012)	LB, Miller broth with 500 µg/mL erythromycin
DH5α pAL1	DH5α harbouring pAL1*; Kan^r *pAL1: Shuttle expression vector with *rofA* promoter.	Gift from Scott Hultgren lab	LB, Miller broth with 50 µg/mL kanamycin
DH5α pAL1-*srtA*-6his	DH5α harbouring pAL1-*srtA*-6his; Kan^r	Gift from Scott Hultgren lab	

E. faecalis			
OG1RF	Fus^r, Rif^r, wild-type strain	American Type Culture Collection (ATCC© 47077™)	BHI (Neogen, USA)
OG1RF Δ*floA*	Fus^r, Rif^r, Δ*floA*	This study. Constructed by Jermain Goh.	
OG1RF Δ*floT*	Fus^r, Rif^r, Δ*floT*	This study. Constructed by Jermain Goh.	
OG1RF Δ*floA*Δ*floT*	Fus^r, Rif^r, Δ*floA*Δ*floT*	This study. Constructed by Jermain Goh.	
OG1RF pAK1-*srtA*-2HA	Fus^r, Rif^r, pAK1-*srtA*-2HA	(Kandaswamy et al., 2013)	BHI with 500 µg/mL kanamycin
OG1RF Δ*floA*Δ*floT* pAK1-*srtA*-2HA	Fus^r, Rif^r, Δ*floA*Δ*floT*, pAK1-*srtA*-2HA	This study. Constructed by Dion Chan.	
OG1RF pCYW2-*floA*-2HA	Fus^r, Rif^r, pCYW2-*floA*-2HA	This study. Constructed by Jermain Goh.	
OG1RF pCYW2-*floA*-6his	Fus^r, Rif^r, pCYW2-*floA*-6his	This study. Constructed by Jermain Goh.	
OG1RF pCYW2-*floT*-2HA	Fus^r, Rif^r, pCYW2-*floT*-2HA	This study. Constructed by Jermain Goh.	
OG1RF pCYW2-*floT*-6his	Fus^r, Rif^r, pCYW2-*floT*-6his	This study. Constructed by Jermain Goh.	
OG1RF pGCP123	Fus^r, Rif^r, pGCP123	Lab stock	
OG1RF pAL1-*srtA*-6his	Fus^r, Rif^r, pAL1-*srtA*-6his	This study	
OG1RF pAL1	Fus^r, Rif^r, pAL1	This study	
OG1RF pCYW2-*floT*-2HA pMSP3545zn-*floA*-6his	Fus^r, Rif^r, pCYW2-*floT*-2HA, pMSP3545zn-*floA*-6his	This study. Constructed by Jermain Goh.	BHI with 500 µg/mL kanamycin and 100 µg/mL erythromycin
OG1RF pAL1	Fus^r, Rif^r, pAL1	This study	BHI with 500 µg/mL kanamycin
OG1RF pAL1-*srtA*-6his	Fus^r, Rif^r, pAL1-*srtA*-6his	This study	

B. subtilis			
168	*trpC2*, wild-type strain	Strains were a gift from Marc Bramkamp, Ludwig-Maximilians-Universität München, Germany (Bach and Bramkamp, 2013)	LB, Miller broth
168 Δ*floT*Δ*floA*	*trpC2*, *yuaG*::pDrive erm; *yqfA*::tet		

4.2.2. Immunofluorescence assay

Immunofluorescence microscopy was performed as previously described with the following modifications (Kandaswamy et al., 2013). Overnight cultures were subcultured twice, grown to mid-log phase and cells harvested for fixation. After fixation, cells were treated with 10 mg/mL lysozyme in lysis buffer for 45 mins at 37 °C followed by permeabilization with 0.1% (v/v) triton-X for 5 mins at 37 °C. The primary and secondary antibodies used were rabbit anti-HA (1:500 dilution) and anti-rabbit Alexa Fluor™ 488 (1:1000 dilution).

Slides were imaged with a Zeiss Axio observer Z1 inverted microscope (Carl-Zeiss, Germany) with a 100X oil immersion objective (NA 1.4, optovar 1.6X), AF488/FITC filter cube (460 – 490 nm band pass excitation filter, 515–550 nm bandpass barrier filter). Phase contrast and fluorescence images were captured. Fluorescence along the cell perimeter was quantified using Projected System of Internal Coordinates from Interpolated Contours (PSICIC) on MATLAB (Guberman et al., 2008).

4.2.3. Growth curves

Overnight stationary phase cultures were normalised to OD_{600} of 0.7 and diluted 200-fold before inoculating in 200 µL of media in 96-well plates in a ratio of 1:25 for growth assessment in BHI. The 96-well plates were incubated at 37 °C in a Tecan Infinite© M200 Pro spectrophotometer (Tecan, Switzerland) with

absorbance read at 600 nm every 10 mins for 72 hrs. The components in the CDM used are shown in **table 4.3** below.

Table 4.3 Components in chemically defined media (CDM)

Component	g/L	Component	g/L
KH_2PO_4	3.6000	D-glucose	15.0000
NaCl	3.0000	L-histidine	0.1700
$(NH_4)_2SO_4$	1.0000	L-isoleucine	0.2400
MOPS	13.0500	L-leucine	1.0000
K-acetate	0.9000	L-methionine	0.0600
$(NH_4)_6Mo_7O_{24} \cdot 4H_2O$	0.0002	L-valine	0.7000
$ZnSO_4 \cdot 7H_2O$	0.0050	L-arginine	0.7200
$CoCl_2 \cdot 6H_2O$	0.0002	L-glutamic acid	0.7200
$CuSO_4 \cdot 5H_2O$	0.0002	Glycine	0.3600
H_3BO_3	0.0008	L-serine	0.6000
K_2SO_4	0.0230	L-threonine	0.6000
KI	0.0001	$MgSO_4 \cdot 7H_2O$	1.0000
L-tryptophan	0.2400	$CaCl_2 \cdot 2H_2O$	0.0400
L-cysteine HCl	0.2400	Inositol	0.0020
Ca-pantothenate	0.0012	Biotin	0.0060
Pyridoxal HCl	0.0048	Niacin	0.0009
Riboflavin	0.0009	p-aminobenzoic acid	0.0001
Folic acid	0.0006	Tricine (4C)	1.3050
Thiamine-HCl	0.0006	Glutathione	0.0150
		Iron (II) sulfate heptahydrate	0.0040

4.2.4. Membrane fluidity assay by Laurdan staining

Overnight stationary phase cultures of *E. faecalis* wild type, Δ*floA*, Δ*floT* and Δ*floA*Δ*floT* were normalised to OD_{600} of 0.7 while *B. subtilis* wild type and Δ*floA*Δ*floT* were normalised to OD_{600} of 2.0 (both corresponding to approximately 10^8 CFU/mL). Normalised cell suspensions were stained with 10 μM Laurdan dye (Sigma Aldrich, USA) for 10 mins at 30 °C before washing twice with PBS. Supernatants were used as blanks for unbound Laurdan background fluorescence. The blanks, PBS control and cell suspensions were aliquoted into 96-well plate and incubated for 30 mins at 30 °C. 50 mM of membrane fluidizer, benzyl alcohol (Sigma Aldrich), was also spiked into some of the cultures as a control. Fluorescence measurements with excitation wavelength (350 nm) and

emission wavelength (435; 500 nm) were taken using Infinite 200 PRO microplate reader. Generalized polarization was calculated using:

$$\mathrm{GP} = \frac{\mathrm{I}_{435\mathrm{nm}} - \mathrm{I}_{500\mathrm{nm}}}{\mathrm{I}_{435\mathrm{nm}} + \mathrm{I}_{500\mathrm{nm}}}$$

4.2.5. Minimal inhibitory concentration assay (microplate dilution)

Stationary phase cultures to be tested were grown till mid-log phase and normalised to OD_{600} of 0.7. MIC assays were performed in a 96-well plate as described previously (Wiegand et al., 2008), with the following modifications. Antibiotics were diluted in BHI media in 2-fold dilutions, from 256.0 µg/mL to 0.5 µg/mL of the respective antibiotics **(table 4.4)**. Cultures were incubated for 16-18 hrs at 37 ºC in static conditions before assessing for growth in the wells to estimate the MIC.

Table 4.4. List of antibiotics used

Antibiotic	Antibiotic Class
Penicillin G (Sigma-aldrich, USA) Ampicillin (MP Biomedicals, USA)	Penicillin
Meropenem (Sigma-aldrich, USA)	Carbapenem
Cefotaxime (Sigma-aldrich, USA)	Cephalosporin
Gentamicin Sulfate (MP Biomedicals, USA)	Aminoglycoside
Daptomycin (Peptide Institute, Japan)	Cyclic lipopeptides

4.2.6. Bulk secretion assay

OD_{600} of stationary phase cultures of *E. faecalis* wild type, Δ*floA*, Δ*floT* and Δ*floA*Δ*floT* and *B. subtilis* wild type and Δ*floA*Δ*floT* were measured for data normalisation. Supernatants of the cultures were harvested and filtered using 0.2 µm syringe filters. 1.6 mL of filtered supernatant was mixed with 400 µL of 100% tricholoroacetic acid (TCA) solution (1:4 ratio of TCA to sample) and

incubated at 4 °C for 10 mins. Tubes were centrifuged at 14000 rpm for 15 mins at 4 °C. The precipitated protein pellet was washed once with 2 mL of 100% ice-cold acetone and placed on a 98 °C heat block to evaporate residual acetone. The pellets were resuspended in 500 µL of PBS. 25 µL of these protein solutions were used for the for estimation of protein content using the Pierce® BCA Protein Assay Kit (Thermoscientific, USA) in a microtiter plate format according to the manufacturer's protocol. Protein concentrations of the samples were then normalized to OD_{600} of 1.0 based on the respective OD_{600} readings of the individual cultures.

4.2.7. Western blot

SDS-PAGE and western blot were performed as described in a previous study (Nielsen et al., 2012). 4-12% or 12% NuPAGE® Bis-Tris mini gel in a XCell SureLock® Mini-Cell filled with either 1x MES or 1x MOPs SDS running buffer (Invitrogen, USA) were used and ran at 140 V for 90 mins. Proteins were transferred to nitrocellulose membranes using the iBlot™ Dry Blotting System (Invitrogen, USA) according to the manufacturer's protocol. The antibodies and developing solutions used are shown in below **(table 4.5)**.

Table 4.5. Antibodies and developing solution used in western immunoblots

Target of interest	Primary Antibody Dilution; Host	Secondary Antibody Dilution; Host	Developing Solution; Dilution Ratios (Luminol:Peroxide:Water)
6his	Mouse anti-6his 1:1000 (Thermoscientific, USA)	Goat anti-mouse HRP 1:5000 (Thermoscientific, USA)	SuperSignal™ West Femto Maximum Sensitivity Substrate 1:1:8
2HA	Mouse anti-HA 1:1000 (Thermoscientific, USA)	Goat anti-mouse HRP 1:5000 (Thermoscientific, USA)	SuperSignal™ West Femto Maximum Sensitivity Substrate 1:1:8
FtsH	Guinea pig anti-FtsH 1:4000 (Lab stock)	Goat anti-guinea pig HRP 1:6000 (Thermoscientific, USA)	SuperSignal™ West Femto Maximum Sensitivity Substrate 1:1:8

4.2.8. Membrane isolation

2 L of *E. faecalis* wild type pGCP123, pCYW2-*floA*-6his, pCYW2-*floT*-6his and pAL1-*srtA*-6his were cultured to mid-log phase (OD_{600} 0.5 ± 0.05) and cell pellets harvested. Membrane isolation was performed as described previously (Maddalo et al., 2011). with the following modifications: mutanolysin was not used, cells were lysed by sonication 60% amplitude for 2 mins (5 seconds on, 5 seconds off) in SMA solubilization buffer (50 mM Tris-HCl, pH 8.0, 500mM NaCl, 10% v/v glycerol) with EDTA-free protease inhibitor, and membrane fractions were resuspended to 80 mg/mL in SMA solubilization buffer.

4.2.9. Detergent-sensitive and resistant membrane fractionation

Isolated membranes were treated with CelLytic™ Membrane Protein Extraction Kit (Sigma Aldrich, USA) with the following modifications. Detergent sensitive membrane (DSM) and detergent resistant membrane (DRM) fractions were normalised against the whole membrane volume with PBS or 20% w/v sodium dodecyl sulfate (SDS), respectively. 100 µL of samples were then boiled with 33.4 µL of NuPAGE LDS Sample Buffer (4X) and 10 µL of 1M dithiothreitol (DTT). Sample mixtures were then run on SDS-PAGE. Either western blot was done as described earlier or gels were silver stained. Silver staining was performed by fixation with 50% v/v methanol and 5% v/v acetic acid solution, sensitizing with 0.02% w/v sodium thiosulfate solution, silver-stained with 0.1% w/v silver nitrate and 3% v/v formalin solution and developed using 2% w/v sodium carbonate and 1.5% v/v formalin solution. Using densitometric analysis of the silver stained gels, relative protein levels were estimated, and information used to normalise loading of samples based on total protein levels for SDS-PAGE. Western blot and silver stain were performed on these gels. Whole lane bands were excised for analysis at Taplin Mass Spectrometry Facility, Harvard Medical School, Boston, Massachusetts, USA for peptide mass spectrometry and proteomic analysis.

Peptide counts were normalised using tweeDEseq (TMM normalisation) and statistics were done using Reproducibility-Optimized Test Statistic (ROTS) (Esnaola et al., 2013; Suomi et al., 2017).

4.2.10. Styrene-maleic acid (SMA) based isolation of membrane microdomains

SMA lipid particles (SMALP) generation and purification was adapted from a previously described protocol (Lee et al., 2016). Activated styrene-maleic acid (2:1) copolymer was kindly gifted by Michael Overduin, University of Alberta, Canada. Isolated membrane suspensions were treated with 2% w/v styrene maleic acid co-polymer (2:1). SMA-solubilised membranes were loaded onto HisPur™ Ni-NTA spin columns (Thermoscientific, USA) for binding overnight, washed with 14 column volumes of SMA solubilization buffer containing 20 mM imidazole before eluting step wise with SMA solubilization buffer containing 50 – 500 mM imidazole. Fractions eluted were analysed by SDS-PAGE followed by western blot and silver staining as described in the earlier sections. Fractions containing SrtA-6his were pooled for size-exclusion chromatography (SEC). SEC was was performed using Superdex® 200 Increase 10/300 GL column attached to ÄKTA protein purification system with 1 mL of sample loaded at 0.4 mL/min with protein elution monitored by absorbance at 280 nm. Peaks containing the samples were pooled and concentrated using a Pierce™ Protein Concentrator PES, 10K MWCO (Thermoscientific, USA). Concentrated samples were then analysed again using SDS-PAGE with silver stain and western blot.

Transmission electron microscopy (TEM) was also performed on the concentrated samples to confirm for the presence of SMALPs (Performed by Choo Pei Yi). Four microliters of samples were spotted onto glow-discharged carbon coated EM grids (mesh 200) and allowed to adsorb for 1 min before excess was wicked away with the edge of a filter paper. The grids were stained

with 5 µL of 2.5% uranyl acetate for 1 min and excess was wicked away. Grids were air dried completely before imaging under Tecnai T12 transmission electron microscope operating at an acceleration voltage of 120 kV. Images were collected at 30, 000 X and 68, 000 X magnification.

4.2.11. Molecular cloning

The respective plasmids were extracted from *E. coli* strains harbouring them using the Monarch® Plasmid Miniprep Kit (New England BioLabs, USA) according to the manufacturer's instructions.

To generate constructs and ligate inserts into vectors, plasmids were first linearized by PCR and inserts generated by PCR using *E. faecalis* OG1RF genomic DNA as a template. PCR was performed using Q5® High-Fidelity DNA Polymerase (New England BioLabs, USA) according to the manufacturer's instructions. Linearized plasmids and their corresponding inserts were then ligated using the In-Fusion HD Cloning system (Takara, Japan) and transformed into Stellar™ Competent Cells (Takara, Japan) according to the manufacturer's instructions. Plasmids were then extracted from the stellar competent cells using the Monarch® Plasmid Miniprep Kit and then transformed into electrocompetent *E. faecalis*. PCR to create flanking gene regions as inserts for in-frame deletion by homologous recombination were done by overlap extension PCR. pGCP213 and pCYW2 were linearised by restriction digestion with EcoRI and NotI instead of linearization by PCR.

Transformants were selected by BHI or LB agar containing the appropriate antibiotics as listed in **table 4.2**. All screening of transformants were done using colony PCR using Taq DNA Polymerase, recombinant (5 U/µL) (Thermo Scientific, USA) according to the manufacturer's instructions. Gel electrophoresis to assess for product sizes were performed using 1% w/v

agarose gel in TAE buffer ran at 100 V for 30 mins followed by ethidium bromide staining for 10-15 mins. After each transformation step, if plasmids passed the colony PCR verification, they were extracted and sent for Sanger sequencing for their inserts to ensure the correct sequence is present (1st BASE DNA Sequencing Services, Singapore). PCR purification was done using Wizard® SV Gel and PCR Clean-Up System (Promega, USA) according to the manufacturer's instructions. Sequences of the primers used for PCR are shown below **(table 4.6)**. Verification of protein expression of the affinity tagged constructs (6his or 2HA) were done by western immunoblot **(supplementary figure S4.1)**.

To construct the pMSP3545zn plasmid, first the nisin inducible promoter of pMSP3545 was removed via inverse PCR to exclude that region. Next, PCR was carried on the pCYW2 plasmid to obtain an insert containing the *srtA* promoter which was then ligated into the pMSP3545 plasmid with its promoter removed. After which, the nisin two-component system was removed by inverse PCR and ligated. PCRs were done using Q5® High-Fidelity DNA Polymerase was used with the primers as stated in **table 4.6** and ligation were done using the In-Fusion HD Cloning system and transformed into Stellar™ Competent Cells. The plasmid map is shown in **supplementary figure S4.2**.

To create in-frame deletion mutants, the inserts containing the flanking regions of the gene to be deleted are ligated with the temperature sensitive vector pGCP213. Serial passaging and selection was done to induce for homologous recombination that result in the in-frame deletion as previously described (Nielsen et al., 2012; Ruiz et al., 1998).

Table 4.6. PCR Primers			
Primer	**Target(s)**	**Sequence**	**Purpose / Remarks**
M13F	- pCYW2-*floA*-6his - pCYW2-*floA*-2HA - pCYW2-*floT*-6his - pCYW2-*floT*-2HA	GTAAAACGACGGCCAG	Screening for transformants targeting the insert
M13R		CAGGAAACAGCTATGAC	Same primers used for Sanger sequencing
pABG5-EcoRI_F	- pAL1-srtA-6his	AGGGGTCCCTTTCCTTGATA	Screening for transformants targeting the insert
pABG5-PstI_R		TGCCTAAAGACAAGCCACCT	Same primers used for Sanger sequencing
M13F (-20)	- pMSP3545zn-floA-6his	GTAAAACGACGGCCAGT	Screening for transformants targeting the insert
M13R_pUC (-26)		GTCATAGCTGTTTCCTG	Same primers used for Sanger sequencing
FloA_R	- *E. faecalis* gDNA	GCTTGATATCGAATTATGAGTTAGGAGAGTGAAACAGAT	To create insert *floA-6his* For ligation into pCYW2
FloA_6his_F		GTGGATCCCCCGGGCCTACTAGTGGTGATGGTGATGATGAGAAGAAACATCGCCTGTATTAAT	
FloA_R	- *E. faecalis* gDNA	GCTTGATATCGAATTATGAGTTAGGAGAGTGAAACAGAT	To create insert *floA-2HA* For ligation into pCYW2
FloA_2HA_F		GTGGATCCCCCGGGCCTACTAAGCGTAATCTGGAACATCGTATGGGTAAGCGTAATCTGGAACATCGTATGGGTAAGAAGAAACATCGCCTGTATTAAT	
FloT_F	- *E. faecalis* gDNA	GCTTGATATCGAATTGAGAGAAGAAAATGGGGATTTTGT	To create insert *floA-6his* For ligation into pCYW2 and pMSP3545zn
FloT_6his_R		GTGGATCCCCCGGGCTTATTAGTGGTGATGGTGATGATGTTCTTTTTCTGAACCTTCTGTTGCAT	
FloT_F	- *E. faecalis* gDNA	GCTTGATATCGAATTGAGAGAAGAAAATGGGGATTTTGT	To create insert *floA-2HA* For ligation into pCYW2
FloT_2HA_R		GTGGATCCCCCGGGCTTATTAAGCGTAATCTGGAACATCGTATGGGTAAGCGTAATCTGGAACATCGTATGGGTATTCTTTTTCTGAACCTTCTGTTGCAT	
pMSP-edit-openV-F	- pMSP3545	AGATCTGATCCGTAGCGGT	To remove the nisin inducible promoter of pMSP3545.
pMSP-edit-openV-R		TTCTAGAGAGCTCAAGCTTTCTTTG	

PsrtA-Insert-F	- pCYW2	CTACGGATCAGATCTGTAAAACGACGGCCAGTGA	To create a fragment containing PsrtA and multiple cloning site to replace the nisin inducible promoter of pMSP3545
pSrtA-Insert-R		TTGAGCTCTCTAGAACAGGAAACAGCTATGACTTACGCCAAGCGCGC	
Nisin-del_F	- pMSP3545 with nisin inducible promoter replaced with PsrtA	CATGAGAATTCTATTTAATCACTTTGACTAGC	To remove the nisin two component system in pMSP3535
Nisin-del_R		AATAGAATTCTCATGTAATCTCTAAGGATTACTTTTTTTGTTTCG	
Lin_3545_F	- pMSP3545zn	AATTCGATATCAAGCTTATCGATACC	To linearise pMSP3545zn
Lin_3545_R		GCCCGGGGGATCCACTAG	
(1) FloA_F	- *E. faecalis* gDNA - Products of first PCR in a 1:1 mix used as a template for the second PCR	CATGCTCGAGCGGCCTTAGTCGCTTGGGAGAAATC	To create insert for deletion of *floA* by overlap extension PCR. First PCR (1)+(2), (3)+(4). Second PCR (1)+(4) on 1:1 mix of products of first PCR. For ligation into pGCP213
(2) FloA_SewR		ATTTCTTTGTTCTCAGTATACTACAAGAGGAAGGAGTTATTACATTCATGAAACCAT	
(3) FloA_SewF		ATGGTTTCATGAATGTAATAACTCCTTCCTCTTGTAGTATACTGAGAACAAAGAAAT	
(4) FloA_R		CAGTGTGCTGGAATTTTGTCACCATTTAGCCTTTTCG	
(1) FloT_F	- *E. faecalis* gDNA - Products of first PCR in a 1:1 mix used as a template for the second PCR	CATGCTCGAGCGGCCATTCGAGAACTTTCCACGATTAAG	To create insert for deletion of floT by overlap extension PCR. First PCR (1)+(2), (3)+(4). Second PCR (1)+(4) on 1:1 mix of products of first PCR. For ligation into pGCP213
(2) FloT_SewR		AGTAACGAAATACGATTCGCTTTTTCTTCTCTCCTACTCTATATTTTTAGACTG	
(3) FloT_SewF		CAGTCTAAAAATATAGAGTAGGAGAGAAGAAAAAGCGAATCGTATTTCGTTACT	
(4) FloT_R		CAGTGTGCTGGAATTGATATGACACCCAACCACTT	

4.3. Results

4.3.1. Flotillin homologs exist in *E. faecalis*

Flotillins are key players involved in membrane microdomain assembly and are important for recruitment of FMM constituent proteins (Langhorst et al., 2005; Lopez and Koch, 2017). Flotillins exist in various bacterial species, in Gram positive bacteria such as *B. subtilis* and *S. aureus*, in Gram negative bacteria such as *E. coli* and *Pseudomonas*, and even in archaea such as *Halobacterium* (Bramkamp and Lopez, 2015). Given their prevalence across different species, we hypothesized that homologs of flotillins also exist in *E. faecalis*.

Protein BLAST searches using flotillins of *B. subtilis* 168, FloA and FloT, revealed protein homologs of FloA and FloT in *E. faecalis* OG1RF. A FloT protein homolog, annotated as SPFH (stomatin, prohibitin, flotillin, and HflK/C) domain/band 7 family protein encoded by OG1RF_11094 (Whole protein identity: 69.94%) and a FloA homolog, another SPFH domain/band 7 family protein encoded by OG1RF_11500 (Whole protein identity: 25.64%) were identified **(figure 4.1A)**. Both of these predicted homologs possess the SPFH superfamily and PHB (prohibitin homologues) conserved domains which are frequently present in flotillins (Bramkamp and Lopez, 2015; Rivera-Milla et al., 2006; Tavernarakis et al., 1999; Yokoyama and Matsui, 2020). Hence, it is highly likely that OG1RF_11500 and OG1RF_11904 are the *floA* and *floT* homologs, respectively, and will be referred to as such throughout the rest of this chapter.

To determine how structurally similar *E. faecalis* flotillins might be to those of *B. subtilis*, structural alignment was performed on predicted structures of both using the DALI structural comparisons server (Holm, 2020) **(figure 4.1B, C)**. Alignment of predicted FloT structures gave 59% identity while FloA structures were not able to be aligned, suggesting that *E. faecalis* FloA is more structurally dissimilar

to its *B. subtilis* homolog than FloT. However, it is important to note that these were based off predicted structures.

A **Protein Sequence Alignments**

B. subtilis FloA vs *E. faecalis* FloA

Protein BLAST (blastp)	
Query cover	17%
E-value	0.86
Identity	25.64%

B. subtilis FloT vs *E. faecalis* FloT

Protein BLAST (blastp)	
Query cover	92%
E-value	0.00
Identity	69.94%

B **Structure Prediction**

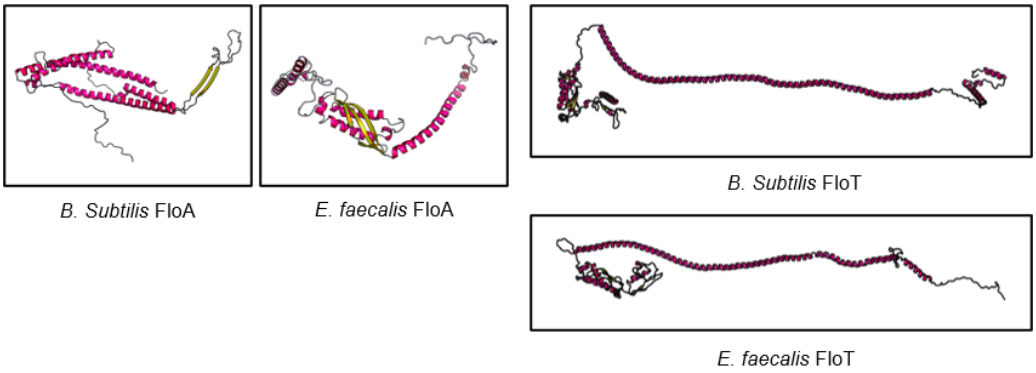

B. Subtilis FloA

E. faecalis FloA

B. Subtilis FloT

E. faecalis FloT

C **Structural Alignments of Predicted Structures**

B. subtilis FloA vs *E. faecalis* FloA

Structural Alignment	
Z-score	Unable to align
RMSD	Unable to align
Identity	Unable to align

B. subtilis FloT vs *E. faecalis* FloT

Structural Alignment	
Z-score	22.3
RMSD	14.5
Identity	59%

Figure 4.1. Protein sequence and structural alignment of predicted FloA and FloT structures. (A) Protein sequence alignment using protein-protein Basic Local Alignment Tool (BLAST). **(B)** Structure predictions using RaptorX. **(C)** Structure alignment results using the pairwise comparison on the DALI structural comparisons server (Holm, 2020).

4.3.2. Flotillin homologs colocalise at the septum similar to SrtA

Virulence factor assembly by sortase A (SrtA), the ATPase component (SecA) of the secretion machinery, as well as anionic lipids are enriched at the septum. Furthermore, they are preferentially targeted by cationic antimicrobials (Kandaswamy et al., 2013; Kline et al., 2009; Tran et al., 2013). These findings suggest that functional membrane microdomains (FMMs) likely exist at the septum. Since FMMs are organised and coordinated by flotillins in other species, we hypothesize that the septal FMMs are likely coordinated by the FloA and FloT homologs in *E. faecalis* as well (Bramkamp and Lopez, 2015; Lopez and Koch, 2017).

To determine if FloA and FloT localise to the same region as SrtA, immunofluorescence microscopy was carried out on wild type *E. faecalis* expressing affinity tagged proteins for each flotillin. SrtA was enriched at the septum as previously reported (Kline et al., 2009). FloA similarly displayed fluorescence along the perimeter with focal enrichment at the septum, whereas FloT was excluded from the poles and septum **(figure 4.2A, B)**. This suggests that FloA and SrtA might be co-enriched at the septum and septal microdomains could be organised by FloA. Furthermore, FloT could be responsible for organising a separate set of domains that are not septum linked.

To investigate the roles and functions of flotillins in *E. faecalis*, flotillin in-frame deletion mutants, Δ*floA*, Δ*floT*, Δ*floA*Δ*floT*, were generated. We hypothesized that the loss of flotillins might affect the proper localisation of SrtA at the septum. Immunofluorescence microscopy was carried out on Δ*floA*Δ*floT* expressing SrtA-2HA. However, the absence of flotillins did not affect the localisation of SrtA and it remained septally enriched in Δ*floA*Δ*floT* like the wild type **(figure 4.2C, D)**.

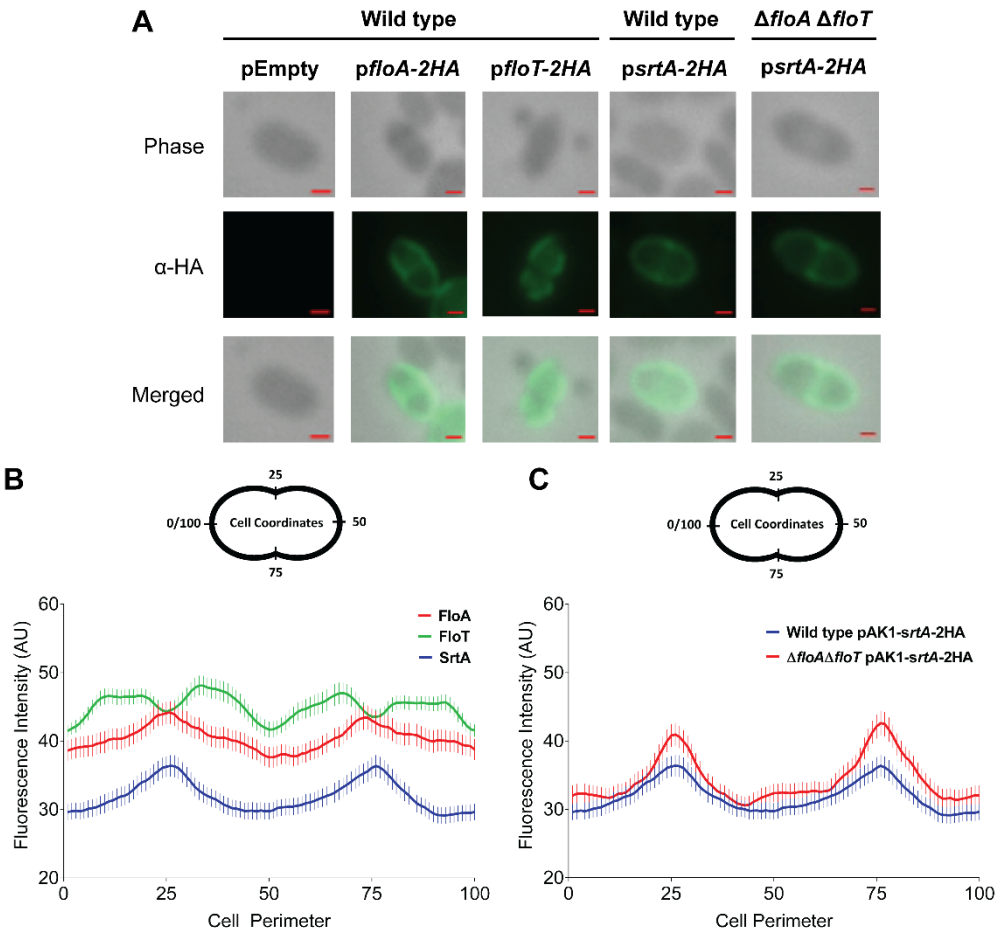

Figure 4.2. Immunofluorescence microscopy of *E. faecalis* pEmpty, pAK1-*srtA*-2HA, pCYW2-*floA*-2HA, pCYW2-*floT*-2HA and Δ*floA*Δ*floT* pAK1-*srtA*-2HA. (A) Representative images of *E. faecalis* wild-type pAK1-*srtA-2HA* and pCYW2-*floT-2HA* pMSP3545ZN-*floA-6his* in phase contrast, fluorescence, and merged channels (scale bar: 0.5 µm). **(B)** Fluorescence intensity distribution of FloA-6his (red), FloT-2HA (green) and SrtA-2HA (blue) across the cell perimeter. **(C)** Fluorescence intensity distribution of SrtA in the wild type (blue) and SrtA in Δ*floA*Δ*floT* (red) across the cell perimeter. Cell perimeter position 0/100 and 50 corresponding to cell poles, and 25 and 75 corresponding to the septum. Cell surface fluorescence intensities were measured using PSICIC software on MATLAB. >100 cells were analysed. Performed by Dion Chan. Representative data from 2 independent experiments.

4.3.3. *floA* is essential for growth in nutrient limited conditions

To determine if flotillins have any effect on fitness, the growth of the flotillin mutants were assessed in both BHI and a more nutrient-limited condition in CDM (chemically defined media) **(figure 4.3)**. CDM is considered to be more nutrient limited as compared to BHI due to the absence of fatty acids and other lipids as well as other carbon sources apart from glucose. All strains grew equally well under nutrient rich conditions with Δ*floA*Δ*floT* growing to significantly higher end point absorbance values of 0.9 as compared to around 0.7 for the rest of the strains **(figure 4.3A, C)**.

Under more nutrient limited CDM, all strains displayed slower growth rates possibly due to nutrient restriction, with extended lag phases likely due to the switch in media environments **(figure 4.3B, C)**. Interestingly, both Δ*floA* and Δ*floA*Δ*floT* were unable to grow at all in CDM indicating that *floA* might be influencing growth only under nutrient limited conditions **(figure 4.3B)**. Furthermore, Δ*floT* also displayed faster growth than the wild type in CDM with log phase growth starting at around 33 hrs as compared to around 37 hrs for wild type, with lower end point absorbance of ~0.6 instead of ~0.7 **(figure 4.3B, C)**. These data suggest that *floA* plays an essential role for growth under a more nutrient limited CDM environment. As for the difference in endpoint absorbances observed in both BHI and CDM, the strains could have different cell morphology or different degrees of cell chaining which should be investigated with microscopy in future.

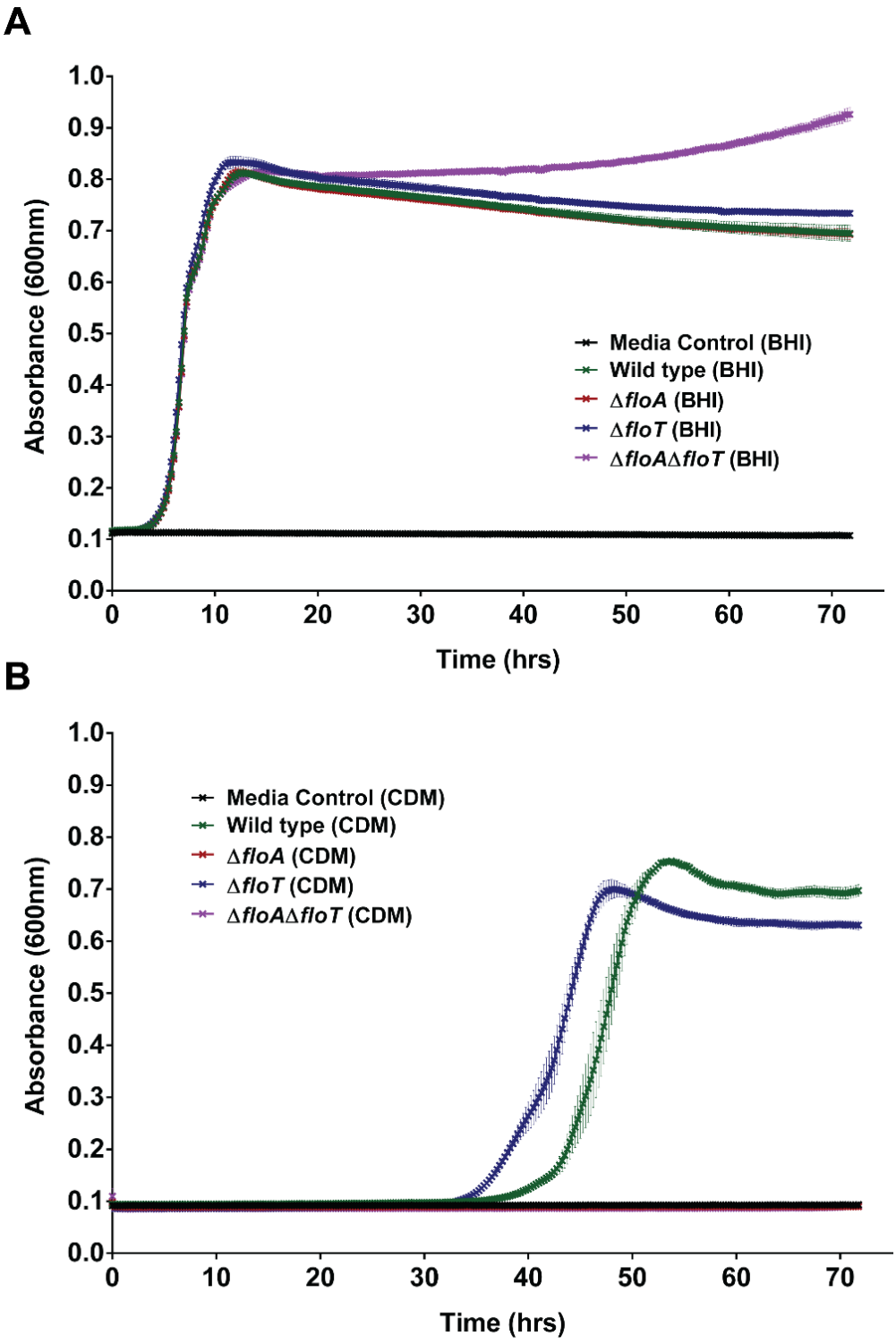
A
Absorbance (600nm)
Time (hrs)
Media Control (BHI)
Wild type (BHI)
ΔfloA (BHI)
ΔfloT (BHI)
ΔfloAΔfloT (BHI)
B
Absorbance (600nm)
Time (hrs)
Media Control (CDM)
Wild type (CDM)
ΔfloA (CDM)
ΔfloT (CDM)
ΔfloAΔfloT (CDM)

C

Media	Strain	Specific growth rate (h^{-1})		Endpoint absorbance (600nm)		Lag phase duration (h)
BHI	Wild-type	0.613 ± 0.016	-	0.695 ± 0.022	-	3
	Δ*floA*	0.620 ± 0.018	ns	0.693 ± 0.014	ns	3
	Δ*floT*	0.575 ± 0.071	ns	0.734 ± 0.004	ns	3
	Δ*floA* Δ*floT*	0.600 ± 0.006	ns	0.926 ± 0.018	****	3
CDM	Wild-type	0.201 ± 0.051	-	0.698 ± 0.016	-	33
	Δ*floA*	No growth		No growth		No growth
	Δ*floT*	0.165 ± 0.038	ns	0.631 ± 0.012	**	37
	Δ*floA* Δ*floT*	No growth		No growth		No growth

Figure 4.3. Growth curves of *E. faecalis* wild type, Δ*floA*, Δ*floT*, Δ*floA*Δ*floT*. Absorbance (600nm) over time of wild type, Δ*floA*, Δ*floT*, Δ*floA*Δ*floT* grown in **(A)** nutrient rich media (BHI), **(B)** and nutrient limited media (CDM – chemically defined media). Error bars refer to standard error of mean (SEM) of 3 biological replicates with 3 technical replicates each. Each biological replicate consists of averaged values from their constituent technical replicates. Experiment was performed by Jermain Goh. **(C)** Calculated specific growth rate of each strain based on the exponential phase of the growth curves (from A and B) with their respective end point absorbance. **, p=0.001 to 0.01; ****, p⩽0.0001; Dunnett's test for ANOVA for the **(A)**, T-test for **(B)**.

4.3.4. *floT* has a minor effect on membrane fluidity under nutrient limited conditions

In *B. subtilis*, flotillins are responsible for spatial organisation of membrane domains of high rigidity, preventing their fusion into large rigid membrane sections, where the loss of flotillins results in more rigid membranes (Bach and Bramkamp, 2013). We hypothesized that *E. faecalis* flotillins might serve similar functions. To analyse membrane fluidity levels, we utilised a fluorescent dye sensitive to changes in membrane fluidity, Laurdan, for which its emission spectra is red-shifted when membranes are more liquid disordered (L_d) and fluid, and blue-shifted when membranes are more liquid ordered (L_o) and rigid (Harris et al., 2002). To detect the emission shift, emission was measured at two wavelengths of 435 nm and 500 nm, and calculated as a ratio termed generalised polarisation (GP). High GP values indicate less fluid membranes, while low GP values indicate more fluid membranes.

When membrane fluidity was assayed, there was a significant increase in membrane fluidity in *B. subtilis* Δ*floA*Δ*floT* by 0.2, compared to wild type, as previously reported (P = 0.0001 to 0.001) (Bach and Bramkamp, 2013) **(figure 4.4A)**. The membrane fluidizer, benzyl alcohol, used as a control, successfully showed a decrease in GP value of 0.1 after treatment indicating fluidized membranes **(figure 4.4)**. However, when grown in BHI, the *E. faecalis* flotillin mutants displayed no difference in membrane fluidity as compared to wild type **(figure 4.4A)**. We hypothesized that the nutrient rich environment of BHI could be masking phenotypes that might otherwise be present. To address this, we grew the *E. faecalis* flotillin mutants in CDM, and observed a slight decrease in membrane fluidity in Δ*floT* of about 0.02 as compared to the wild type (P = 0.001 to 0.01) **(figure 4.4B)**. Since Δ*floA* and Δ*floA*Δ*floT* were not able to grow in CDM, we were unable to assess their membrane fluidity under these conditions. Hence,

out of the 2 homologs, *floT* mildly influences membrane fluidity only under more nutrient limited conditions.

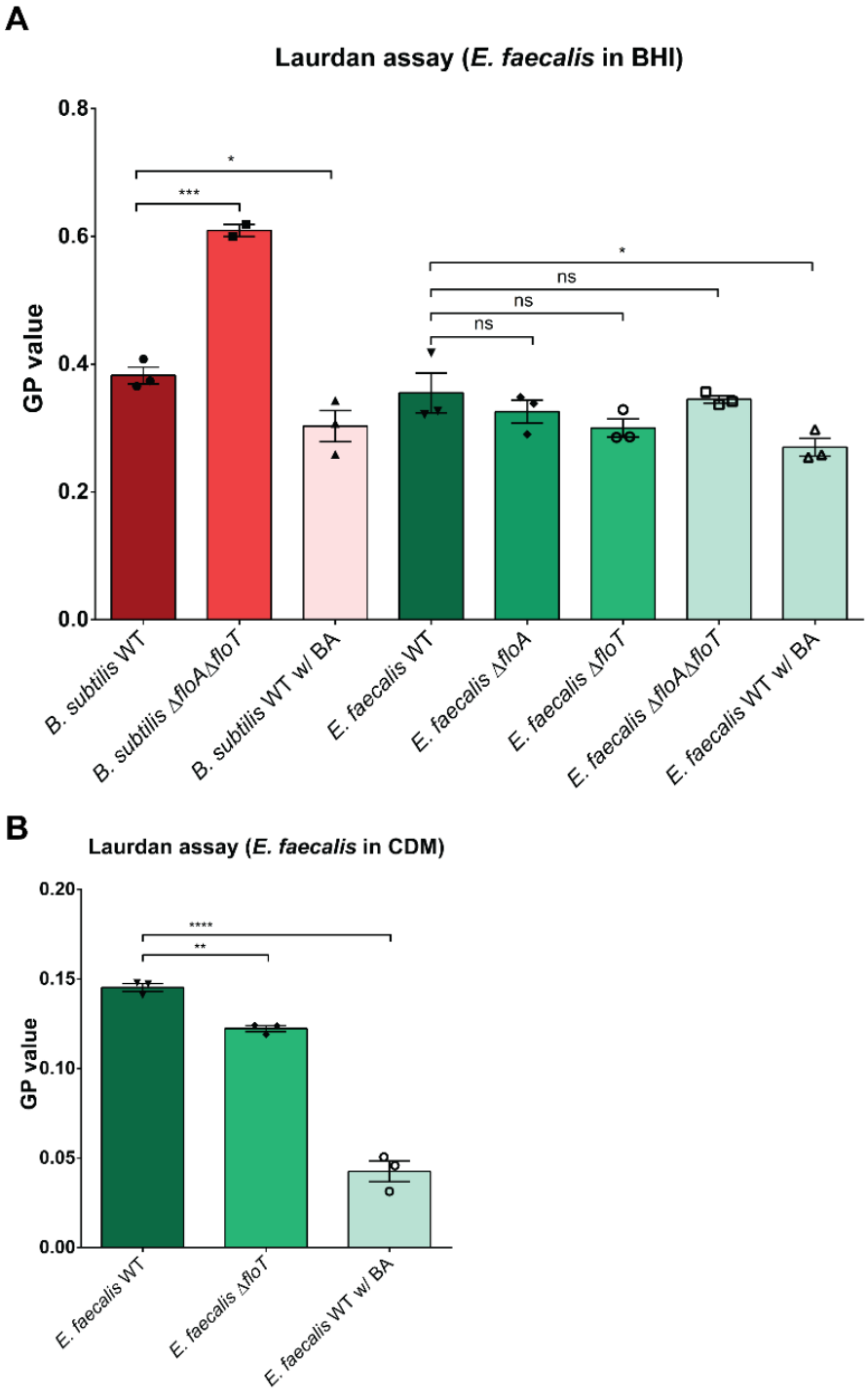

Figure 4.4. Membrane fluidity of the flotillin mutants measured by laurdan spectroscopy. (A) General polarisation values (GP) of *B. subtilis* controls and *E. faecalis* flotillin mutants grown to late stationary phase in LB and BHI, respectively and measured by spectrometry. **(B)** GP values of *E. faecalis* flotillin mutants grown to late stationary phase in CDM. Membrane fluidizer, benzyl alcohol (BA) was added as a

control to fluidize membranes. Larger GP values refer to less fluid and more rigid membranes, while smaller GP values refer to more fluid and less rigid membranes. Error bars refer to standard error of mean (SEM) of 3 biological replicates with 3 technical replicates each. Each biological replicate consists of averaged values from their constituent technical replicates. Statistical analysis was performed using Dunnett's test for one-way ANOVA comparison between each flotillin mutant against wild type. *, p=0.05 to 0.01; **, p=0.001 to 0.01; ***, p=0.0001 to 0.001; ****, p⩽0.0001. Experiments were performed by Jermain Goh.

4.3.5. Flotillins are not involved in beta-lactam resistance and secretion

In methicillin-resistant *S. aureus* (MRSA), deletion of *floA* led to increased sensitivity to beta-lactams due to disruption of FloA microdomains and their associated penicillin-binding proteins (García-Fernández et al., 2017). To determine if the same phenomenon occurs for *E. faecalis*, minimal inhibitory concentrations of beta-lactams such as penicillin G (penicillin), ampicillin (penicillin), and cefotaxime (cephalosporin) were tested for the wild type and ∆*floA*∆*floT* in BHI **(figure 4.5A)**. However, there were no difference in MICs between the two strains. A membrane targeting antibiotic, daptomycin, was also tested to determine if possible microdomain disruption might affect its MIC, which it did not. To serve as a control, an antibiotic that *E. faecalis* is known to be resistant to (gentamicin sulfate) was also tested, where it displayed high level of resistance with MIC of 256 µg/mL in both strains **(figure 4.5A)**.

In *B. subtilis*, the loss of flotillins also resulted in impaired bulk secretion (Bach and Bramkamp, 2013). To determine if the same might be occurring in *E. faecalis*, the protein content in supernatants of wild type and flotillin mutants from both *E. faecalis* and *B. subtilis* were quantified using the BCA assay **(figure 4.5B, C)**. *B. subtilis* displayed the previously reported impairment in bulk secretion, with > 40% decrease in secretion **(figure 4.5B, C)**. When grown under either BHI or more nutrient limited CDM, no difference in bulk secretion was detected

in any of the *E. faecalis* flotillin mutants **(figure 4.5B, C)**. Hence, unlike *S. aureus* and *B. subtilis*, in *E. faecalis*, flotillins are not associated with beta-lactam resistance or secretion.

A

Minimal inhibitory concentrations (MICs) (µg/mL)			
Antibiotic	**Class**	**Wild type**	**Δ*floA*Δ*floT***
Penicillin G	β-lactam	1	1
Ampicillin	β-lactam	0.5	0.5
Cefotaxime	β-lactam	2	2
Gentamicin Sulfate	Aminoglycoside	256	256
Daptomycin	Lipopeptide	8	8

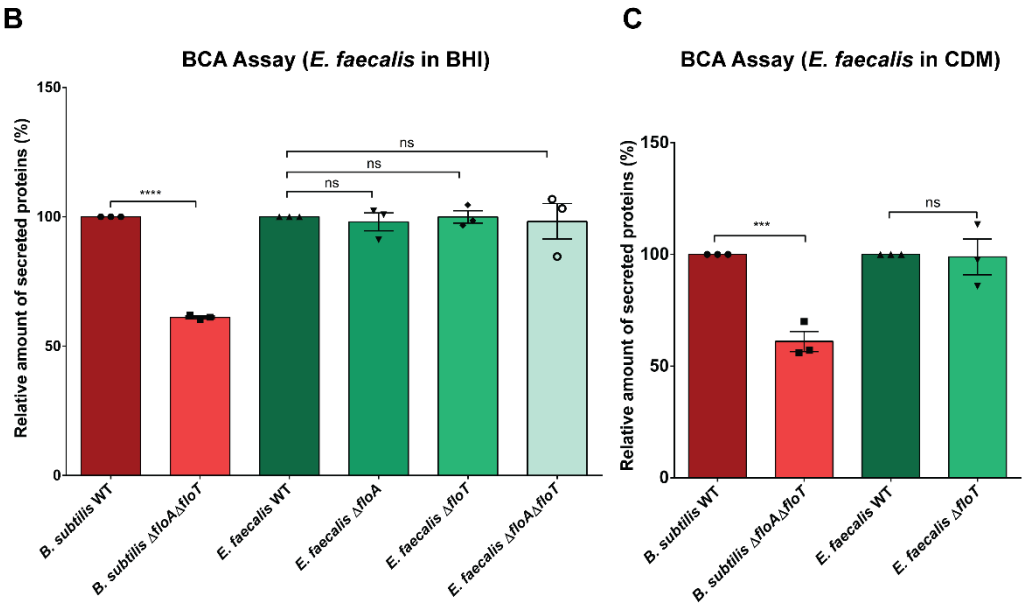

Figure 4.5. Antibiotic minimal inhibitory concentration (MICs) and bulk secretion of the flotillin mutants. (A) Minimal inhibitory concentrations of a series of β-lactam antibiotics, gentamicin and daptomycin in wild type and Δ*floA*Δ*floT*. Assay tested in a microdilution-based assay. Data was obtained from 3 biological replicates. Bulk secretion determined by BCA assay quantification of late stationary phase supernatants from *E. faecalis* wild type and flotillin mutants grown in **(B)** BHI (nutrient rich condition), and **(C)** CDM (nutrient limited condition). *B. subtilis* wild type and Δ*floA*Δ*floT* were grown in LB and used as controls. Error bars refer to standard error of mean (SEM) of 3 biological replicates with 3 technical replicates each. Each biological replicate consists of averaged values from their constituent technical replicates. Statistical analysis was performed using Dunnett's test for one-way ANOVA with comparisons between each flotillin mutant against wild type. ***, p=0.0001 to 0.001; ****, p⩽0.0001. Part (A) was performed by Dion Chan and parts (B, C) were performed by Jermain Goh.

4.3.6. Detergent-based extraction and analysis of flotillin and SrtA microdomains

The only roles for *E. faecalis* uncovered at this point were a role of *floA* in supporting growth in nutrient limited CDM, and a minor role for *floT* in membrane fluidity. In an attempt to predict additional functions of *E. faecalis* flotillins, we characterised of the membrane microdomain composition that these flotillins reside in, since functions of flotillins are tied to microdomain assembly, and recruitment and proper function of microdomain-linked proteins (Lopez and Koch, 2017).

To characterise the membrane domain environment, we took advantage of the property that microdomain proteins tend to be enriched in detergent resistant membrane (DRM) partitions when cell membranes are treated with non-ionic detergents to isolate and characterise the microdomain proteome in *E. faecalis* (Brown, 2002). It is important to note that the DRM fractions are not equated to microdomains but are instead simply enriched in proteins present in them. We employed a similar method previously used to isolate *B. subtilis* microdomains to obtain the DRM partition in *E. faecalis* (Bach and Bramkamp, 2013; Lopez and Kolter, 2010). This was performed on *E. faecalis* transformed with the plasmids p*srtA*-6his, *pfloA*-6his, or *floT*-6his to determine the level of enrichment of these proteins in the DRM fraction by western blot and to allow for eventual direct comparisons of these fractions with nanodisc-mediated isolation that will be described in the next section. *B. subtilis* was used as a positive control.

We observed that the whole membrane for all samples partitioned into detergent soluble membrane (DSM) and DRM fractions containing different enrichments of proteins, as observed from SDS-PAGE and silver staining of all the samples, which was consistent as previously reported in *B. subtilis* (Lopez and Kolter, 2010) **(Supplementary Figure S4.3)**.

Based off whole lane densitometric measurements, the total protein content of each partition together with the whole membrane was normalised to allow for comparisons of protein enrichment across samples by western blot. Western blot analysis of normalised samples of *E. faecalis* p*srtA*-6his, *E. faecalis* p*floA*-6his and *E. faecalis pfloT*-6his revealed that SrtA, FloA and FloT do not appear to be greatly enriched within the DRM fraction **(Figure 4.6A-D)**. We also probed for the presence of FtsH, which is commonly associated with membrane microdomains of other organisms such as *B. subtilis*, *S. aureus*, *B. burgdorferi* as a control (Lopez and Koch, 2017). Similar to these other organisms, but in contrast to what we observed for SrtA, FloA, and FloT, FtsH was enriched in the *E. faecalis* DRM fractions **(Figure 4.6A-D)**.

To determine the protein cargo enriched within the DRM fraction, the DSM and DRM fractions of *E. faecalis* p*floT-6his* were analysed by peptide mass spectrometry to serve as a representative for *E. faecalis* DRM fractions and the associated microdomain environment. p*srtA*-6his and *pfloA*-6his DRM fractions will be analysed in future to determine consistency of the results.

When protein abundances were compared between the DRM and the DSM fractions, several proteins were discovered to be enriched within the DRM fraction **(Figure 4.6E, Supplementary Table S4.1)**. Components of the Sec secretion machinery (SecY) was enriched within the DRM fraction ($log_2FC = 2.08$) **(Figure 4.6E)**. FtsH was also slightly enriched in the DRM fraction ($log_2FC = 0.33$) (Data not shown since $log_2FC<1$). This corroborates with the western blot findings despite the low fold-change difference **(Figure 4.6A-D)**. Enrichment of ABC transporters (OG1RF_11197, 11135, 12369, 10897, 11354, 11774 and PotD) were also observed **(Figure 4.6E)**. Of the proteins enriched in the DRM fraction, amidase (OG1RF_10473), RseP (RIP metalloprotease) and a putative ABC superfamily ATP binding cassette transporter (OG1RF_10191) are part of

a putative complex as determined by a previous membrane proteome survey conducted in *E. faecalis* (Maddalo et al., 2011).

Interestingly, we also observed strong enrichment of MprF2 in the DRM fraction ($log_2FC = 2.75$), indicating that MprF2 could be coordinated within DRM-linked microdomains **(Figure 4.6E)**. We also observed enrichment of SrtA within the DRM fraction ($log_2FC = 1.06$) **(Supplementary Table S4.1)**, also indicating possible association with DRM-linked microdomains. However, in *E. faecalis* p*srtA*-6his samples, this was not observed in anti-6his western blots **(Figure 4.6A)**. This discrepancy could be due to the western blot only detecting the 6his-tagged variants and not the native SrtA which could be contributing to its abundance in the DRM fraction. This will need to be verified in future with peptide MS analysis of the *E. faecalis* p*srtA*-6his samples. Preliminarily, it appears that SrtA-linked septal microdomains could be partly associated with the DRM fraction and some of the protein hits could be predictive of SrtA-linked septal microdomain function. This will need to be verified by complementary experiments to confirm their vicinity and/or interaction with SrtA such as SrtA nanodisc isolation as described in the next section, or by bacterial two hybrid assays.

However, unlike previously reported microdomains, we do not observe enrichment of flotillins in the DRM or DSM fractions and they appear equally represented in these fractions based on western blot analysis **(Figure 4.6 A-D)**. This finding suggests that flotillins and their associated microdomains in *E. faecalis* are likely not associated with the DRM fraction.

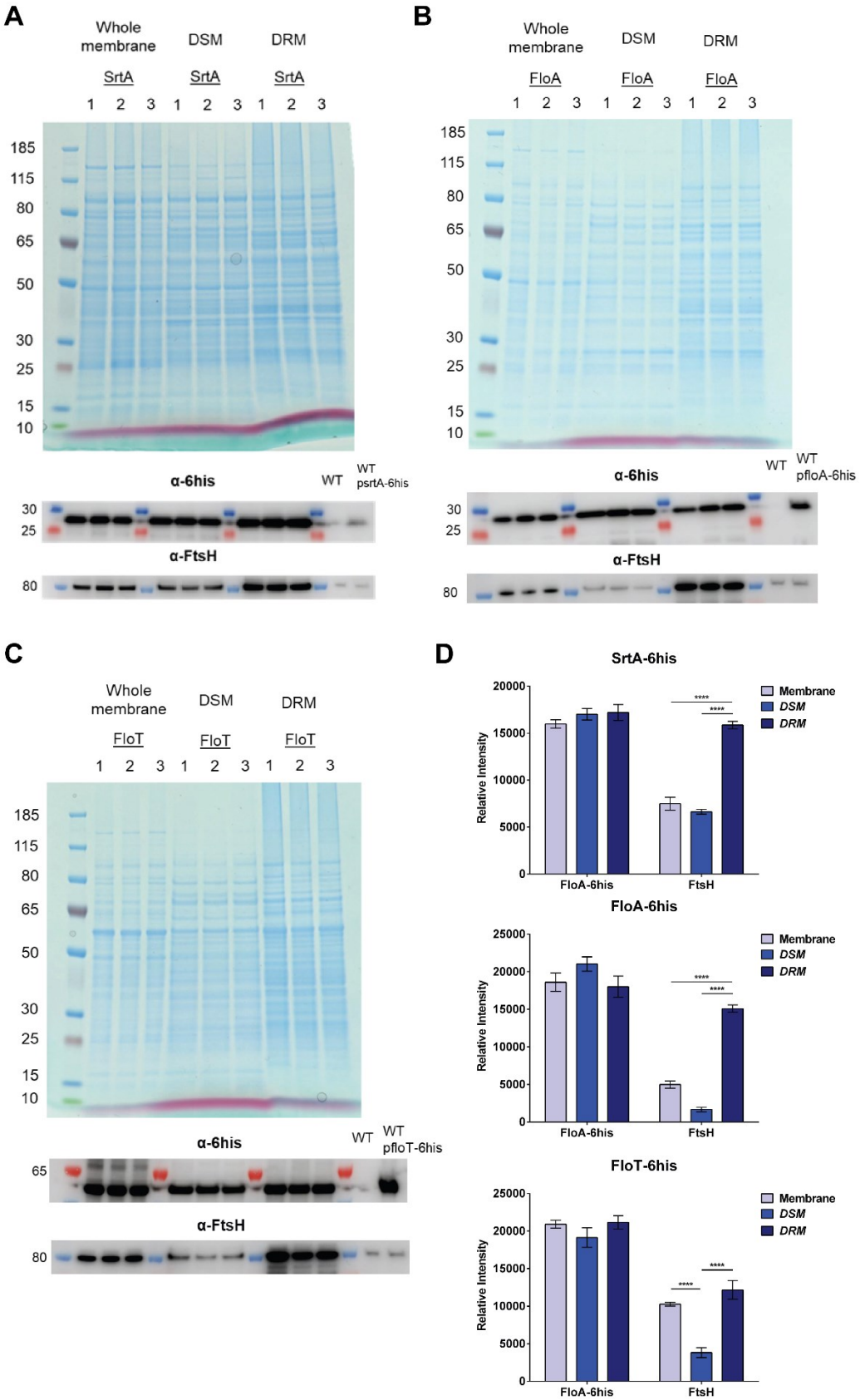
A
Whole membrane
DSM
DRM
SrtA
1 2 3 1 2 3 1 2 3
185
115
80
65
50
30
25
15
10
α-6his
WT
WT psrtA-6his
30
25
α-FtsH
80
B
Whole membrane
DSM
DRM
FloA
1 2 3 1 2 3 1 2 3
185
115
80
65
50
30
25
15
10
α-6his
WT
WT pfloA-6his
30
25
α-FtsH
80
C
Whole membrane
DSM
DRM
FloT
1 2 3 1 2 3 1 2 3
185
115
80
65
50
30
25
15
10
α-6his
WT
WT pfloT-6his
65
α-FtsH
80
D
SrtA-6his
FloA-6his
FloT-6his
Relative Intensity
20000
15000
10000
5000
0
25000
FloA-6his
FtsH
****
Membrane
DSM
DRM

E

Top 20 most enriched proteins enriched in the DRM Fractions				
Annotation	**Gene Symbol**	**LogFC**	**P-value**	**FDR**
ABC superfamily ATP binding cassette transporter, membrane protein	OG1RF_11197	3.2146	0.0080	0.0141
Bifunctional lysylphosphatidylglycerolflippase/synthetase MprF	*mprF2*	2.7525	0.0127	0.0141
Sugar ABC superfamily ATP binding cassette transporter, sugar-binding protein	OG1RF_11135	2.6648	0.0155	0.0141
Amidase	OG1RF_10473	2.6025	0.0183	0.0141
Peptidase propeptide and YPEB domain protein	OG1RF_11807	2.5938	0.0350	0.0315
ABC superfamily ATP binding cassette transporter, ABC protein	OG1RF_12369	2.5575	0.0103	0.0141
Glutamine ABC superfamily ATP binding cassette transporter, binding protein	OG1RF_10897	2.4467	0.0030	0.0000
Polysaccharide biosynthesis family protein	OG1RF_10400	2.3900	0.0306	0.0179
Iron (Fe) ABC superfamily ATP binding cassette transporter, binding protein	OG1RF_11354	2.3643	0.0043	0.0141
Rhodanese-like domain-containing protein	OG1RF_12146	2.3481	0.0332	0.0315
Cell wall surface anchor family protein	OG1RF_12451	2.2605	0.0408	0.0350
CPA1 family monovalent cation:proton (H+) antiporter-1	OG1RF_11293	2.2516	0.0408	0.0350
Sugar ABC superfamily ATP binding cassette transporter, sugar-binding protein	OG1RF_11774	2.2335	0.0408	0.0350
Spermidine/putrescine ABC superfamily ATP binding cassette transporter, binding protein	*potD*	2.1950	0.0448	0.0412
Uncharacterized protein	OG1RF_10612	2.1640	0.0253	0.0179
Integral membrane protein	OG1RF_11154	2.1640	0.0469	0.0412
Brp/Blh family beta-carotene 15,15'-monooxygenase	OG1RF_11723	2.1308	0.0272	0.0179
Protein translocase subunit SecY	*secY*	2.0816	0.0199	0.0141
RIP metalloprotease RseP	*rseP*	2.0566	0.0025	0.0000
Energy-coupling factor transporter ATP-binding protein EcfA	*ecfA*	1.9743	0.0286	0.0179

Figure 4.6. Analysis of detergent resistant membrane (DRM) and detergent soluble membrane (DSM) fractions from *E. faecalis*. Coomassie blue stained SDS-PAGE gels showing whole membrane, DRM and DSM fractions from *E. faecalis* **(A)** p*srtA*-6his, **(B)** p*floA*-6his, and **(C)** p*floT*-6his. Western blots against 6his and FtsH (a DRM marker) are shown below each respective Coomassie stained gel. **(D)** Densitometric analysis of westernblots in **(A-C)**. ****, $p \leqslant 0.0001$; Tukey's test for ANOVA. **(E)** List of the top 20 most enriched proteins in the DRM fractions from peptide MS performed on the p*floT*-

6his fractions as representative fractions of *E. faecalis* membrane. 3 biological replicates were analysed. Comparisons were done with DRM against DSM. Results were filtered as -1>Log_2FC>1, p-value>0.05, FDR>0.05. Full list of enriched and depleted proteins in DRM with respect to the DSM fraction is shown in **Supplementary Table S4.1**.

4.3.7. Non-detergent based extraction and analysis of SrtA microdomains

Since flotillins in *E. faecalis* are not associated with DRM-linked microdomains, we hypothesized that they form and organise microdomains that are not enriched within the DRM. To more specifically target and characterise flotillin associated microdomains and SrtA-associated septal microdomains we next used a non-detergent based extraction method based on styrene-maleic acid (SMA) co-polymers.

SMA co-polymers can spontaneously insert into hydrophobic cores of membranes and extract membrane nanodiscs of ~10nm in diameter, retaining native proteins and lipids within them while preserving protein stability and native interactions (Dörr et al., 2016). Hence, by using SMA on *E. faecalis* expressing 6his-tagged SrtA and flotillins, we could isolate the constituent lipids and proteins in their local environment, which should correspond to their respective membrane microdomains. Utilising this method also overcomes the pitfalls of detergent based extraction which include the potential loss of native membrane structure and native interactions, where DRMs tend to have large size distributions with lower protein stability (Dörr et al., 2016; Magee and Parmryd, 2003).

As a proof of concept that such a method is viable in *E. faecalis*, we first attempted to sample SrtA-linked microdomains by generating SrtA associated SMA lipid particles (SMALPs). Membranes from *E. faecalis* p*srtA-6his* were solubilised in SMA generating lipid nanodiscs (also known interchangeably as SMALPs). SMALPs associated with SrtA-6his were purified using immobilized

metal affinity chromatography (IMAC) with nickel columns. Wash fractions from the nickel column showed no elution of proteins after washing with 14 column volumes of wash buffer, indicating that most of the non-specific interacting proteins have been washed off **(Supplementary Figure S4.4A)**. In the stepwise elution of the column thereafter, proteins were eluted with increasing concentrations of imidazole, with SrtA-6his present in the eluted fractions as determined by western blot **(Supplementary Figure S4.4B).** Other proteins were observed to be eluted along with SrtA-6his, starting from 50 μM of imidazole.

To further purify the SrtA-SMALP preparation and remove any unspecific interacting proteins, size exclusion chromatography (SEC) was conducted. The SEC chromatogram displayed elution of a major peak at 8-9 mL of elution volume which is consistent to a previously reported isolation of a ZipA SMALPs from *E. coli* (Lee et al., 2016). Western blot and sliver stain analysis of fractions corresponding to this peak show the presence of SrtA-6his together with other proteins **(Supplementary Figure S4.4C)**.

To verify that the SEC purified SrtA-SMALPs indeed contain SMALPs, negative-stain transmission electron microscopy (TEM) was carried on the pooled SEC fractions containing SrtA-6his. Particles were observed in the SrtA SMALP samples which were absent in the buffer control, which display the signature double gaussian distribution with a mean diameter of 11.5 ± 2.5 nm, which is within the size range of previously reported SMALPs (Dörr et al., 2014; Knowles et al., 2009; Laursen et al., 2016; Long et al., 2013) **(Figure 4.7)**.

Hence, we have successfully shown that isolation of SrtA-6his SMALPs is a viable option in *E. faecalis*. Increased replicates of SrtA-6his as well as preparations for FloA-6his and FloT-6his SMALPs will be prepared for both

proteomic and lipidomic characterisation as a means of better understanding their associated membrane microdomain environment in future.

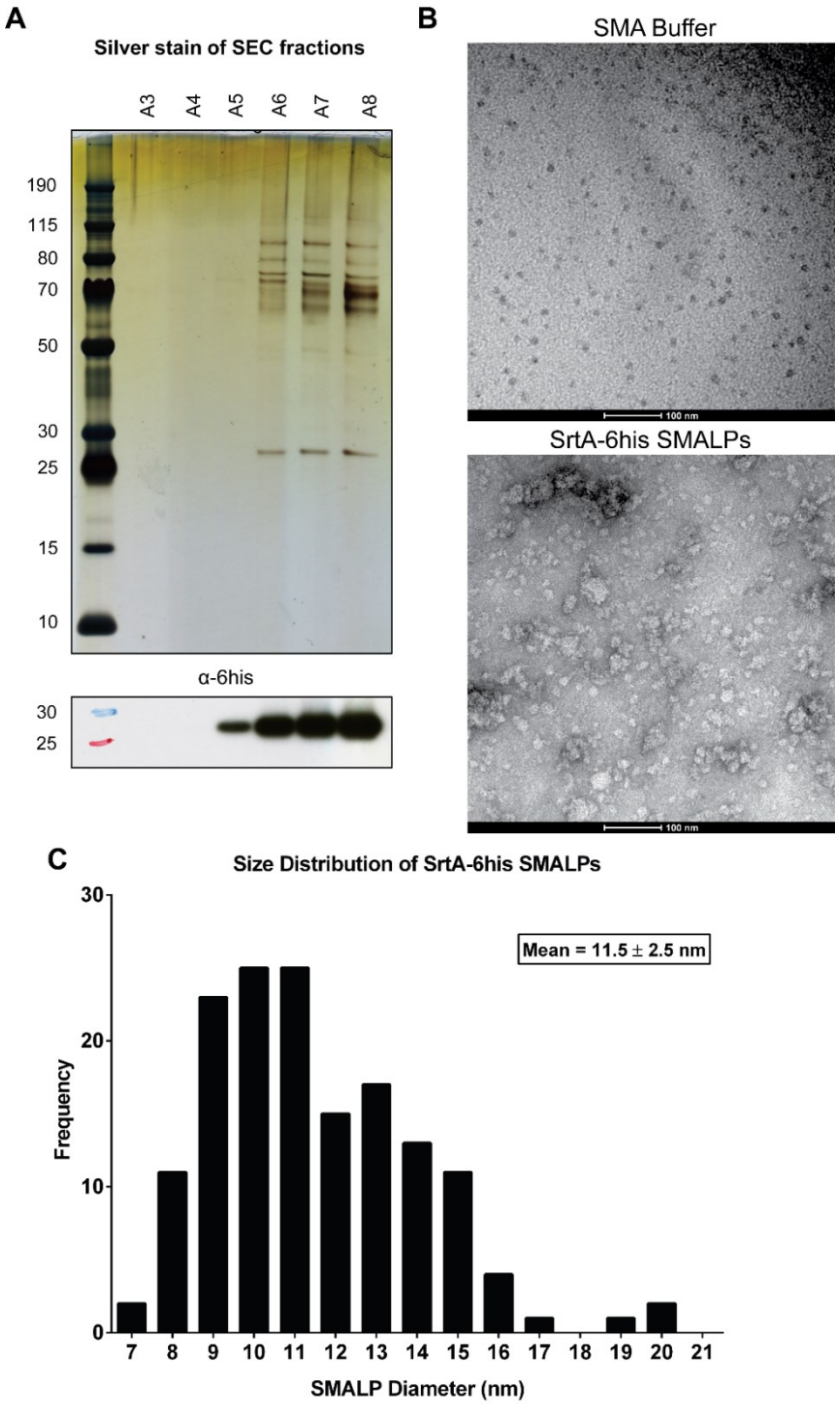

Figure 4.7. Styrene-maleic acid (SMA) based isolation of SrtA-6his SMA-lipid particles (SMALPs). (A) Silver stain and anti-6his western blots of SrtA-6his SMALP fractions after size-exclusion chromatography (SEC). Gel images of the preceding steps of nickel column chromatography and the SEC chromatogram are shown in **Supplementary Figure S4.4. (B)** Representative transmission electron micrographs of

SrtA-6his SMALPs showing nanodiscs from pooled SEC fractions (A5-A8) and corresponding buffer control. Images at 68, 000 X magnification. Performed by Choo Pei Yi. **(C)** Size distribution of SrtA-6his SMALPs as determined from the micrographs showing the signature double gaussian distribution. >100 particles were analysed.

4.4. Discussion

Sortases are an important class of enzymes responsible for anchoring virulence factors to the cell wall to allow for their proper surface display in Gram positive bacteria (Schneewind and Missiakas, 2012). Sortase A in *E. faecalis* is responsible for surface sorting of substrates, such as aggregation substance, and focally localises to the septum of mid-log phase cells (Kline et al., 2009). The mid-log septum is also the site of focal enrichment of anionic lipids, SecA of the Sec secretion machinery, as well as focal targeting of CAMPs and daptomycin (Kandaswamy et al., 2013; Kline et al., 2009; Tran et al., 2013). The coordination of these processes at this site suggests the presence of septal microdomains. Microdomains are laterally organised regions in the membrane where the unique lipid environment, and proper recruitment and assembly of domain-associated proteins are essential for the domains' function. Such microdomains have been described in *S. pyogenes* wherein its ExPortal domains are responsible for coordinating secretion, as well as functional membrane microdomains in *B. subtilis* that are responsible for coordinating membrane fluidity, biofilm formation related signalling and secretion (Bach and Bramkamp, 2013; Donovan and Bramkamp, 2009; Schneider et al., 2015; Vega and Caparon, 2012). Microdomains are also frequently associated with flotillins as their key scaffolding protein required for domain assembly and recruitment of domain-associated proteins, as in the case of *B. subtilis* and *S. aureus* (Dempwolff et al., 2016; Donovan and Bramkamp, 2009; Mielich-Süss et al., 2017). Hence, we hypothesize that flotillins could be coordinating septal

microdomains and their functions could be similar as those reported in other gram-positive organisms such as *B. subtilis* and *S. aureus*.

Through protein sequence comparisons of *B. subtilis* flotillins against *E. faecalis*, we identified two flotillin homogs, FloA and FloT (encoded by OG1RF_11500 and OG1RF_11094 respectively) **(Figure 4.1)**.

Investigation into phenotypes previously associated with flotillins revealed that the *E. faecalis* flotillin homologs are not implicated in secretion or beta-lactam resistance as previously reported in *B. subtilis* and *S. aureus* when bulk secretion and MICs for a series of beta-lactams were tested (Bach and Bramkamp, 2013; García-Fernández et al., 2017) **(Figure 4.5)**. Interestingly, amongst the *E. faecalis* flotillins, *floA* was discovered to be essential for growth when grown under a more nutrient limited conditions CDM, which was otherwise not the case when grown under BHI **(Figure 4.3)**. This suggests that *floA* might be responsible for recruiting proteins involved in the biosynthesis of the missing components in CDM such as fatty acids and other compounds. However, while *floT* was dispensable for growth in CDM, it was the only homolog that mildly affects membrane fluidity when grown under nutrient limited CDM conditions but not BHI **(Figure 4.3B, 4.4)**. This suggests that FloA and FloT have different functions in *E. faecalis* which are only apparent under nutrient limited conditions.

The results from this chapter also suggests that flotillins are likely not associated with septal microdomains. Immunofluorescence microscopy to assay for cell surface localisation and distribution revealed that FloA and SrtA are enriched at the septum while FloT is excluded from the septum and cell poles in mid log phase cells **(Figure 4.2)**. However, investigation of DRM fractions did not reveal FloA or FloT to be enriched in the DRM fraction, whereas SrtA was enriched in the DRM **(Figure 4.6)**. Taking the localisation data and DRM proteomic analyses together, these results suggest that FloA, FloT and SrtA are likely part of

separate and distinct microdomains. This is especially likely since FloA and FloT are linked to different phenotypes.

Since FloA and FloT are not enriched in the DRM, and it is widely known that DRM fractions do not equate to microdomains and are simply enriched in their associated proteins based on their tendency to resist non-ionic detergents, we also used styrene-maleic acid (SMA) co-polymers that spontaneously integrate into the membrane and excise ~10 nm diameter nanodiscs / SMA lipid particles (SMALPs) (Dörr et al., 2014). Initial experiments isolating SrtA-containing SMALPs demonstrated this to be a viable method with it successfully isolating SMALPs containing SrtA with an average diameter of 11.5 ± 2.5 nm, which is well within previously reported size ranges (Dörr et al., 2014; Knowles et al., 2009; Laursen et al., 2016; Long et al., 2013) **(Figure 4.7)**.

Consistent with previous reports, our analysis of DRM fractions yielded enrichment of similar microdomain-linked proteins such as FtsH, components of the Sec secretion machinery (SecY) along with a large number of ABC transporters, all of which are commonly found in reported DRM fractions of *S. aureus*, *B. subtilis* and *B. burgdoferi* (Lopez and Kolter, 2010; Lopez and Koch, 2017; Toledo et al., 2015) **(Figure 4.6, Supplementary Table S4.1)**.

However, unlike these studies, the flotillin homologs in *E. faecalis* are not enriched within the DRM and are equally represented in the DRM and DSM fractions **(Figure 4.6)**. These findings can also explain the reason for observed lack of secretion defects that was otherwise reported in *B. subtilis* since they are not co-enriched with the high SecY representation in the DRM (Bach and Bramkamp, 2013) **(Figure 4.5B, C)**. It can also explain their lack of influence on SrtA localisation in Δ*floA*Δ*floT* since they are also not co-enriched with higher SrtA representation in the DRM **(Figure 4.2C)**. Furthermore, they were also not associated with beta-lactam resistance as reported in *S. aureus*, which suggests

that *E. faecalis* flotillins are likely not associated with penicillin binding proteins (PBPs) in a way that affects resistance (García-Fernández et al., 2017) **(Figure 4.5A)**. In addition, only *floT* was implicated in membrane fluidity. However, its involvement is unlike that of *B. subtilis* where loss of flotillins resulted in increased membrane rigidity, where instead the loss of *floT* in *E. faecalis* only under nutrient limited conditions of CDM led to more fluid membranes instead (Bach and Bramkamp, 2013) **(Figure 4.4)**. These findings suggest that flotillins in *E. faecalis* likely coordinate separate and distinct microdomains and their functions differ from that of previously described flotillins in other bacteria.

Taken together, our findings provide the first characterisation of flotillins in *E. faecalis* and describe their roles in survival and membrane fluidity under more nutrient limited conditions. We also provide the first proteomic characterisation of DRM and DSM fractions in *E. faecalis* which can serve as a framework for other studies investigating proteins enriched within either of these fractions. Furthermore, from our successful trials in isolating SMALPs, it serves as a proof of concept that SMA-mediated extraction of nanodiscs within *E. faecalis* is possible and a viable option. This not only provides an avenue for microdomain studies that we propose here but could have extended utility in membrane protein isolation for structural and interactome investigations.

The difference in phenotypes and DRM partitioning of the flotillins in *E. faecalis* suggest that these flotillins possess unique characteristics. However, much is still unknown about its functions. This can be investigated by characterising their interactome through protein pull-downs. Proteomic and lipidomic analysis of their local membrane environment can also be done which we propose to do in future work. Furthermore, mechanistic insight into the nutrient specific phenotypes of growth and fluidity in the flotillin mutants is also needed. The exact differences between BHI and CDM contributing to these phenotypes needs to

be investigated to better understand flotillin functions. This can be done either through transcriptomic analysis of cells grown in each of these media to determine differences in metabolic responses or metabolomic analysis of the media to determine the largest differences in their constituents. The fact that the loss of *floA* affects growth in this environment also presents it as an enticing target for antimicrobial therapeutic development.

However, there are several caveats to take note of from our findings. We currently only report the mid-log phase localisations of FloA, FloT and SrtA, while it is known that localisation of flotillins and SrtA are dynamic and can change across the cell cycle (Dempwolff et al., 2016; Donovan and Bramkamp, 2009; Kandaswamy et al., 2013). This will be investigated in future work with fluorescent protein fusions to better trace localisation dynamics. Furthermore, only the DRM fractions of *E. faecalis* p*floT-6his* and the SMALP extracts of *E. faecalis psrtA-6his* were analysed which may not provide the complete picture of the DRM and microdomain environments of flotillins and SrtA. Future work will include characterisation of 6his tagged *floA, floT* and *srtA* and their DRM and DSM fractions to assess the consistency of protein representation in their fractions as well as SMALPs for each of these proteins. Proteomic and lipidomic analysis and comparisons between DRM and SMALP environments will not only help in a more complete characterisation of the microdomain environment but will also provide an assessment of SMA-based investigations as an alternative to characterising microdomains as compared to the widely used DRM fractionation method.

Furthermore, improvements can also be made to the experiments conducted. For instance, spatial information on the distribution of GP values across the cell surface cannot be determined by the spectrometry-based measurements performed in the laurdan staining assays. Future experiments should

incorporate super resolution-based microscopy to obtain this information. In addition, from the stepwise elution of the nickel column bound with SMA solubilised membranes, it was observed that elution of proteins occurred early in the imidazole gradient at 50 mM and continued to elute throughout **(Supplementary Figure S4.4B).** This makes it challenging to determine if the imidazole concentrations used allowed for specific elution of SMA lipid particles. In future a lower starting gradient should be used together with a fast protein liquid chromatography (FPLC) system for better control of the gradient and monitoring of the elution fractions.

4.5. Conclusion

In this chapter we have shown that flotillin homologs, FloA and FloT, exist in *E. faecalis* and they possess functions which are different from previous reports in other organisms. Their phenotypes only manifest under a more nutrient limited environment where *floA* is required for growth and *floT* has a minor influence on membrane fluidity. Localisation and DRM proteomic data also revealed that FloA, FloT and SrtA are likely part of separate and distinct microdomains. We also demonstrate the successful use of a SMA-mediated approach to isolate the local membrane environment of SrtA. This method can be extended to FloA and FloT, and aid in membrane microdomain characterisations when coupled with future proteomic and lipidomic analyses. These findings provide the first description of flotillins and their functions in *E. faecalis* together with a proteomic map of proteins enriched within the DRM and DSM fractions. Since *floA* is essential for growth when certain nutrients are limiting, it presents it as an enticing target for antimicrobial therapeutic development

4.6. References

Bach, J.N., Bramkamp, M., 2013. Flotillins functionally organize the bacterial membrane. Molecular microbiology 88, 1205-1217.

Banning, A., Tomasovic, A., Tikkanen, R., 2011. Functional aspects of membrane association of reggie/flotillin proteins. Current protein & peptide science 12, 725-735.

Bramkamp, M., Lopez, D., 2015. Exploring the Existence of Lipid Rafts in Bacteria. Microbiology and Molecular Biology Reviews : MMBR 79, 81-100.

Brown, D.A., 2002. Isolation and Use of Rafts. Current protocols in immunology 51, 11.10.11-11.10.23.

Bryan, E.M., Bae, T., Kleerebezem, M., Dunny, G.M., 2000. Improved vectors for nisin-controlled expression in gram-positive bacteria. Plasmid 44, 183-190.

Dempwolff, F., Schmidt, F.K., Hervás, A.B., Stroh, A., Rösch, T.C., Riese, C.N., Dersch, S., Heimerl, T., Lucena, D., Hülsbusch, N., Stuermer, C.A.O., Takeshita, N., Fischer, R., Eckhardt, B., Graumann, P.L., 2016. Super Resolution Fluorescence Microscopy and Tracking of Bacterial Flotillin (Reggie) Paralogs Provide Evidence for Defined-Sized Protein Microdomains within the Bacterial Membrane but Absence of Clusters Containing Detergent-Resistant Proteins. PLoS Genet 12, e1006116-e1006116.

Donovan, C., Bramkamp, M., 2009. Characterization and subcellular localization of a bacterial flotillin homologue. Microbiology (Reading, England) 155, 1786-1799.

Dörr, J.M., Scheidelaar, S., Koorengevel, M.C., Dominguez, J.J., Schäfer, M., van Walree, C.A., Killian, J.A., 2016. The styrene–maleic acid copolymer: a versatile tool in membrane research. European Biophysics Journal 45, 3-21.

Dörr, J.M., Koorengevel, M.C., Schafer, M., Prokofyev, A.V., Scheidelaar, S., van der Cruijsen, E.A., Dafforn, T.R., Baldus, M., Killian, J.A., 2014. Detergent-free isolation, characterization, and functional reconstitution of a tetrameric K+ channel: the power of native nanodiscs. Proceedings of the National Academy of Sciences of the United States of America 111, 18607-18612.

Dunny, G.M., Brown, B.L., Clewell, D.B., 1978. Induced cell aggregation and mating in Streptococcus faecalis: evidence for a bacterial sex pheromone. Proceedings of the National Academy of Sciences of the United States of America 75, 3479-3483.

Esnaola, M., Puig, P., Gonzalez, D., Castelo, R., Gonzalez, J.R., 2013. A flexible count data model to fit the wide diversity of expression profiles arising from extensively replicated RNA-seq experiments. BMC bioinformatics 14, 254.

García-Fernández, E., Koch, G., Wagner, R.M., Fekete, A., Stengel, S.T., Schneider, J., Mielich-Süss, B., Geibel, S., Markert, S.M., Stigloher, C., Lopez, D., 2017. Membrane Microdomain Disassembly Inhibits MRSA Antibiotic Resistance. Cell 171, 1354-1367.e1320.

Guberman, J.M., Fay, A., Dworkin, J., Wingreen, N.S., Gitai, Z., 2008. PSICIC: Noise and Asymmetry in Bacterial Division Revealed by Computational Image Analysis at Sub-Pixel Resolution. PLOS Computational Biology 4, e1000233.

Harris, F.M., Best, K.B., Bell, J.D., 2002. Use of laurdan fluorescence intensity and polarization to distinguish between changes in membrane fluidity and phospholipid order. Biochimica et biophysica acta 1565, 123-128.

Holm, L., 2020. DALI and the persistence of protein shape. Protein Science 29, 128-140.

Kandaswamy, K., Liew, T.H., Wang, C.Y., Huston-Warren, E., Meyer-Hoffert, U., Hultenby, K., Schröder, J.M., Caparon, M.G., Normark, S., Henriques-Normark, B., Hultgren, S.J., Kline, K.A., 2013. Focal targeting by human β-defensin 2 disrupts localized virulence factor assembly sites in Enterococcus faecalis. Proceedings of the National Academy of Sciences 110, 20230-20235.

Kline, K.A., Kau, A.L., Chen, S.L., Lim, A., Pinkner, J.S., Rosch, J., Nallapareddy, S.R., Murray, B.E., Henriques-Normark, B., Beatty, W., Caparon, M.G., Hultgren, S.J., 2009. Mechanism for Sortase Localization and the Role of Sortase Localization in Efficient Pilus Assembly in Enterococcus faecalis. Journal of Bacteriology 191, 3237-3247.

Knowles, T.J., Finka, R., Smith, C., Lin, Y.-P., Dafforn, T., Overduin, M., 2009. Membrane Proteins Solubilized Intact in Lipid Containing Nanoparticles

Bounded by Styrene Maleic Acid Copolymer. Journal of the American Chemical Society 131, 7484-7485.

Kristich, C.J., Manias, D.A., Dunny, G.M., 2005. Development of a method for markerless genetic exchange in Enterococcus faecalis and its use in construction of a srtA mutant. Appl Environ Microbiol 71, 5837-5849.

Lajoie, P., Nabi, I.R., 2010. Lipid rafts, caveolae, and their endocytosis. International review of cell and molecular biology 282, 135-163.

Langhorst, M.F., Reuter, A., Stuermer, C.A.O., 2005. Scaffolding microdomains and beyond: the function of reggie/flotillin proteins. Cellular and Molecular Life Sciences CMLS 62, 2228-2240.

Laursen, T., Borch, J., Knudsen, C., Bavishi, K., Torta, F., Martens, H.J., Silvestro, D., Hatzakis, N.S., Wenk, M.R., Dafforn, T.R., Olsen, C.E., Motawia, M.S., Hamberger, B., Moller, B.L., Bassard, J.E., 2016. Characterization of a dynamic metabolon producing the defense compound dhurrin in sorghum. Science (New York, N.Y.) 354, 890-893.

Lee, S.C., Knowles, T.J., Postis, V.L., Jamshad, M., Parslow, R.A., Lin, Y.P., Goldman, A., Sridhar, P., Overduin, M., Muench, S.P., Dafforn, T.R., 2016. A method for detergent-free isolation of membrane proteins in their local lipid environment. Nature protocols 11, 1149-1162.

Lingwood, D., Simons, K., 2010. Lipid rafts as a membrane-organizing principle. Science (New York, N.Y.) 327, 46-50.

Long, A.R., O'Brien, C.C., Malhotra, K., Schwall, C.T., Albert, A.D., Watts, A., Alder, N.N., 2013. A detergent-free strategy for the reconstitution of active enzyme complexes from native biological membranes into nanoscale discs. BMC Biotechnology 13, 41.

Lopez, D., Kolter, R., 2010. Functional microdomains in bacterial membranes. Genes Dev 24, 1893-1902.

Lopez, D., Koch, G., 2017. Exploring functional membrane microdomains in bacteria: an overview. Current opinion in microbiology 36, 76-84.

Maddalo, G., Chovanec, P., Stenberg-Bruzell, F., Nielsen, H.V., Jensen-Seaman, M.I., Ilag, L.L., Kline, K.A., Daley, D.O., 2011. A reference map of the membrane proteome of Enterococcus faecalis. Proteomics 11, 3935-3941.

Magee, A.I., Parmryd, I., 2003. Detergent-resistant membranes and the protein composition of lipid rafts. Genome Biology 4, 234.

Mielich-Süss, B., Wagner, R.M., Mietrach, N., Hertlein, T., Marincola, G., Ohlsen, K., Geibel, S., Lopez, D., 2017. Flotillin scaffold activity contributes to type VII secretion system assembly in Staphylococcus aureus. PLOS Pathogens 13, e1006728.

Nielsen, H.V., Guiton, P.S., Kline, K.A., Port, G.C., Pinkner, J.S., Neiers, F., Normark, S., Henriques-Normark, B., Caparon, M.G., Hultgren, S.J., 2012. The Metal Ion-Dependent Adhesion Site Motif of the Enterococcus faecalis EbpA Pilin Mediates Pilus Function in Catheter-Associated Urinary Tract Infection. mBio 3.

Rivera-Milla, E., Stuermer, C.A.O., Málaga-Trillo, E., 2006. Ancient origin of reggie (flotillin), reggie-like, and other lipid-raft proteins: convergent evolution of the SPFH domain. Cellular and Molecular Life Sciences CMLS 63, 343-357.

Rosch, J.W., Caparon, M.G., 2005. The ExPortal: an organelle dedicated to the biogenesis of secreted proteins in Streptococcus pyogenes. Molecular microbiology 58, 959-968.

Ruiz, N., Wang, B., Pentland, A., Caparon, M., 1998. Streptolysin O and adherence synergistically modulate proinflammatory responses of keratinocytes to group A streptococci. Molecular microbiology 27, 337-346.

Schneewind, O., Missiakas, D.M., 2012. Protein secretion and surface display in Gram-positive bacteria. Philos Trans R Soc Lond B Biol Sci 367, 1123-1139.

Schneider, J., Mielich-Suss, B., Bohme, R., Lopez, D., 2015. In vivo characterization of the scaffold activity of flotillin on the membrane kinase KinC of Bacillus subtilis. Microbiology 161, 1871-1887.

Singer, S.J., Nicolson, G.L., 1972. The fluid mosaic model of the structure of cell membranes. Science (New York, N.Y.) 175, 720-731.

Suomi, T., Seyednasrollah, F., Jaakkola, M.K., Faux, T., Elo, L.L., 2017. ROTS: An R package for reproducibility-optimized statistical testing. PLOS Computational Biology 13, e1005562.

Tavernarakis, N., Driscoll, M., Kyrpides, N.C., 1999. The SPFH domain: implicated in regulating targeted protein turnover in stomatins and other membrane-associated proteins. Trends in Biochemical Sciences 24, 425-427.

Toledo, A., Pérez, A., Coleman, J.L., Benach, J.L., 2015. The lipid raft proteome of *Borrelia burgdorferi*. Proteomics 15, 3662-3675.

Tran, T.T., Panesso, D., Gao, H., Roh, J.H., Munita, J.M., Reyes, J., Diaz, L., Lobos, E.A., Shamoo, Y., Mishra, N.N., Bayer, A.S., Murray, B.E., Weinstock, G.M., Arias, C.A., 2013. Whole-genome analysis of a daptomycin-susceptible enterococcus faecium strain and its daptomycin-resistant variant arising during therapy. Antimicrobial agents and chemotherapy 57, 261-268.

Vega, L.A., Caparon, M.G., 2012. Cationic antimicrobial peptides disrupt the Streptococcus pyogenes ExPortal. Molecular microbiology 85, 1119-1132.

Wiegand, I., Hilpert, K., Hancock, R.E., 2008. Agar and broth dilution methods to determine the minimal inhibitory concentration (MIC) of antimicrobial substances. Nature protocols 3, 163-175.

Yepes, A., Schneider, J., Mielich, B., Koch, G., García-Betancur, J.C., Ramamurthi, K.S., Vlamakis, H., López, D., 2012. The biofilm formation defect of a Bacillus subtilis flotillin-defective mutant involves the protease FtsH. Molecular microbiology 86, 457-471.

Yokoyama, H., Matsui, I., 2020. The lipid raft markers stomatin, prohibitin, flotillin, and HflK/C (SPFH)-domain proteins form an operon with NfeD proteins and function with apolar polyisoprenoid lipids. Critical reviews in microbiology 46, 38-48.

Zhao, F., Zhang, J., Liu, Y.-S., Li, L., He, Y.-L., 2011. Research advances on flotillins. Virology Journal 8, 479.

5. CHAPTER V:

Conclusions and future perspectives

5.1. Conclusions

Enterococci are of great clinical importance due to their roles in nosocomial infections and their tendency to be resistant to a wide range of antimicrobials. They are not only able to acquire resistance to antibiotics of last resort, such as vancomycin and daptomycin, for the treatment of multi-drug resistant infections but also possess mechanisms to overcome the action of host-derived cationic antimicrobial peptides (CAMPs). Interestingly, some of these cationic antimicrobials such as human beta-defensin 2 and daptomycin focally target the septum of *E. faecalis* which are coincident with sites of virulence factor assembly, secretion and enriched in anionic lipids. These facts together suggest that membrane microdomains may reside within the septum which are targeted by cationic antimicrobials.

However, despite the importance of septal targeting by antimicrobials, not much is known about the interaction of antimicrobials with the *E. faecalis* membrane, particularly the dynamics behind targeting, microdomain assembly, and membrane and genetic factors involved in targeting and resistance. This thesis aims to address this by investigating an enzyme implicated in CAMP-resistance, MprF (multiple peptide resistance factor), daptomycin resistance acquisition in the absence of *mprF*, as well as characterisation of microdomains within *E. faecalis*.

MprF is a membrane bound enzyme which modifies phosphatidylglycerol (PG) in the membrane to lysyl-PG (Lys-PG) and in doing so reduces the negative charge of the cell membrane and its affinity to cationic antimicrobials. The two paralogs in *E. faecalis*, *mprF1* and *mprF2*, were characterised in **Chapter 2**.

Deletion of *mprF* led to a loss of Lys-PG where *mprF2* is more involved in PG lysinylation as compared to *mprF1* **(Figure 2.2A)**. Loss of *mprF* also results in other unexpected lipidomic changes in other lipid classes with a decrease in the major phospholipid, PG and increases in glycerophosphoryl-diglucosyl-diacylglycerol (GPDGDAG), D-ala-GPDGDAG and a phosphorous-containing lipid of unknown identity **(Figure 2.2B, 2.3)**. In terms of fatty acid composition, Δ*mprF1*Δ*mprF2* exhibits an increase in palmitic acid ($C_{16:0}$) and decrease in stearic acid ($C_{18:0}$) when grown in BHI, and an increase in palmitic acid ($C_{16:0}$) and decreases in *cis*-vaccenic acid ($C_{18:1\ \omega7\ cis}$) and $C_{19\ cyclo\ \omega7}$ when grown in chemically defined media (CDM) **(Figure 2.6)**. In addition, genes in fatty acid biosynthesis were also transcriptionally downregulated, resulting in growth defects in CDM and dependence on exogenously supplied fatty acids **(Figure 2.4, 2.5, Supplementary Figure S2.8)**. These lipidomic changes in combination results in functional outcomes in terms of enhanced CAMP binding and susceptibility, increased membrane rigidity and compromised Sec-mediated secretion **(Figure 2.1, 2.8)**. This work paints a far more complex role *mprF* has in cell physiology that extends beyond just its catalytic function.

MprF also possesses daptomycin protective effects as evidenced in decreased in MIC upon *mprF2* deletion (Iris Gao, unpublished), and gain of function mutations and increased expression in daptomycin resistance (DAP^R) isolates of *S. aureus* (Ernst et al., 2018; Mishra et al., 2009; Sabat et al., 2018). To determine DAP^R associated mutations that might be masked by MprF protective activity, *in vitro* evolution was carried out in the *mprF* mutants revealing several novel mutations, one of which was the conserved metalloprotease FtsH (Iris Gao, unpublished) **(Figure 3.1)**. Loss of function mutations frequently occurred in *ftsH* early in evolution and only within Δ*mprF1*Δ*mprF2*. **Chapter 3** investigates this gene in detail and deconstructs its role in DAP^R acquisition. Excitingly, we found

that *ftsH* is essential in wild type *E. faecalis* but dispensable in the *mprF* double mutant where MprF loss of function accelerates the rate of DAP^R acquisition and basal mutation rates **(Figure 3.2, 3.3)**. The growth defects in wild type *E. faecalis* under FtsH dysfunction is likely due combined metabolic effects of differential transcriptomic regulation of oxidative phosphorylation, shikimate pathway and glycolysis coupled with proteomic depletion of glycosyl hydrolase (TrePP) and lysine-tRNA ligase (LysS) **(Figure 3.4, 3.5, 3.6)**. FtsH dysfunction also contributes to accelerated DAP^R acquisition rates through a combination of positive influence of lactose utilisation protein (*lutA*) and beta-glucosidase (*yckE*) and negative influence of a heat inducible transcription repressor (*hrcA*) **(Figure 3.7)**. Putative substrates of FtsH were also determined to be YckE, LysS, PyrB, LutA, GelE, TrePP, CryZ and HrcA.

Since septal microdomains in *E. faecalis* are implicated in CAMP binding and targeting, which *mprF* also influences, it is important that microdomains in *E. faecalis* are characterised. Since flotillins are generally recognised as main players in coordinating microdomain assembly, their functions were also characterised in **Chapter 4**. From localisation data of the flotillin homologs, FloA and FloT as well as SrtA, together with proteomic analysis of the detergent resistant membrane (DRM) fractions within which microdomain proteins are enriched, FloA and FloT appear to be part of separate and distinct microdomains **(Figure 4.2, 4.6)**. Unlike previous reports in *B. subtilis* and *S. aureus*, *E. faecalis* *floA* and *floT* were not implicated in membrane fluidity, secretion and beta-lactam resistance when grown in nutrient rich BHI (Bach and Bramkamp, 2013; García-Fernández et al., 2017) **(Figure 4.4A, 4.5A, B)**. However, under nutrient limitation in CDM, *floA* was essential for growth while *floT* had a minor effect on membrane fluidity **(Figure 4.3B, 4.4B)**. We also demonstrate the successful use of styrene-maleic acid (SMA) extraction of lipid nanodiscs as a method to

characterise microdomains by isolating the local environment around a protein of interest as an alternative method for future characterisation of FloA, FloT and SrtA-associated microdomains.

In summary, this work has provided the first detailed description of *mprF's* extended role in cell physiology beyond its catalytic function, and in its absence, uncovered FtsH's novel role in accelerating DAP^R acquisition and its conditional essentiality in the wild type **(Figure 5.1)**. This work also provides the first insight into *E. faecalis* flotillins which possess atypical characteristics in terms of functions that only manifest under a more nutrient limited environment and their non-enrichment in DRM fractions. We also provide the first description of FtsH's putative substrates, and proteomic map of the DRM and DSM fractions in the context of *E. faecalis*. Taken as a whole, this thesis gives a better understanding on the physiology of *E. faecalis* and reinforces the importance of how metabolic networks, membrane lipid composition, microdomains and functional outcomes are all closely intertwined, and holistic approaches in investigation should always be employed.

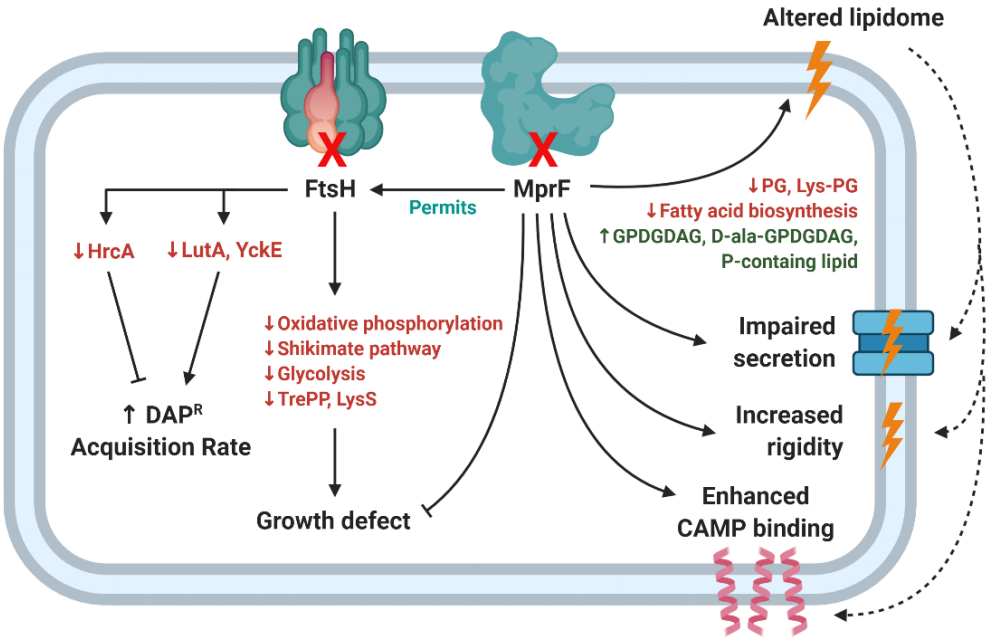

Figure 5.1. Model for MprF influence on *E. faecalis* cell physiology and FtsH influence on growth and DAP^R acquisition. MprF deletion alters the lipidome composition resulting in impaired secretion, increased rigidity, and enhanced CAMP binding. MprF deletion also permits FtsH loss of function, which results in increased DAP^R acquisition rate and contributes to a growth defect that only occurs in the presence of MprF. Created with Biorender.com.

5.2. Future perspectives

This thesis provides insight into the role of *mprF* in affecting cell physiology, FtsH in daptomycin resistance and characterisation of membrane microdomains in *E. faecalis*. The findings described in this thesis also provide multiple avenues for further exploration and investigation, which will be detailed here.

5.2.1. Investigating the mechanism behind the observed phenotypes in Δ*mprF*

In **chapter 2**, the loss of *mprF* was shown to result in global lipidomic changes and a range of pleiotropic phenotypes. However, information on exactly how these changes are mediated is still incomplete. One hypothesis is that these changes could be mediated via the interacting partners of MprF whose functions might be compromised in its absence. Another hypothesis is that the MprF paralogs could be residing in membrane microdomains and their loss could destabilise their microdomains and the functions of their resident proteins. Furthermore, metabolons, which are transient association of sequential enzymes of a biochemical pathway organised within the membrane or cytoskeleton, could be also associated with *mprF* (Hoppert and Mayer, 1999; Moraes and Reithmeier, 2012). To jointly address these hypotheses, profiling the interactome of the MprF paralogs through protein pull-downs and validation through bacterial two-hybrid assays can be done to identify the interacting partners of MprF in the cytoplasmic compartment. Styrene-maleic acid (SMA) mediated isolation of membrane nanodiscs corresponding to the MprF local environment could also be done to both characterise its microdomain environment as well as to identify any metabolon complexes which might be coordinated together with MprF. This method has been successfully used previously to characterise a metabolon coordinating the production of a defence compound, dhurrin, in plants (Laursen et al., 2016).

Another intriguing finding is that of the two *mprF* paralogs, *mprF2* appears to be the major contributor to the catalytic function of PG lysinylation and most of the other observed phenotypes. One reason for this difference could be the different processivity of the two paralogs due to differences in their protein structure and how well they bind to their substrates and process them to Lys-PG. Purification, crystallisation and solving the structures of these two paralogs might help answer this. Furthermore, biochemical investigations in the MprF paralogs activity in catalysing Lys-PG synthesis can be done through *in vitro* functional assays to determine processivity of the paralogs. In addition, Isothermal Titration Calorimetry (ITC) can also be carried to assess the possible differences in thermodynamic binding of its substrates, lysine, and PG to the enzyme.

5.2.2. Implications of chaperone activity on DAP^R acquisition and DAP mechanisms of action

In **chapter 3**, disruption of heat-inducible transcription repressor *hrcA* was discovered to be detrimental to daptomycin DAP^R acquisition rates **(Figure 3.7B)**. *hrcA* encodes a heat-inducible negative regulator of the *grpE-dnaK-dnaJ* and *groEL-groES* chaperone operons in *B. subtilis* (Roncarati and Scarlato, 2017; Schulz and Schumann, 1996). This suggests that the loss of active HrcA leads to up-regulation of chaperones in these operons that could be lowering mutation rates. If the reverse is true, that chaperone inhibition accelerates DAP^R acquisition rates, it holds important implications in cancer therapeutics that utilise chaperone inhibitors. Molecular chaperone inhibitors are typically used in combinatorial anti-cancer therapies to reduce the ability of cancer cells to respond to pharmacological and environmental stressors (Lazarev et al., 2018; Li et al., 2009; Shevtsov et al., 2019). Many of these target chaperones possess homologs found in prokaryotes (Henderson et al., 2006). Hence, it could be possible that if chaperone inhibitors are administered together with long term

courses of antibiotics in cancer patients with chronic infections, there might be accelerated instances of antibiotic resistance. Given, the possible implication of this finding, detailed investigation is warranted. First, *in vitro* evolution of strains overexpressing chaperones will need to be conducted to determine if they indeed accelerate resistance acquisition to daptomycin and other. This will also need to be repeated with the chaperone inhibitors currently used for cancer therapies to verify if co-administration of them with antibiotics might affect resistance acquisition.

Previous studies identifying and characterising the genes implicated in *E. faecalis* DAP^R mostly revealed genes implicated in membrane remodelling (*gdpD*, *cls, liaF, liaX*), oxidative stress response (*gsh*, *yybT*, *selA*) and drug efflux (*mdpA*) (Arias et al., 2011; Khan et al., 2019; Miller et al., 2013; Mishra et al., 2012). These findings suggest that resistance mechanisms tend to involve prevention of daptomycin insertion and penetration into the cell membrane and part of daptomycin's mechanism of action might involve inducing oxidative stress. However, at present not much is known about daptomycin's mechanism of action after it gains entry to the cell and what other cytotoxic effects might it be coordinating besides membrane disruption. To investigate this, the Cellular Thermal Shift Assay (CETSA) can be used to determine novel protein binding targets of daptomycin that might help inform on its mechanism of action. CETSA is able to determine these targets based on the principle of ligand-induced thermal stabilisation of ligand-bound proteins that result in a detectable thermal shift (Molina et al., 2013).

5.2.3. More extensive characterisation of virulence factor and flotillin associated microdomains and their dynamics

In **Chapter 4**, *E. faecalis* SrtA and flotillin associated microdomains were shown to be likely part of distinct and separate domains based on localisation data, and that these flotillins are not selectively enriched within the detergent resistant membrane (DRM) fraction unlike those reported in other organisms (Lopez and Koch, 2017) **(Figure 4.2, 4.6)**. Hence, profiling microdomains using DRM partitioning alone is insufficient in the context of *E. faecalis* and much is still unknown about the characteristics of these microdomains. We have shown that SMA mediated nanodisc generation to sample the microdomain environment is a viable option and propose that this can be used as an alternative to characterise these microdomains in detail **(Figure 4.7)**. Local membrane environments of SrtA and flotillins, should be isolated using this method and extensively characterised through lipidomics and proteomics to determine what process might be governed by their microdomains. Local membrane environments of other membrane bound virulence factors should also be isolated for characterisation as coordination of other virulence factor related activities could also be microdomain influenced.

Furthermore, there is evidence that microdomains are not static structures but instead are dynamic and transient in nature. This is indicated by the fact that flotillins and SrtA change their membrane localisation across the cell cycle (Dempwolff et al., 2016; Kandaswamy et al., 2013). Furthermore, lipid rafts (the eukaryotic analogue of microdomains) are temporally transient, and are assembled when required and remain so for varying durations (Kinoshita et al., 2018; Lillemeier et al., 2010; Pike, 2006). Hence, it is likely that the microdomains in *E. faecalis* are just as dynamic and profiling of these domains should be done across different stages of the cell cycle to explore the temporal

dynamics of their resident lipids and proteins. Furthermore, localisation of these microdomain-linked proteins should be traced across the cell cycle with live cell imaging under high resolution microscopy to better characterise localisation changes.

SMA-based isolations of membrane nanodiscs also offers the opportunity to study part of the membrane microdomain environment in isolation. This allows for biophysical characterisation of these domain sections in terms of membrane fluidity and charge. This method has also been used previously to isolate nanodiscs of a K^+ channel from *E. coli* and reconstitute it into an artificial bilayer for functional characterisation highlighting the potential for studying microdomains in isolation within a native environment (Dörr et al., 2014). For instance, this can be used to determine the sufficiency of SrtA-associated microdomains in guiding CAMP targeting by using reintegrating SrtA nanodiscs into artificial bilayers and treating them with fluorescent antimicrobials to determine if they specifically target SMALPs.

In **Chapter 2**, *mprF* deletion changes the lipidome of *E. faecalis* and results in functional outcomes such as impaired secretion **(Figure 2.2, 2.3, 2.8B, C)**. Since secretion is likely coordinated within the septal microdomains as explained earlier, it is possible that the altered lipidome might be changing the lipid composition of septal microdomains resulting in altered function of the Sec-secretion machinery. This might also hold true for other microdomains within *E. faecalis*. Hence, it is worthwhile to investigate the possible changing lipidome profiles of microdomains under global lipidomic changes. This can also be extended to determine both proteomic and lipidomic changes in microdomains under specific lipid depletion such as Lys-PG, PG or other lipid classes to better understand microdomain biology and determine essential lipids needed for proper domain assembly and function.

5.2.4. Bacterial lipidome alterations in infection

E. faecalis can uptake and integrate exogenous fatty acids from the environment into its lipidome, which has functional effects on daptomycin and bile resistance (Brewer et al., 2020; Saito et al., 2014). In this thesis we show that upon the loss of *mprF*, *E. faecalis* becomes dependent on exogenously supplied lipids when grown in chemically defined media **(Figure 2.5, Supplementary Figure S2.8)**. Despite this, *mprF* mutants were outcompeted in a previously reported *in vivo* competitive murine wound infection model, while in a bacteriaemia single infection model in another study, and a gut competitive infection model reported here, there were no differences reported in colonisation as compared to the wild type (Bao et al., 2012; Chong et al., 2017) **(Figure 2.9)**. These findings might suggest that despite the dependence on exogenous fatty acids, the *mprF* mutant likely encounters different fatty acid combinations in the different colonisation niches which results in niche-specific fitness outcomes. Hence, it would be interesting to profile the lipidome changes in *E. faecalis* in both wild type and *mprF* mutant backgrounds in different infection niches and tease apart the interplay between membrane homeostasis and the external host environment, and their influence on fitness and virulence through membrane alterations. This can be done by separating host and bacterial cells post infection via cell sorting and performing lipidomic characterisation on the bacterial components.

5.3. References

Arias, C.A., Panesso, D., McGrath, D.M., Qin, X., Mojica, M.F., Miller, C., Diaz, L., Tran, T.T., Rincon, S., Barbu, E.M., Reyes, J., Roh, J.H., Lobos, E., Sodergren, E., Pasqualini, R., Arap, W., Quinn, J.P., Shamoo, Y., Murray, B.E., Weinstock, G.M., 2011. Genetic basis for in vivo daptomycin resistance in enterococci. The New England journal of medicine 365, 892-900.

Bach, J.N., Bramkamp, M., 2013. Flotillins functionally organize the bacterial membrane. Molecular microbiology 88, 1205-1217.

Bao, Y., Sakinc, T., Laverde, D., Wobser, D., Benachour, A., Theilacker, C., Hartke, A., Huebner, J., 2012. Role of mprF1 and mprF2 in the pathogenicity of Enterococcus faecalis. PloS one 7, e38458.

Brewer, W., Harrison, J., Saito, H.E., Fozo, E.M., 2020. Induction of Daptomycin Tolerance in Enterococcus faecalis by Fatty Acid Combinations. Appl Environ Microbiol 86, e01178-01120.

Chong, K.K.L., Tay, W.H., Janela, B., Yong, A.M.H., Liew, T.H., Madden, L., Keogh, D., Barkham, T.M.S., Ginhoux, F., Becker, D.L., Kline, K.A., 2017. Enterococcus faecalis Modulates Immune Activation and Slows Healing During Wound Infection. The Journal of infectious diseases 216, 1644-1654.

Dempwolff, F., Schmidt, F.K., Hervás, A.B., Stroh, A., Rösch, T.C., Riese, C.N., Dersch, S., Heimerl, T., Lucena, D., Hülsbusch, N., Stuermer, C.A.O., Takeshita, N., Fischer, R., Eckhardt, B., Graumann, P.L., 2016. Super Resolution Fluorescence Microscopy and Tracking of Bacterial Flotillin (Reggie) Paralogs Provide Evidence for Defined-Sized Protein Microdomains within the Bacterial Membrane but Absence of Clusters Containing Detergent-Resistant Proteins. PLoS Genet 12, e1006116-e1006116.

Dörr, J.M., Koorengevel, M.C., Schafer, M., Prokofyev, A.V., Scheidelaar, S., van der Cruijsen, E.A., Dafforn, T.R., Baldus, M., Killian, J.A., 2014. Detergent-free isolation, characterization, and functional reconstitution of a tetrameric K+ channel: the power of native nanodiscs. Proceedings of the National Academy of Sciences of the United States of America 111, 18607-18612.

Ernst, C.M., Slavetinsky, C.J., Kuhn, S., Hauser, J.N., Nega, M., Mishra, N.N., Gekeler, C., Bayer, A.S., Peschel, A., 2018. Gain-of-Function Mutations in the Phospholipid Flippase MprF Confer Specific Daptomycin Resistance. mBio 9, e01659-01618.

García-Fernández, E., Koch, G., Wagner, R.M., Fekete, A., Stengel, S.T., Schneider, J., Mielich-Süss, B., Geibel, S., Markert, S.M., Stigloher, C., Lopez, D., 2017. Membrane Microdomain Disassembly Inhibits MRSA Antibiotic Resistance. Cell 171, 1354-1367.e1320.

Henderson, B., Allan, E., Coates, A.R.M., 2006. Stress wars: the direct role of host and bacterial molecular chaperones in bacterial infection. Infect Immun 74, 3693-3706.

Hoppert, M., Mayer, F., 1999. Principles of macromolecular organization and cell function in bacteria and archaea. Cell Biochemistry and Biophysics 31, 247-284.

Kandaswamy, K., Liew, T.H., Wang, C.Y., Huston-Warren, E., Meyer-Hoffert, U., Hultenby, K., Schröder, J.M., Caparon, M.G., Normark, S., Henriques-Normark, B., Hultgren, S.J., Kline, K.A., 2013. Focal targeting by human β-defensin 2 disrupts localized virulence factor assembly sites in Enterococcus faecalis. Proceedings of the National Academy of Sciences 110, 20230-20235.

Khan, A., Davlieva, M., Panesso, D., Rincon, S., Miller, W.R., Diaz, L., Reyes, J., Cruz, M.R., Pemberton, O., Nguyen, A.H., Siegel, S.D., Planet, P.J., Narechania, A., Latorre, M., Rios, R., Singh, K.V., Ton-That, H., Garsin, D.A., Tran, T.T., Shamoo, Y., Arias, C.A., 2019. Antimicrobial sensing coupled with cell membrane remodeling mediates antibiotic resistance and virulence in *Enterococcus faecalis*. Proceedings of the National Academy of Sciences 116, 26925.

Kinoshita, M., Suzuki, K.G.N., Murata, M., Matsumori, N., 2018. Evidence of lipid rafts based on the partition and dynamic behavior of sphingomyelins. Chemistry and Physics of Lipids 215, 84-95.

Laursen, T., Borch, J., Knudsen, C., Bavishi, K., Torta, F., Martens, H.J., Silvestro, D., Hatzakis, N.S., Wenk, M.R., Dafforn, T.R., Olsen, C.E., Motawia, M.S., Hamberger, B., Møller, B.L., Bassard, J.-E., 2016. Characterization of a

dynamic metabolon producing the defense compound dhurrin in sorghum. Science (New York, N.Y.) 354, 890-893.

Lazarev, V.F., Sverchinsky, D.V., Mikhaylova, E.R., Semenyuk, P.I., Komarova, E.Y., Niskanen, S.A., Nikotina, A.D., Burakov, A.V., Kartsev, V.G., Guzhova, I.V., Margulis, B.A., 2018. Sensitizing tumor cells to conventional drugs: HSP70 chaperone inhibitors, their selection and application in cancer models. Cell Death & Disease 9, 41.

Li, Y., Zhang, T., Schwartz, S.J., Sun, D., 2009. New developments in Hsp90 inhibitors as anti-cancer therapeutics: mechanisms, clinical perspective and more potential. Drug Resist Updat 12, 17-27.

Lillemeier, B.F., Mörtelmaier, M.A., Forstner, M.B., Huppa, J.B., Groves, J.T., Davis, M.M., 2010. TCR and Lat are expressed on separate protein islands on T cell membranes and concatenate during activation. Nature Immunology 11, 90-96.

Lopez, D., Koch, G., 2017. Exploring functional membrane microdomains in bacteria: an overview. Current opinion in microbiology 36, 76-84.

Miller, C., Kong, J., Tran, T.T., Arias, C.A., Saxer, G., Shamoo, Y., 2013. Adaptation of Enterococcus faecalis to daptomycin reveals an ordered progression to resistance. Antimicrobial agents and chemotherapy 57, 5373-5383.

Mishra, N.N., Yang, S.-J., Sawa, A., Rubio, A., Nast, C.C., Yeaman, M.R., Bayer, A.S., 2009. Analysis of cell membrane characteristics of in vitro-selected daptomycin-resistant strains of methicillin-resistant Staphylococcus aureus. Antimicrobial agents and chemotherapy 53, 2312-2318.

Mishra, N.N., Bayer, A.S., Tran, T.T., Shamoo, Y., Mileykovskaya, E., Dowhan, W., Guan, Z., Arias, C.A., 2012. Daptomycin Resistance in Enterococci Is Associated with Distinct Alterations of Cell Membrane Phospholipid Content. PloS one 7, e43958.

Molina, D.M., Jafari, R., Ignatushchenko, M., Seki, T., Larsson, E.A., Dan, C., Sreekumar, L., Cao, Y., Nordlund, P., 2013. Monitoring Drug Target Engagement in Cells and Tissues Using the Cellular Thermal Shift Assay. Science (New York, N.Y.) 341, 84-87.

Moraes, T.F., Reithmeier, R.A.F., 2012. Membrane transport metabolons. Biochimica et Biophysica Acta (BBA) - Biomembranes 1818, 2687-2706.

Pike, L.J., 2006. Rafts defined: a report on the Keystone symposium on lipid rafts and cell function. Journal of Lipid Research 47, 1597-1598.

Roncarati, D., Scarlato, V., 2017. Regulation of heat-shock genes in bacteria: from signal sensing to gene expression output. FEMS Microbiology Reviews 41, 549-574.

Sabat, A.J., Tinelli, M., Grundmann, H., Akkerboom, V., Monaco, M., Del Grosso, M., Errico, G., Pantosti, A., Friedrich, A.W., 2018. Daptomycin Resistant Staphylococcus aureus Clinical Strain With Novel Non-synonymous Mutations in the mprF and vraS Genes: A New Insight Into Daptomycin Resistance. Front Microbiol 9, 2705-2705.

Saito, H.E., Harp, J.R., Fozo, E.M., 2014. Incorporation of exogenous fatty acids protects Enterococcus faecalis from membrane-damaging agents. Appl Environ Microbiol 80, 6527-6538.

Schulz, A., Schumann, W., 1996. hrcA, the first gene of the Bacillus subtilis dnaK operon encodes a negative regulator of class I heat shock genes. J Bacteriol 178, 1088-1093.

Shevtsov, M., Multhoff, G., Mikhaylova, E., Shibata, A., Guzhova, I., Margulis, B., 2019. Combination of Anti-Cancer Drugs with Molecular Chaperone Inhibitors. Int J Mol Sci 20, 5284.

6. APPENDIX

6.1. Supplementary information for Chapter 2

Table S2.1. DGDAG Species detected in *E. faecalis*

				MS1			MS2				
Lipid Species	**Molecular Ion**	**RT [min]**	**Sum Composition**	**Observed m/z**	**Theoretical m/z**	**Δppm**	**Observed m/z**	**Neutral loss**	**Theoretical m/z**	**Δppm**	**Identity**
Wild type											
DGDAG	[M+NH4+]	1.00 – 1.30	28:1	852.5682	852.5679	0.35	not fragmented				
DGDAG	[M+NH4+]	1.00 – 1.30	28:0	854.5838	854.5835	0.30	495.439	359.1448	359.1422	7.24	Loss of 2 glucose
DGDAG	[M+NH4+]	1.00 – 1.30	30:1	880.5948	880.5992	-4.99	521.4569	359.1379	359.1422	-11.97	Loss of 2 glucose
DGDAG	[M+NH4+]	1.00 – 1.30	30:0	882.6154	882.6148	0.63	523.4711	359.1443	359.1422	5.85	Loss of 2 glucose
DGDAG	[M+NH4+]	1.00 – 1.30	32:2	906.6158	906.6148	1.05	547.4696	359.1462	359.1422	11.14	Loss of 2 glucose
DGDAG	[M+NH4+]	1.00 – 1.30	32:1	908.6321	908.6305	1.76	549.4873	359.1448	359.1422	7.24	Loss of 2 glucose
DGDAG	[M+NH4+]	1.00 – 1.30	32:0	910.6468	910.6461	0.72	551.5036	359.1432	359.1422	2.78	Loss of 2 glucose
DGDAG	[M+NH4+]	1.00 – 1.30	34:2	934.6478	934.6461	1.77	575.505	359.1428	359.1422	1.67	Loss of 2 glucose
DGDAG	[M+NH4+]	1.00 – 1.30	34:1	936.6634	936.6618	1.71	577.5207	359.1427	359.1422	1.39	Loss of 2 glucose
DGDAG	[M+NH4+]	1.00 – 1.30	34:0	938.674	938.6774	-3.67	not fragmented				
DGDAG	[M+NH4+]	1.00 – 1.30	35:2	948.6626	948.6618	0.85	not fragmented				
DGDAG	[M+NH4+]	1.00 – 1.30	35:1	not detected			not detected				
DGDAG	[M+NH4+]	1.00 – 1.30	36:2	962.6786	962.6774	1.20	603.5351	359.1435	359.1422	3.62	Loss of 2 glucose
DGDAG	[M+NH4+]	1.00 – 1.30	36:1	964.6919	964.6931	-1.24	not fragmented				
DGDAG	[M+NH4+]	1.00 – 1.30	37:2	not detected			not detected				

Δ*mprF1*											
DGDAG	[M+NH4+]	1.00 – 1.30	28:1	852.5709	852.5679	3.52	not fragmented				
DGDAG	[M+NH4+]	1.00 – 1.30	28:0	854.5862	854.5835	3.10	495.4396	359.1466	359.1422	12.25	Loss of 2 glucose
DGDAG	[M+NH4+]	1.00 – 1.30	30:1	880.6028	880.5992	4.09	521.4566	359.1462	359.1422	11.14	Loss of 2 glucose
DGDAG	[M+NH4+]	1.00 – 1.30	30:0	882.6184	882.6148	4.02	523.4723	359.1461	359.1422	10.86	Loss of 2 glucose
DGDAG	[M+NH4+]	1.00 – 1.30	32:2	906.6183	906.6148	3.81	547.4725	359.1458	359.1422	10.02	Loss of 2 glucose
DGDAG	[M+NH4+]	1.00 – 1.30	32:1	908.6348	908.6305	4.74	549.4893	359.1455	359.1422	9.19	Loss of 2 glucose
DGDAG	[M+NH4+]	1.00 – 1.30	32:0	910.6494	910.6461	3.57	not fragmented				
DGDAG	[M+NH4+]	1.00 – 1.30	34:2	not detected			not detected				
DGDAG	[M+NH4+]	1.00 – 1.30	34:1	936.6662	936.6618	4.70	577.5194	359.1468	359.1422	12.81	Loss of 2 glucose
DGDAG	[M+NH4+]	1.00 – 1.30	34:0	938.6766	938.6774	-0.90	not fragmented				
DGDAG	[M+NH4+]	1.00 – 1.30	35:2	not detected			not detected				
DGDAG	[M+NH4+]	1.00 – 1.30	35:1	950.6778	950.6774	0.37	591.5375	359.1403	359.1422	-5.29	Loss of 2 glucose
DGDAG	[M+NH4+]	1.00 – 1.30	36:2	962.6814	962.6774	4.11	not fragmented				
DGDAG	[M+NH4+]	1.00 – 1.30	36:1	964.6951	964.6931	2.08	not fragmented				
DGDAG	[M+NH4+]	1.00 – 1.30	37:2	976.6922	976.6931	-0.92	not fragmented				
Δ*mprF2*											
DGDAG	[M+NH4+]	1.00 – 1.30	28:1	852.5679	852.5679	0.00	493.4217	359.1462	359.1422	11.14	Loss of 2 glucose
DGDAG	[M+NH4+]	1.00 – 1.30	28:0	854.5839	854.5835	0.41	495.4408	359.1431	359.1422	2.51	Loss of 2 glucose
DGDAG	[M+NH4+]	1.00 – 1.30	30:1	880.6003	880.5992	1.25	521.4563	359.1440	359.1422	5.01	Loss of 2 glucose
DGDAG	[M+NH4+]	1.00 – 1.30	30:0	882.616	882.6148	1.31	523.4703	359.1457	359.1422	9.75	Loss of 2 glucose
DGDAG	[M+NH4+]	1.00 – 1.30	32:2	906.6162	906.6148	1.49	547.4759	359.1403	359.1422	-5.29	Loss of 2 glucose
DGDAG	[M+NH4+]	1.00 – 1.30	32:1	908.6322	908.6305	1.87	549.4875	359.1447	359.1422	6.96	Loss of 2 glucose
DGDAG	[M+NH4+]	1.00 – 1.30	32:0	910.6468	910.6461	0.72	551.5027	359.1441	359.1422	5.29	Loss of 2 glucose
DGDAG	[M+NH4+]	1.00 – 1.30	34:2	934.6482	934.6461	2.20	575.5036	359.1446	359.1422	6.68	Loss of 2 glucose

DGDAG	[M+NH4+]	1.00 – 1.30	34:1	936.6634	936.6618	1.71	577.5199	359.1435	359.1422	3.62	Loss of 2 glucose
DGDAG	[M+NH4+]	1.00 – 1.30	34:0	938.6743	938.6774	-3.35	not fragmented				
DGDAG	[M+NH4+]	1.00 – 1.30	35:2	948.6621	948.6618	0.32	589.5195	359.1426	359.1422	1.11	Loss of 2 glucose
DGDAG	[M+NH4+]	1.00 – 1.30	35:1	950.6777	950.6774	0.27	591.5343	359.1434	359.1422	3.34	Loss of 2 glucose
DGDAG	[M+NH4+]	1.00 – 1.30	36:2	962.6787	962.6774	1.30	603.5361	359.1426	359.1422	1.11	Loss of 2 glucose
DGDAG	[M+NH4+]	1.00 – 1.30	36:1	964.6922	964.6931	-0.93	not fragmented				
DGDAG	[M+NH4+]	1.00 – 1.30	37:2	976.6919	976.6931	-1.23	617.5485	359.1434	359.1422	3.34	Loss of 2 glucose
Δ*mprF1* Δ*mprF2*											
DGDAG	[M+NH4+]	1.00 – 1.30	28:1	852.5684	852.5679	0.59	493.427	359.1414	359.1422	-2.23	Loss of 2 glucose
DGDAG	[M+NH4+]	1.00 – 1.30	28:0	854.5837	854.5835	0.18	not fragmented				
DGDAG	[M+NH4+]	1.00 – 1.30	30:1	880.6007	880.5992	1.71	521.4542	359.1465	359.1422	11.97	Loss of 2 glucose
DGDAG	[M+NH4+]	1.00 – 1.30	30:0	882.6162	882.6148	1.53	523.471	359.1452	359.1422	8.35	Loss of 2 glucose
DGDAG	[M+NH4+]	1.00 – 1.30	32:2	906.6162	906.6148	1.49	547.4692	359.1470	359.1422	13.37	Loss of 2 glucose
DGDAG	[M+NH4+]	1.00 – 1.30	32:1	908.6323	908.6305	1.98	549.4876	359.1447	359.1422	6.96	Loss of 2 glucose
DGDAG	[M+NH4+]	1.00 – 1.30	32:0	910.6468	910.6461	0.72	551.5028	359.1440	359.1422	5.01	Loss of 2 glucose
DGDAG	[M+NH4+]	1.00 – 1.30	34:2	934.6494	934.6461	3.48	575.5037	359.1457	359.1422	9.75	Loss of 2 glucose
DGDAG	[M+NH4+]	1.00 – 1.30	34:1	936.6636	936.6618	1.92	577.5205	359.1431	359.1422	2.51	Loss of 2 glucose
DGDAG	[M+NH4+]	1.00 – 1.30	34:0	938.6735	938.6774	-4.21	not fragmented				
DGDAG	[M+NH4+]	1.00 – 1.30	35:2	948.6627	948.6618	0.95	589.5177	359.1450	359.1422	7.80	Loss of 2 glucose
DGDAG	[M+NH4+]	1.00 – 1.30	35:1	950.6771	950.6774	-0.37	591.5355	359.1416	359.1422	-1.67	Loss of 2 glucose
DGDAG	[M+NH4+]	1.00 – 1.30	36:2	962.679	962.6774	1.61	603.5355	359.1435	359.1422	3.62	Loss of 2 glucose
DGDAG	[M+NH4+]	1.00 – 1.30	36:1	964.6891	964.6931	-4.14	not fragmented				
DGDAG	[M+NH4+]	1.00 – 1.30	37:2	976.692	976.6931	-1.12	617.549	359.1430	359.1422	2.23	Loss of 2 glucose

DGDAG species detected in the various *mprF* mutants of *E. faecalis* as confirmed by the observed MS1 and MS2 peaks' m/z.

Table S2.2 - MRM transition list for DGDAG and MGDAG			
Lipid Species	**Ion Mode**	**Precursor Ion**	**Product Ion**
MGDAG 34:1	Positive	774.6	313.3
DGDG 28:1	Positive	852.6	493.5
DGDG 28:0	Positive	854.6	495.5
DGDG 30:1	Positive	880.6	521.5
DGDG 30:0	Positive	882.6	523.5
DGDG 32:2	Positive	906.6	547.5
DGDG 32:1	Positive	908.6	549.5
DGDG 32:0	Positive	910.6	551.5
DGDG 34:2	Positive	934.6	575.5
DGDG 34:1	Positive	936.7	577.6
DGDG 34:0	Positive	938.7	579.6
DGDG 35:2	Positive	948.7	589.6
DGDG 35:1	Positive	950.7	591.6
DGDG 36:2	Positive	962.7	603.6
DGDG 36:1	Positive	964.7	605.6
DGDG 37:2	Positive	976.7	617.6

Table S2.3 - Untargeted MS analysis of TLC spots											
				MS1			MS2				
Lipid Class	Molecular Ion	RT [min]	Sum Composition	Observed m/z	Theoretical m/z	Δppm	Observed m/z	Neutral loss	Theoretical m/z	Δppm	Identity
Spot 1 - WT											
DGDAG	[M+NH4+]	1 - 1.5	32:1	908.6312	908.6305	0.77	549.4878	359.1434	359.1422	3.34	2 Glucose
DGDAG	[M+NH4+]	1 - 1.5	32:0	910.6466	910.6461	0.50	551.5021	359.1445	359.1422	6.40	2 Glucose
DGDAG	[M+NH4+]	1 - 1.5	34:2	934.6473	934.6461	1.23	575.5027	359.1446	359.1422	6.68	2 Glucose
DGDAG	[M+NH4+]	1 - 1.5	34:1	936.6625	936.6618	0.75	577.5192	359.1433	359.1422	3.06	2 Glucose
DGDAG	[M+NH4+]	1 - 1.5	34:0	938.6743	938.6774	-3.35	579.5312	359.1431	359.1422	2.51	2 Glucose
DGDAG	[M+NH4+]	1 - 1.5	35:2	948.6608	948.6618	-1.05	not fragmented				
DGDAG	[M+NH4+]	1 - 1.5	35:1	950.6765	950.6774	-1.00	not fragmented				
DGDAG	[M+NH4+]	1 - 1.5	35:0	952.6827	952.6931	-10.91	591.5363	359.1402	359.1422	-5.57	2 Glucose
DGDAG	[M+NH4+]	1 - 1.5	36:2	962.6766	962.6774	-0.88	not fragmented				
DGDAG	[M+NH4+]	1 - 1.5	36:1	964.692	964.6931	-1.14	603.5348	359.1418	359.1422	-1.11	2 Glucose
DGDAG	[M+NH4+]	1 - 1.5	36:0	966.6999	966.7087	-9.15	605.549	359.143	359.1422	2.23	2 Glucose
Spot 1 - ΔmprF1Δ*mprF2*											
DGDAG	[M+NH4+]	1 - 1.5	30:0	882.6153	882.6148	0.51	523.4720	359.1433	359.1422	3.06	2 Glucose
DGDAG	[M+NH4+]	1 - 1.5	32:2	906.6159	906.6148	1.16	not fragmented				
DGDAG	[M+NH4+]	1 - 1.5	32:1	908.6312	908.6305	0.77	549.4877	359.1435	359.1422	3.62	2 Glucose
DGDAG	[M+NH4+]	1 - 1.5	32:0	910.6455	910.6461	-0.71	551.5019	359.1436	359.1422	3.90	2 Glucose
DGDAG	[M+NH4+]	1 - 1.5	33:2	920.6318	920.6305	1.41	not fragmented				
DGDAG	[M+NH4+]	1 - 1.5	33:1	922.6466	922.6461	0.49	not fragmented				
DGDAG	[M+NH4+]	1 - 1.5	34:2	934.6469	934.6461	0.80	575.5027	359.1442	359.1422	5.57	2 Glucose
DGDAG	[M+NH4+]	1 - 1.5	34:1	936.6621	936.6618	0.32	577.5189	359.1432	359.1422	2.78	2 Glucose

DGDAG	[M+NH4+]	1 - 1.5	34:0	938.6727	938.6774	-5.06	579.5306	359.1421	359.1422	-0.28	2 Glucose
DGDAG	[M+NH4+]	1 - 1.5	35:2	948.661	948.6618	-0.84	589.5192	359.1418	359.1422	-1.11	2 Glucose
DGDAG	[M+NH4+]	1 - 1.5	35:1	950.6762	950.6774	-1.31	591.5357	359.1405	359.1422	-4.73	2 Glucose
DGDAG	[M+NH4+]	1 - 1.5	36:2	962.6765	962.6774	-0.98	603.5344	359.1421	359.1422	-0.28	2 Glucose
DGDAG	[M+NH4+]	1 - 1.5	36:1	964.6918	964.6931	-1.35	605.5482	359.1436	359.1422	3.90	2 Glucose
DGDAG	[M+NH4+]	1 - 1.5	36:0	966.7002	966.7087	-8.84	not fragmented				
DGDAG	[M+NH4+]	1 - 1.5	37:2	976.6923	976.6931	-0.82	not fragmented				
DGDAG	[M+NH4+]	1 - 1.5	37:1	978.7075	978.7087	-1.28	not fragmented				
DGDAG	[M+NH4+]	1 - 1.5	38:2	990.7088	990.7087	0.05	not fragmented				
DGDAG	[M+NH4+]	1 - 1.5	38:1	992.7237	992.7244	-0.70	not fragmented				
Spot 2 - WT											
No spot available											
Spot 2 - ΔmprF1ΔmprF2											
unknown	[M-H+]	0-2.0	unknown	909.5777			227.2012		227.2017	-2.00	FA 14:0
							255.2325		255.2330	-1.78	FA 16:0
							379.1237				
							397.1342				
							415.1447				
unknown	[M-H+]	0-2.0	unknown	935.5933			227.2013		227.2017	-1.56	FA 14:0
							253.2169		253.2173	-1.59	FA 16:1
							255.2325		255.2330	-1.78	FA 16:0
							281.2480		281.2486	-2.15	FA 18:1
							379.1239				
							397.1342				
							415.1447				

unknown	[M-H+]	0-2.0	unknown	938.6125			227.2012	227.2017	-2.00	FA 14:0
							255.2325	255.2330	-1.78	FA 16:0
							379.1238			
							397.1342			
							415.1447			
unknown	[M-H+]	0-2.0	unknown	953.5957			255.2325	255.2330	-1.78	FA 16:0
							281.2479	281.2486	-2.50	FA 18:1
							379.1236			
							397.1342			
							415.1467			
unknown	[M-H+]	0-2.0	unknown	963.6237			255.2325	255.2330	-1.78	FA 16:0
							281.2480	281.2486	-2.15	FA 18:1
							379.1239			
							397.1343			
							415.1446			
unknown	[M-H+]	0-2.0	unknown	977.6393			255.2326	255.2330	-1.39	FA 16:0
							295.2638	295.2643	-1.54	FA 19:1
							379.1240			
							397.1344			
							415.1447			
Spot 3 - WT										
PG	[M-H+]	2-2.4	32:1	719.485	719.4869	-2.58	152.9954	152.9953	0.65	GP
							227.2012	227.2017	-2.00	FA 14:0
							253.2168	253.2173	-1.99	FA 16:1
							255.2324	255.2330	-2.17	FA 16:0

							281.2479	281.2486	-2.50	FA 18:1
PG	[M-H+]	2-2.4	32:0	721.5006	721.5025	-2.65	152.9951	152.9953	-1.31	GP
							227.2012	227.2017	-2.00	FA 14:0
							255.2325	255.2330	-1.78	FA 16:0
							283.2634	283.2643	-3.01	FA 18:0
PG	[M-H+]	2-2.4	33:1	733.5007	733.5025	-2.47	152.9955	152.9953	1.31	GP
							227.2013	227.2017	-1.56	FA 14:0
							255.2325	255.2330	-1.78	FA 16:0
							295.2633	295.2643	-3.23	FA 19:1
PG	[M-H+]	2-2.4	34:1	747.5167	747.5182	-1.95	152.9955	152.9953	1.31	GP
							255.2325	255.2330	-1.78	FA 16:0
							281.2478	281.2486	-2.86	FA 18:1
PG	[M-H+]	2-2.4	34:0	749.5319	749.5338	-2.55	152.9954	152.9953	0.65	GP
							255.2325	255.2330	-1.78	FA 16:0
							283.2634	283.2643	-3.01	FA 18:0
PG	[M-H+]	2-2.4	35:2	759.5161	759.5182	-2.71	152.9955	152.9953	1.31	GP
							253.2168	253.2173	-1.99	FA 16:1
							295.2634	295.2643	-2.89	FA 19:1
PG	[M-H+]	2-2.4	35:1	761.5314	761.5338	-3.16	152.9954	152.9953	0.65	GP
							255.2325	255.2330	-1.78	FA 16:0
							295.2634	295.2643	-2.89	FA 19:1
PG	[M-H+]	2-2.4	36:2	773.5307	773.5338	-4.02	152.9956	152.9953	1.96	GP
							281.2481	281.2486	-1.79	FA 18:1
PG	[M-H+]	2-2.4	36:1	775.5465	775.5495	-3.82	152.9955	152.9953	1.31	GP
							255.2324	255.2330	-2.17	FA 16:0

							269.2116			
							281.2479	281.2486	-2.50	FA 18:1
							295.2634	295.2643	-2.89	FA 19:1
							309.2789	309.2799	-3.25	FA 20:1
PG	[M-H+]	2-2.4	37:2	787.5465	787.5495	-3.76	152.9955	152.9953	1.31	GP
							281.2479	281.2486	-2.50	FA 18:1
							295.2636	295.2643	-2.21	FA 19:1
PG	[M-H+]	2-2.4	Iodinylated PG	863.3916			126.9048	126.9045	2.36	Iodine adduct
							152.9956	152.9953	1.96	GP
							227.2014	227.2017	-1.12	FA 14:0
				891.4229			255.2325	255.2330	-1.78	FA 16:0
							269.2116			
							297.2429			
PG	[M-H+]	2-2.4	Iodinylated PG	903.422			126.9047	126.9045	1.58	Iodine adduct
							152.9955	152.9953	1.31	GP
							269.2115			
							295.2634	295.2643	-2.89	FA 19:1
PG	[M-H+]	2-2.4	Iodinylated PG	919.4531			126.9047	126.9045	1.58	Iodine adduct
							152.9955	152.9953	1.31	GP
							269.2115			
							295.2634	295.2643	-2.89	FA 19:1
PG	[M-H+]	2-2.4	Iodinylated PG	931.4535			126.9047	126.9045	1.58	Iodine adduct
							152.9955	152.9953	1.31	GP
							297.2430			
PG	[M-H+]	2-2.4	Iodinylated PG	1017.3195			126.9047	126.9045	1.58	Iodine adduct

							152.9955	152.9953	1.31	GP
							255.2324	255.2330	-2.17	FA 16:0
							761.4946			
PG	[M-H+]	2-2.4	Iodinylated PG	1033.3136			126.9047	126.9045	1.58	Iodine adduct
							152.9954	152.9953	0.65	GP
							269.2115			
							297.2430			
							777.4895			
Spot 3 - Δ*mprF1*Δ*mprF2*										
PG	[M-H+]	2-2.4	32:1	719.485	719.4869	-2.58	152.9955	152.9953	1.31	GP
							227.2013	227.2017	-1.56	FA 14:0
							253.2168	253.2173	-1.99	FA 16:1
							255.2325	255.2330	-1.78	FA 16:0
							281.2478	281.2486	-2.86	FA 18:1
PG	[M-H+]	2-2.4	32:0	721.5006	721.5025	-2.65	152.9954	152.9953	0.65	GP
							227.2012	227.2017	-2.00	FA 14:0
							255.2325	255.2330	-1.78	FA 16:0
							283.2634	283.2643	-3.01	FA 18:0
PG	[M-H+]	2-2.4	33:1	733.5006	733.5025	-2.60	152.9954	152.9953	0.65	GP
							227.2012	227.2017	-2.00	FA 14:0
							255.2325	255.2330	-1.78	FA 16:0
							295.2632	295.2643	-3.57	FA 19:1
PG	[M-H+]	2-2.4	34:1	747.5164	747.5182	-2.35	152.9955	152.9953	1.31	GP
							255.2326	255.2330	-1.39	FA 16:0
							281.2478	281.2486	-2.86	FA 18:1

PG	[M-H+]	2-2.4	34:0	749.5317	749.5338	-2.81	152.9955	152.9953	1.31	GP
							255.2325	255.2330	-1.78	FA 16:0
							283.2633	283.2643	-3.37	FA 18:0
PG	[M-H+]	2-2.4	35:2	759.516	759.5182	-2.84	152.9954	152.9953	0.65	GP
							253.2167	253.2173	-2.38	FA 16:1
							295.2633	295.2643	-3.23	FA 19:1
PG	[M-H+]	2-2.4	35:1	761.5313	761.5338	-3.29	152.9954	152.9953	0.65	GP
							255.2325	255.2330	-1.78	FA 16:0
							295.2634	295.2643	-2.89	FA 19:1
PG	[M-H+]	2-2.4	Iodinylated PG	763.5372			126.9048	126.9045	2.36	Iodine adduct
							152.9954	152.9953	0.65	GP
							255.2325	255.2330	-1.78	FA 16:0
							296.2667			
PG	[M-H+]	2-2.4	Iodinylated PG	861.4565			126.9047	126.9045	1.58	Iodine adduct
							152.9954	152.9953	0.65	GP
PG	[M-H+]	2-2.4	Iodinylated PG	863.3916			126.9047	126.9045	1.58	Iodine adduct
							152.9955	152.9953	1.31	GP
							227.2012	227.2017	-2.00	FA 14:0
							255.2324	255.2330	-2.17	FA 16:0
							269.2115			
							297.2429			
PG	[M-H+]	2-2.4	Iodinylated PG	889.4073			126.9048	126.9045	2.36	Iodine adduct
							152.9955	152.9953	1.31	GP
							253.2167	253.2173	-2.38	FA 16:1
							269.2116			

					281.2478	281.2486	-2.86	FA 18:1
					297.2430			
PG	[M-H+]	2-2.4	Iodinylated PG	891.4228	126.9047	126.9045	1.58	Iodine adduct
					152.9955	152.9953	1.31	GP
					255.2324	255.2330	-2.17	FA 16:0
					297.2430			
PG	[M-H+]	2-2.4	Iodinylated PG	893.429	126.9047	126.9045	1.58	Iodine adduct
					152.9955	152.9953	1.31	GP
					255.2324	255.2330	-2.17	FA 16:0
					297.2429			
PG	[M-H+]	2-2.4	Iodinylated PG	903.4224	126.9047	126.9045	1.58	Iodine adduct
					152.9955	152.9953	1.31	GP
					269.2115			
					295.2633	295.2643	-3.23	FA 19:1
PG	[M-H+]	2-2.4	Iodinylated PG	917.4383	126.9047	126.9045	1.58	Iodine adduct
					152.9955	152.9953	1.31	GP
					281.2478	281.2486	-2.86	FA 18:1
					297.2431			
PG	[M-H+]	2-2.4	Iodinylated PG	919.452	126.9047	126.9045	1.58	Iodine adduct
					255.2324	255.2330	-2.17	FA 16:0
					283.2634	283.2643	-3.01	FA 18:0
					297.2429			
PG	[M-H+]	2-2.4	Iodinylated PG	931.4538	126.9047	126.9045	1.58	Iodine adduct
					152.9955	152.9953	1.31	GP
					297.2429			

PG	[M-H+]	2-2.4	Iodinylated PG	1033.3136			126.9047	126.9045	1.58	Iodine adduct
							152.9955	152.9953	1.31	GP
							269.2115			
							297.2429			
PG	[M-H+]	2-2.4	Iodinylated PG	1061.3448			126.9048	126.9045	2.36	Iodine adduct
							152.9956	152.9953	1.96	GP
							297.2431			
Spot 4 - WT										
Lys-PG	[M-H+]	4.2-4.6	30:0	821.5641	821.5656	-1.83	not fragmented			
Lys-PG	[M-H+]	4.2-4.6	32:1	847.5794	847.5813	-2.24	not fragmented			
Lys-PG	[M-H+]	4.2-4.6	32:0	849.5949	849.5969	-2.35	145.0980	145.0977	2.07	lysine
							227.2012	227.2017	-2.00	FA 14:0
							255.2324	255.2330	-2.17	FA 16:0
							283.2634	283.2643	-3.01	FA 18:0
unknown	[M-H+]	4.2-4.6	unknown	851.6012			not fragmented			
Lys-PG	[M-H+]	4.2-4.6	33:1	861.595	861.5969	-2.21	not fragmented			
unknown	[M-H+]	4.2-4.6	unknown	863.6016			not fragmented			
Lys-PG	[M-H+]	4.2-4.6	34:1	875.6017	875.6126	-12.45	145.0979	145.0977	1.38	lysine
							255.2324	255.2330	-2.17	FA 16:0
							281.2478	281.2486	-2.86	FA 18:1
Lys-PG	[M-H+]	4.2-4.6	34:0	877.6265	877.6282	-1.94	145.0979	145.0977	1.38	lysine
							255.2324	255.2330	-2.17	FA 16:0
							283.2639	283.2643	-1.25	FA 18:0
unknown	[M-H+]	4.2-4.6	unknown	879.6327			not fragmented			
Lys-PG	[M-H+]	4.2-4.6	35:2	887.6106	887.6126	-2.25	not fragmented			

Lys-PG	[M-H+]	4.2-4.6	35:1	889.626	889.6282	-2.47	145.0979	145.0977	1.38	lysine
							255.2324	255.2330	-2.17	FA 16:0
							295.2636	295.2643	-2.21	FA 19:1
Lys-PG	[M-H+]	4.2-4.6	35:0	891.6323	891.6439	-13.01	145.0980	145.0977	2.07	lysine
							255.2325	255.2330	-1.78	FA 16:0
							297.2423			
Lys-PG	[M-H+]	4.2-4.6	36:2	901.626	901.6282	-2.44	not fragmented			
Lys-PG	[M-H+]	4.2-4.6	36:1	903.6422	903.6439	-1.88	not fragmented			
Lys-PG	[M-H+]	4.2-4.6	36:0	905.6565	905.6595	-3.31	not fragmented			
Lys-PG	[M-H+]	4.2-4.6	37:2	915.6418	915.6439	-2.29	not fragmented			
Lys-PG	[M-H+]	4.2-4.6	37:1	917.6569	917.6595	-2.83	not fragmented			
unknown	[M-H+]	4.2-4.6	unknown	919.6367			not fragmented			
Lys-PG	[M-H+]	4.2-4.6	Iodinylated Lys-PG	991.4863			126.9047	126.9045	1.58	Iodine adduct
							145.0980	145.0977	2.07	lysine
							227.2012	227.2017	-2.00	FA 14:0
Lys-PG	[M-H+]	4.2-4.6	Iodinylated Lys-PG	1019.5176			126.9047	126.9045	1.58	Iodine adduct
							145.0979	145.0977	1.38	lysine
							255.2324	255.2330	-2.17	FA 16:0
							297.2429			
Lys-PG	[M-H+]	4.2-4.6	Iodinylated Lys-PG	1047.5486			126.9047	126.9045	1.58	Iodine adduct
							145.0980	145.0977	2.07	lysine
							173.0928			
							255.2325	255.2330	-1.78	FA 16:0
							297.2432			

Spot 4 - Δ*mprF1*Δ*mprF2*										
No spot available										
Spot 5 - WT										
No spot available										
Spot 5 - Δ*mprF1*Δ*mprF2*										
D-ala-GPDGDAG	[M-H+]	3.0-3.5	unknown	1142.6511	1142.6609	-8.59	88.0399	88.0399	0.27	Alanine
							152.9955	152.9953	1.31	GP
Spot 6 - WT										
GPDGDAG	[M-H+]	3.0-3.5	30:0	1017.5748	1017.5769	-2.06	not fragmented			
GPDGDAG	[M-H+]	3.0-3.5	32:1	1043.5905	1043.5925	-1.92	not fragmented			
GPDGDAG	[M-H+]	3.0-3.5	32:0	1045.606	1045.6082	-2.10	152.9955	152.9953	1.31	GP
							171.0061			
							315.0482	315.0488	-1.90	Glucosyldiacylglycerol
GPDGDAG	[M-H+]	3.0-3.5	34:1	1071.6216	1071.6238	-2.05	152.9954	152.9953	0.65	GP
							171.0057			
							315.0481	315.0488	-2.22	Glucosyldiacylglycerol
GPDGDAG	[M-H+]	3.0-3.5	34:0	1073.6368	1073.6395	-2.51	152.9955	152.9953	1.31	GP
							315.0482	315.0488	-1.90	Glucosyldiacylglycerol
GPDGDAG	[M-H+]	3.0-3.5	35:1	1085.6373	1085.6395	-2.03	152.9954	152.9953	0.65	GP
							315.0483	315.0488	-1.59	Glucosyldiacylglycerol
Spot 6 - Δ*mprF1*Δ*mprF2*										
GPDGDAG	[M-H+]	3.0-3.5	30:0	1017.5756	1017.5769	-1.28	not fragmented			
GPDGDAG	[M-H+]	3.0-3.5	32:1	1043.5913	1043.5925	-1.15	not fragmented			
GPDGDAG	[M-H+]	3.0-3.5	32:0	1045.6065	1045.6082	-1.63	152.9955	152.9953	1.31	GP

							171.0060			
							315.0482	315.0488	-1.90	Glucosyldiacylglycerol
GPDGDAG	[M-H+]	3.0-3.5	33:1	1057.6065	1057.6082	-1.61	not fragmented			
GPDGDAG	[M-H+]	3.0-3.5	34:2	1069.6076	1069.6082	-0.56	not fragmented			
GPDGDAG	[M-H+]	3.0-3.5	34:1	1071.6222	1071.6238	-1.49	152.9955	152.9953	1.31	GP
							171.0061			
							315.0481	315.0488	-2.22	Glucosyldiacylglycerol
GPDGDAG	[M-H+]	3.0-3.5	34:0	1073.6363	1073.6395	-2.98	152.9956	152.9953	1.96	GP
							315.0483	315.0488	-1.59	Glucosyldiacylglycerol
GPDGDAG	[M-H+]	3.0-3.5	35:2	1083.6224	1083.6238	-1.29	not fragmented			
GPDGDAG	[M-H+]	3.0-3.5	35:1	1085.6377	1085.6395	-1.66	152.9955	152.9953	1.31	GP
							315.0483	315.0488	-1.59	Glucosyldiacylglycerol
GPDGDAG	[M-H+]	3.0-3.5	36:2	1097.6379	1097.6395	-1.46	not fragmented			
GPDGDAG	[M-H+]	3.0-3.5	36:1	1099.6522	1099.6551	-2.64	not fragmented			
GPDGDAG	[M-H+]	3.0-3.5	37:2	1111.6532	1111.6551	-1.71	not fragmented			

Identities of the peaks of the observed precursor ion and product ion masses are also shown. GP refers to glycerophosphate, and FA refers to fatty acid.

Table S2.4 - RNAseq Results (Δ*mprF1*Δ*mprF2* vs WT)						
Locus Tag	**Log_2 FC**	**Log CPM**	**PValue**	**FDR**	**Gene**	**Annotation**
OG1RF_10760	-13.07	6.83	4.08E-62	1.05E-58	*mprF2*	lysyl-tRNA synthetase
OG1RF_10101	6.95	10.42	3.91E-55	5.07E-52	*arcC*	carbamate kinase
OG1RF_10100	7.37	11.43	4.31E-48	3.72E-45	*arcB*	ornithine carbamoyltransferase
OG1RF_10102	6.38	9.53	4.25E-47	2.75E-44	*ntcA*	global nitrogen regulator NtcA
OG1RF_10099	6.80	11.65	7.57E-41	3.92E-38	*arcA*	arginine deiminase
OG1RF_10103	5.94	9.87	2.38E-38	1.03E-35	-	UIT3 family protein
OG1RF_10098	3.72	6.20	4.62E-17	1.71E-14	*argR*	arginine repressor
OG1RF_10017	2.34	10.12	2.99E-15	9.68E-13	*levR*	transcriptional regulatory protein LevR
OG1RF_10073	2.34	7.40	8.64E-13	2.48E-10	-	transglycosylase associated protein
OG1RF_11922	-2.60	6.73	1.43E-12	3.71E-10	-	M protein trans-acting positive regulator
OG1RF_10068	2.20	9.27	5.97E-12	1.40E-09	*fabG*	3-oxoacyl-ACP reductase
OG1RF_10072	2.22	8.91	1.34E-11	2.89E-09	-	stress response regulator Gls24
OG1RF_10069	2.20	9.12	1.75E-11	3.48E-09	-	hypothetical protein
OG1RF_11923	-2.60	6.00	2.37E-10	4.38E-08	-	hypothetical protein
OG1RF_10181	-2.29	5.49	2.92E-10	5.04E-08	-	M20D family peptidase
OG1RF_10071	2.22	9.16	4.25E-10	6.88E-08	-	stress response regulator Gls24
OG1RF_10070	2.14	7.00	1.23E-09	1.87E-07	-	hypothetical protein
OG1RF_12256	-2.12	7.13	1.87E-09	2.70E-07	*mutS2*	DNA mismatch repair protein MutS2
OG1RF_10029	-2.84	3.88	2.10E-09	2.86E-07	*mprF1*	hypothetical protein
OG1RF_10752	2.78	8.41	3.96E-09	5.13E-07	-	PTS family lactose/cellobiose (lac) porter component IIC
OG1RF_11797	-2.74	4.60	4.99E-09	6.15E-07	*pbuX*	xanthine permease
OG1RF_11798	-3.11	3.67	1.60E-08	1.88E-06	*xpt*	xanthine phosphoribosyltransferase
OG1RF_10753	2.68	6.21	2.12E-08	2.39E-06	*bglA2*	6-phospho-beta-glucosidase
OG1RF_10451	2.12	3.74	4.47E-08	4.60E-06	-	hypothetical protein
OG1RF_12425	1.72	9.12	4.52E-08	4.60E-06	*trePP*	glycosyl hydrolase
OG1RF_11753	2.34	6.05	4.62E-08	4.60E-06	*treB*	PTS family trehalose porter, IIBC component
OG1RF_11156	2.25	8.05	5.16E-08	4.85E-06	-	hypothetical protein
OG1RF_12255	-2.03	6.30	5.25E-08	4.85E-06	*phoB*	alkaline phosphatase
OG1RF_10857	2.32	3.52	8.63E-08	7.70E-06	-	GNAT family acetyltransferase
OG1RF_11927	-1.97	6.37	1.53E-07	1.32E-05	*azlC*	LIV-E family branched chain amino acid exporter AzlC
OG1RF_12456	1.81	8.12	1.61E-07	1.33E-05	-	WxL domain surface protein
OG1RF_11519	2.49	4.87	1.64E-07	1.33E-05	*gspA1*	general stress protein A
OG1RF_10022	-2.16	7.04	1.83E-07	1.43E-05	-	hypothetical protein
OG1RF_10552	2.58	9.42	4.06E-07	3.09E-05	*rplY*	50S ribosomal protein L25
OG1RF_12453	1.95	6.54	7.74E-07	5.72E-05	-	WxL domain surface protein
OG1RF_12452	1.86	6.77	1.12E-06	8.07E-05	*ubiD*	UbiD family decarboxylase
OG1RF_10856	2.25	5.44	1.24E-06	8.65E-05	-	streptomycin 3"-adenylyltransferase
OG1RF_12421	-2.75	3.45	1.68E-06	1.13E-04	-	S-layer protein
OG1RF_12031	-2.28	6.01	1.70E-06	1.13E-04	-	integral membrane protein
OG1RF_11442	-1.67	7.87	2.27E-06	1.47E-04	*mdlB*	multidrug ABC superfamily ATP binding cassette transporter, ABC protein
OG1RF_12084	-1.57	9.02	2.83E-06	1.79E-04	-	ABC superfamily ATP binding cassette transporter, ABC protein
OG1RF_12422	-2.84	2.10	3.23E-06	1.99E-04	-	S-layer protein
OG1RF_11497	-3.33	1.73	3.95E-06	2.38E-04	*purC*	phosphoribosylaminoimidazolesuccinocarboxamide synthase
OG1RF_10754	1.38	6.90	4.13E-06	2.43E-04	-	GNAT family acetyltransferase

OG1RF_10018	-2.24	9.15	4.36E-06	2.47E-04	*manX*	PTS family mannose/fructose/sorbose porter component IIB
OG1RF_10353	2.33	6.11	4.39E-06	2.47E-04	-	LemA family protein
OG1RF_10019	-2.29	10.70	4.54E-06	2.50E-04	*manX 2*	PTS system mannose transporter subunit IIAB
OG1RF_10021	-2.28	10.10	6.08E-06	3.28E-04	-	PTS system mannose/fructose/sorbose transporter subunit IID
OG1RF_11875	-1.80	4.33	6.94E-06	3.66E-04	-	acyl-CoA thioester hydrolase
OG1RF_10536	-2.00	4.01	7.37E-06	3.82E-04	-	hypothetical protein
OG1RF_10615	-1.94	5.82	7.64E-06	3.88E-04	-	group 2 glycosyl transferase
OG1RF_10180	-1.58	5.89	1.19E-05	5.85E-04	-	hypothetical protein
OG1RF_10614	-1.63	6.06	1.22E-05	5.85E-04	-	hypothetical protein
OG1RF_11615	3.22	1.60	1.22E-05	5.85E-04	*ulaB*	PTS family ascorbate porter, IIB component
OG1RF_10097	1.71	7.67	1.26E-05	5.89E-04	-	ArgR family transcriptional regulator
OG1RF_10551	1.94	5.38	1.27E-05	5.89E-04	-	hypothetical protein
OG1RF_11520	2.45	4.61	1.42E-05	6.35E-04	*gspA2*	general stress protein A
OG1RF_11682	-2.92	2.03	1.42E-05	6.35E-04	-	ABC superfamily ATP binding cassette transporter, binding protein
OG1RF_10020	-2.24	9.41	1.45E-05	6.35E-04	*manY*	PTS family mannose/fructose/sorbose porter component IIC
OG1RF_11443	-1.39	7.83	1.51E-05	6.52E-04	*mdlA*	multidrug ABC superfamily ATP binding cassette transporter, ABC protein
OG1RF_10616	-1.52	7.65	1.57E-05	6.68E-04	-	cellulose synthase catalytic subunit
OG1RF_11684	-2.85	1.79	2.01E-05	8.40E-04	-	ABC superfamily ATP binding cassette transporter, binding protein
OG1RF_10855	2.01	5.12	2.73E-05	1.11E-03	-	GNAT family acetyltransferase
OG1RF_12446	1.46	9.61	2.74E-05	1.11E-03	*dapE*	succinyl-diaminopimelate desuccinylase
OG1RF_11878	1.46	4.19	3.05E-05	1.21E-03	*comEC*	competence protein ComEC
OG1RF_11494	-2.38	2.85	3.54E-05	1.39E-03	*purL*	phosphoribosylformylglycinamidine synthase
OG1RF_11925	-1.29	6.85	3.64E-05	1.41E-03	-	hypothetical protein
OG1RF_12288	1.77	4.02	3.77E-05	1.44E-03	-	hypothetical protein
OG1RF_12302	-2.45	2.01	4.04E-05	1.48E-03	-	DAACS family dicarboxylate/amino acid:cation symporter
OG1RF_10457	-1.76	5.58	4.08E-05	1.48E-03	-	voltage-gated chloride channel family protein
OG1RF_11074	-1.52	5.47	4.09E-05	1.48E-03	*mgtA*	magnesium-importing ATPase
OG1RF_11928	-1.79	4.43	4.11E-05	1.48E-03	*azlD*	LIV-E family branched chain amino acid exporter AzlD
OG1RF_11201	-2.02	4.03	4.24E-05	1.50E-03	*msrA*	ABC superfamily ATP binding cassette transporter, ABC protein
OG1RF_11308	-1.67	5.02	4.50E-05	1.57E-03	-	N-acetyltransferase
OG1RF_12132	-1.92	3.24	4.62E-05	1.59E-03	*yniG*	EmrB/QacA family drug resistance transporter
OG1RF_10952	1.73	8.00	4.67E-05	1.59E-03	-	hypothetical protein
OG1RF_12184	-1.51	10.05	4.89E-05	1.64E-03	*fabG3*	3-oxoacyl-ACP reductase
OG1RF_11069	-1.93	3.74	5.03E-05	1.67E-03	-	putative transcriptional regulator
OG1RF_11493	-2.22	2.04	5.29E-05	1.73E-03	*purF*	amidophosphoribosyltransferase
OG1RF_11464	1.87	9.30	5.35E-05	1.73E-03	-	hypothetical protein
OG1RF_10627	1.92	10.71	5.68E-05	1.81E-03	*aad*	aldehyde-alcohol dehydrogenase
OG1RF_12480	-1.40	6.48	6.11E-05	1.93E-03	-	DEAH-box family ATP-dependent helicase
OG1RF_12484	-1.49	5.33	6.30E-05	1.97E-03	-	hypothetical protein

OG1RF_11979	-1.41	6.57	6.45E-05	1.99E-03	-	FMN-dependent NADH-azoreductase
OG1RF_10292	-1.59	4.37	7.05E-05	2.15E-03	*mtlA*	PTS family mannitol porter, EIICB component
OG1RF_10133	1.39	9.23	7.79E-05	2.34E-03	*deoB*	phosphopentomutase
OG1RF_10618	-1.64	4.68	7.92E-05	2.36E-03	-	hypothetical protein
OG1RF_11616	3.73	1.99	8.05E-05	2.37E-03	-	PTS system mannose/fructose/sorbose transporter subunit IIA
OG1RF_10617	-1.45	6.10	8.54E-05	2.48E-03	-	hypothetical protein
OG1RF_10761	-1.45	5.34	9.17E-05	2.64E-03	-	alpha/beta hydrolase fold family hydrolase
OG1RF_12098	1.50	7.99	9.30E-05	2.65E-03	-	gfo/Idh/MocA family oxidoreductase
OG1RF_12426	1.34	6.67	9.90E-05	2.79E-03	*yvdM*	beta-phosphoglucomutase
OG1RF_10882	-2.36	2.76	1.01E-04	2.80E-03	-	APC family amino acid-polyamine-organocation transporter
OG1RF_12185	-1.64	10.37	1.04E-04	2.85E-03	*fabD*	malonyl-CoA-[acyl-carrier-protein] transacylase
OG1RF_10293	-1.30	5.46	1.06E-04	2.88E-03	-	mannitol operon transcriptional antiterminator
OG1RF_10135	1.36	7.88	1.14E-04	3.08E-03	-	purine nucleoside phosphorylase
OG1RF_11254	1.77	3.61	1.20E-04	3.17E-03	-	outer surface protein
OG1RF_12557	-1.50	8.58	1.20E-04	3.17E-03	*trmE*	tRNA modification GTPase TrmE
OG1RF_11489	-1.84	3.24	1.21E-04	3.17E-03	*purD*	phosphoribosylamine--glycine ligase
OG1RF_11223	-1.81	2.80	1.23E-04	3.17E-03	-	hypothetical protein
OG1RF_12078	1.41	5.18	1.25E-04	3.20E-03	-	AraC family transcriptional regulator
OG1RF_10354	2.35	6.80	1.28E-04	3.24E-03	-	hypothetical protein
OG1RF_12454	1.72	6.43	1.30E-04	3.25E-03	*ubiD2*	UbiD family decarboxylase
OG1RF_12181	-1.22	9.12	1.37E-04	3.42E-03	*fabZ2*	(3R)-hydroxymyristoyl-ACP dehydratase
OG1RF_11498	-1.75	2.43	1.46E-04	3.60E-03	*purK*	phosphoribosylaminoimidazole carboxylase ATPase subunit PurK
OG1RF_11067	-1.92	2.78	1.53E-04	3.74E-03	-	PadR family transcriptional regulator
OG1RF_11926	-1.12	7.04	1.59E-04	3.85E-03	-	cro/CI family transcriptional regulator
OG1RF_12201	1.28	9.49	1.65E-04	3.96E-03	-	D-isomer specific 2-hydroxyacid dehydrogenase
OG1RF_11631	-1.77	5.76	1.67E-04	3.98E-03	-	putative phosphomethylpyrimidine kinase
OG1RF_10769	1.49	3.79	1.93E-04	4.55E-03	*ndk*	nucleoside diphosphate kinase
OG1RF_12294	-1.33	4.55	1.96E-04	4.58E-03	*pmr1*	P-ATPase superfamily P-type ATPase cation transporter
OG1RF_11146	1.29	8.24	2.00E-04	4.62E-03	*gldA*	glycerol dehydrogenase
OG1RF_11598	-1.78	3.27	2.15E-04	4.93E-03	*yedF*	PTS family porter component IIABC
OG1RF_11490	-1.79	3.27	2.21E-04	5.02E-03	*purH*	bifunctional purine biosynthesis protein PurH
OG1RF_11309	1.66	5.82	2.23E-04	5.02E-03	-	AraC family transcriptional regulator
OG1RF_10136	-2.50	6.30	2.25E-04	5.02E-03	-	iron (Fe3+) ABC superfamily ATP binding cassette transporter, binding protein
OG1RF_12129	-1.98	6.79	2.27E-04	5.02E-03	-	ABC superfamily ATP binding cassette transporter, ABC protein
OG1RF_12183	-1.33	10.71	2.29E-04	5.02E-03	*fabF2*	beta-ketoacyl-acyl-carrier-protein synthase II
OG1RF_11311	-1.52	3.96	2.40E-04	5.23E-03	-	ABC superfamily ATP binding cassette transporter, ABC/membrane protein

OG1RF_10496	-1.26	11.69	2.48E-04	5.34E-03	*glnP*	amino acid ABC superfamily ATP binding cassette transporter, binding/permease protein
OG1RF_12305	1.30	8.41	2.66E-04	5.68E-03	*htrA*	serine protease HtrA
OG1RF_12556	-1.32	9.50	2.91E-04	6.17E-03	*gidA*	tRNA uridine 5-carboxymethylaminomethyl modification protein GidA
OG1RF_12284	-1.70	3.65	3.13E-04	6.60E-03	-	sulfate transporter/STAS domain protein
OG1RF_11346	-1.15	6.77	3.24E-04	6.76E-03	-	sensor histidine kinase
OG1RF_10983	1.50	10.08	3.42E-04	7.08E-03	*npr*	NADH peroxidase
OG1RF_10765	1.07	7.87	3.67E-04	7.55E-03	*drrC*	daunorubicin resistance protein
OG1RF_11390	1.30	7.83	3.72E-04	7.56E-03	-	putative lipoprotein
OG1RF_10613	-1.18	6.23	3.74E-04	7.56E-03	-	hypothetical protein
OG1RF_10307	-1.08	6.49	3.84E-04	7.67E-03	*lmrB*	MFS family lincomycin resistance protein LmrB
OG1RF_10148	-1.45	4.64	3.86E-04	7.67E-03	*thiD*	phosphomethylpyrimidine kinase
OG1RF_12242	3.15	5.01	3.93E-04	7.77E-03	-	DMT superfamily drug/metabolite transporter
OG1RF_11720	-1.31	5.78	3.99E-04	7.82E-03	-	group 2 glycosyl transferase
OG1RF_12186	-1.64	10.34	4.17E-04	8.11E-03	*fabK*	enoyl-ACP reductase
OG1RF_11523	-1.80	4.50	4.47E-04	8.63E-03	-	LysR family transcriptional regulator
OG1RF_10858	-1.78	3.17	4.60E-04	8.82E-03	-	MFS family major facilitator transporter
OG1RF_10134	1.31	8.69	4.91E-04	9.13E-03	*deoD*	purine-nucleoside phosphorylase
OG1RF_10358	-1.38	7.98	4.92E-04	9.13E-03	*nrdH*	glutaredoxin
OG1RF_10603	1.05	8.86	4.93E-04	9.13E-03	*copB*	P-ATPase superfamily P-type ATPase copper (Cu) transporter
OG1RF_12501	-2.61	1.58	4.93E-04	9.13E-03	-	hypothetical protein
OG1RF_12128	-1.97	5.17	4.94E-04	9.13E-03	-	cobalt transporter
OG1RF_11907	1.19	9.12	5.17E-04	9.48E-03	-	penicillin-binding protein 4
OG1RF_12138	-2.47	2.32	5.26E-04	9.57E-03	*thiW*	ThiW protein
OG1RF_11908	1.13	8.70	5.32E-04	9.57E-03	-	hypothetical protein
OG1RF_11432	-2.00	3.16	5.33E-04	9.57E-03	*upp*	uracil phosphoribosyltransferase
OG1RF_10685	-1.59	3.01	5.52E-04	9.86E-03	*rgfB*	endonuclease/exonuclease/ phosphatase family protein RgfB
OG1RF_10357	-1.45	7.29	5.86E-04	1.04E-02	*nrdI*	ribonucleotide-diphosphate reductase subunit gamma
OG1RF_11629	-1.71	5.01	5.92E-04	1.04E-02	*ywlG*	hypothetical protein
OG1RF_12481	1.58	7.43	5.98E-04	1.05E-02	-	choline binding protein
OG1RF_12066	1.46	8.19	6.87E-04	1.19E-02	-	hypothetical protein
OG1RF_12182	-1.35	9.73	6.90E-04	1.19E-02	*accB*	acetyl-CoA carboxylase biotin carboxyl carrier subunit
OG1RF_10495	-1.02	9.77	7.05E-04	1.21E-02	-	ABC superfamily ATP binding cassette transporter, ABC protein
OG1RF_11430	-1.54	5.15	7.09E-04	1.21E-02	*pyrB*	aspartate carbamoyltransferase
OG1RF_10994	-2.17	3.27	7.20E-04	1.22E-02	*ade*	adenine deaminase
OG1RF_11880	2.35	0.81	7.34E-04	1.23E-02	*comEA*	competence protein comEA
OG1RF_12127	-1.96	5.53	7.68E-04	1.28E-02	*tenA*	thiaminase
OG1RF_12455	1.64	4.44	7.79E-04	1.29E-02	-	hypothetical protein
OG1RF_12276	1.10	7.60	7.96E-04	1.31E-02	-	hypothetical protein
OG1RF_11082	1.14	6.69	8.08E-04	1.32E-02	-	serine/threonine protein phosphatase
OG1RF_12130	-1.88	5.02	8.46E-04	1.38E-02	-	ABC superfamily ATP binding cassette transporter, membrane protein
OG1RF_12485	-1.18	10.99	8.64E-04	1.38E-02	*mdoB*	phosphatidylglycerol--membrane-oligosaccharide glycerophosphotransferase

OG1RF_11924	-1.13	9.67	8.65E-04	1.38E-02	-	cell wall surface anchor family protein
OG1RF_10520	-1.46	2.94	8.71E-04	1.38E-02	-	TetR family transcriptional regulator
OG1RF_12180	-1.11	11.70	8.84E-04	1.39E-02	*accC*	acetyl-CoA carboxylase subunit A
OG1RF_10991	-3.03	0.76	9.35E-04	1.47E-02	-	spermidine/putrescine ABC superfamily ATP binding cassette transporter, permease protein
OG1RF_10497	1.13	9.11	9.63E-04	1.50E-02	*uvrB*	excision endonuclease subunit UvrB
OG1RF_10490	-1.54	6.14	9.67E-04	1.50E-02	-	cell wall surface anchor family protein
OG1RF_12134	-2.43	1.60	9.93E-04	1.53E-02	-	MarR family transcriptional regulator
OG1RF_10083	-1.83	3.20	1.00E-03	1.53E-02	-	M protein trans-acting positive regulator
OG1RF_10228	-1.05	7.86	1.00E-03	1.53E-02	*pyrDA*	dihydroorotate oxidase
OG1RF_10187	-1.41	3.92	1.02E-03	1.55E-02	*brnQ*	LIVCS family branched chain amino acid:cation symporter
OG1RF_10848	1.68	3.40	1.03E-03	1.55E-02	*galM*	galactose mutarotase
OG1RF_11643	1.73	7.59	1.04E-03	1.55E-02	-	universal stress protein
OG1RF_10651	1.03	6.78	1.04E-03	1.55E-02	-	hypothetical protein
OG1RF_12404	3.05	3.01	1.07E-03	1.57E-02	-	D-isomer specific 2-hydroxyacid dehydrogenase
OG1RF_11315	1.13	6.36	1.11E-03	1.61E-02	*phrB*	deoxyribodipyrimidine photolyase
OG1RF_11681	-1.33	3.27	1.12E-03	1.61E-02	*hipO2*	aminoacylase
OG1RF_12135	-2.29	2.66	1.12E-03	1.61E-02	*thiD2*	phosphomethylpyrimidine kinase
OG1RF_11426	-1.67	5.90	1.13E-03	1.61E-02	*pyrK*	dihydroorotate dehydrogenase electron transfer subunit
OG1RF_11326	-1.02	7.65	1.13E-03	1.61E-02	-	hypothetical protein
OG1RF_12451	1.29	6.43	1.14E-03	1.62E-02	-	cell wall surface anchor family protein
OG1RF_10291	1.37	5.04	1.16E-03	1.64E-02	-	HAD phosphatase superfamily protein
OG1RF_10030	-5.13	0.31	1.19E-03	1.67E-02	*mprF1*	ABC superfamily ATP binding cassette transporter permease subunit
OG1RF_11694	-1.26	7.44	1.19E-03	1.67E-02	-	ABC superfamily ATP binding cassette transporter, ABC protein
OG1RF_10294	-1.40	3.72	1.21E-03	1.68E-02	*mltF*	PTS family fructose/mannitol porter component IIA
OG1RF_11431	-1.58	5.32	1.22E-03	1.68E-02	*pyrP*	NCS family uracil:cation symporter
OG1RF_10781	-1.03	8.89	1.26E-03	1.74E-02	*rpmF*	50S ribosomal protein L32
OG1RF_10210	-1.08	8.69	1.29E-03	1.77E-02	*hslO*	chaperonin HslO
OG1RF_11147	1.15	6.79	1.33E-03	1.80E-02	-	glycerone kinase PTS family porter component IIA
OG1RF_10540	1.08	8.45	1.35E-03	1.82E-02	-	oligopeptide ABC superfamily ATP binding cassette transporter, binding protein
OG1RF_10659	1.13	3.36	1.39E-03	1.87E-02	-	hypothetical protein
OG1RF_10529	-1.24	6.78	1.41E-03	1.89E-02	-	radical SAM protein
OG1RF_10111	-1.58	1.73	1.45E-03	1.92E-02	-	ornithine cyclodeaminase/mu-crystallin family protein
OG1RF_11491	-2.08	1.78	1.50E-03	1.97E-02	*purN*	phosphoribosylglycinamide formyltransferase
OG1RF_12067	1.28	9.86	1.51E-03	1.97E-02	-	tellurite resistance protein
OG1RF_10431	1.73	2.47	1.52E-03	1.98E-02	*fruK*	1-phosphofructokinase
OG1RF_11261	-1.44	9.06	1.53E-03	1.98E-02	-	hypothetical protein
OG1RF_10673	1.37	5.77	1.56E-03	2.00E-02	-	hypothetical protein
OG1RF_12488	1.47	10.26	1.58E-03	2.02E-02	*dps*	DNA starvation/stationary phase protection protein Dps

OG1RF_11656	1.36	8.34	1.58E-03	2.02E-02	-	ABC superfamily ATP binding cassette transporter, permease protein
OG1RF_11012	-1.69	2.32	1.64E-03	2.08E-02	-	hypothetical protein
OG1RF_12179	-1.01	10.28	1.65E-03	2.08E-02	*accD*	acetyl-coA carboxylase carboxyl transferase subunit beta
OG1RF_12569	1.49	5.05	1.66E-03	2.09E-02	*gcdB*	glutaconyl-CoA decarboxylase
OG1RF_10380	-1.72	2.86	1.67E-03	2.09E-02	-	nitroreductase
OG1RF_10821	-5.20	0.26	1.71E-03	2.13E-02	-	hypothetical protein
OG1RF_10289	-1.11	4.32	1.77E-03	2.19E-02	-	MarR family transcriptional regulator
OG1RF_10995	-1.98	2.96	1.86E-03	2.28E-02	*mtaD*	putative S-adenosylhomocysteine deaminase
OG1RF_12547	1.65	6.90	1.87E-03	2.28E-02	*mycA*	myosin-cross-reactive antigen
OG1RF_10476	-1.48	5.09	1.88E-03	2.28E-02	-	hypothetical protein
OG1RF_11071	-2.12	2.85	1.89E-03	2.28E-02	-	FtsW/RodA/SpovE family cell division protein
OG1RF_11428	-1.55	6.26	1.90E-03	2.28E-02	*carA*	carbamoyl-phosphate synthase small subunit
OG1RF_11693	-1.24	5.79	1.92E-03	2.30E-02	-	cobalt (Co2+) ABC superfamily ATP binding cassette transporter, membrane protein
OG1RF_11427	-1.44	8.60	1.93E-03	2.30E-02	*carB*	carbamoyl-phosphate synthase large subunit
OG1RF_11539	-1.15	4.84	1.97E-03	2.34E-02	-	membrane protein
OG1RF_11495	-2.96	1.00	1.98E-03	2.34E-02	*purL2*	phosphoribosylformylglycinamidine synthase
OG1RF_12523	-1.43	3.93	2.01E-03	2.36E-02	-	hydantoinase/oxoprolinase
OG1RF_10626	-1.16	6.27	2.05E-03	2.39E-02	-	hypothetical protein
OG1RF_11369	1.94	3.20	2.09E-03	2.43E-02	-	regulatory protein
OG1RF_11368	2.02	3.55	2.14E-03	2.47E-02	-	LysR family transcriptional regulator
OG1RF_10528	-1.19	6.10	2.16E-03	2.49E-02	-	rRNA methylase
OG1RF_10530	-1.35	5.57	2.25E-03	2.58E-02	*pap2?*	type 2 phosphatidic acid phosphatase
OG1RF_11429	-1.54	6.44	2.27E-03	2.59E-02	*pyrC*	dihydroorotase
OG1RF_10910	1.04	6.00	2.28E-03	2.59E-02	-	hypothetical protein
OG1RF_10672	-1.23	4.75	2.30E-03	2.60E-02	-	GNAT family acetyltransferase
OG1RF_11195	1.24	2.68	2.44E-03	2.72E-02	-	hypothetical protein
OG1RF_12407	-1.59	2.69	2.48E-03	2.75E-02	-	hypothetical protein
OG1RF_10543	-1.52	2.33	2.49E-03	2.75E-02	-	hypothetical protein
OG1RF_11743	1.14	7.39	2.60E-03	2.85E-02	-	TetR family transcriptional regulator
OG1RF_10585	-1.12	5.09	2.61E-03	2.86E-02	-	M protein trans-acting positive regulator
OG1RF_12238	-1.25	4.51	2.67E-03	2.90E-02	-	NCS2 family xanthine/uracil permease family protein
OG1RF_10334	-1.03	7.54	2.70E-03	2.91E-02	*menH*	putative 2-succinyl-6-hydroxy-2,4-cyclohexadiene-1-carboxylate synthase
OG1RF_11680	-1.13	5.36	2.71E-03	2.91E-02	-	ABC superfamily ATP binding cassette transporter, ABC protein
OG1RF_11045	-1.16	3.71	2.75E-03	2.95E-02	-	hypothetical protein
OG1RF_10107	1.42	5.56	2.86E-03	3.02E-02	-	family 20 glycosyl hydrolase
OG1RF_11614	2.28	1.57	2.88E-03	3.02E-02	-	PTS family mannose/fructose/sorbose porter component IIC
OG1RF_12487	-1.08	10.96	2.88E-03	3.02E-02	*rplM*	50S ribosomal protein L13
OG1RF_10898	-1.62	6.69	2.88E-03	3.02E-02	-	ABC superfamily ATP binding cassette transporter, ABC protein
OG1RF_11114	-1.62	2.44	3.07E-03	3.20E-02	-	hypothetical protein
OG1RF_12167	1.58	4.28	3.09E-03	3.20E-02	*endOF3*	mannosyl-glycoprotein endo-beta-N-acetylglucosaminidase

OG1RF_11672	-1.03	4.75	3.09E-03	3.20E-02	-	major facilitator family transporter
OG1RF_10719	1.05	7.22	3.11E-03	3.21E-02	-	cation transporter
OG1RF_11463	1.37	5.92	3.15E-03	3.24E-02	-	PspC domain-containing protein
OG1RF_10601	-1.49	5.38	3.17E-03	3.24E-02	-	potassium uptake protein
OG1RF_10762	1.12	6.64	3.20E-03	3.26E-02	-	hypothetical protein
OG1RF_10492	-1.37	5.29	3.22E-03	3.27E-02	-	M protein trans-acting positive regulator
OG1RF_10474	-2.58	3.93	3.25E-03	3.29E-02	-	NMN family nicotinamide monnucleotide uptake permease
OG1RF_12391	-1.17	7.01	3.28E-03	3.30E-02	*gmk2*	guanylate kinase
OG1RF_10296	1.93	5.43	3.40E-03	3.37E-02	*mtlA2*	PTS family mannitol porter, EIICB component
OG1RF_10698	1.26	2.26	3.41E-03	3.37E-02	-	hypothetical protein
OG1RF_11424	-1.30	5.32	3.41E-03	3.37E-02	*pyrF*	orotidine-5'-phosphate decarboxylase
OG1RF_12050	-1.92	1.01	3.44E-03	3.39E-02	-	HAD-superfamily hydrolase
OG1RF_10763	1.09	7.37	3.57E-03	3.50E-02	-	endonuclease/exonuclease/ phosphatase
OG1RF_11425	-1.50	6.24	3.63E-03	3.54E-02	*pyrDB*	dihydroorotate oxidase
OG1RF_10090	1.28	6.41	3.70E-03	3.60E-02	-	putative lipoprotein
OG1RF_10764	1.04	6.21	3.76E-03	3.65E-02	-	phosphorylase
OG1RF_10648	-1.10	3.80	4.00E-03	3.85E-02	-	sulfate transporter
OG1RF_11096	-1.01	5.30	4.06E-03	3.89E-02	-	hypothetical protein
OG1RF_10491	-1.19	5.09	4.09E-03	3.90E-02	-	
OG1RF_10556	-1.32	4.66	4.15E-03	3.92E-02	*udk*	uridine kinase
OG1RF_10674	1.16	7.20	4.20E-03	3.93E-02	*ppx2*	exopolyphosphatase
OG1RF_11384	1.15	5.25	4.21E-03	3.93E-02	-	permease protein
OG1RF_11462	1.45	5.93	4.21E-03	3.93E-02	-	hypothetical protein
OG1RF_11230	-1.15	7.26	4.24E-03	3.94E-02	*sacT*	SacPA operon antiterminator
OG1RF_11231	-1.09	8.91	4.28E-03	3.95E-02	*ptsG*	PTS family glucose porter, IICBA component
OG1RF_10256	-1.19	5.65	4.42E-03	4.06E-02	-	HAD-superfamily hydrolase
OG1RF_10054	-1.31	3.86	4.48E-03	4.10E-02	*purR*	purine operon repressor
OG1RF_10656	-1.24	4.25	4.52E-03	4.12E-02	-	amino acid permease
OG1RF_10751	1.44	5.81	4.67E-03	4.21E-02	*lacF*	PTS family lactose/cellobiose porter component IIA
OG1RF_12512	-1.34	3.70	4.69E-03	4.21E-02	-	heptaprenyl diphosphate synthase component I
OG1RF_10355	-1.38	10.15	4.69E-03	4.21E-02	*nrdF*	ribonucleotide-diphosphate reductase subunit beta
OG1RF_10981	1.16	3.73	4.72E-03	4.21E-02	-	putative histidine kinase
OG1RF_10854	1.06	4.86	4.77E-03	4.24E-02	-	hypothetical protein
OG1RF_11135	2.15	6.08	4.94E-03	4.36E-02	-	sugar ABC superfamily ATP binding cassette transporter, sugar-binding protein
OG1RF_10223	-1.05	6.66	4.97E-03	4.37E-02	-	hypothetical protein
OG1RF_11741	-1.28	2.92	5.29E-03	4.62E-02	-	flavodoxin
OG1RF_12133	-1.44	2.29	5.49E-03	4.78E-02	-	major facilitator family transporter
OG1RF_10356	-1.27	11.46	5.53E-03	4.80E-02	*nrdE*	ribonucleotide-diphosphate reductase subunit alpha
OG1RF_12249	1.62	5.63	5.60E-03	4.84E-02	-	BglG family transcriptional antiterminator
OG1RF_12025	1.00	5.44	5.67E-03	4.89E-02	-	cro/CI family transcriptional regulator
OG1RF_11793	1.01	9.18	5.69E-03	4.89E-02	*clpB*	chaperone protein ClpB
OG1RF_12536	1.35	8.75	5.70E-03	4.89E-02	-	sensor histidine kinase

Results filtered by log_2FC >1, P-value<0.05, FDR<0.05.

Table S2.5 - Fatty acids present within BHI			
Fatty acid species	**Normalised Peak Area**		
	BHI #1	**BHI #2**	**BHI #3**
$C_{14:1\ \omega7\ cis}$	N.D.	N.D.	N.D.
$C_{14:1\ \omega5\ cis}$	N.D.	N.D.	N.D.
$C_{14:0}$	N.D.	N.D.	N.D.
$C_{15:0}$	N.D.	N.D.	N.D.
$C_{16:1\ \omega7\ cis}$	N.D.	N.D.	N.D.
$C_{16:1\ \omega7\ trans}$	N.D.	N.D.	N.D.
$C_{16:1\ \omega6\ cis}$	N.D.	N.D.	N.D.
$C_{16:0}$	66000.01	290020.4	78558.25
$C_{17:1\ \omega7\ cis}$	N.D.	N.D.	N.D.
$C_{17:1\ \omega7\ trans}$	N.D.	N.D.	N.D.
$C_{17:1\ \omega6\ cis}$	N.D.	N.D.	N.D.
$C_{17:0}$	N.D.	N.D.	N.D.
$C_{18:1\ \omega9\ cis}$	N.D.	N.D.	N.D.
$C_{18:1\ \omega7\ cis}$	N.D.	N.D.	N.D.
$C_{18:0}$	24739.47	109245.5	23707.07
$C_{18:1\ \omega7\ cis\ 11\text{-}methyl}$	N.D.	N.D.	N.D.
$C_{19:1\ ISO\ \omega8\ cis}$	N.D.	N.D.	N.D.
$C_{19:1\ ISO\ \omega5\ cis}$	N.D.	N.D.	N.D.
$C_{19:1\ ISO\ \omega4\ cis}$	N.D.	N.D.	N.D.
$C_{19:1\ \omega9\ cis}$	N.D.	N.D.	N.D.
$C_{19:1\ \omega9\ trans}$	N.D.	N.D.	N.D.
$C_{19:1\ \omega7\ cis}$	N.D.	N.D.	N.D.
$C_{19:1\ \omega7\ trans}$	N.D.	N.D.	N.D.
$C_{19:1\ \omega6\ cis}$	N.D.	N.D.	N.D.
$C_{19\ cyclo\ \omega7}$	N.D.	N.D.	N.D.
$C_{11\text{-}MeO\text{-}17:0}$	N.D.	N.D.	N.D.
$C_{20:1\ \omega7\ cis}$	N.D.	N.D.	N.D.
$C_{20:0}$	N.D.	N.D.	N.D.
$C_{22:1}$	N.D.	N.D.	N.D.

N.D. = not detected

Table S2.6 - Fatty acids detected in WT and Δ*mprF1*Δ*mprF2* grown in BHI or CDM				
Fatty acid Species	**% of total membrane fatty acid content**			
	BHI WT	**BHI Δ*mprF1* Δ*mprF2***	**CDM WT**	**CDM Δ*mprF1* Δ*mprF2***
$C_{14:1\ \omega7\ cis}$	0.25 ± 0.04	0.24 ± 0.03	0.31 ± 0.05	0.42 ± 0.07
$C_{14:1\ \omega5\ cis}$	N.D.	N.D.	N.D.	0.11 ± 0.06
$C_{14:0}$	3.17 ± 0.33	3.23 ± 0.55	1.99 ± 0.24	3.65 ± 0.17
$C_{15:0}$	0.07 ± 0.03	0.09 ± 0.03	0.03 ± 0.01	0.07 ± 0.01
$C_{16:1\ \omega7\ cis}$	2.73 ± 0.28	2.86 ± 0.59	3.25 ± 0.41	2.86 ± 1.34
$C_{16:1\ \omega7\ trans}$	0.63 ± 0.28	0.66 ± 0.33	1.5 ± 0.18	1.87 ± 0.24
$C_{16:1\ \omega6\ cis}$	0.05 ± 0.01	0.03 ± 0.01	N.D.	N.D.
$C_{16:0}$	52.55 ± 1.43	54.36 ± 1.92	50.8 ± 1.62	61.91 ± 2.76
$C_{17:1\ \omega7\ cis}$	0.49 ± 0.26	0.3 ± 0.16	0.76 ± 0.55	0.29 ± 0.32
$C_{17:1\ \omega7\ trans}$	N.D.	N.D.	N.D.	0.16 ± 0.25
$C_{17:1\ \omega6\ cis}$	0.16 ± 0.04	0.19 ± 0.05	0.05 ± 0.03	0.08 ± 0.08
$C_{17:0}$	0.07 ± 0.01	0.03 ± 0.01	0.02 ± 0	0.03 ± 0
$C_{18:1\ \omega9\ cis}$	0.27 ± 0.02	0.18 ± 0.04	N.D.	N.D.
$C_{18:1\ \omega7\ cis}$	28.39 ± 0.56	28.79 ± 0.74	34.31 ± 0.21	23.83 ± 0.75
$C_{18:0}$	4.65 ± 0.37	2.29 ± 0.46	1.16 ± 0.5	1.01 ± 0.12
$C_{18:1\ \omega7\ cis\ 11\text{-}methyl}$	0.34 ± 0.11	0.32 ± 0.07	0.29 ± 0.18	0.55 ± 0.2
$C_{19:1\ ISO\ \omega8\ cis}$	0.04 ± 0.02	0.04 ± 0.02	0.1 ± 0.08	0.16 ± 0.03
$C_{19:1\ ISO\ \omega5\ cis}$	0.04 ± 0.02	0.04 ± 0.01	0.08 ± 0.05	0.12 ± 0.02
$C_{19:1\ ISO\ \omega4\ cis}$	0.02 ± 0.01	0.02 ± 0.01	0.08 ± 0.02	0.09 ± 0.02
$C_{19:1\ \omega9\ cis}$	0.23 ± 0.06	0.23 ± 0.07	0.34 ± 0.21	0.42 ± 0.11
$C_{19:1\ \omega9\ trans}$	N.D.	N.D.	N.D.	0.11 ± 0.03
$C_{19:1\ \omega7\ cis}$	N.D.	N.D.	0.06 ± 0.02	0.08 ± 0.01
$C_{19:1\ \omega7\ trans}$	N.D.	N.D.	0.04 ± 0.01	0.05 ± 0.01
$C_{19:1\ \omega6\ cis}$	0.08 ± 0.03	0.08 ± 0.02	0.18 ± 0.14	0.32 ± 0.17
$C_{19\ cyclo\ \omega7}$	4.99 ± 0.46	4.97 ± 1.06	4.06 ± 0.92	1.5 ± 1.11
$C_{11\text{-}MeO\text{-}17:0}$	0.31 ± 0.11	0.32 ± 0.07	0.3 ± 0.08	0.16 ± 0.03
$C_{20:1\ \omega7\ cis}$	0.21 ± 0.02	0.11 ± 0.01	0.2 ± 0.02	0.07 ± 0.02
$C_{20:0}$	0.05 ± 0.01	0.02 ± 0.01	0.01 ± 0	0 ± 0
$C_{22:1}$*	0.07 ± 0.01	0.05 ± 0.01	0 ± 0	N.D.
Saturated Sum	60.55 ± 0.81	60 ± 1.1	54.01 ± 1.83	66.68 ± 2.57
Unsaturated Sum	38.91 ± 0.68	39.04 ± 1.42	45.61 ± 1.81	33.09 ± 2.48
Ratio (Sat/Unsat)	1.56 ± 0.05	1.54 ± 0.08	1.19 ± 0.09	2.03 ± 0.23

Data shows mean values from 5 biological replicates with standard deviation. N.D. = not detected. * peak area was too low to determine double bond position.

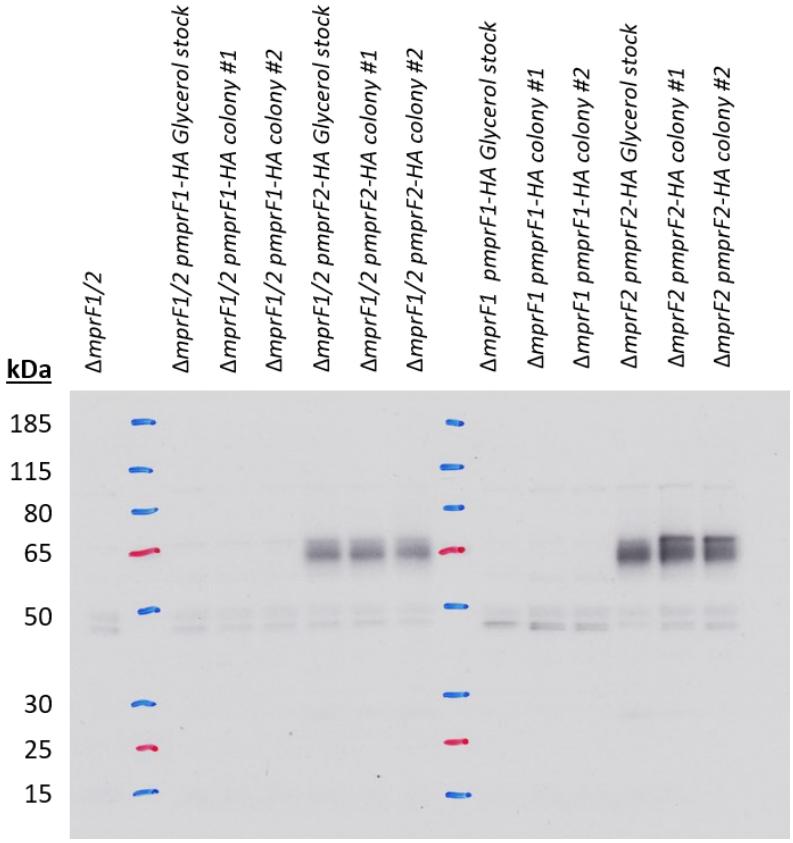

Figure S2.1. Anti-HA western immunoblot of *E. faecalis* strains containing p*mprF1-HA* and *pmprF2-HA*. Strains harbouring *pmprF2*-HA display expression while those harbouring *pmprF1*-HA do not. Δ*mprF1/2* refers to Δ*mprF1*Δ*mprF2*. Predicted protein size of MprF1 and MprF2 is ~96 kDa

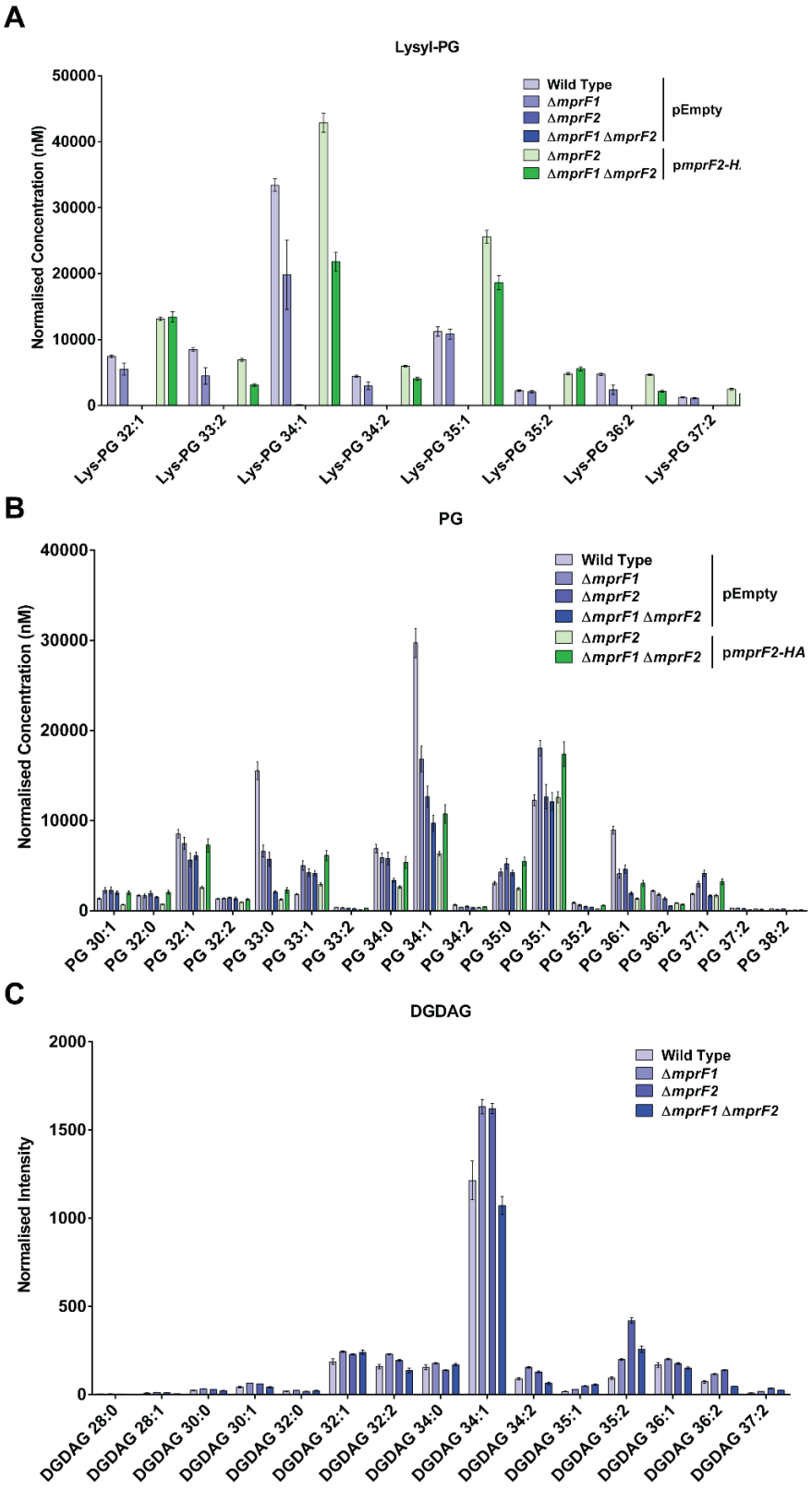

Figure. S2.2. Loss of *mprF* contributes to changes in individual species of Lysyl-PG, PG and DGDAG. Normalized quantities of **(A)** 8 native lysyl-PG species, **(B)** 18 native PG species and semi-quantitative analysis of **(C)** 15 native DGDAG species in the *mprF* mutants. Samples were normalised against internal standards and dry sample weight.

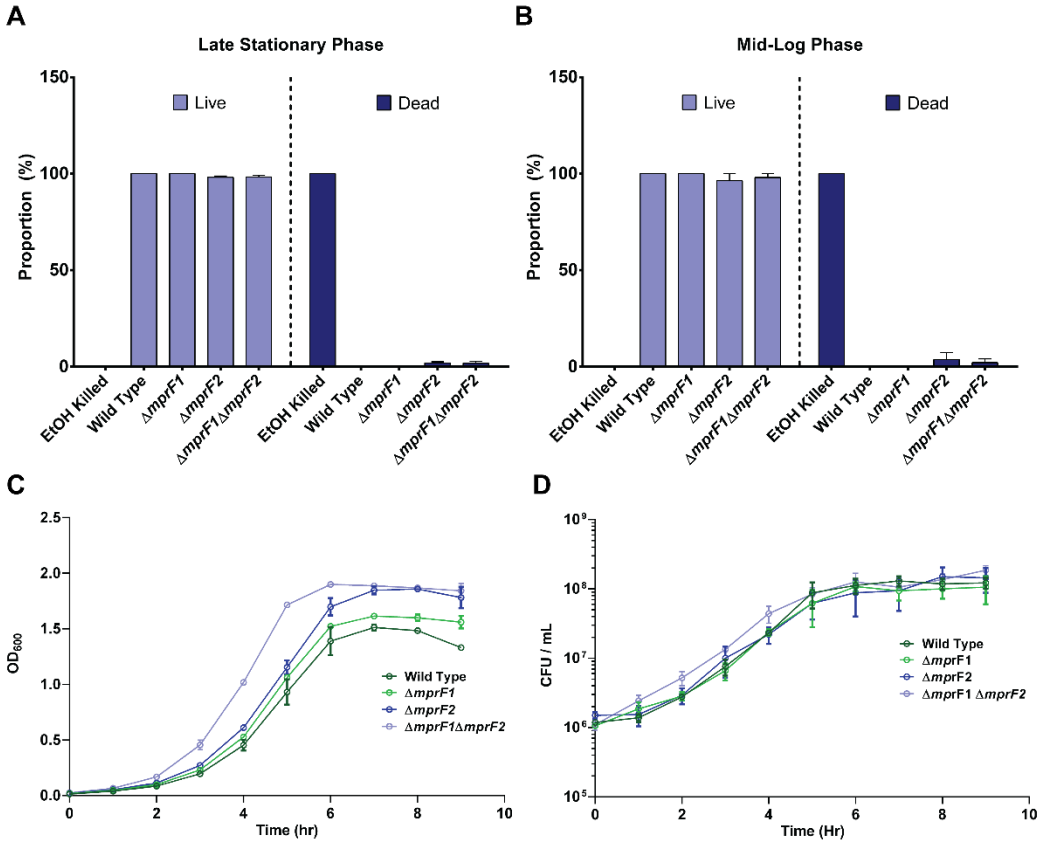

Figure. S2.3. *mprF* mutants display no difference in viability and membrane permeability to propidium iodide (PI). Live-dead staining of the wild type and *mprF* mutants in **(A)** late stationary and **(B)** mid-log phases. Microscopy of stained cells were carried out and percentage of live and dead cells were quantified. Error bars represent the standard error of mean from 2 biological replicates with at least 100 cells analysed per replicate. Not significant, $p>0.05$. **(C)** OD_{600} measurements and **(D)** CFU enumeration of the *mprF* mutants over time.

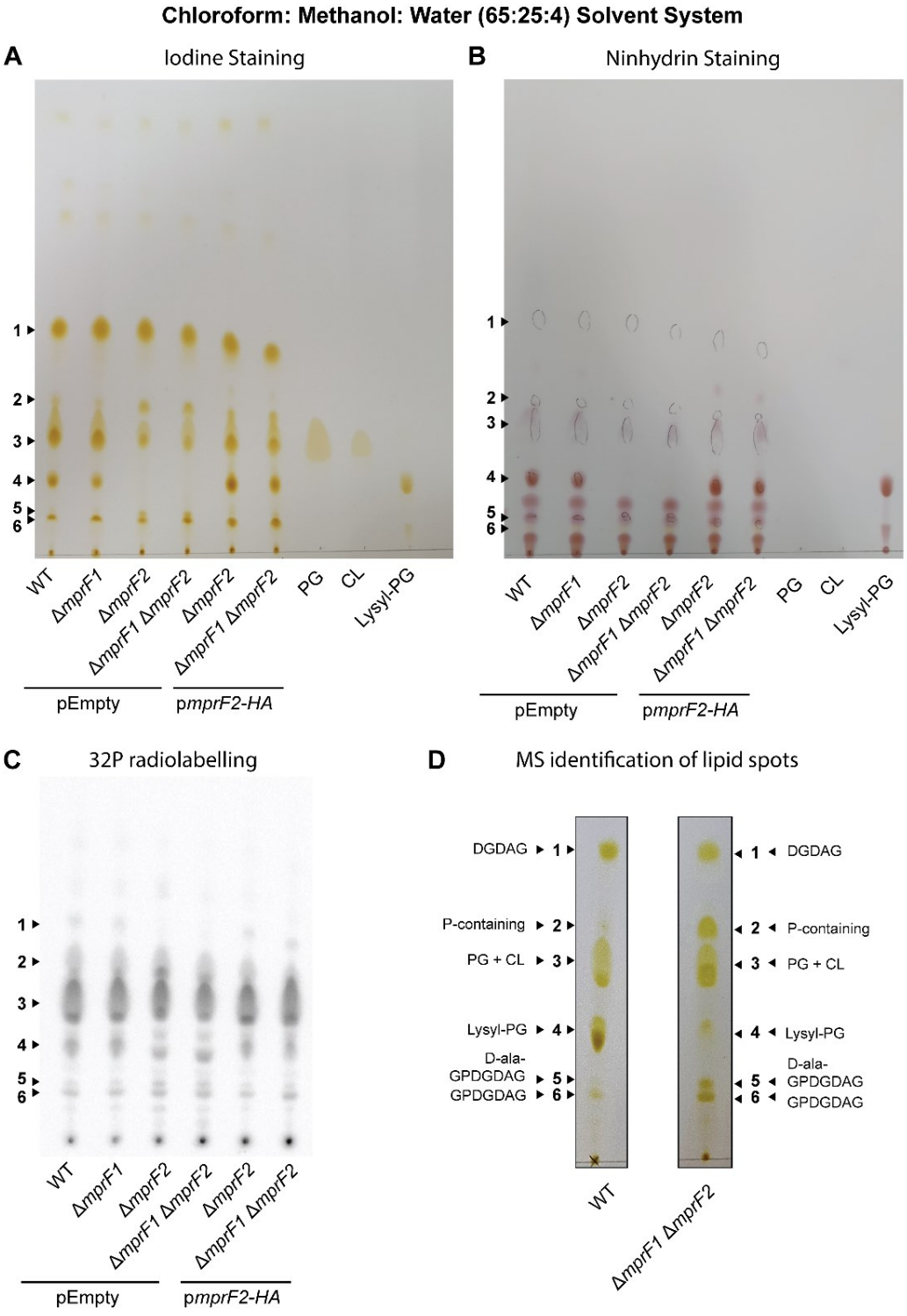
Chloroform: Methanol: Water (65:25:4) Solvent System
A
Iodine Staining
B
Ninhydrin Staining
1
2
3
4
5
6
WT
ΔmprF1
ΔmprF2
ΔmprF1 ΔmprF2
ΔmprF2
ΔmprF1 ΔmprF2
PG
CL
Lysyl-PG
pEmpty
pmprF2-HA
C
32P radiolabelling
D
MS identification of lipid spots
DGDAG
P-containing
PG + CL
Lysyl-PG
D-ala-GPDGDAG
GPDGDAG

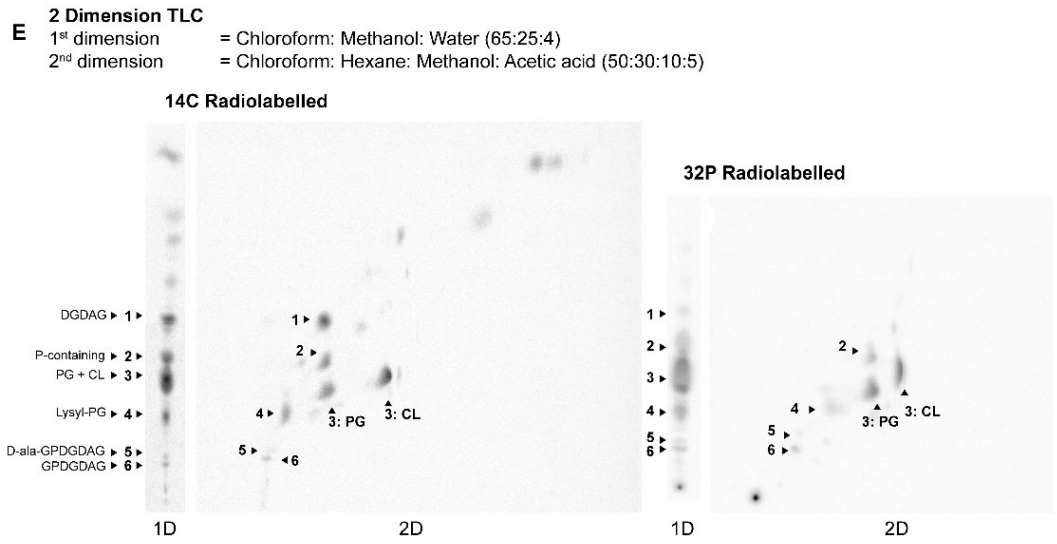

Figure. S2.4. Identification of lipid spots in 1D- and 2D-TLCs of lipid extracts from WT and the *mprF* mutants. (A) Iodine staining, **(B)** ninhydrin staining and **(C)** 32P radiolabelling staining of 1D-TLCs of empty vector controls of WT, Δ*mprF1*, Δ*mprF2*, Δ*mprF1*Δ*mprF2* and p*mprF2*-HA complemented Δ*mprF2*, Δ*mprF1*Δ*mprF2* together with PG, CL and lysyl-PG standards under chloroform: methanol: water (65:25:4) solvent system. Iodine stains most lipids while ninhydrin stains amino modified lipids. 6 major spots were observed. **(D)** These spots were scrapped off iodine strained TLC plates of WT and Δ*mprF1*Δ*mprF2* and placed through lipid extraction before analysis using LC-MS. Spots were identified and labelled accordingly. **(E)** 1D and 2-D TLCs of 14C and 32P labelled lipid extracts of wild type and Δ*mprF1*Δ*mprF2*. chloroform: methanol: water (65:25:4) solvent system was used in the first dimension while chloroform: hexane, methanol, acetic acid (50:30:10:5) was used in the second dimension. Comparing positions of the spots in the first and second dimension, we can resolve the positions of PG and CL. In the solvent system used in the second dimension, CL migrates ahead of PG.

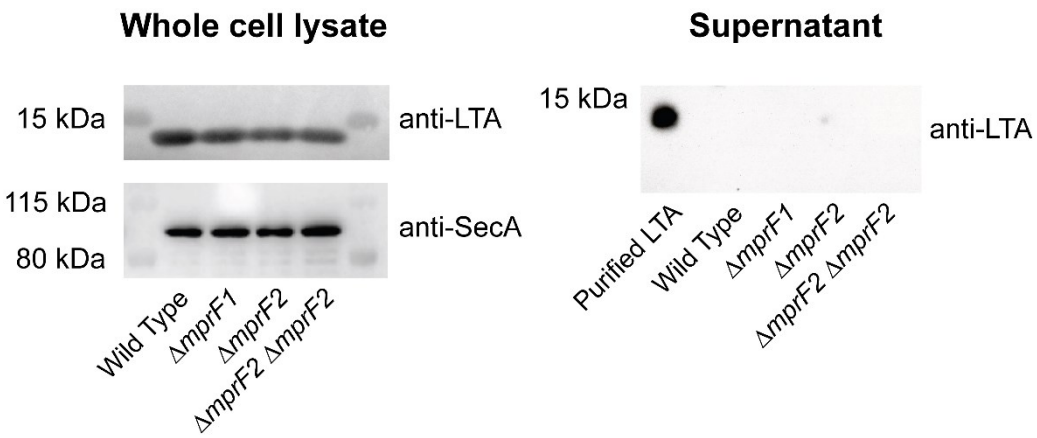

Figure. S2.5. *mprF* mutants do not display detectable differences in lipoteichoic acid (LTA) levels. Western immunoblots for LTA in whole cell lysates and supernatants using anti-polyglycerophosphate antibodies. SecA immunoblots were used as a loading control. No detectable levels of LTA were present in the supernatant of all samples.

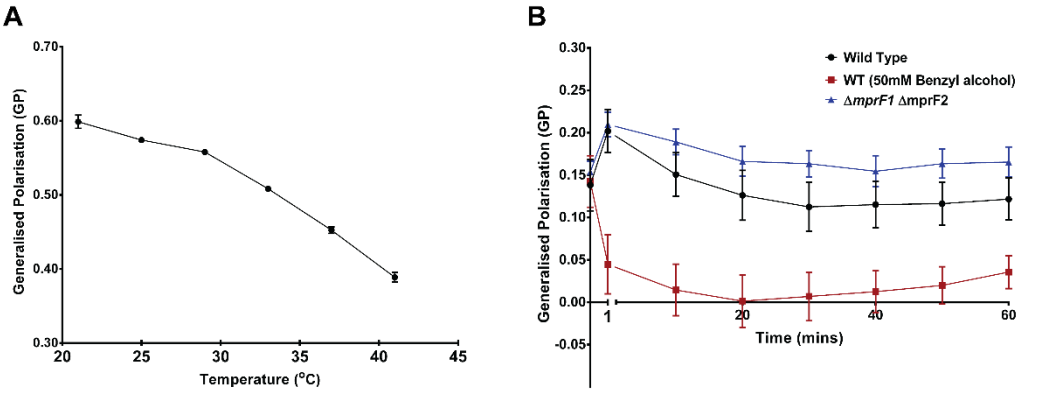

Figure. S2.6. Membrane fluidity measurements by Laurdan. Membrane fluidity measurements using Laurdan can detect for **(A)** changes in membrane fluidity in response to temperature and **(B)** in the presence of membrane fluidizer, benzyl alcohol. Benzyl alcohol was spiked in just after the initial reading at time, t = 0 minutes. Experiments are done in a microtiter plate set-up with measurements taken using a plate reader instead due to the technical constraints in the microscope set up in **figure 2.10A**. Each bar represents the mean ± standard error of measurement calculated from 3 biological replicates.

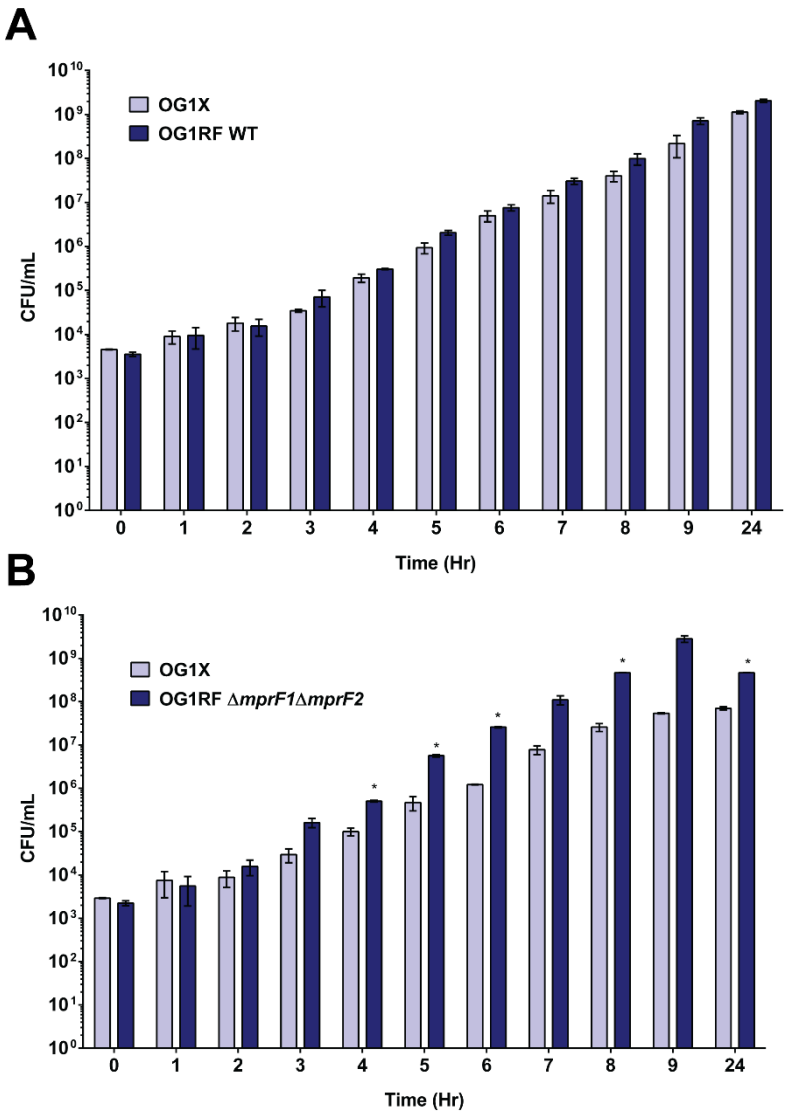

Figure. S2.7. *In vitro* competitive planktonic growth assay. Either **(A)** OG1RF WT or **(B)** OG1RF Δ*mprF1*Δ*mprF2* were co-cultured with OG1X at 10^8 CFU/mL of inoculum per strain in BHI and CFU of the strains were enumerated across 24 hours. Error bars represent the standard error of mean from 2 biological replicates. Statistical comparisons made for OG1RF Δ*mprF1*Δ*mprF2* against OG1X WT. Multiple t-tests. *, p=0.05 to 0.01.

A

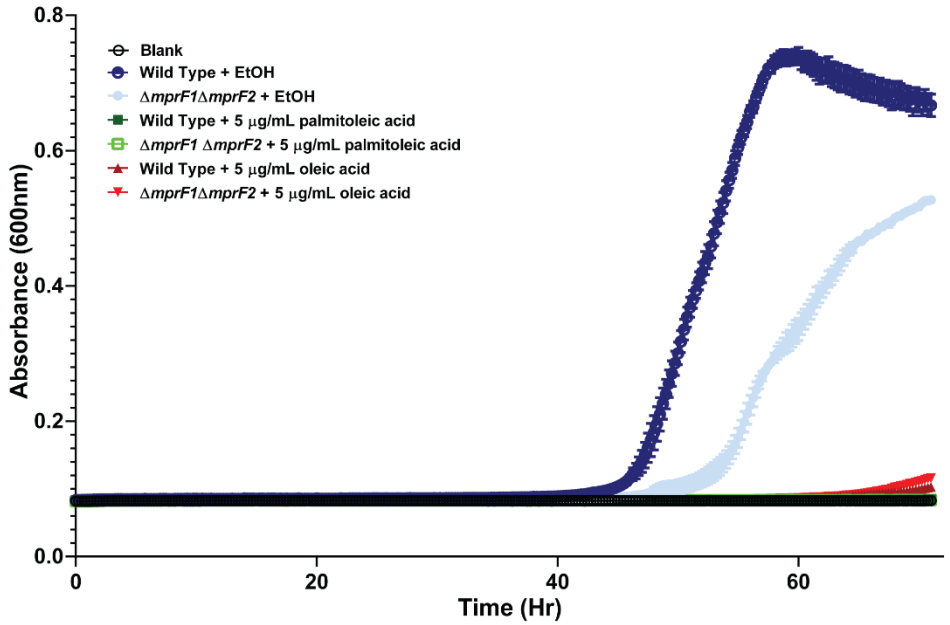
Unsaturated Fatty Acid Supplementation
Blank
Wild Type + EtOH
ΔmprF1ΔmprF2 + EtOH
Wild Type + 5 μg/mL palmitoleic acid
ΔmprF1 ΔmprF2 + 5 μg/mL palmitoleic acid
Wild Type + 5 μg/mL oleic acid
ΔmprF1ΔmprF2 + 5 μg/mL oleic acid
Absorbance (600nm)
0.0
0.2
0.4
0.6
0.8
0
20
40
60
Time (Hr)

B

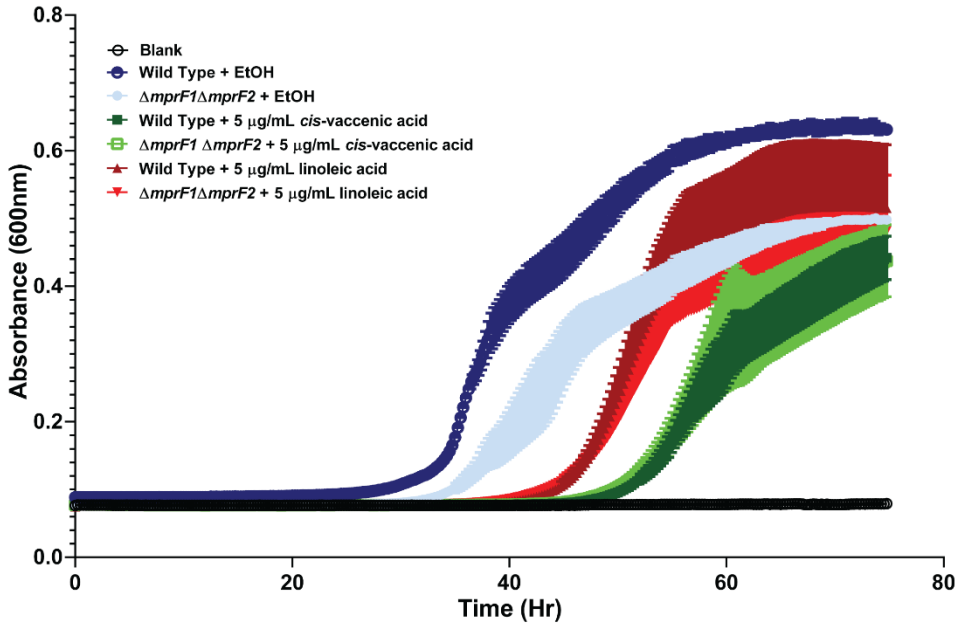
Unsaturated Fatty Acid Supplementation
Blank
Wild Type + EtOH
ΔmprF1ΔmprF2 + EtOH
Wild Type + 5 μg/mL cis-vaccenic acid
ΔmprF1 ΔmprF2 + 5 μg/mL cis-vaccenic acid
Wild Type + 5 μg/mL linoleic acid
ΔmprF1ΔmprF2 + 5 μg/mL linoleic acid
Absorbance (600nm)
0.0
0.2
0.4
0.6
0.8
0
20
40
60
80
Time (Hr)

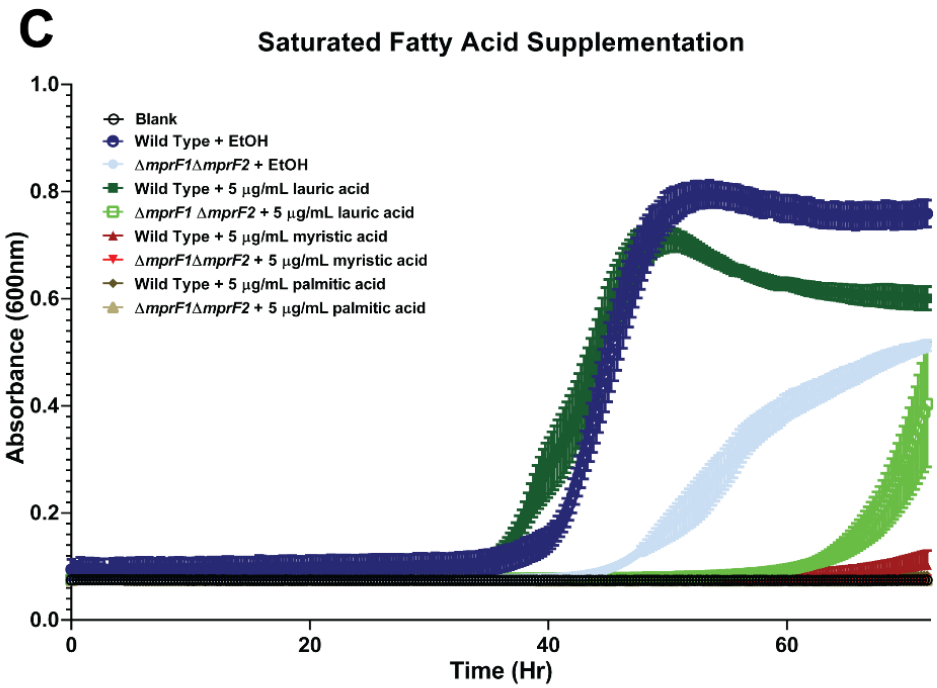
C
Saturated Fatty Acid Supplementation
Blank
Wild Type + EtOH
ΔmprF1ΔmprF2 + EtOH
Wild Type + 5 μg/mL lauric acid
ΔmprF1 ΔmprF2 + 5 μg/mL lauric acid
Wild Type + 5 μg/mL myristic acid
ΔmprF1ΔmprF2 + 5 μg/mL myristic acid
Wild Type + 5 μg/mL palmitic acid
ΔmprF1ΔmprF2 + 5 μg/mL palmitic acid
Absorbance (600nm)
Time (Hr)

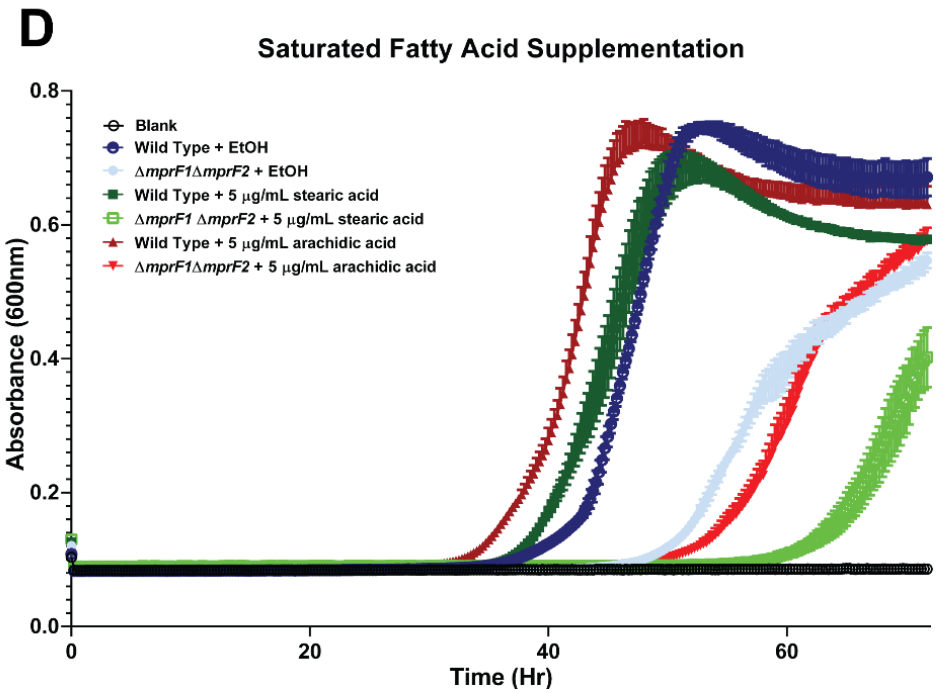
D
Saturated Fatty Acid Supplementation
Blank
Wild Type + EtOH
ΔmprF1ΔmprF2 + EtOH
Wild Type + 5 μg/mL stearic acid
ΔmprF1 ΔmprF2 + 5 μg/mL stearic acid
Wild Type + 5 μg/mL arachidic acid
ΔmprF1ΔmprF2 + 5 μg/mL arachidic acid
Absorbance (600nm)
Time (Hr)

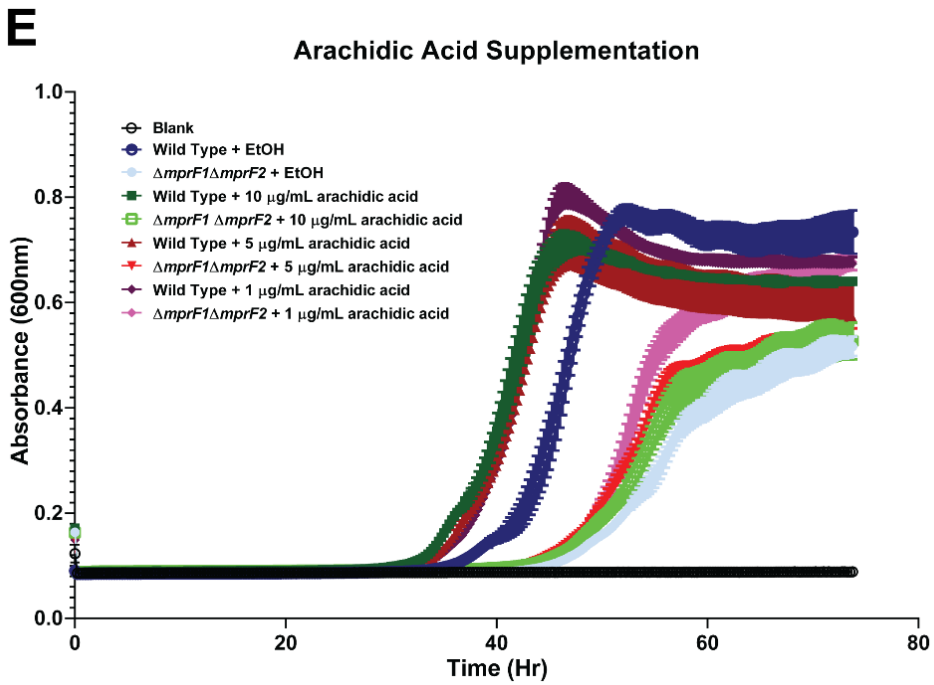

Figure S2.8. *mprF* mutants grown in chemically defined media (CDM) with individual fatty acid supplementation. Growth curves of wild type and Δ*mprF1*Δ*mprF2* grown under unsaturated fatty acid supplementation of **(A)** palmitoleic acid ($C_{16:1\ cis-9}$), oleic acid ($C_{18:1\ cis-9}$) and **(B)** cis-vaccenic acid ($C_{18:1\ cis-7}$) and linoleic acid ($C_{18:2\ cis-9,12}$). As well as **(C)** lauric acid ($C_{12:0}$), myristic acid ($C_{14:0}$), palmitic acid ($C_{16:0}$) and **(D)** stearic acid ($C_{18:0}$) and arachidic acid ($C_{18:0}$). Fatty acids were supplemented at 5 μg/mL and equal volume of ethanol (EtOH) was used as the solvent control for comparison. **(E)** Growth curves with arachidic acid at a range of concentrations (1, 5, 10 μg/mL) was also supplemented into CDM. Data points for all graphs represents the mean ± standard error of measurement calculated from 3 biological replicates with 3 technical replicates each.

6.1.1. Supplementary section – TLC spot identification

To identify spots in the 1D TLC in **figure 2.9A**, iodine and ninhydrin staining of 1D-TLCs of empty vector controls of WT, Δ*mprF1*, Δ*mprF2*, Δ*mprF1*Δ*mprF2* and p*mprF2*-HA complemented Δ*mprF2*, Δ*mprF1*Δ*mprF2* together with PG, CL and lysyl-PG standards was done. **(Figure S2.4A, B)**. 32P radiolabelled lipids of the same samples were also ran as 1D TLCs **(Figure S2.4C)**. In the iodine stained TLC, 6 major spots were identified, labelled 1 to 6.

Spot 3's migration position matches that of the PG and CL standards, suggesting that spot 3 might contain PG and CL that co-migrate together **(Figure S2.4A)**. Spot 3 was also not strongly stained with ninhydrin and were present in the 32P radiolabelled samples **(Figure S2.4B, C)**. This highly suggests that PG and CL comigrate together in spot 3 since neither PG and CL are amino modified and have phosphate present in their glycerophosphate headgroup.

Spot 4's migration position corresponds with lys-PG and is also absent in empty vector controls of Δ*mprF2* and Δ*mprF1*Δ*mprF2* **(Figure S2.4A)**. Furthermore, spot 4 is stained with ninhydrin along with the lys-PG control at the same location and this spot was also present in the 32P radiolabelled samples **(Figure S2.4B, C)**. Taken together this suggests that spot's 4 identity is lys-PG, since it is amino-modified, and phosphate is present in their glycerophosphate headgroup.

The other spots that do not match the migration of the standards are spots 1, 2, 5 and 6. To assign identities to these spots, WT and Δ*mprF1*Δ*mprF2* lipid extracts were ran as 1D-TLCs under the same conditions and all spots were scrapped off and lipids extracted for LC-MS/MS analysis **(Figure S2.4D)**. The observed masses for each of the spots and identities are listed in **supplementary table S2.3.** Spot 1 was found to contain DGDAG, spot 3 was confirmed to contain PG. CL however was unable to be detected in spot 3 due to the difficulty in ionising CL for MS. spot 4 was confirmed to contain lys-PG

and spot 6 was confirmed to contain GPDGDAG **(Table S2.3)**. Spot 5's identity is likely to be a D-alanine modified GPDGDAG (D-ala-GPDGDAG) while spot 2's identity is unclear although they do contain fatty acyl chains **(Table S2.3)**.

Hence, the spot 2's identity has been assigned according to **figure S2.4D** where it is renamed as unknown spot P-containing untargeted MS data and the fact that it is present in 32P labelled samples.

To separate the co-migrating PG and CL spots, 2D-TLC was performed. Using correspond locations on 1D-TLC plates, spots on 2D-TLC plates can be assigned. As for the co-migrating PG and CL in spot 3, the distal spot was assigned as CL and the proximal spot PG since the solvent system in the second dimension is known to cause CL to migrate ahead of PG with theoretical Rf values of 0.38 for CL and 0.31 for PG (TLC Solvent Systems – Lipid Migration, Avanti Polar Lipids Inc.) **(figure S2.4E)**. To verify that these two spots are truly PG and CL, 32P-labelling was carried out with 2D-TLC in the same solvent systems. Indeed, these 2 spots appear in the 32P-labelled samples as well.

6.1.2. Supplementary method – mass spectrometry of TLC spots

TLC spots to be identified were scrapped and silica fragments were collected in Eppendorf tubes. Lipid extraction was carried out as described in the main methods section. Chromatography separation was achieved by hydrophilic interaction liquid chromatography (HILIC) on a Phenomenex Kinetex HILIC column (150 x 2.10 mm, 2.6µM, 100Å), using Vanquish LC system (ThermoScientific). The column temperature was 40 °C, the autosampler was kept at 10 °C, and 1 µL of sample was injected. Solvent A was acetonitrile/25mM aqueous ammonium formate pH4.6 (1/1 v/v), solvent B was acetonitrile/25mM aqueous ammonium formate pH4.6 (95/5 v/v. Gradient elution started at 1 % solvent A, increased linearly to 75% A in 6 min, then increased linearly to 90 % A in 1 min, then decreased back at 1 % A in 0.1 min, and held for 3 min (total

runtime 10.1 min). The flow rate was 500µL/min. The column effluent was introduced into a Thermo QExactive plus mass spectrometer.

FT-MS spectra in the range of m/z 250-1250 were acquired in profile mode at a resolution setting of 140,000 (FWHM at m/z 200) with an AGC setting of 3x106 and maximum ion time of 200 ms. Product ion scans in centroid mode were acquired in data-dependent analysis mode, with a resolution setting of 17500 (FWHM at m/z 200), AGC setting of 1x105, normalized collision energy of 25, and isolation window of 1.4 m/z, and fixed first mass m/z 80. Samples were analysed in positive and negative ionisations.

6.2. Supplementary information for Chapter 3

Table S3.1. List of genes with mutations and sequence of occurrence

Mutant	Strain	Early ≤ 16 µg/mL DAP	Intermediate ≤ 64 ug/mL DAP	Late ≤ 256 ug/mL DAP
9	Wild type	OG1RF_12213	OG1RF_11464	OG1RF_11036 *cls1* OG1RF_11507
42	Δ*mprF1*	cls2 OG1RF_11464 OG1RF_11507		
11	Δ*mprF1*	OG1RF_11464		*cls1*
13	Δ*mprF2*	OG1RF_10260 OG1RF_11464		*cls1*
36	Δ*mprF2*	*ftsH*	OG1RF_11464	*cls1* *cls2* OG1RF_10437 OG1RF_11840 OG1RF_10531 OG1RF_11172
37	Δ*mprF2*	*ftsH*	*cls2* OG1RF_11463	OG1RF_11464 OG1RF_11036 *pgsA*
38	Δ*mprF2*	*ftsH*	OG1RF_10176 OG1RF_11162 OG1RF_12410^ 12411	cls1 OG1RF_11464 OG1RF_10453 OG1RF_10784^ 10785
39	Δ*mprF2*	OG1RF_11162	*ftsH*	*cls1* OG1RF_11464 OG1RF_10437 OG1RF_11036 OG1RF_12387
40	Δ*mprF2*	*ftsH*	*cls1* OG1RF_11464	OG1RF_12388 *pgsA*
41	Δ*mprF2*	*ftsH* OG1RF_11162	*cls1*	OG1RF_10437 OG1RF_10743
18	Δ*mprF1*Δ*mprF2*	*ftsH* OG1RF_12493 OG1RF_11876^ 11877	OG1RF_10437 cls2 OG1RF_12387 OG1RF_12502	OG1RF_11464
43	Δ*mprF1*Δ*mprF2*	*ftsH*	OG1RF_10437 OG1RF_11466	*cls1* *cls2* OG1RF_12193
44	Δ*mprF1*Δ*mprF2*	*ftsH* OG1RF_12208	OG1RF_10437 OG1RF_11464	OG1RF_11481 OG1RF_11901
45	Δ*mprF1*Δ*mprF2*	*ftsH*	*cls2* OG1RF_11464	OG1RF_10437
46	Δ*mprF1*Δ*mprF2*	*ftsH* OG1RF_10437	*cls2* *clpP* OG1RF_10506	OG1RF_11901 OG1RF_11172
47	Δ*mprF1*Δ*mprF2*	*ftsH* OG1RF_10437 OG1RF_10784^ 10785	*cls1*	OG1RF_11901 OG1RF_12189
48	Δ*mprF1*Δ*mprF2*	*ftsH*	OG1RF_10437 cls2 OG1RF_11464	OG1RF_11901
49	Δ*mprF1*Δ*mprF2*	*ftsh*	*cls1*	OG1RF_11901
50	Δ*mprF1*Δ*mprF2*	*ftsH* OG1RF_10437	OG1RF_10364 OG1RF_10387	OG1RF_11901 OG1RF_11713

^ indicates mutations found within intergenic regions of the listed genes.

Table S3.2 - RNAseq Results (WT p6his-*ftsH(H456Y)* vs WT p6his-*ftsH*)						
Locus Tag	**Log FC**	**Log CPM**	**PValue**	**FDR**	**Gene**	**Annotation**
OG1RF_10090	2.73	3.41	8.70E-04	1.89E-02	-	lipoprotein
OG1RF_10661	2.61	3.12	2.35E-03	4.10E-02	-	TatD family hydrolase
OG1RF_11482	2.47	3.28	7.30E-04	1.66E-02	-	hypothetical protein
OG1RF_10482	2.36	3.23	1.31E-03	2.59E-02	-	hypothetical protein
OG1RF_11464	2.31	9.72	2.69E-167	6.74E-164	-	hypothetical protein
OG1RF_10353	2.07	4.67	2.66E-08	1.59E-06	-	hypothetical protein
OG1RF_10354	1.81	5.88	3.16E-13	3.60E-11	-	hypothetical protein
OG1RF_10133	1.78	6.28	3.39E-13	3.69E-11	*deoB*	phosphopentomutase
OG1RF_10708	1.72	4.89	5.23E-07	2.62E-05	*pepQ*	peptidase M24
OG1RF_10775	1.68	3.83	2.94E-03	4.95E-02	-	multidrug resistance protein
OG1RF_11463	1.68	7.22	4.27E-19	7.64E-17	-	PspC family transcriptional regulator
OG1RF_10505	1.63	7.03	2.38E-16	3.32E-14	*clpP*	ATP-dependent Clp protease proteolytic subunit
OG1RF_11677	1.62	4.21	4.08E-04	9.92E-03	-	ABC transporter ATP-binding protein
OG1RF_10338	1.59	6.18	9.64E-13	9.66E-11	*ohr*	osmotically inducible protein C
OG1RF_12006	1.58	8.38	2.05E-35	2.57E-32	*groEL*	molecular chaperone GroEL
OG1RF_11055	1.57	5.80	4.07E-10	3.00E-08	-	phage major tail protein, TP901-1 family
OG1RF_11078	1.53	10.10	7.69E-34	6.42E-31	*dnaK*	molecular chaperone DnaK
OG1RF_10823	1.52	4.53	8.92E-05	2.66E-03	-	ATP-binding nuclease
OG1RF_12446	1.50	6.24	2.10E-11	1.88E-09	*dapE*	succinyl-diaminopimelate desuccinylase
OG1RF_10209	1.46	10.90	2.09E-29	1.31E-26	*ftsH*	cell division protein FtsH
OG1RF_11626	1.45	9.31	2.14E-21	4.47E-19	*gap2*	type I glyceraldehyde-3-phosphate dehydrogenase
OG1RF_12067	1.43	7.93	1.52E-22	4.22E-20	-	tellurite resistance protein
OG1RF_12066	1.41	6.11	3.26E-10	2.48E-08	-	hypothetical protein
OG1RF_10367	1.37	7.73	4.56E-22	1.14E-19	*decarboxylase*	tyrosine decarboxylase
OG1RF_10149	1.35	4.85	7.85E-05	2.40E-03	*cfa*	cyclopropane-fatty-acyl-phospholipid synthase
OG1RF_11214	1.34	5.82	2.28E-07	1.27E-05	*atpB*	ATP synthase subunit beta
OG1RF_10444	1.34	9.31	6.06E-25	2.53E-22	*clpE*	ATP-dependent Clp protease ATP-binding subunit
OG1RF_12508	1.32	5.16	2.55E-05	9.01E-04	-	thiamine biosynthesis protein ApbE
OG1RF_11076	1.32	7.47	2.41E-14	3.01E-12	*hrcA*	HrcA family transcriptional regulator
OG1RF_12375	1.30	4.46	1.22E-03	2.45E-02	*asp2*	hypothetical protein
OG1RF_11140	1.26	5.42	1.73E-05	6.29E-04	*mgtA2*	magnesium-translocating P-type ATPase
OG1RF_11793	1.24	7.83	1.15E-12	1.11E-10	*clpB*	chaperone protein ClpB
OG1RF_10886	1.22	5.20	1.32E-04	3.81E-03	-	Fe-S oxidoreductase
OG1RF_12509	1.19	6.89	3.79E-06	1.64E-04	-	FMN-binding domain-containing protein
OG1RF_10500	1.19	4.77	1.43E-03	2.75E-02	-	RNase adaptor protein RapZ
OG1RF_12530	1.15	6.95	2.00E-10	1.57E-08	*clpC*	ATP-dependent Clp protease ATP-binding subunit ClpC
OG1RF_11208	1.13	5.19	2.04E-04	5.50E-03	*atpI*	V-type ATP synthase subunit I
OG1RF_10606	1.13	5.48	1.65E-04	4.65E-03	*polA*	DNA polymerase I
OG1RF_11077	1.13	6.25	3.63E-07	1.90E-05	*grpE*	nucleotide exchange factor GrpE
OG1RF_11215	1.08	5.37	2.56E-03	4.39E-02	*atpD*	V-type ATP synthase subunit D
OG1RF_10531	1.08	6.20	1.90E-05	6.79E-04	-	hypothetical protein
OG1RF_12046	1.02	5.43	9.28E-04	1.98E-02	*mecA*	adapter protein MecA
OG1RF_11999	0.98	5.56	3.43E-04	8.60E-03	-	cobalt ABC transporter ATP-binding protein
OG1RF_10917	0.96	5.18	1.92E-03	3.49E-02	*gloA5*	lactoylglutathione lyase
OG1RF_10983	0.96	7.74	3.19E-12	2.96E-10	*npr*	NADH peroxidase
OG1RF_10402	0.94	7.07	2.87E-07	1.56E-05	*pepV*	dipeptidase PepV

OG1RF_11060	0.94	6.20	1.36E-05	5.29E-04	-	structural protein
OG1RF_10019	0.94	6.50	1.54E-06	7.28E-05	*manX2*	PTS mannose transporter subunit EIIAB
OG1RF_10603	0.90	5.48	2.89E-03	4.90E-02	*copB*	copper-translocating P-type ATPase
OG1RF_11213	0.89	5.53	2.83E-03	4.83E-02	*atpA*	V-type ATP synthase alpha chain
OG1RF_11265	0.88	5.75	1.08E-03	2.23E-02	-	peptidase M23
OG1RF_10915	0.87	5.99	2.61E-04	6.83E-03	*dkgB*	glyoxal reductase
OG1RF_10447	0.84	5.65	1.84E-03	3.44E-02	*ptsH*	phosphocarrier protein HPr
OG1RF_11241	0.82	5.92	1.20E-03	2.42E-02	*dnaG*	DNA primase
OG1RF_11625	0.81	7.02	4.48E-05	1.48E-03	*pgk*	phosphoglycerate kinase
OG1RF_11988	0.79	7.70	1.53E-07	8.91E-06	*atpA2*	ATP synthase subunit alpha
OG1RF_11624	0.79	7.06	6.91E-05	2.14E-03	*tpiA*	triose-phosphate isomerase
OG1RF_11056	0.78	5.98	1.42E-03	2.75E-02	-	hypothetical protein
OG1RF_11987	0.73	6.60	1.93E-04	5.32E-03	*atpG*	ATP synthase subunit gamma
OG1RF_11876	0.72	6.62	2.43E-04	6.42E-03	*panE2*	2-dehydropantoate 2-reductase
OG1RF_11058	0.71	7.18	9.17E-06	3.69E-04	-	hypothetical protein
OG1RF_11156	0.71	7.35	2.66E-05	9.27E-04	-	hypothetical protein
OG1RF_11246	0.70	7.80	1.17E-06	5.77E-05	*gap*	type I glyceraldehyde-3-phosphate dehydrogenase
OG1RF_11427	0.67	6.61	9.31E-04	1.98E-02	*carB*	carbamoyl phosphate synthase large subunit
OG1RF_10368	0.66	6.58	5.73E-04	1.36E-02	-	amino acid permease
OG1RF_12309	0.65	6.56	6.61E-04	1.52E-02	*pepA2*	glutamyl aminopeptidase
OG1RF_10199	0.64	6.85	3.49E-04	8.65E-03	*ldh1*	L-lactate dehydrogenase
OG1RF_12492	-0.38	8.90	1.13E-03	2.30E-02	*rpoC*	DNA-directed RNA polymerase subunit beta'
OG1RF_10448	-0.50	9.52	1.64E-07	9.32E-06	*ptsI*	phosphoenolpyruvate--protein phosphotransferase
OG1RF_10952	-0.58	7.48	2.16E-03	3.82E-02	-	hypothetical protein
OG1RF_11269	-0.67	9.40	3.63E-11	3.14E-09	*hup*	transcriptional regulator
OG1RF_12510	-0.68	7.28	6.10E-04	1.42E-02	*ndh3*	NADH dehydrogenase
OG1RF_11696	-0.69	6.59	5.58E-04	1.33E-02	*glmM*	phosphoglucosamine mutase
OG1RF_11283	-0.71	6.45	1.85E-03	3.44E-02	*aroC*	chorismate synthase
OG1RF_10099	-0.73	7.68	4.70E-05	1.51E-03	*arcA*	arginine deiminase
OG1RF_12374	-0.76	6.84	1.72E-04	4.78E-03	-	hypothetical protein
OG1RF_11832	-0.76	7.51	1.99E-04	5.41E-03	*tsf*	elongation factor Ts
OG1RF_10731	-0.81	6.00	2.06E-03	3.65E-02	*ylmE*	YggS family pyridoxal phosphate enzyme
OG1RF_10732	-0.82	6.68	1.12E-04	3.30E-03	-	cell division protein SepF
OG1RF_10101	-0.84	7.57	4.24E-06	1.80E-04	*arcC*	carbamate kinase 1
OG1RF_11847	-0.86	6.69	2.93E-05	1.01E-03	-	hypothetical protein
OG1RF_11665	-0.86	6.82	5.09E-05	1.61E-03	*cydB*	cytochrome c oxidase assembly protein
OG1RF_10479	-0.88	6.13	8.01E-04	1.79E-02	-	L-cystine transporter tcyP
OG1RF_12188	-0.88	6.16	1.68E-03	3.21E-02	*fabH*	3-oxoacyl-ACP synthase III
OG1RF_10100	-0.89	7.81	1.90E-10	1.54E-08	*arcB*	ornithine carbamoyltransferase
OG1RF_10705	-0.95	7.27	1.54E-08	1.04E-06	*rpmA*	50S ribosomal protein L27
OG1RF_11663	-0.96	7.05	4.62E-07	2.36E-05	-	amino acid ABC transporter ATP-binding protein
OG1RF_12063	-0.98	6.31	3.49E-05	1.18E-03	*mtnN*	5'-methylthioadenosine/S-adenosylhomocysteine nucleosidase
OG1RF_12180	-1.00	6.05	6.79E-05	2.13E-03	*accC*	acetyl-CoA carboxylase biotin carboxylase subunit
OG1RF_11525	-1.05	9.24	3.21E-23	1.00E-20	*sprE*	serine protease
OG1RF_12143	-1.06	5.72	1.71E-03	3.25E-02	-	DUF3042 domain-containing protein
OG1RF_10924	-1.08	5.36	8.34E-04	1.83E-02	*pyrG*	CTP synthetase
OG1RF_10932	-1.08	5.36	5.83E-04	1.37E-02	*nth*	endonuclease III
OG1RF_10355	-1.09	5.32	1.25E-03	2.49E-02	*nrdF*	ribonucleoside-diphosphate reductase

OG1RF_12242	-1.10	5.77	1.19E-04	3.46E-03	-	ribose transporter RbsU
OG1RF_10396	-1.10	6.32	2.21E-06	9.87E-05	-	hypothetical protein
OG1RF_10102	-1.10	6.96	2.59E-08	1.59E-06	*ntcA*	Crp/Fnr family transcriptional regulator
OG1RF_12179	-1.11	5.37	1.96E-03	3.50E-02	*accD*	acetyl-CoA carboxylase subunit beta
OG1RF_11527	-1.13	6.56	1.59E-05	5.86E-04	*fsrC*	histidine kinase
OG1RF_11285	-1.16	5.06	1.34E-03	2.62E-02	*aroA*	3-phosphoshikimate 1-carboxyvinyltransferase
OG1RF_10923	-1.17	5.83	3.98E-05	1.33E-03	*rpoE*	DNA-directed RNA polymerase subunit delta
OG1RF_11751	-1.18	6.15	1.38E-05	5.29E-04	-	hypothetical protein
OG1RF_10103	-1.20	7.94	1.44E-16	2.12E-14	-	C4-dicarboxylate ABC transporter
OG1RF_10875	-1.21	5.35	3.09E-04	7.81E-03	-	streptococcin A-M57
OG1RF_12109	-1.23	6.92	2.04E-09	1.42E-07	*dltD*	D-alanyl-lipoteichoic acid biosynthesis protein DltD
OG1RF_11144	-1.26	9.40	9.49E-18	1.58E-15	*lpd*	dihydrolipoyl dehydrogenase
OG1RF_10948	-1.29	7.77	1.19E-17	1.87E-15	*rpmE*	50S ribosomal protein L31 type B
OG1RF_11980	-1.30	5.41	8.08E-05	2.44E-03	-	AI-2E family transporter
OG1RF_11571	-1.31	6.73	9.71E-10	6.96E-08	-	membrane protein
OG1RF_10070	-1.31	4.87	8.08E-04	1.79E-02	-	DUF2273 domain-containing protein
OG1RF_11420	-1.34	4.52	2.20E-03	3.86E-02	-	GntR family transcriptional regulator
OG1RF_11128	-1.40	5.30	1.50E-04	4.27E-03	*trxB*	thioredoxin-disulfide reductase
OG1RF_11998	-1.43	5.66	2.95E-06	1.30E-04	-	hypothetical protein
OG1RF_11231	-1.43	6.62	4.79E-11	4.00E-09	*ptsG*	PTS N-acetylglucosamine transporter subunit IIABC
OG1RF_11608	-1.46	7.92	1.70E-23	6.07E-21	-	hypothetical protein
OG1RF_11281	-1.47	5.47	4.69E-06	1.96E-04	*aroF*	3-deoxy-7-phosphoheptulonate synthase
OG1RF_11282	-1.49	6.02	2.65E-08	1.59E-06	*aroB*	3-dehydroquinate synthase
OG1RF_11442	-1.49	4.92	2.96E-04	7.57E-03	*mdlB*	ABC transporter ATP-binding protein
OG1RF_10918	-1.53	4.54	1.02E-03	2.12E-02	-	NUDIX hydrolase
OG1RF_11621	-1.54	6.79	2.83E-13	3.38E-11	-	NgoFVII restriction endonuclease
OG1RF_11985	-1.57	8.13	1.17E-21	2.67E-19	*atpC2*	ATP synthase epsilon chain
OG1RF_11679	-1.59	7.99	3.82E-29	1.92E-26	-	manganese ABC transporter substrate-binding protein
OG1RF_11618	-1.60	7.29	1.02E-15	1.35E-13	-	hypothetical protein
OG1RF_10594	-1.60	4.33	1.85E-03	3.44E-02	*opuCB*	choline ABC transporter permease
OG1RF_11528	-1.63	5.53	3.23E-07	1.72E-05	*fsrB*	protein FsrB
OG1RF_11792	-1.65	4.21	2.43E-03	4.20E-02	-	nucleoside 2-deoxyribosyltransferase
OG1RF_10971	-1.71	4.08	1.88E-03	3.45E-02	*ycgQ*	phosphate ABC transporter substrate-binding protein
OG1RF_12460	-1.77	7.67	6.24E-20	1.20E-17	*lrgB*	antiholin
OG1RF_12433	-1.79	5.05	7.90E-06	3.25E-04	*maf*	maf-like protein
OG1RF_11753	-1.79	5.66	2.44E-08	1.57E-06	*treB*	PTS maltose transporter subunit IIBC
OG1RF_11887	-1.90	4.81	9.27E-06	3.69E-04	-	hypothetical protein
OG1RF_12152	-1.97	4.85	1.55E-05	5.81E-04	-	hypothetical protein
OG1RF_10228	-1.97	4.26	5.54E-04	1.33E-02	*pyrDA*	dihydroorotate oxidase
OG1RF_10639	-2.01	6.06	8.07E-13	8.43E-11	*oppF*	peptide ABC transporter ATP-binding protein
OG1RF_10190	-2.03	4.11	9.56E-04	2.01E-02	-	peptide ABC transporter ATP-binding protein
OG1RF_10045	-2.09	3.91	1.87E-03	3.44E-02	*cysS2*	Mini-ribonuclease 3
OG1RF_11577	-2.22	3.71	9.13E-04	1.97E-02	-	N-acetylmannosamine kinase
OG1RF_10876	-2.45	4.41	2.09E-04	5.56E-03	-	hypothetical protein
OG1RF_10288	-2.49	4.98	1.67E-08	1.10E-06	*nhaC*	Na+/H+ antiporter NhaC

OG1RF_10847	-2.69	4.03	4.62E-05	1.50E-03	-	hypothetical protein
OG1RF_10080	-2.82	4.43	1.66E-06	7.55E-05	-	hypothetical protein
OG1RF_12116	-2.86	4.46	1.26E-06	6.09E-05	*nrdG*	anaerobic ribonucleoside-triphosphate reductase activating protein
OG1RF_12400	-3.28	3.44	1.00E-03	2.09E-02	*sorB2*	PTS sorbose transporter subunit IIB
OG1RF_10395	-3.41	3.52	4.03E-04	9.91E-03	-	hypothetical protein
OG1RF_11584	-4.71	2.94	1.95E-03	3.50E-02	-	C4-dicarboxylate ABC transporter
OG1RF_12459	-5.43	3.36	2.75E-04	7.11E-03	*entB2*	isochorismatase

Results filtered by $\log_2$FC >1, P-value<0.05, FDR<0.05.

Table S3.3 - Proteomics Results (WT p6his-*ftsH(H456Y)* vs WT p6his-*ftsH*)			
Membrane			
Gene	**logFC**	**PValue**	**FDR**
OG1RF_10669	2.60	4.36E-03	0.00E+00
arcB	2.53	8.94E-03	1.72E-02
cls	2.46	1.01E-02	1.72E-02
OG1RF_10473	2.36	1.72E-02	4.05E-02
OG1RF_11656	2.31	4.88E-03	0.00E+00
OG1RF_11718	2.24	1.84E-02	4.05E-02
ziaA	1.83	6.62E-04	0.00E+00
OG1RF_12464	1.51	1.19E-02	1.72E-02
OG1RF_11761	1.29	6.33E-03	1.72E-02
mdlB2	1.28	1.11E-02	1.72E-02
atpI	1.17	3.00E-03	0.00E+00
OG1RF_11679	1.14	2.18E-03	0.00E+00
OG1RF_11938	1.13	1.66E-03	0.00E+00
yckE	-2.77	1.01E-02	1.72E-02
lysS	-2.69	1.41E-02	3.08E-02
pyrB	-2.66	8.94E-03	1.72E-02
OG1RF_10886	-2.07	1.01E-02	1.72E-02
gelE	-2.03	4.03E-03	0.00E+00
trePP	-1.97	1.44E-02	3.08E-02
carB	-1.83	3.31E-04	0.00E+00
cryZ	-1.72	1.47E-02	3.08E-02
hrcA	-1.63	4.71E-03	0.00E+00
ileS	-1.55	4.97E-04	0.00E+00
glyS	-1.52	1.66E-04	0.00E+00
fabF	-1.52	1.82E-03	0.00E+00
OG1RF_11694	-1.29	1.59E-02	4.05E-02
OG1RF_12202	-1.23	1.82E-02	4.05E-02
sufB	-1.20	7.31E-03	1.72E-02
valS	-1.18	5.21E-03	0.00E+00
prfC	-1.16	2.34E-03	0.00E+00
efp	-1.16	7.96E-03	1.72E-02
tig	-1.15	8.28E-04	0.00E+00
purB	-1.10	8.12E-03	1.72E-02
glmM	-1.07	7.47E-03	1.72E-02
pyk	-1.04	1.49E-03	0.00E+00
cmk	-1.02	1.09E-02	1.72E-02
ftsY	-1.00	5.05E-03	0.00E+00
Whole cell lysate			
cls	1.77	1.81E-02	6.45E-02
OG1RF_10473	1.33	8.72E-02	3.57E-01
OG1RF_12485	1.27	6.62E-02	2.94E-01
arcB	1.19	5.64E-02	2.53E-01
OG1RF_10669	1.26	7.86E-03	0.00E+00
OG1RF_11313	1.25	3.82E-02	1.57E-01
yckE	-2.77	2.51E-03	0.00E+00
lysS	-2.69	3.93E-03	0.00E+00
pyrB	-2.54	5.40E-03	0.00E+00
OG1RF_11789	-2.16	1.47E-02	6.45E-02
OG1RF_12227	-2.13	4.62E-03	0.00E+00
ahpC	-2.13	7.86E-03	0.00E+00
OG1RF_10886	-2.01	2.20E-03	0.00E+00
OG1RF_10960	-1.99	1.82E-02	6.45E-02
gelE	-1.95	1.39E-03	0.00E+00
dapB	-1.88	1.20E-02	6.12E-02
OG1RF_12011	-1.88	7.24E-03	0.00E+00

trePP	-1.86	8.02E-03	0.00E+00
OG1RF_10302	-1.85	6.47E-03	0.00E+00
relA	-1.71	3.47E-02	1.46E-01
carB	-1.69	3.11E-04	0.00E+00
OG1RF_11294	-1.67	1.08E-02	6.12E-02
cryZ	-1.67	3.14E-03	0.00E+00
ctsR	-1.64	3.79E-02	1.57E-01
OG1RF_11098	-1.64	5.90E-02	2.67E-01
OG1RF_11724	-1.62	1.46E-02	6.45E-02
OG1RF_10898	-1.58	5.04E-02	2.26E-01
OG1RF_12306	-1.58	3.38E-02	1.46E-01
hrcA	-1.56	1.71E-03	0.00E+00
OG1RF_10435	-1.55	7.05E-02	3.11E-01
azoR	-1.53	3.53E-02	1.51E-01
rep	-1.53	7.84E-02	3.25E-01
tsf	-1.53	7.40E-02	3.17E-01
OG1RF_11029	-1.46	7.09E-03	0.00E+00
gnd	-1.46	5.24E-03	0.00E+00
ileS	-1.41	4.67E-04	0.00E+00
truA	-1.38	1.10E-02	6.12E-02
fabF	-1.36	9.38E-04	0.00E+00
addA	-1.36	5.43E-02	2.37E-01
xseA	-1.35	2.67E-03	0.00E+00
carA	-1.33	7.09E-03	0.00E+00
gmk2	-1.33	1.21E-02	6.12E-02
glyS	-1.30	1.56E-04	0.00E+00
ftsQ	-1.28	1.31E-02	6.45E-02
OG1RF_10181	-1.20	7.55E-03	0.00E+00
bbvIM	-1.19	5.28E-02	2.32E-01
OG1RF_11694	-1.18	5.86E-03	0.00E+00
ptsI	-1.12	3.87E-02	1.57E-01
gcp	-1.11	9.20E-02	3.76E-01
uppS	-1.11	9.51E-02	3.82E-01
OG1RF_12202	-1.10	1.53E-02	6.45E-02
pepF	-1.09	2.16E-02	1.01E-01
sufB	-1.08	8.33E-03	0.00E+00
glyQ	-1.07	1.03E-02	6.12E-02
metG	-1.07	1.03E-02	6.12E-02
efp	-1.07	4.93E-03	0.00E+00
valS	-1.05	7.40E-03	0.00E+00
thrS	-1.02	9.17E-03	2.50E-02
menB	-1.02	9.17E-03	2.50E-02
prfC	-1.00	2.82E-03	0.00E+00

Membrane fraction hits are filtered by P-value<0.05, FDR<0.05, log2FC>1. Whole cell lysates are filtered by P-value<0.1, log2FC>1 instead due to high lysozyme contamination reducing sensitivity of detection.

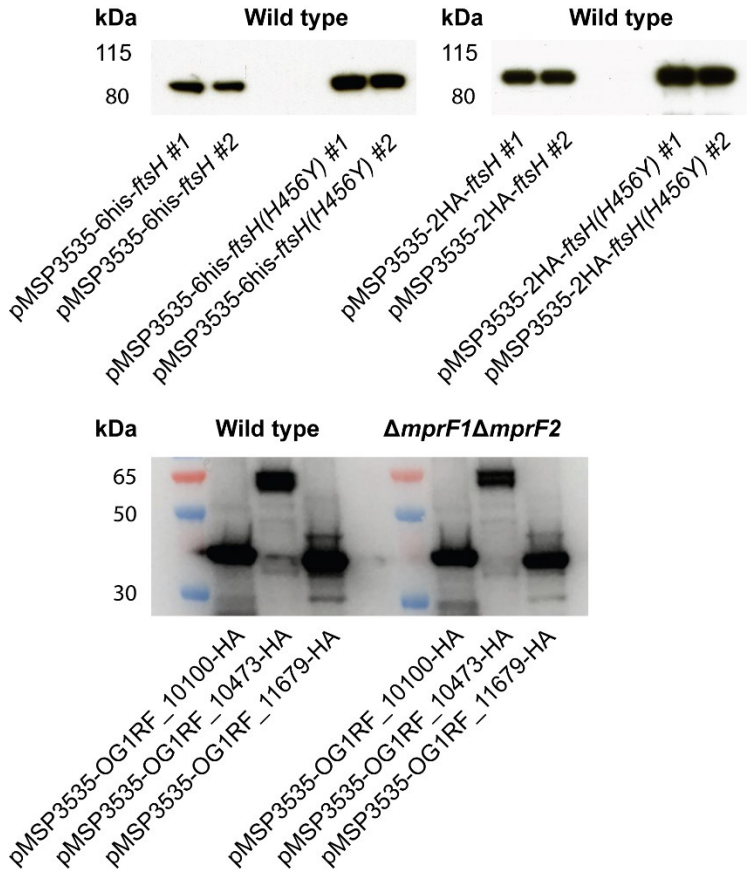

Figure S3.1. Anti-HA western immunoblot of *E. faecalis* strains expressing 6his and/or HA tagged *ftsH*, *ftsH(H456Y)*, OG1RF_10100 (*arcB*), OG1RF_11679, OG1RF_10473. All constructs display expression. The predicted protein sizes are: FtsH (~80 kDa), OG1RF_10100 (~38.6 kDa), OG1RF_10473 (~59.6 kDa) and OG1RF_11679 (~35.2 kDa).

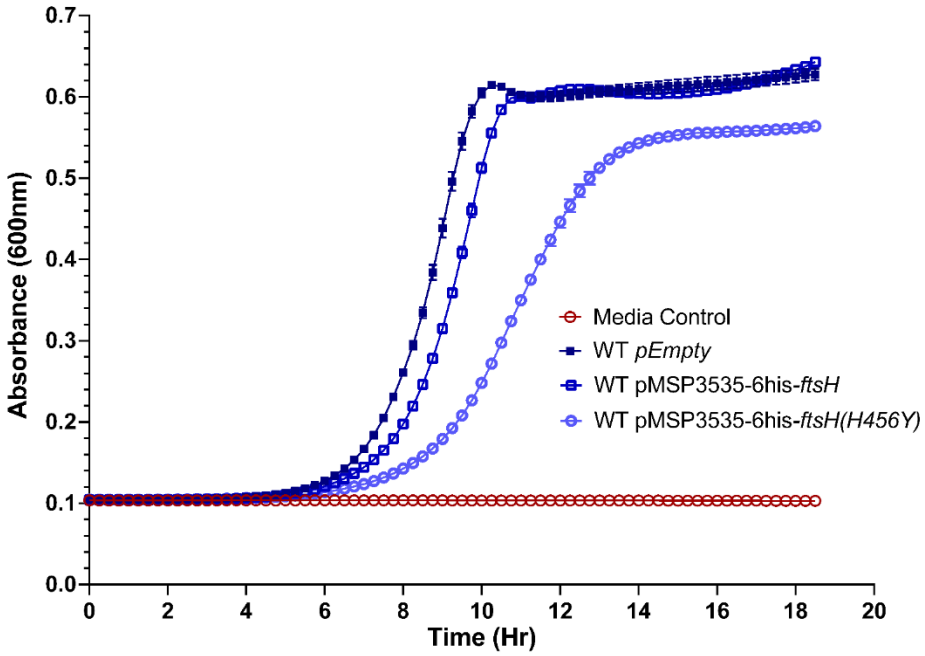

Figure S3.2. Inducible expression of inactive *ftsH* variant, *ftsH(H456Y)* leads to growth defect in the wild type. Growth curve of inducible heterologous expression of wild type *ftsH* and protease inactive variant, *ftsH(H456Y)*. Growth curve was done under induction with 125 ng/mL nisin.

Mutation occurrence detected by PCR			
Mutants (out of 8 colonies)	Bio-rep 1	Bio-rep 2	Bio-rep 3
Day 3	0	3	3
Day 6	1	4	1
Day 9	2	4	2

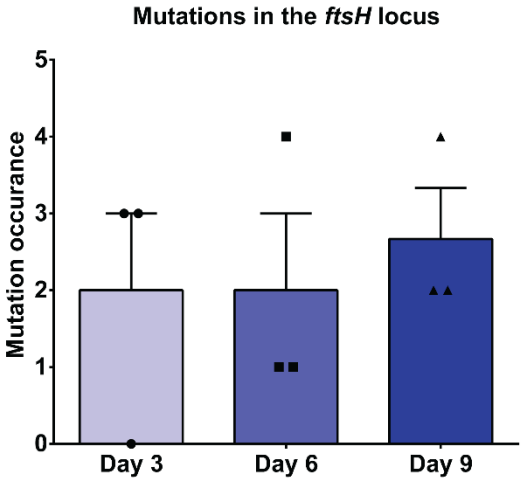

Figure S3.3. PCR amplification of the *ftsH* locus of Δ*mprF1*Δ*mprF2* passage control isolates from day 3, 6, 9 of evolution. PCR of the *ftsH* locus inclusive of its native promoter was conducted to detect for any size shifts or missing products indicating possible mutations in the locus. 8 colonies for each biological replicate were tested. Results are presented in a tabular and graphical format.

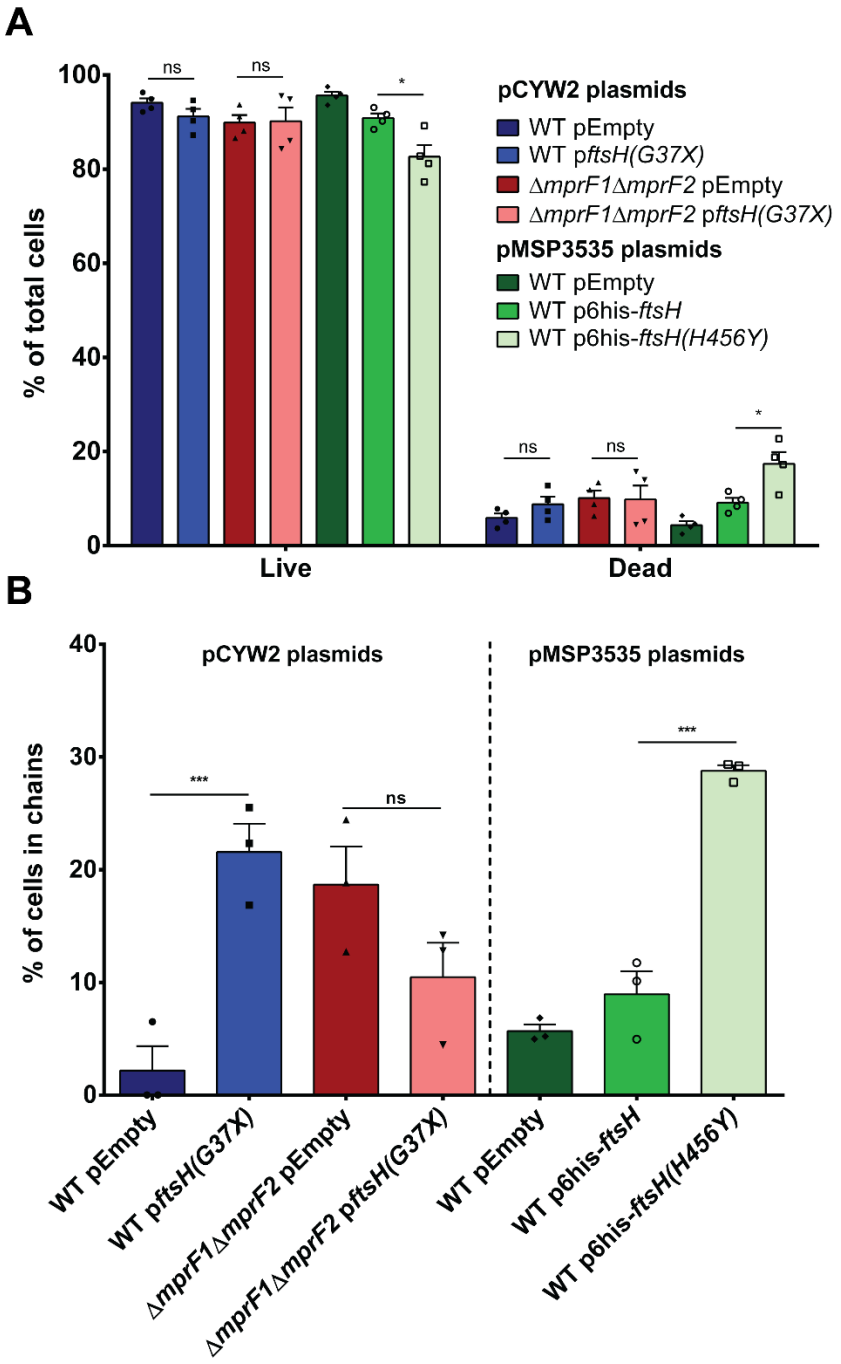

Figure S3.4. *ftsH* dysfunction has a minor effect on cell viability and increases cell chaining in the wild type. (A) Live dead staining on stationary phase cultures. Error bars represent the standard error of mean from 4 biological replicates. At least 100 cells per replicate were analysed. Tukey's test for ANOVA. *, p=0.05 to 0.01. **(B)** Enumeration of cells in chains from phase contrast microscopy. Chaining cells are defined as 3 or more cells adjacent to each other. Error bars represent the standard error of mean from 3 biological replicates. At least 100 cells per replicate were analysed. Tukey's test for ANOVA. ***, p=0.0001 to 0.001. pCYW2 plasmids are under constitutive expression of a PsrtA promoter. Constructs in pMSP3535 plasmids are under a nisin inducible promoter induced with 125 ng/mL nisin.

6.3. Supplementary information for Chapter 4

Table S4.1. Results of proteomic analysis of p*floT-6his* DRM vs DSM				
Enriched in DRM Fraction (DRM vs DSM)				
Gene Symbol	**Annotation**	**P-value**	**FDR**	**LogFC**
OG1RF_11197	ABC superfamily ATP binding cassette transporter, membrane protein	0.0080	0.0141	3.2146
mprF2	Lysyl-tRNA synthetase (Class II)	0.0127	0.0141	2.7525
OG1RF_11135	Sugar ABC superfamily ATP binding cassette transporter, sugar-binding protein	0.0155	0.0141	2.6648
OG1RF_10473*	Amidase	0.0183	0.0141	2.6025
OG1RF_11807	Peptidase propeptide and YPEB domain protein	0.0350	0.0315	2.5938
OG1RF_12369	ABC superfamily ATP binding cassette transporter, ABC protein	0.0103	0.0141	2.5575
OG1RF_10897	Glutamine ABC superfamily ATP binding cassette transporter, binding protein	0.0030	0.0000	2.4467
OG1RF_10400	Polysaccharide biosynthesis family protein	0.0306	0.0179	2.3900
OG1RF_11354	Iron (Fe) ABC superfamily ATP binding cassette transporter, binding protein	0.0043	0.0141	2.3643
OG1RF_12146	Rhodanese family protein	0.0332	0.0315	2.3481
OG1RF_12451	Cell wall surface anchor family protein	0.0408	0.0350	2.2605
OG1RF_11293	CPA1 family monovalent cation:proton (H+) antiporter-1	0.0408	0.0350	2.2516
OG1RF_11774	Sugar ABC superfamily ATP binding cassette transporter, sugar-binding protein	0.0408	0.0350	2.2335
potD	Spermidine/putrescine ABC superfamily ATP binding cassette transporter, binding protein	0.0448	0.0412	2.1950
OG1RF_10612	Uncharacterized protein	0.0253	0.0179	2.1640
OG1RF_11154	Integral membrane protein	0.0469	0.0412	2.1640
OG1RF_11723	Brp/Blh family beta-carotene 15,15'-monooxygenase	0.0272	0.0179	2.1308
secY	Protein translocase subunit SecY	0.0199	0.0141	2.0816
rseP*	RIP metalloprotease RseP	0.0025	0.0000	2.0566
ecfA	Energy-coupling factor transporter ATP-binding protein EcfA	0.0286	0.0179	1.9743
OG1RF_10412	ABC superfamily ATP binding cassette transporter, membrane protein	0.0389	0.0350	1.9690
OG1RF_10669	ABC superfamily ATP binding cassette transporter, membrane protein	0.0389	0.0350	1.9690
OG1RF_11022	ABC superfamily ATP binding cassette transporter, binding protein	0.0306	0.0179	1.9123
OG1RF_10968	Uncharacterized protein	0.0448	0.0412	1.9001
OG1RF_12485	Phosphatidylglycerol--membrane-oligosaccharide glycerophosphotransferase	0.0257	0.0179	1.8908
OG1RF_11721	Bacterial sugar transferase	0.0173	0.0141	1.8633
treB	PTS family trehalose porter, IIBC component	0.0286	0.0179	1.8359

OG1RF_12351	Ferric (Fe+3) ABC superfamily ATP binding cassette transporter, binding protein	0.0297	0.0179	1.8306
OG1RF_10031	ABC superfamily ATP binding cassette transporter, membrane protein	0.0335	0.0315	1.8198
OG1RF_12464	ABC superfamily ATP binding cassette transporter, binding protein	0.0127	0.0141	1.7157
OG1RF_12366	Peptide ABC superfamily ATP binding cassette transporter, binding protein	0.0002	0.0000	1.7035
yclK	Sensor histidine kinase	0.0332	0.0315	1.6053
OG1RF_11255	Cell surface hydrolase	0.0257	0.0179	1.5458
ftsX	Cell division protein FtsX	0.0264	0.0179	1.5156
OG1RF_10103	UIT3 family protein	0.0286	0.0179	1.5148
OG1RF_10040	PIN domain protein	0.0362	0.0315	1.4865
tig2	Peptidyl-prolyl cis-trans isomerase	0.0306	0.0179	1.3333
OG1RF_12014	Glycine betaine/carnitine/choline ABC superfamily ATP binding cassette transporter	0.0088	0.0141	1.3236
atpH	ATP synthase subunit delta	0.0419	0.0405	1.2569
OG1RF_10021	PTS family mannose/fructose/sorbose porter component IID	0.0236	0.0179	1.2552
OG1RF_11664	ABC superfamily ATP binding cassette transporter, ABC/membrane protein	0.0286	0.0179	1.2260
ndvA	ABC superfamily ATP binding cassette transporter, membrane protein	0.0335	0.0315	1.2024
OG1RF_10521	ABC superfamily ATP binding cassette transporter, membrane protein	0.0312	0.0179	1.1910
lepB	Signal peptidase I	0.0236	0.0179	1.1867
oppA	Oligopeptide ABC superfamily ATP binding cassette transporter, binding protein	0.0010	0.0000	1.1863
OG1RF_11761	ABC superfamily ATP binding cassette transporter, binding protein	0.0016	0.0000	1.1429
metQ	Lipoprotein	0.0286	0.0179	1.1209
actP	Copper-exporting ATPase	0.0228	0.0141	1.1168
mdlB2	Multidrug ABC superfamily ATP binding cassette transporter, ABC protein	0.0297	0.0179	1.1033
OG1RF_11679	ABC superfamily ATP binding cassette transporter, binding protein	0.0488	0.0412	1.0951
ecfA	Energy-coupling factor transporter ATP-binding protein EcfA	0.0228	0.0141	1.0898
OG1RF_10191*	Amino acid ABC superfamily ATP binding cassette transporter, membrane protein	0.0039	0.0141	1.0710
srtA	Sortase SrtA	0.0350	0.0315	1.0566
OG1RF_11663	ABC superfamily ATP binding cassette transporter, ABC/membrane protein	0.0155	0.0141	1.0214
OG1RF_12509	Pheromone cAD1 lipoprotein	0.0117	0.0141	1.0163
lytR	Transcriptional regulator LytR	0.0448	0.0412	1.0075
Enriched in DSM Fraction (DRM vs DSM)				
Gene Symbol	**Annotation**	**P-value**	**FDR**	**LogFC**
OG1RF_11061	Uncharacterized protein	0.0008	0.0000	-3.9346
lepA	Elongation factor 4	0.0272	0.0179	-3.0997

trcF	Transcription-repair-coupling factor	0.0210	0.0141	-2.8306
gshAB	Glutathione biosynthesis bifunctional protein GshAB	0.0408	0.0350	-2.8306
OG1RF_10056	5'-nucleotidase	0.0155	0.0141	-2.8003
smc	Chromosome partition protein Smc	0.0272	0.0179	-2.6923
zwf	Glucose-6-phosphate 1-dehydrogenase	0.0350	0.0315	-2.6667
rnr	Ribonuclease R	0.0199	0.0141	-2.5714
OG1RF_12224	Metallo-beta-lactamase superfamily protein	0.0350	0.0315	-2.4406
clpB	Chaperone protein ClpB	0.0080	0.0141	-2.4171
polC	DNA polymerase III PolC-type	0.0408	0.0350	-2.3764
parE	DNA topoisomerase 4 subunit B	0.0448	0.0412	-2.3764
xseA	Exodeoxyribonuclease 7 large subunit	0.0469	0.0412	-2.2381
OG1RF_12445	Uncharacterized protein	0.0448	0.0412	-2.2098
OG1RF_11970	Glyoxalase	0.0297	0.0179	-2.1221
opuAA2	Glycine betaine/L-proline ABC superfamily ATP binding cassette transporter, ABC protein	0.0312	0.0179	-2.0075
prfA	Peptide chain release factor 1	0.0469	0.0412	-1.8813
fhs	Formate-tetrahydrofolate ligase	0.0448	0.0412	-1.8433
mutS	Endonuclease MutS2	0.0362	0.0315	-1.7098
relA	GTP diphosphokinase	0.0448	0.0412	-1.5790
OG1RF_11718	Uncharacterized protein	0.0099	0.0141	-1.5026
uvrA	UvrABC system protein A	0.0183	0.0141	-1.4601
npr	NADH peroxidase	0.0389	0.0350	-1.4554
OG1RF_11908	Uncharacterized protein	0.0054	0.0141	-1.4075
srmB	ATP-dependent RNA helicase DeaD	0.0066	0.0141	-1.3245
glmU	Bifunctional protein GlmU	0.0469	0.0412	-1.2915
argS	Arginine-tRNA ligase	0.0253	0.0179	-1.2552
yhgF	YhgF like protein	0.0389	0.0350	-1.2197
infB	Translation initiation factor IF-2	0.0074	0.0141	-1.2127
tkt	Transketolase	0.0272	0.0179	-1.2028
OG1RF_12015	Uncharacterized protein	0.0286	0.0179	-1.1760
clpC	ATPase/chaperone ClpC, probable specificity factor for ClpP protease	0.0286	0.0179	-1.1707
gnd	6-phosphogluconate dehydrogenase, decarboxylating	0.0408	0.0350	-1.1693
tig	Trigger factor	0.0188	0.0141	-1.1682
ackA	Acetate kinase	0.0257	0.0179	-1.1536
OG1RF_10367	Decarboxylase	0.0488	0.0412	-1.1335
pnp	Polyribonucleotide nucleotidyltransferase	0.0228	0.0141	-1.1264
glyS	Glycine-tRNA ligase beta subunit	0.0127	0.0141	-1.0876
OG1RF_11464	Uncharacterized protein	0.0005	0.0000	-1.0303
recA	Protein RecA	0.0350	0.0315	-1.0210
OG1RF_11724	Group 2 glycosyl transferase	0.0408	0.0350	-1.0201

Results filtered by $-1>Log_2FC>1$, p-value<0.05, FDR<0.05. * refers to proteins found in the same putative complex as determined previously (Maddalo et al., 2011).

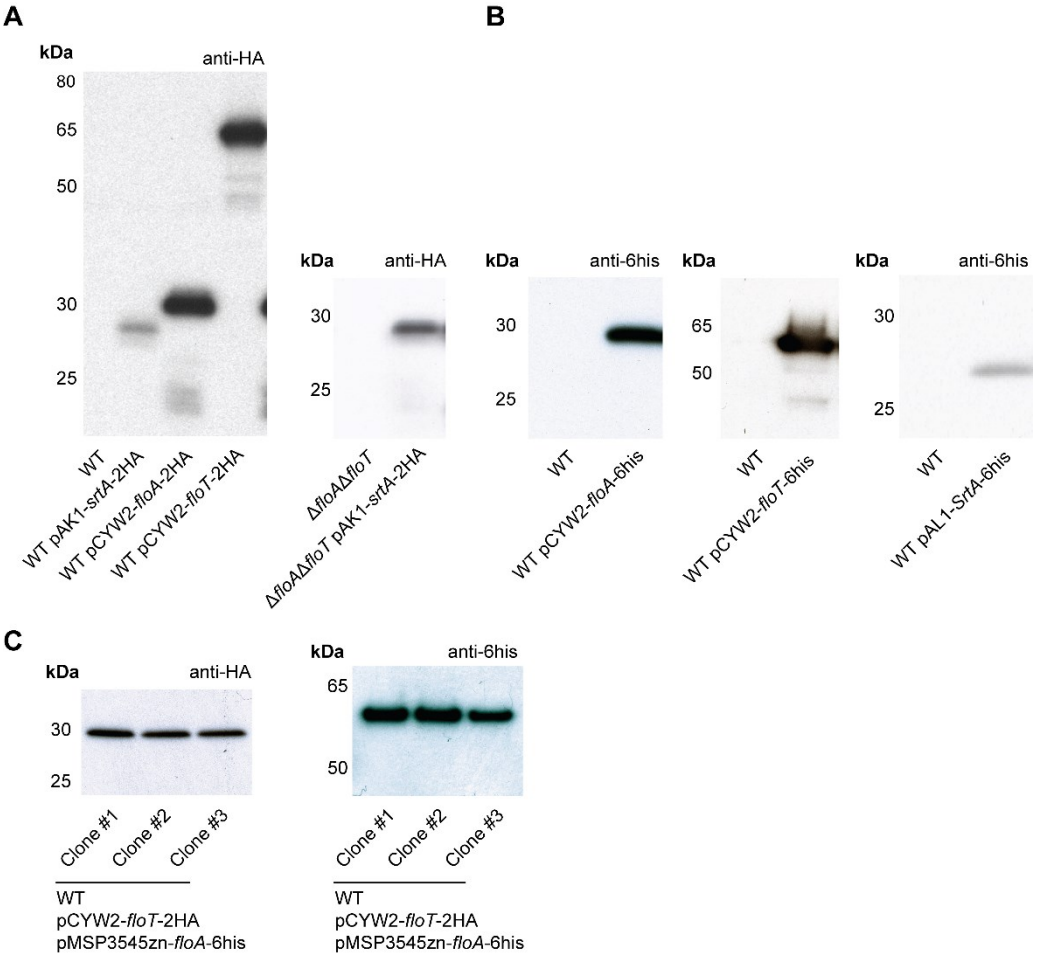

Figure S4.1. Western blot of affinity tagged flotillins and SrtA showing expression. **(A)** Western blots for HA-tagged SrtA and flotillin expression for pAK1-*srtA*-2HA, pCYW2-*floA*-2HA and pCYW2-*floT*-2HA in the wild type and pAK1-*srtA*-2HA in Δ*floA*Δ*floT*. **(B)** Western blots for 6his-tagged flotillin expression for pCYW2-*floA*-6his, pCYW2-*floT*-6his and pAL1-*srtA*-2HA in the wild type. **(C)** Western blots for 6his- and HA-tagged flotillins in dual plasmid containing strain, wild type pCYW2-*floT*-2HA pMSP3545zn-*floA*-6his. Estimated protein sizes are: SrtA-2HA = 29 kDa, FloA-2HA = 36 kDa, FloT-2HA = 57 kDa. SrtA-6his = 28 kDa, FloA-6his = 33 kDa, FloT-6his = 55 kDa. Western blot for pCYW2-*floT*-6his was performed by Daryl Yeong, the other blots were performed by Jermain Goh.

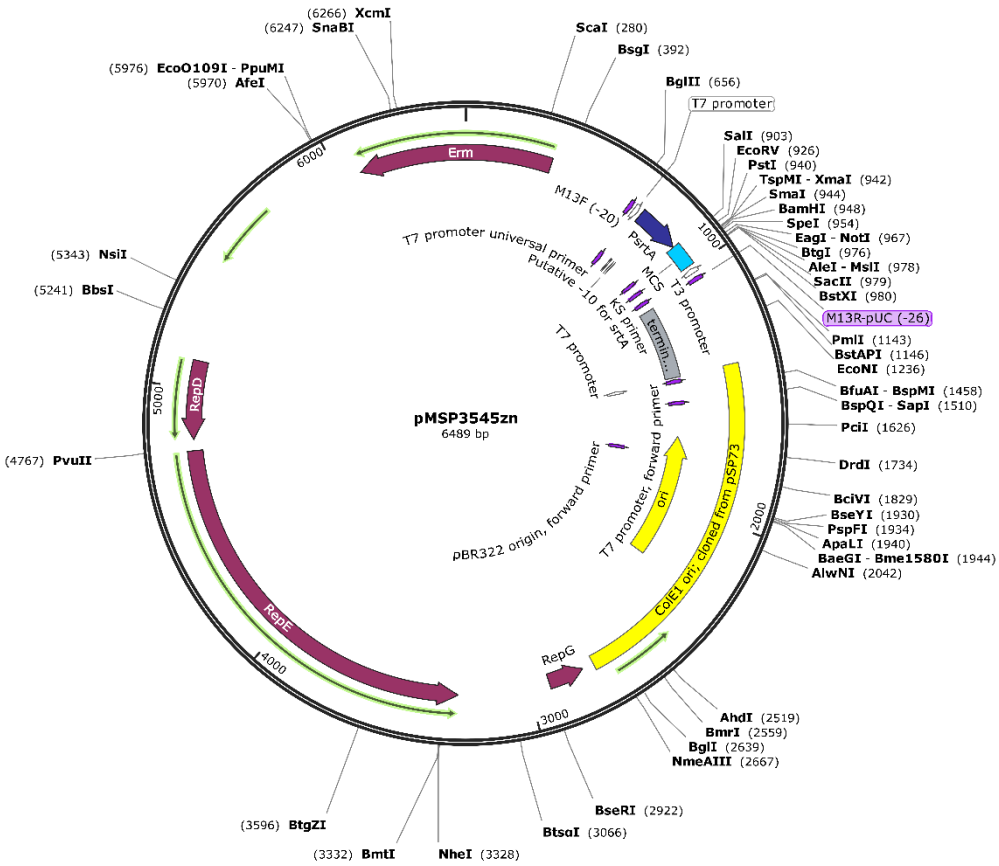

Figure S4.2. Plasmid map of pMSP3545zn. Genes to be expressed were inserted into the multiple cloning site (MCS) downstream of the P*srtA* promoter.

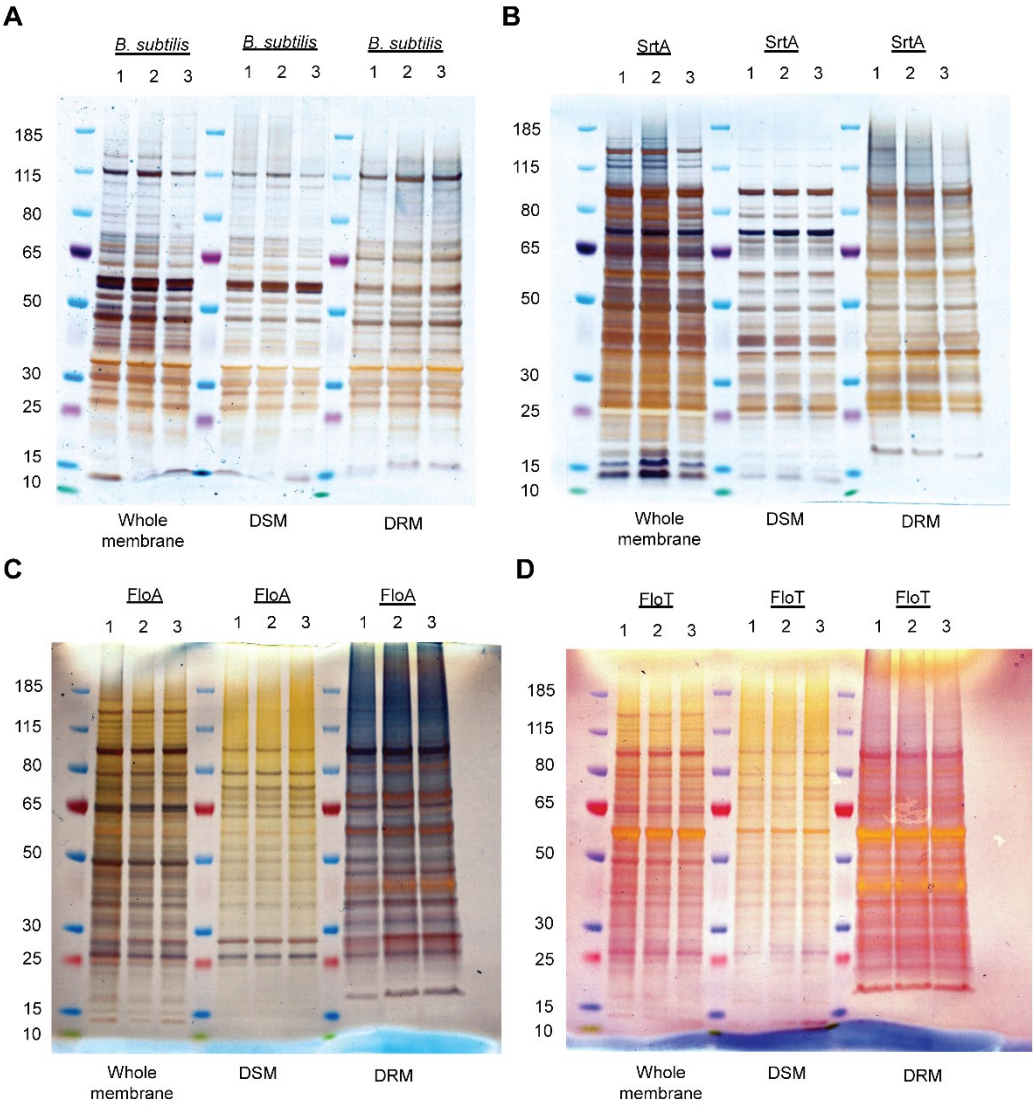

Figure S4.3. Sliver stained SDS-PAGE gels showing partition of proteins into detergent resistant membrane (DRM) and detergent soluble membrane (DSM) fractions. Sliver stained SDS-PAGE gels of whole membranes, DSM and DRM fractions in **(A)** *B. subtilis* and *E. faecalis* **(B)** p*srtA-6his*, **(C)** p*floA-6his*, **(D)** p*floT-6his*. Fractions were normalised to total volume of the detergent mixture to show representative partitions of DSM and DRM sub-sets of the whole membrane. 3 biological replicates were performed for each sample.

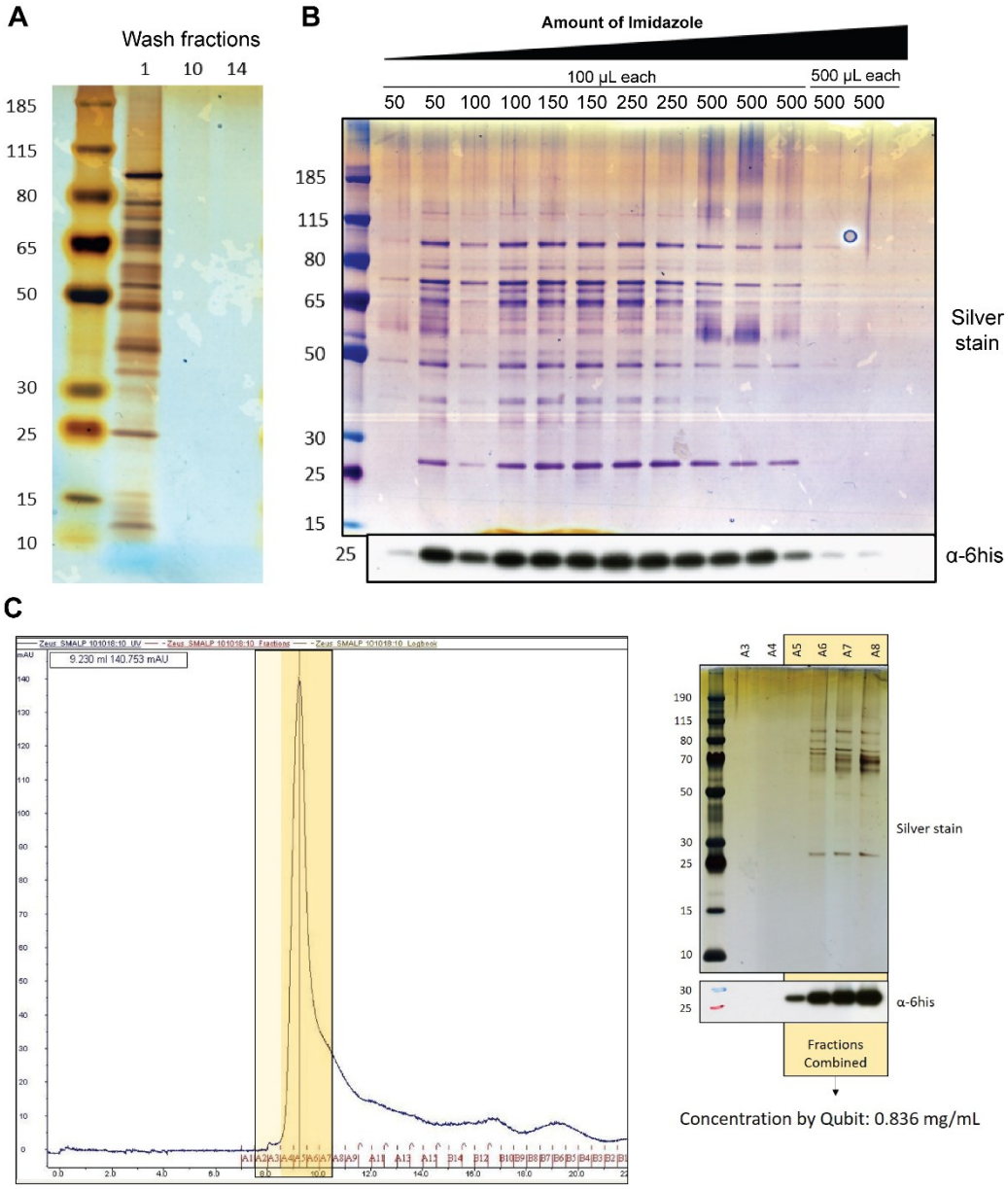

Figure S4.4. SrtA-6his SMALP isolation. Nickel column chromatography of SMA solubilised membranes was performed. **(A)** Wash fractions from the Ni-column showing no eluates at 10 and 14 column volumes from silver stain of the fractions. **(B)** Eluate fractions from the Ni-column at increasing concentrations of imidazole. Silver stain and anti-6his western blots of the fractions are shown. Fractions containing SrtA-6his as determined from the western blot were pooled and placed through size exclusion chromatography (SEC). **(C)** SEC chromatogram showing majority of the proteins eluting from 1 peak. Silver stain and anti-6his western blots of the fractions corresponding to that peak are shown. Fractions containing SrtA-6his were combined and concentration was determined to be 0.836 mg/mL by Qubit protein assay.